Development of new synthetic tools for the preparation of coumarins and thiocoumarins

Olesia Zaitceva

UNIVERSITÉ DE STRASBOURG

ÉCOLE DOCTORALE DES SCIENCES CHIMIQUES

Institut de Chimie, UMR 7177

THÈSE

présentée par :

Olesia ZAITCEVA

soutenue le : **20 juin 2019**

pour obtenir le grade de : **Docteur de l'université de Strasbourg**

Discipline/ Spécialité : Chimie

Development of new synthetic tools for the preparation of coumarins and thiocoumarins.

THÈSE dirigée par :

Mr. LOUIS Benoît	Directeur de Recherche CNRS
Mr. PALE Patrick	Professeur, Université de Strasbourg

RAPPORTEURS :

Ms. IVANOVA Svetlana	Professeur, Université de Séville
Mr. KIRSCH Gilbert	Professeur Emérite, Université de Lorraine

---

AUTRES MEMBRES DU JURY :

Mr. VASILYEV Aleksander	Professeur, Université de Saint-Pétersbourg
Ms. SARACI Erisa	Chercheur, Karlsruhe Institute of Technology

Remerciements

La première personne que j'aimerais remercier est le docteur Benoît Louis. J'aimerais commencer par faire remarquer que cette personne m'a aidée à mieux définir mes intérêts, ainsi que mes priorités professionnelles. Je voudrais souligner sa manière captivante de mener des présentations et ses cours. Il a une capacité exceptionnelle à rendre simple les sujets compliqués à travers son discours. Je suis reconnaissante pour tous les conseils, consignes et explications qu'il m'a donnés durant ces trois années. Ma participation à deux conférences du Groupe d'Étude en Catalyse (GECat) et mon travail dans l'Université forestière de Pékin ont été des expériences inoubliables. Tout cela n'a pu être possible qu'avec les recommandations et le soutien de mon honorable directeur de thèse.

J'aimerais exprimer ma reconnaissance au professeur Patrick Pale qui m'a réservé un accueil chaleureux dans le laboratoire de Synthèse, Réactivité Organiques et Catalyse dont il est le directeur. Merci pour l'ambiance d'entraide et d'amitié qui règne dans votre laboratoire. J'adresse également ma sincère gratitude à toute l'équipe et tous les employés : Dr. Aurélien Blanc, Pr. Jean-Marc Weibel, Dr. Victor Mamane.

J'aimerais mentionner spécialement ma directrice de thèse officieuse, mais qui m'a encadrée au quotidien, Dr. Valérie Bénéteau. Je me sentais absolument à l'aise grâce à elle pendant toute cette période difficile qu'est la vie d'une étudiante en doctorat. De par son propre exemple, Valérie Bénéteau m'a démontré comment résoudre des casse-têtes chimiques, quelles méthodes utiliser pour obtenir un travail efficace, autant avec la littérature qu'avec les expériences. Mille « merci » pour votre travail, votre patience et le cœur que vous mettez dans l'encadrement de chaque étudiant.

Merci beaucoup à Dr. Stefan Chassaing pour votre présence pendant ma mi-thèse en tant que membre du jury. Vos recommandations et vos remarques, votre perspective extérieure ont fait progresser mes recherches. Je suis impressionnée par votre capacité de travail et j'aimerais vraiment que les gens soient aussi ravis en recevant mes mails que j'étais heureuse de voir les vôtres dans ma boîte de réception.

Je suis reconnaissante au Professeur Marcelo Maciel Pereira du laboratoire de Rio de Janeiro pour vos connaissances et conseils exceptionnels, votre énergie, votre esprit, pour votre présence à ma mi-thèse et vos mots « j'ai bien aimé, merci » après la présentation et la session de questions. Le soleil du Brésil est toujours avec vous, peu importe où vous êtes.

J'aimerais ensuite dire quelques mots de gratitude au professeur Qiang Wang de l'Université Forestière de Pékin. Merci pour les excellentes conditions de vie et de travail à Pékin dont j'ai pu profiter et pour la possibilité de réaliser le travail de l'adsorption de toluène sur les zéolithes que vous m'avez donnée.

J'aimerais également mentionner tous les gens qui ont apporté une contribution importante dans mon travail :

- Dr. Ksenia Parkhomenko, je vous admire et je vous remercie pour la formation théorique et pratique à la méthode BET. Merci pour votre aide à plusieurs reprises, votre sentiment chaleureux à mon égard et votre soutien moral permanent.

- Thierry Roméro, un excellent spécialiste dans le domaine du SEM, je vous remercie pour votre travail minutieux avec mes nombreux échantillons, votre vitesse de travail et votre caractère très doux.

- Le service de RMN de la faculté de Chimie de Strasbourg, et particulièrement Bruno Vincent pour l'attention soignée apportée à chaque analyse malgré les très petites quantités de matière parfois. Et, bien sûr, pour sa capacité à comprendre mon français.

J'aimerais évidemment mentionner les amis et collègues que j'ai rencontrés durant mes années d'études en France. Chacun d'entre vous est un vrai travailleur acharné, et une trouvaille particulière de notre groupe scientifique. Je souhaite à chacun de vous un avenir radieux et rempli de succès ! Thomas, Robin, Weiss, Romain Pertschi, Fatih Sirindil, Hugo Loidon.

Solène Miaskiewicz, ou la fille avec qui je vais toujours associer la France. Moderne, déterminée, se précipitant sur les vagues de la vie sur le navire solide de la ténacité. Merci pour la Suisse et pour toi-même, pour tous les mots de soutien que tu m'envoies de différents endroits de la planète.

Pit Losch, le plus intelligent et le plus aimable des jeunes chercheurs, je te remercie pour m'avoir appris certaines méthodes de travail avec les zéolithes et pour ta thèse qui m'a aidée à réaliser mes analyses après ton départ de Strasbourg. Tu es un excellent spécialiste de zéolithes. Merci pour Luxembourg et Saint-Pétersbourg. Je n'arrête pas de rire de ta phrase « c'est la mafia russe ».

Elisa Silva Gomes, je te suis reconnaissante pour ton aide à m'adapter pendant mes premiers mois en France. Je suis ravie de t'avoir rencontrée et, bien-sûr, merci d'avoir trouvé la possibilité de réaliser nos analyses XRF à Paris.

Rogéria Amaral, merci à toi, chérie, pour le travail côte à côte dans le même bureau. C'était le temps où je ne connaissais pas la solitude. Je peux encore reconnaître ton parfum dans la foule, mais je ne sais toujours pas son nom. Je te remercie pour les innombrables heures de discussion, pour la lutte contre un équipement hors service, pour un mois entier à Pékin et des pique-niques au bord de la rivière (au bord de l'Ill) de Strasbourg.

En général, on consacre toujours le moins de lignes aux plus proches.

Merci, maman, de ta foi en moi et la possibilité de réaliser mon rêve.
Merci, papi, de m'avoir parlé des moteurs au lieu de contes populaires.

Merci à ma nouvelle famille : Maksim, Ludmila, Valeriy, Oksana Saenko.
Et la plus joyeuse salutation à mes camarades : Yaroslav, Igor, Asya, Irina, Olya.

RÉSUMÉ EN FRANÇAIS

INTRODUCTION GENERALE

La coumarine a été isolée à l'état naturel en 1820. Depuis, les scientifiques ont isolé et caractérisé plus de 1 400 coumarines naturelles et élaboré plusieurs méthodes de synthèse pour cette famille de composés naturels[1]. L'engouement pour cette famille de composés est également dû à leur potentiel biologique, des activités antibactériennes, antimalaria, antitumorales, anti-VIH ayant notamment été établies. De plus, les coumarines sont aussi utilisées en tant que filtres ultraviolet grâce à leurs propriétés d'absorption. Grâce à ce vaste champ d'applications, nous avons décidé de mettre au point de nouvelles méthodes pour synthétiser ce squelette organique d'intérêt.

Le but principal de notre recherche repose sur le développement de nouvelles méthodes pour la préparation de dérivés de coumarines et de thiocoumarines **2** à partir de dérivés acétyléniques **1** (**Schéma 1**).

Deux stratégies

Catalyse hétérogène avec des zéolithes acides

Catalyse homogène avec un complexe de platine

Zéolithe Y

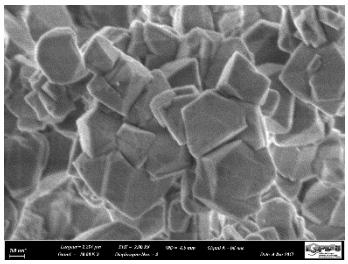

Zéolithe USY

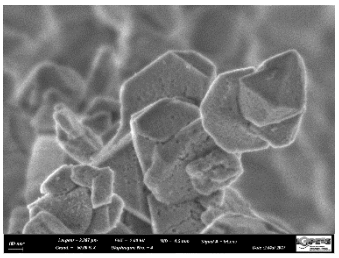

Zéolithe Y – classique FAU (Y), matériaux microporeux
Zéolithe USY CBV-720 (zéolithe ultra-stable Y, commerciales achetées à la société Zeolyst, matériaux micro-mésoporeux)

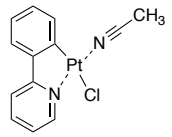

Travail réalisé en collaboration avec des collègues russes (Vasilyev et *al.*).

Schéma 1. Préparation de dérivés de coumarines et de thiocoumarines à partir de dérivés acétyléniques

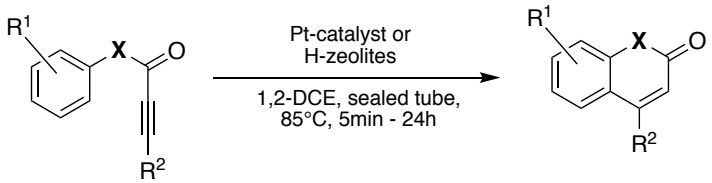

1

X = O, S

2

[1] Ryabukhin, D. S.; Vasilyev, A.V. *Russ. Chem. Rev.* **2016**, 85 (6), 637-665

PREMIERE PARTIE. Catalyse homogène avec un complexe de platine

Synthèse du complexe de platine pour la catalyse

Plusieurs catalyseurs à base de métaux de transition, notamment à base de Pd(II), [2] Au(I),[3] et Pt(IV),[4] sont décrits dans la littérature pour réaliser la transformation des esters d'aryles **1** en coumarines **2**. Les sels de Pt(II) ont en revanche été trés peu utilisés dans ce domaine. Notre attention s'est portée sur l'utilisation d'un complexe de Pt(II) (**3**, voir **Schéma 2**), normalement moins électrophile, mais dont la solubilité et la réactivité sont influencées par la nature des ligands.[5]

Nous avons ainsi montré que le complexe **3**, en combinaison avec un sel d'Ag(I), conduit efficacement à l'obtention des coumarines **2**.

Schéma 2. Étapes pour synthétiser le complexe de platine (PPy)PtCl(MeCN) **3**

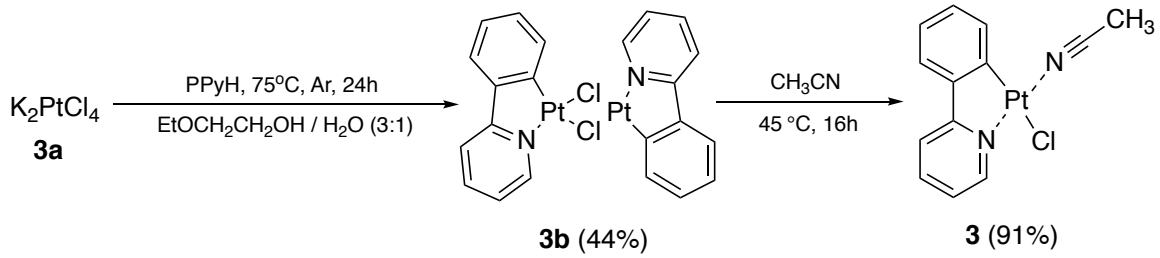

Synthèse des *O*- et *S*-esters propioniques 1 :

Les précurseurs de la cyclisation (*O*- et *S*- esters propioniques **1**) ont été obtenus par réaction entre des acides propynoïques substitués **4** et des phénols ou thiophénols substitués **5**, en présence de dicyclohexylcarbodiimide (DCC). Les rendements se sont avérés souvent bons, entre 40 et 90 %.

Schéma 3. Préparation des esters O- et S-aryl d'acides 3-arylpropynoïques **1**

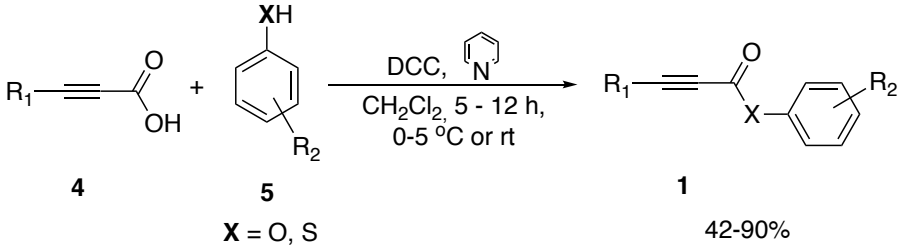

Etude de la cyclisation intramoléculaire des esters 1 en (thio)coumarines 2.

L'optimisation des conditions opératoires a conduit à l'utilisation de 5 mol % de complexe **3** avec 15 mol % de AgSbF6, dans le dichloroéthane, à 85°C. A titre comparatif, $PtCl_2$ et $PtCl_4$ se sont montrés moins performants dans la réaction modèle (voir **Tableau 1**).

Tableau 1. Preuve de l'efficacité du complexe au platine **3**

Catalyseurs	Ester	H	Conv, %	Rend[t], %	Produit
(PPy)PtCl(MeCN) + $AgSbF_6$	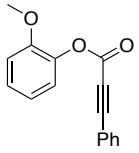	24 h	100	86	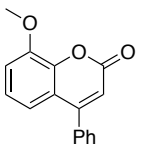
$PtCl_2$ + $AgSbF_6$		24 h	54	48	
$PtCl_4$ + $AgSbF_6$		24 h	37	30	

Le champ d'application du complexe **3** dans la cyclisation étudiée a ensuite été exploré en faisant varier la nature des substituants sur la partie phénolique (R^1) et sur la partie acétylénique (R^2) (**Schéma 4**, **Tableau 2**).

---

[2] Jia C.; Piao D.; Oymada J.; Kitamura T.; Fujiwara Y. *J. Org. Chem.* 2000, 65, 7516.
[3] Menon R.S.; Findlay A.D.; Bissember A.C.; Banwell M.C. *J. Org. Chem.* 2009, 74, 8901
[4] Pastine, S. J.; Youn, S. W.; Sames, D. *Org. Lett.* 2003, 5(7), 1055-1058
[5] Fuerstner, A.; Davies, P. W. *Angew. Chem. Int. Ed.* 2007, 46, 3410 – 3449

Schéma 4. Synthèse des coumarines **2a-2l**

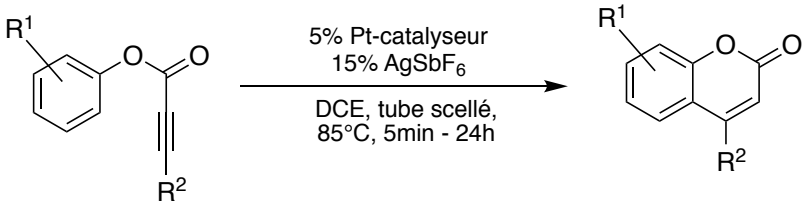

Tableau 2. Comparaison de l'effet des substituants

1	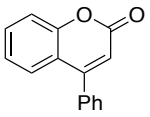	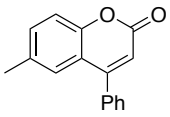	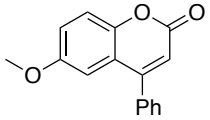	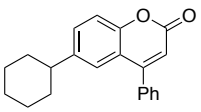	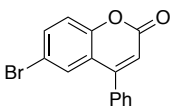	5-24h
	2a, 54%	2b, 89%	2c, 84%	2d, 72%	2e, 25%	
2	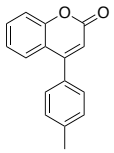	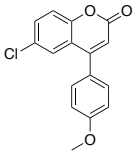	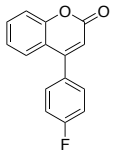			10-24h
	2f, 59%	2g, 50%	2h, 50%			
3	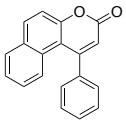	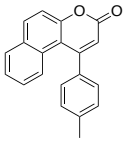	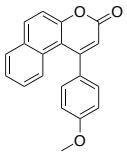	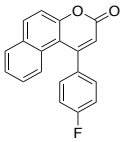		5-45 min
	2i, 99%	2j, 74%	2k, 99%	2l, 99%		

Conformément au mécanisme supposé, et au vu des résultats du **Tableau 2**, il apparait qu'un substituant électrodonneur sur le substituant phénolique est favorable à la cyclisation (**2b-d**), alors que la présence d'un brome conduit au produit de cyclisation avec un faible rendement de 25% (**2e**). La nature électronique du substituant sur le phényle acétylénique ne semble pas influencer de façon majeure l'efficacité de la cyclisation (**2f-h**). Les meilleurs résultats ont été obtenus à partir des esters issus du 2-naphtol, avec des rendements en coumarines parfois quantitatifs, dans des temps de réaction très courts (**2i-l**).

Conclusion de la première partie.

Un nouveau système catalytique combinant un complexe de platine et un sel d'argent a été identifié pour la transformation d'esters en coumarines. A l'aide de ce système catalytique, de bonnes conversions des dérivés acétyléniques **1**, ainsi qu'une bonne sélectivité pour les coumarines, ont été obtenues. Le complexe de Pt(II) **3** s'est avéré efficace dans la cyclisation de *O*-aryl propinoates, mais complètement inopérant au départ des analogues soufrés. Pour pallier cela, nous avons envisagé l'utilisation de zéolithes acides en tant que promoteurs dans la cyclisation étudiée.

SECONDE PARTIE. Catalyse hétérogène avec des zéolithes acides

Nous avons également décidé d'évaluer le potentiel catalytique des zéolithes pour réaliser la synthèse de coumarines à partir des précurseurs acétyléniques **1** (**Schéma 1**). Les zéolithes sont des aluminosilicates microporeux de la famille des tectosilicates. Ce sont des polymères inorganiques de silice et d'aluminium, consistant en un enchaînement de tétraèdres de SiO_4 et de AlO_4 liés entre eux par des atomes d'oxygène. [6]

[6] Flanigen, E. M.; Broach, R. W.; Wilson, S. T. *Edited by Kulprathipanja, S. Zeolites in Industrial Separation and Catalysis.* **2010**, 1-26.

Les zéolithes sont reconnues pour leur propriété en que catalyseurs acides hétérogènes. En plus de leur forte acidité, ces matériaux ont l'avantage d'être peu coûteux et thermiquement stables.[7]

Tout d'abord, afin de tester le potentiel catalytique des zéolithes pour la formation de coumarines, nous avons procédé à une première série d'expériences, visant à comparer l'efficacité de la zéolithe FAU avec l'efficacité de divers acides forts et superacides (**Figure 1** & **Schéma 5**). Cette première série d'expériences a été réalisée avec le substrat modèle représenté sur le Schéma 5 et les meilleurs résultats ont été obtenus en présence de la zéolithe (**Figure 1**).

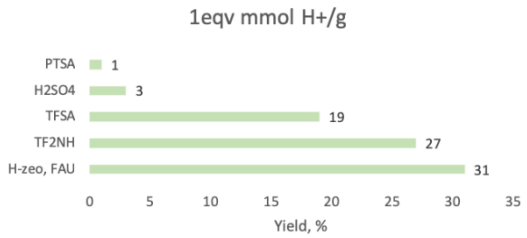

Figure 1. Comparaison de l'efficacité des zéolithes avec les (super)acides

Schéma 5. Comparaison de l'efficacité de la zéolithe avec divers acides forts et superacides

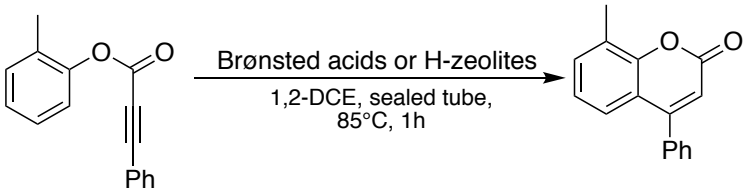

Dans un second temps, nous avons étudié différents types de zéolithes (MFI, MOR, BEA, FAU) et comparé leur efficacité. Parmi les zéolithes microporeuses ainsi évaluées, nous avons retenu les zéolithes Y (FAU) qui se sont avérées les plus efficaces (**Figure 2**). Afin d'optimiser cette transformation et comme la microporosité peut empêcher la diffusion efficace de larges molécules organiques à l'intérieur de la zéolithe, nous nous sommes d'une part tournés vers un analogue commercial de zéolithe micro-mésoporeuse et d'autre part, nous avons réalisé des modifications sur la zéolithe microporeuse « parente ».

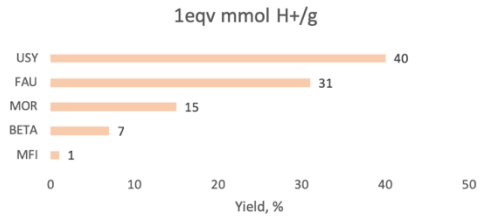

Figure 2. Comparaison de l'efficacité de divers types de zéolithes

Cette étude nous a permis d'identifier les zéolithes USY comme meilleurs catalyseurs pour la réaction de cyclisation intramoléculaire souhaitée. Toujours dans un souci d'optimisation, divers paramètres du matériau, dont son acidité, l'effet de l'eau adsorbée, son ratio Si/Al, l'influence de la mésoporosité, ont également été examinés quant à leurs effets sur le rendement de coumarines et thiocoumarines. A l'aide des conditions optimales, nous avons pu obtenir une large variété de coumarines et thiocoumarines, dont certaines sont tout-à-fait originales. Les résultats principaux sont résumés dans le **Tableau 2**.

Schéma 6. Cyclisation de propynoates/propynethiolates d'aryle en coumarines/thiocoumarines à l'aide de zéolithes.

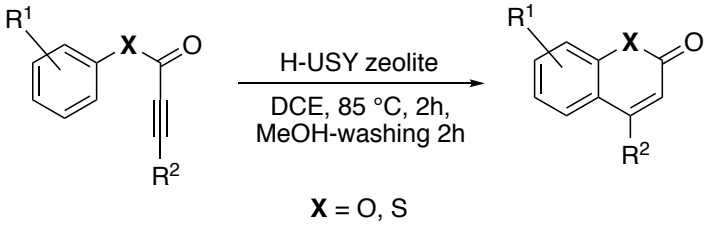

[7] Chassaing, S.; Beneteau, V.; Louis, B.; Pale, P. *Curr. Org. Chem.* **2017**, 21(9), 779-793.

Tableau 3. Cyclisation d'aryl propynoates ou propynethioates en coumarines ou thiocoumarines catalysée par la zéolite CBV-720.

Coumarines				Thiocoumarines			
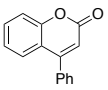	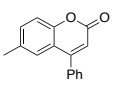	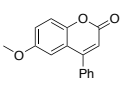	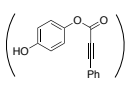	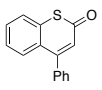	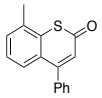	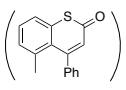	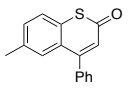
2^{a} 82%	2^{b} 44%	2^{c} 60%	$2^{c'}$20%	2^{k} 84%	2^{l} 0%	$2^{l'}$40%	2^{n} 99%
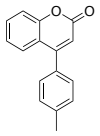	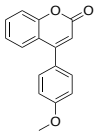	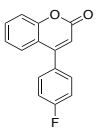	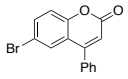	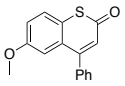	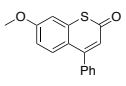	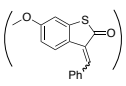	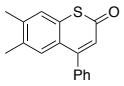
2^{e} 80%	2^{f} 88%	2^{g} 73%	2^{d} 84%	2^{o} 90%	2^{p} 24%	$2^{p'}$ 8%	2^{m} 99% (1/0.45)
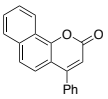	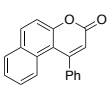			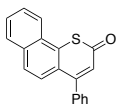	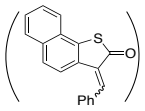	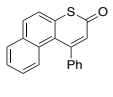	
2^{h} 28%	2^{i} 65%			2^{q} 33%	$2^{q'}$ 5%	2^{r} 95%	

Au regard de ces résultats, l'influence de l'effet électronique des substituants présents sur la partie (thio)phénolique ou sur le phényle porté par la triple liaison carbone-carbone ne semble pas prépondérante. Dans la moitié des cas, des rendements en (thio)coumarine supérieurs à 80% ont été obtenus (**2a**, **2d-f**, **2k**, **2m-o**, **2r**). Dans l'autre moitié des cas, des rendements plus modestes ont été constatés, essentiellement pour 3 raisons : une conversion en réactif incomplète, l'apparition de produits secondaires (**2c'**, **2p'**, **2q', 2l'**), ou une perte de matière organique à l'intérieur du matériau (**2b**, **2l**, **2p**, **2h**, **2q**) entraînant un bilan de masse déficient.

Conclusion de la seconde partie.

Grâce à cette étude, nous avons pu montrer que les zéolithes sont des catalyseurs acides efficaces pour la cyclisation intramoléculaire de propynoates d'aryle en coumarines. L'utilisation d'un catalyseur zéolithique est compatible avec les réactifs soufrés, puisque des thiocoumarines (très peu décrites dans la littérature[8]) ont pu être obtenues avec de bons rendements. De plus, il a été montré que la zéolithe pouvait être facilement récupérée par simple filtration et réutilisée jusqu'à 5 fois sans perte d'activité catalytique.

Conclusion générale

Les résultats des travaux entrepris dans le cadre de cette thèse, par catalyse homogène avec un complexe de platine et en parallèle par catalyse hétérogène avec des zéolithes acides, ont permis d'identifier des conditions pour la cyclisation de *O*- et *S*-aryl propinoates en coumarines et thiocoumarines.

Alors que le complexe de Pt(II) 3 s'est avéré performant pour la cyclisation de O-aryl propinoates en coumarines, les zéolithes apparaissent comme des catalyseurs acides efficaces pour l'accès non seulement aux coumarines, mais aussi aux thiocoumarines très peu décrites dans la littérature.

L'ensemble de ces résultats fait l'objet de deux manuscrits qui seront très prochainement soumis pour publication. L'un est intitulé «Zeolite-promoted synthesis of coumarins and thiocoumarins», l'autres «Intramolecular cyclization of aryl 3-arylpropynoates into 4-arylcoumarins catalyzed by platinacycle complexes».

[8] Ryabukhin, D. S.; Vasilyev, A. V.; Vyazmin, S. Yu. *Russian Chemical Bulletin*. **2012**, 61(4), 843-846.

Table of contents

GENERAL INTRODUCTION

1. COUMARINS, THIOCOUMARINS.

Coumarins (2H-1-benzopyran-2-one or 2H-chromen-2-one) are aromatic organic chemical compounds, made of fused benzene and α-pyrone rings. These compounds can be also considered as a subclass of lactones.

Simple coumarin was first extracted independently by Vogel and Guibourt in 1820 from the tonka seeds of the tree *Dipteryx odorata*, common in Central and South America (**Fig. 1**). Local people call this tree «coumarou», hence the name. [9] They used these aromatic seeds as an amulet against evil spirits and food additives.

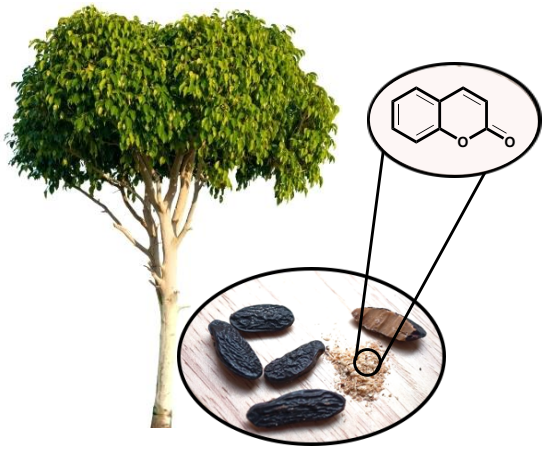

Figure 1. *Dipteryx odorata* tree
Tonka seeds

Historically, the first use of simple coumarin was in perfumery. Interestingly its smell varies along different concentrations from new-mown hay to vanilla, nutmeg, cinnamon, almond. On this base, the House of Houbigant created the «Fougère Royale» perfume in 1882. Unbelievably, this perfume can still be purchased today. From that day forward, coumarins were widely used as an aroma in perfumery, cosmetics and as additives in tobacco and alcohol.

Since the 19th century, coumarins have become a huge class of natural products, because scientists extracted more than 1300 natural coumarins from plants, bacteria, and fungi. [10] In nature, coumarins are secondary metabolites and often play protective functions in inhibiting various biological processes. As a result, humans use these substances as biologically active compounds for pharmaceuticals and medicine. Based on their chemical structure, coumarins can be divided into several subgroups according to their substituent nature, and each type exhibit different biological activities. (**Fig. 2**).

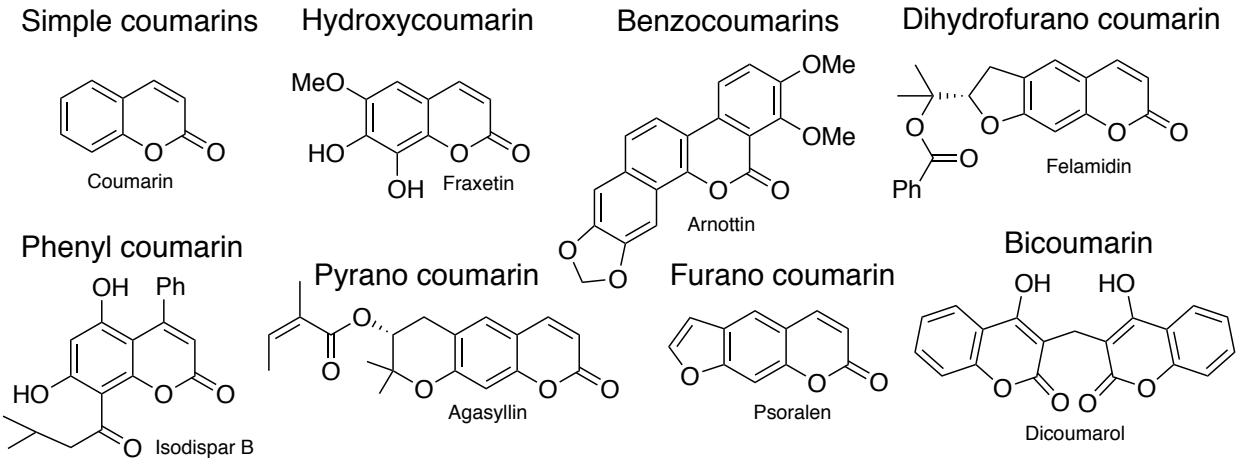

Figure 2: Subgroups of coumarins according to their substituent nature.

[9] Sardari, S.; Nishibe, S.; Daneshtalab, M. *Stud. Nat. Prod. Chem.* **2000**, 23, 335-393.
[10] Venugopala, K. N.; Rashmi, V.; Odhav, B. *BioMed Res. Int.* **2013**, 963248, 14 pp.

Overall, coumarins exhibit:

- pharmaceuticals and medicinal activities, for example, antibacterial (Agasyllin and Felamidin - anti-TB), antiviral - HIV (inophyllums and calanolides), treatment of various skin diseases (Psoralen); anticoagulant (Dicoumarol); anti-inflammatory (coumarin, Esculetin); antifungal, antioxidant (Esculetin); they act as selective enzyme inhibitors; they are able to selectively interact with targets helping in the treatment of diseases such as Alzheimer's and Parkinson's diseases [11]
- optical properties with, for example, application as organic light-emitting diode (OLED) [12]
- interest in photochemistry and photobiology, due to their fluorescence properties. They can act as fluorescent sensors or tags or as optical control of biochemical reactions [13]

In contrast to coumarins, thiocoumarins can not be found in nature. Thiocoumarins were first described by A. Clayton and W. Godden in 1912. [14] This class is much less represented than coumarins, but finds application in similar areas like:

- inhibition of cell adhesion molecules (**Fig. 3a**) [15] or inhibitors of the zinc metalloenzyme carbonic anhydrase, [16] an enzyme that maintains acid-base balance in the body, transporting CO_2 (**Fig. 3b**); antimicrobial and antifungal activities, for example towards respectively (*Staphylococcus aureus, Escherichia coli*) and as (*Aspergillus fumigatus, Candida albicans/glabrata*) (**Fig. 3d**). [17]
- in signaling supramolecular systems: thiocoumarins exhibits chemodosimetric behavior toward Hg^{2+}, [18] Au^{3+} [19]. Upon complexation with such ions, the compound is converted to a coumarin derivative by desulfurization, which changes the color of the complex (**Fig. 3c**)

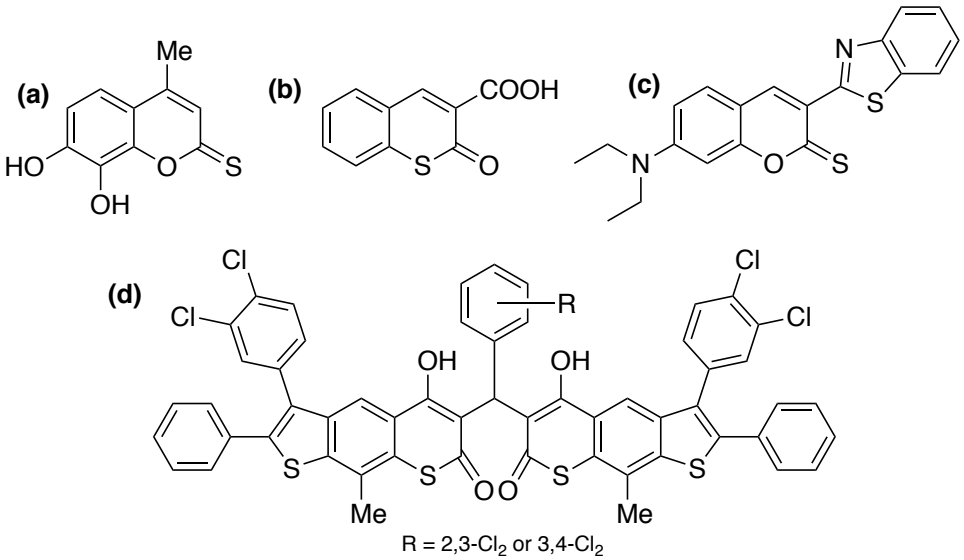

Figure 3: Some examples of thiocoumarins which have found applications in therapeutic (**a**, **b**, **d**) or signaling supramolecular systems (**c**).

---

[11] Stefanachi A., Leonetti F., Pisani F., Catto M., Carotti A. *Molecules* **2018**, 23 (2), 250/1-250/34.
[12] Trenor S. R., Shultz A. R., Love B. J., Long T. E. *Chem. Rev*. **2004**, 104 (6), 3059–3077.
[13] a) Chen, X.; Wang, F.; Hyun, J. Y.; Wei, T.; Qiang, J.; Ren, X.; Shin, I. *Chem. Soc. Rev.* **2016**, 45 (10), 2976-3016. b) Lee, M. H.; Sharma, A.; Chang, M. J.; Lee, J.; Son, S.; Sessler, J. L.; Kang, C.; *Chem. Soc. Rev.* **2018**, 47(1), 28-52.
[14] Clayton A., Godden W., J. *Chem. Soc. Trans.* **1912**, 101, 210-216.
[15] Kayal, G.; Jain, K.; Malviya, S.; Kharia, A. *Int J. Pharm. Sci. Res.* **2014**, 5 (9), 3577-3583
[16] Maresca, A.; Temperini, C.; Pochet, L.; Masereel, B.; Scozzafava, A. *J. Med. Chem.* **2010**, 53(1), 335-344.
[17] Reddy, P. V. K.; Kumar, P. N.; Chandramouli, G. V. P. *J. Heterocycl. Chem*. **2005**, 42 (2), 283-286.
[18] Choi, M. G.; Kim, Y. H.; Namgoong, J. E.; Chang, S.-K. *Chem Commun (Camb)* **2009**, 24, 3560-3562.
[19] Park J. E., Choi M. G., Chang S. K. *Inorg. Chem.* **2012**, 51 (5), 2880-2884.

2. CONTEXT

I was interested and impressed by the wide area of applications and the large potential of coumarins and thiocoumarins. In the process of thorough work with publications concerning syntheses or uses of coumarins, I have often seen the expression «unceasing» or «increasing» interest. To check that this expression was not inflated, I turned to statistics, and analyzed selected reviews data related to the coumarins's studies for the last 25 years, according to the ACS website. Thiocoumarins were not considered in these statistics, as they are poorly represented in the literature. The pie chart on the right (**Fig. 4a**) shows the most common topics of these reviews.

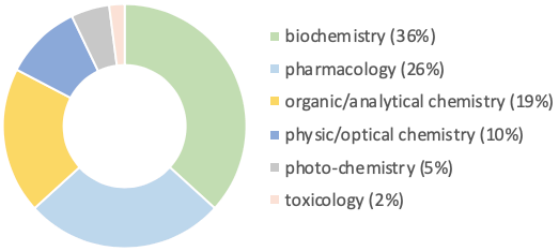

Figure 4a: The percentage of articles about coumarins on selected subjects from 1992 to 2017

The graph (**Fig. 4b**) clearly shows, that between 1992 and 2008 a maximum of 12 reviews per year dealt with the coumarin subject. Since 2008, the number of reviews has increased by a factor of almost five/ OR increased five times, and in 2017 reached 59.

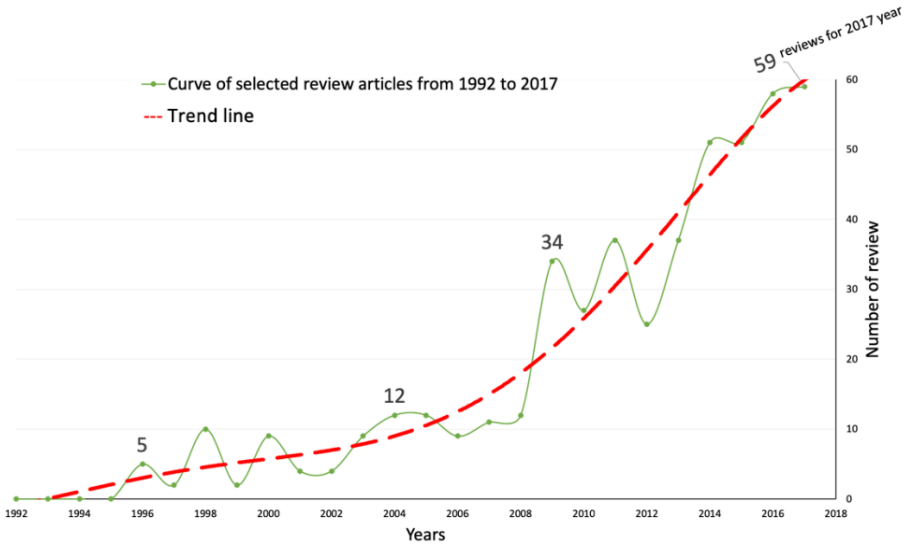

Figure 4b: Schematic representation of selected review articles from 1992 to 2017, according to the ACS website, related to the coumarins and their studies/applications in most common fields [20]

The most important in our view is the trend line. The graph 3a clearly reveals that now studies of coumarin compounds are highly relevant. Thus, based on the wide range of applications and modern technologies in which coumarins have proven to be effective, research aimed at developing new access to the synthesis of coumarins and their little-known thiocoumarin analogs is currently very relevant and important.

3. OBJECTIVE OF THE STUDY

The main goal of our study relies on the development of new, but very simple methods for preparing coumarin and thiocoumarin derivatives **2.** We indeed aim to start from the readily available acetylenic ester or thioester compounds **1** (**Scheme 1**). The work presented in this thesis, is divided into the development of two strategies to reach this goal:

---

[20] https://pubs.acs.org/.
Criteria for charting: search line – coumarin; manuscript type – reviews; subjects - biochemistry (general/microbial/plant), pharmacology/pharmaceuticals, organic/analytical chemistry, physical/electron/optical chemistry, radiation chemistry/photochemistry, toxicology; publication date - each year separately.

- Homogeneous catalysis with platinum complexes
- Heterogeneous catalysis over acidic zeolites

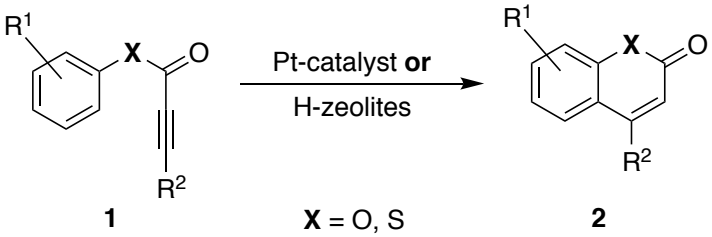

1 **X** = O, S **2**

Scheme 1: General synthesis scheme for preparing coumarin and thiocoumarin derivatives

First strategy: homogeneous catalysis with platinum complexes

Figure 5. Platinum ingot of the highest standard.

Historically, the study of metal complexes began with platinum. Alfred Werner in 1893 created the theory of complex (coordination) compounds mostly by studying ammonia platinum complexes. Later, from the beginning of the 20th century, two chemists from the USSR, Chugaev and Chernyaev, worked on the mutual influence of ligands in the complexes. [21] Platinum complexes have proven to be effective as catalysts in organic reactions such as isomerization, cyclization, oxidation. [22] However, platinum, in comparison with palladium or gold complexes, is not used extensively.

After having studied the literature on the synthesis of coumarins using platinum catalysts, we found only 3 publications in which $PtCl_2$ and $PtCl_4$ have been used. These salts are inorganic polymers and they exhibit very low solubility in organic solvents. Accordingly, only a small soluble percentage reacts. Therefore, we found interesting to synthesize metal-organic catalysts based on platinum, more soluble and more efficient, than Pt chlorides and test them for reactions of intramolecular cyclization of *O*-or *S*-aryl esters of 3-arylpropynoic acids into coumarins.

Second strategy: Heterogeneous catalysis over acidic zeolites

The choice of the second strategy is based on the advantages offered by heterogeneous catalysis in general. For example, they can easily separated from the reaction mixtur, and they can be reused several times.

In the family of heterogeneous catalysts, zeolites occupy a special position, due to of their peculiar structures and the~~ir~~ reactivity they induce. These aluminosilicates materials contain SiO_4 and AlO_4 tetrahedra linked by oxygen atoms in their framework. Such structure creates a curve, microporous surface with interesting properties such as shape selectivity, confinement effect and high acidity.

With the latter, zeolites exhibit interesting and useful catalytic activity. Zeolites exhibit acidities high enough to be compared to super acids and they are thus called solid superacids. These materials act as very effective catalyst in petrochemical industry inducing various highly selective transformations at large scale. More recently, they have been used in fine organic chemistry. [23]

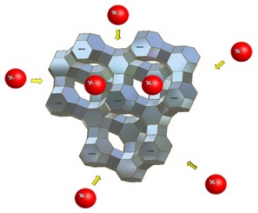

Figure 6. Depicted is a Y zeolite and molecular diffusion.

Working with these materials, we will try to comply with some principles of green chemistry in the synthesis of coumarin and thiocoumarin from *O*-or *S*-aryl esters of 3-arylpropynoic acids using acid sites in zeolite.

---

[21] Kauffman, G. B. *Platinum Metals Rev.* **1973**, 17 (4), 144-148
[22] https://ipa-news.com (The International Platinum Group Metals Association (IPA))
[23] Chassaing, S.; Beneteau, V.; Louis, B.; Pale, P. *Curr. Org. Chem.* **2017**, 21 (9), 779-793.

FIRST PART.

CHAPTER I. Literature background

1. Metal-free methods for the synthesis of coumarins and their optimization

In the literature, five main reactions have been applied for the synthesis of coumarins. They all rely on the condensation of carbonyl compounds with substituted phenols to form coumarins. These reactions were discovered between 1868 and 1926 and got the name of their discoverers: Perkin, Pechmann, Knoevenagel, Houben-Hoesch, Ponndorf (**Scheme 2**). These reactions have been well studied and extensively applied. Many reviews mention these transformations.[24]

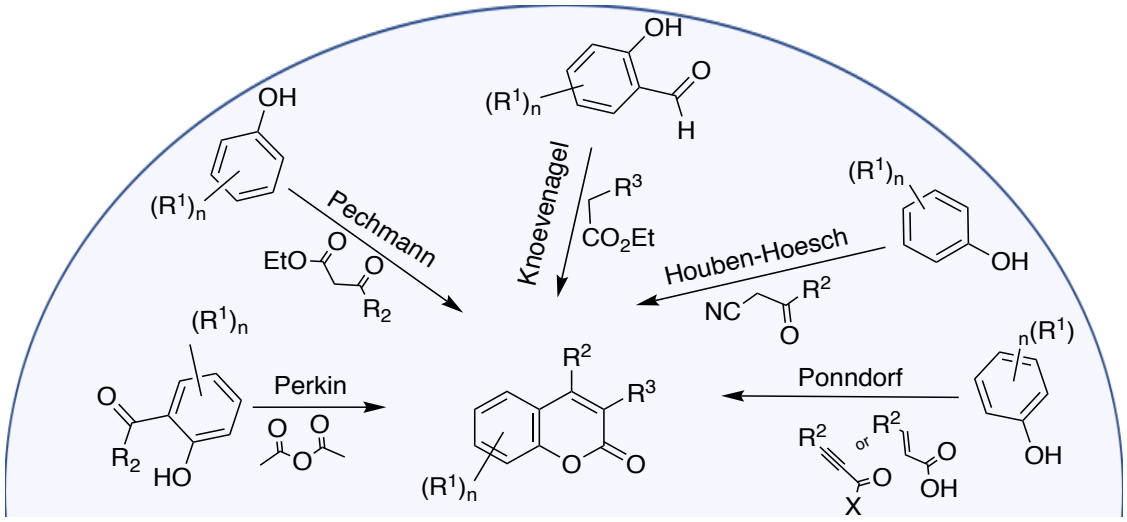

Scheme 2: Condensation of carbonyl compounds with various phenols (or derivatives) for coumarin synthesis.

The first synthesis of coumarins were described by Henry Perkin, an English chemist, in 1868. [25] This reaction was possible due to the interaction of o-hydroxybenzophenones of various structure with acetic anhydride, in the presence of sodium or potassium salt and heating.

The Pechmann reaction is characterized by the condensation of various phenols with β-ketoesters. This reaction requires the presence of mineral or strong Lewis acid. Numerous modifications of the Pechmann reaction have been reported. For examples, various catalysts could be used without or with metals ($FeCl_3$-catalysed, $NbCl_5$-catalysed). Catalytic surfaces, such as poly(4-vinylpyridine)-supported copper iodide or sulfuric acid, melamine-formaldehyde resin, ionic liquid or nanoparticles ($CuFe_2O_4$) have also been developed. More details about these methods can be found in a dedicated review. [26]

The preparation of coumarins initially proposed by Knoevenagel usually occurs from condensation of salicylaldehydes and ethyl acetoacetate or derivatives and subsequent intramolecular cyclisation in the presence of a basic catalyst. [27]

Houben-Hoesch condensation relies on reaction between substituted β-ketonitriles and phenol derivatives under the action of Lewis acid or hydrochloric acid, and a subsequent cyclisation. [16]

According to the Ponndorf method, coumarin derivatives are formed by the interaction of unsaturated carboxylic acid and phenol derivatives. [28] As for the other related reaction, this method requires the presence of a strong acid and high temperature.

---

[24] a) Garazd, M. M.; Garazd, Ya. L.; Khilya, V. P. *Chem. Nat. Compd.* **2005**, 41 (3), 245-271. b) Fedorov A. Yu., Nyuchev A. V., Beletskaya I. P. *Chem. Heterocycl. Compd.* **2012**, 1, 175-186

[25] Perkin W. H. *J. Chem. Soc.* **1868**, 21, 53–63. https://www.name-reaction.com/perkin-reaction

[26] Anuradha T.; Ramit S.; Vikas J. *Eur. J. Med. Chem.* **2015**, 101, 476-495.

[27] Salem,M.A.; Helal, M.H.; Gouda, M.A.; Ammar, Y.A.; El-Gaby, M. *Synth. Commun.* **2018**, 48 (13), 1534-1550

[28] Krajniak, E. R.; Ritchie, E.; Taylor, W. C. *Aust. J. Chem.* **1973**, 26 (4), 899-906.

2. Metal catalysis as a route to coumarin

The chemistry of transition metal complexes has found very important applications in catalysis.

United in d-block, transition elements exhibit partially filled d-orbitals, which give them a great ability to form complexes. These coordination complexes are chemical arrangements consisting of a central metal atom or ion (electron acceptor), surrounded by ligands (electron donors). The bond between the central atom and the ligands arises from the resulting donor – acceptor interactions or coordination bond. These bonds can be more or less labile, allowing ligand exchange. Furthermore, transition metals usually exhibit more than one oxidation state.

The combination of these properties allows transition metal complexes to induce numerous reactions, often under mild conditions, which can lead to useful catalytic processes.

2.1 Intermolecular reactions for the preparation of coumarins

Usually compatible with many functional groups, reactions with transition metals have been logically applied to the synthesis of coumarins. [29]

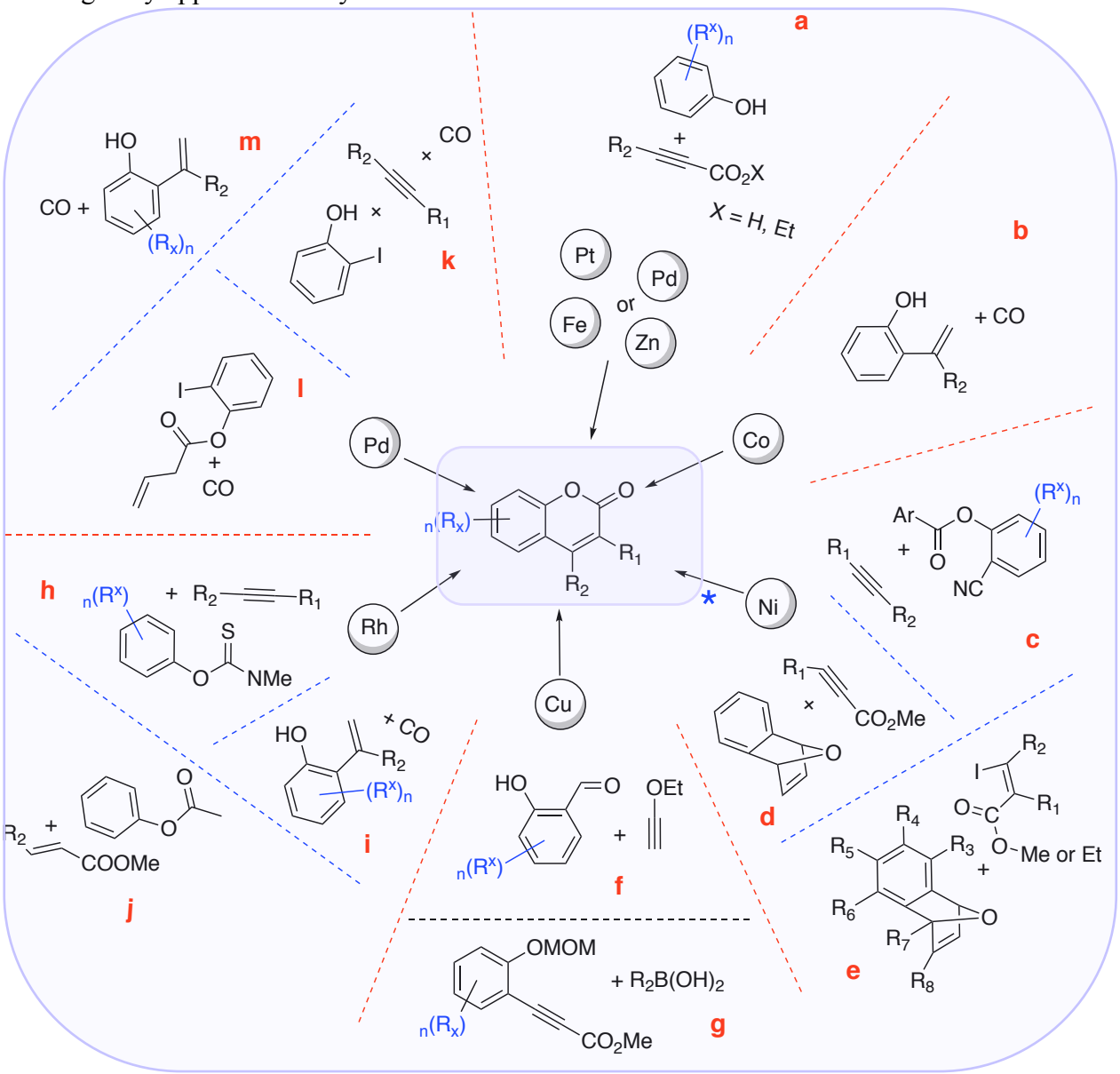

Scheme 3: Metal catalyzed intermolecular reactions for the preparation of coumarins

[29] Sharma, R. K.; Katiyar, D. *Synthesis* **2016**, 48 (15), 2303-2322.

The group of Kitamura used $FeCl_3$/AgOTf, for direct synthesis of coumarins from different phenols and substituted propiolic acids (**Scheme 3, variant a**). [30] There are two possible ways for this reaction (**Scheme 4**) : a) esterification and then intramolecular hydroarylation; b) intermolecular hydroarylation followed by cyclization. No explicit and definitive reaction mechanism was established in this work. However, the authors suggest that these two processes occur simultaneously. With a few exception, high coumarin yields were received. This method is interesting from the point of view of the development of the less popular iron-catalyzed hydroarylation of alkynes reactions.

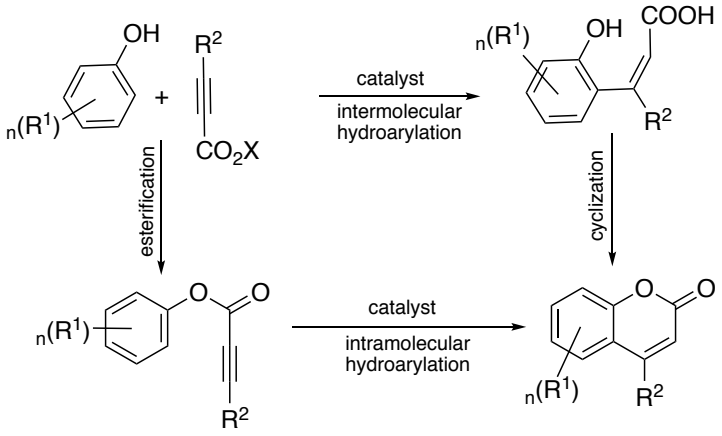

Scheme 4.

In the same year, the Costa group published research results about hydroarylation of propiolates with phenols, where zinc chloride was used as a reaction promoter (**Scheme 3, variant a**). [31] The ability to use solvent-free conditions and only 5% of the catalyst is interesting, however, the yields of naturally occurring coumarins and neoflavones depend on the nature of the phenolic substrates. Unfortunately, the mechanism of this reaction is not specified.

Oyamada and Kitamura used catalytic systems based on platinum such as $PtCl_2$/AgOTf, K_2PtCl_4/AgOTf, and K_2PtCl_4/AgOAc for the preparation of substituted coumarins from various phenols and phenylpropiolic or 2-octynoic or propiolic acids (**Scheme 3, variant a**). [32]

The authors demonstrated a possible reaction mechanism (**Scheme 5**) in which the triple bond is activated at the first stage, followed by intramolecular hydroarylation which results in hydroxy substituted cinnamic acids, and the last stage was intramolecular esterification with the formation of the final product. However, they do not exclude the possibility of an aromatic electrophilic substitution which precedes hydroarylation.

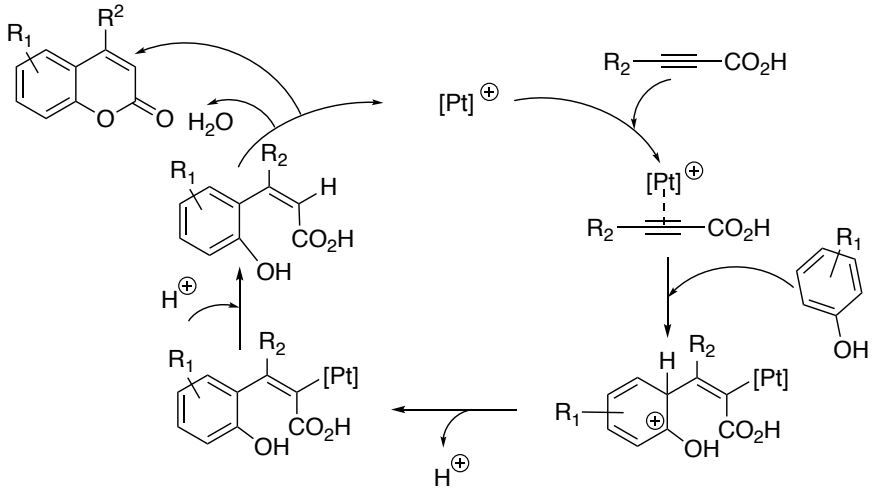

Scheme 5.

[30] Kutubi, Md. S.; Hashimoto, T.; Kitamura, T. *Synthesis* **2011**, 8, 1283-1289.
[31] Leao, R. A. C.; de Moraes, Paula de F.; Pedro, M. C. B. C.; Costa, P. R. R. *Synthesis* **2011**, 22, 3692-3696.
[32] Oyamada J., Kitamura T. *Tetrahedron*, **2006**, 62 (29), 6918-6925

All catalytic systems behaved with variable activity. Reactions even occurred with non- or de-activated phenol (not substituted or bromo-substituted), but with low yields. Among substituted propiolic acids, the highest yields were observed with phenylpropiolic acids compared to 2-octynoic or propiolic acids.

The Pd-catalyzed hydroarylation of alkynes offers an interesting alternative to process to 4-substituted coumarins (**Scheme 3, variant a**). [33] [34] Catalytic activation of C – H bonds of electron-rich phenols forms intermediates, which add to propiolates. Formic acid is used as solvent and seems to also reduce the Pd catalyst. This is a simple and decent method, which makes it possible to use moderate temperatures and produce coumarins in good to high yields.

Cobalt complexes are well known for promoting carbonylation. In this context, Wang-group synthesized coumarins from 2-vinylphenols and CO under pressure in the presence of a Co-catalyst (**Scheme 3, variant b**). [35]

The authors show possible mechanism of this reaction (**Scheme 6**). They suggest that the activation of catalyst $Cp^*Co(CO)I_2$ is possible due to the reaction with activating agents Ag_2CO_3 or $Cu(OAc)_2{}^*H_2O$. After that, ligand replacement with 2-vinylphenol occurs in activated catalyst $Cp^*Co(III)Ln$ creating intermediate **I**. The cyclometalated **III** may be produced by two different ways : *way A* – an intramolecular electrophilic attack of the conjugated alkene to $Cp^*Co(III)$, intermediate **II** followed by a base-assisted deprotonation **III**; way B – concerted metalation deprotonation. It worth noting that the authors adhere to the second way because this was confirmed by Kinetic Isotope Effect (KIE) measurements. Next, CO coordination and formation of intermediate **IV** take place. The coumarin is created due to reductive elimination. The last step in this catalytic cycle is the oxidation of Cp^*Co^I by the copper or silver salt. The main advantage of this work is the possibility of using different substrates. For example, it was possible to get 6-Cl- or 7-Br-substituted coumarins with high yields, respectively 83 % or 71 %

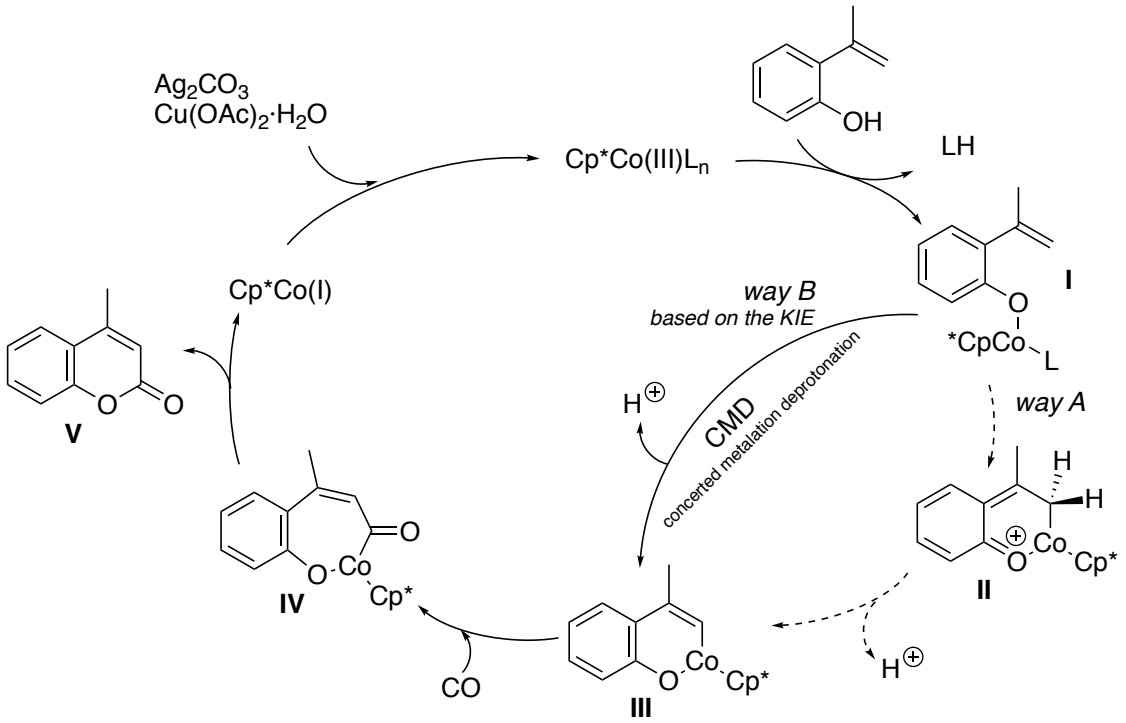

Scheme 6.

[33] Trost, B. M.; Toste, F. D. *J. Am. Chem. Soc.* **1996**, 118 (26), 6305-6306
[34] Trost, B. M.; Toste, F. D.; Greenman, K. *J. Am. Chem. Soc.* **2003**, 125 (15), 4518-4526
[35] Liu, X.-G.; Zhang, S.-S.; Jiang, C.-Yo.; Wu, J.-Q.; Li, Q.; Wang, H. *Org. Lett.* **2015**, 17 (21), 5404-5407.

Alternatively, a nickel (0) catalytic system, produced from $Ni(cod)_2$ together with $P(CH_2Ph)_3$ and methylaluminum bis(2,6-di-tert-butyl-4-methylphenoxide) (MAD), showed a good activity in the synthesis of coumarin derivatives by a intermolecular cycloaddition reaction of o-(arylcarboxy)benzonitrile and various alkynes (**Scheme 3, variant c**). [36] Within the course of this reaction, the cleavage of two sigma bonds C-CN and C-CO occurs.

Further, in 2015, the reaction mechanism has been clarified using the DFT method (**Scheme 7**). [37] According to Matsubara, at the first stage nickel (0) catalyst is coordinated with alkyne (**b**) to form **1**. The next stage is the oxidative addition of Ni-alkyne to the C-CN σ-bond of o-arylcarboxybenzonitrile (**a**), which affords intermediate **2**. After insertion of the so-formed arylnickel, the vinylnickel intermediate **3** is produced. Further isomerization creating intermediate **4** followed by β-aryl elimination and led to ~~5~~ **6**. At the last stage, reductive elimination led to the final product (**c**). The reaction requires the presence of two Al^+. First Al^+ interacts with the cyano-nitrogen atom, thus improving the oxidative addition. The second Al^+ interact with the carbonyl oxygen for a) increasing the electrophilicity of carbonyl carbon (CO) of the carbon-carbonboxybenzonitrile for C-C coupling and b) promotes the β-aryl elimination thanks to the interaction of the aluminum and carbonyl oxygen atom. [38] The yields nevertheless ranged from good to very high (70-99%).

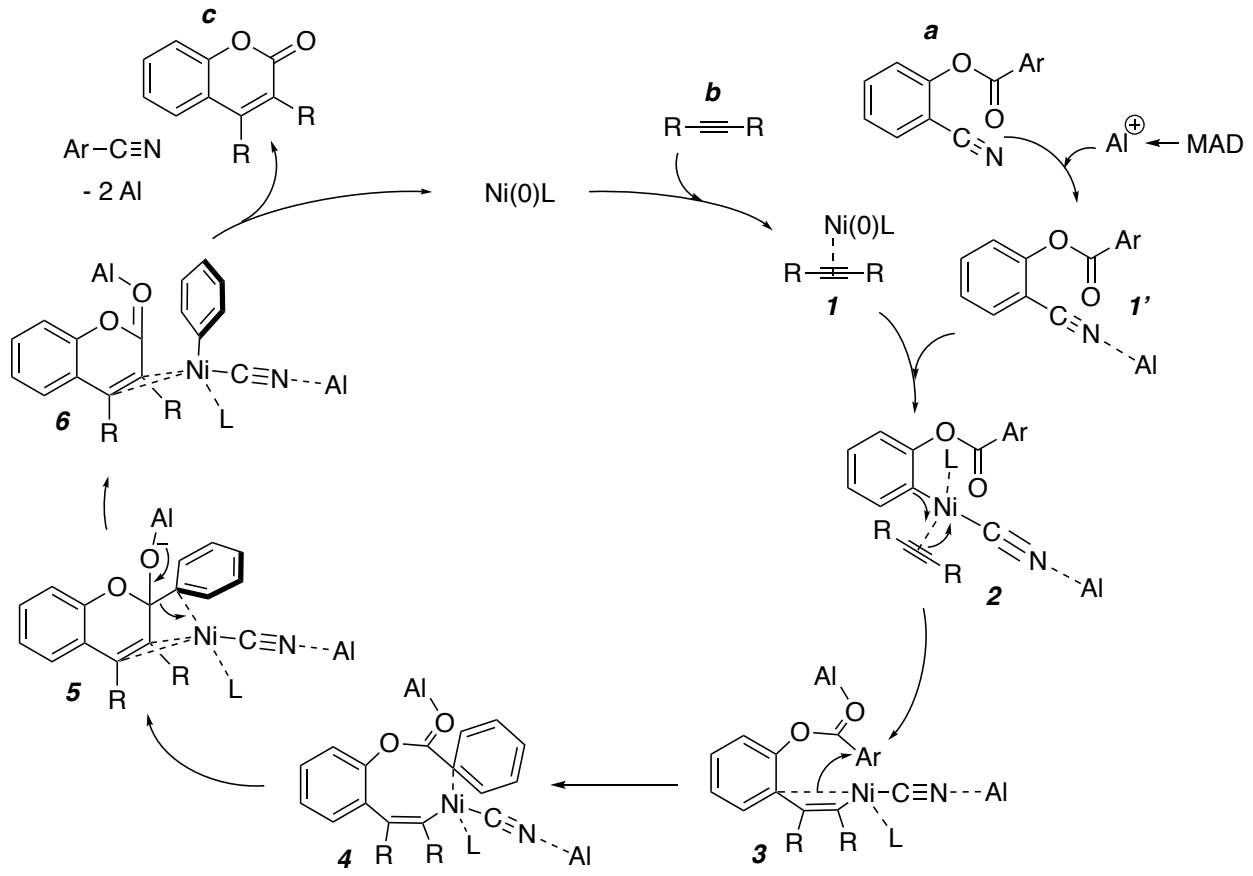

Scheme 7.

[36] Nakai, K.; Kurahashi, T.; Matsubara, S. *J. Am. Chem. Soc.* **2011**, 133 (29), 11066-11068.
[37] Kurahashi, T.; Matsubara, S. *Acc. Chem. Res.* **2015**, 48 (6), 1703-1716.
[38] Guan, W.; Sakaki, S.; Kurahashi, T.; Matsubara, S. *ACS Catal.* **2015**, 5 (1), 1-10.

Substituted benzocoumarins or annulated coumarin derivatives can be synthesized in the presence of nickel salts or complexes from oxabicyclic olefins and propiolates or iodo-substituted propenoates. [39] [40] The best catalyst for this reaction is $NiBr_2$(dppe) which is *in situ* activated by zinc powder (**Schemes 3, variant d and e)**. These methods are a good example of one-step synthesis of complex structures from oxabenzonorbornadienes. The reaction yields are however highly variable.

Surprisingly, the use of copper catalyst for obtaining coumarin is poorly represented in the literature. Nevertheless, an A3 coupling method is known, in which salicylaldehydes, ethoxyacetylene and pyrrolidine act as reagents and CuI is the catalyst for this reaction (**Scheme 3, variant f**). [41] Concerning the reaction mecanism (**Scheme 8**), the authors suppose the creation of intermediate **A** by condensation of salicylaldehyde with pyrrolidine and addition of copper ethoxyacetylide. Next follows cycloisomerization with the phenoxy group, which provides intermediate **B**. Acidic hydrolysis finally led to form a coumarin. It is useful to mention the short reaction time and the good to high yields (50-84%), especially for halogenated salicylaldehydes, for which yields are around 60-65%.

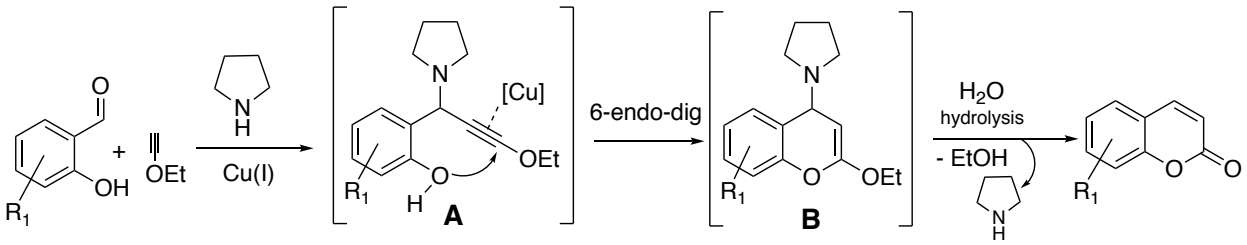

Scheme 8.

Another example of Cu catalyst uses for obtaining coumarins is the hydroarylation of propiolate substrates with arylboronic acids and subsequent cyclization (**Scheme 3, variant g**). [42] Performed in the presence of a catalytic amount of CuOAc in MeOH at rt, this reaction gave high yields, around 75-90 %. Methyl phenylpropiolates having a MOM (methoxymethyl) protection suppress adverse reactions (methoxylation) and after reaction can be easily removed using HCl. Interestingly, electron-donating or electron-withdrawing groups of arylboronic acids had almost no impact on the yield of coumarins. This method of synthesis was applied to the synthesis of some naturally occurring neoflavones in good yields.

Under the action of Rh catalyst, aryl thiocarbamates containing internal alkynes were condensed to a series of 3,4-disubstituted coumarins with variable yields (**Scheme 3, variant h**).[43] This reaction requires both silver and copper salts. An elegant mechanism has been proposed (**Scheme 9**).

AgOTf activates the catalyst $[Cp^*RhCl_2]_2$ *in situ* by forming $[Cp^*Rh^{III}](OTf)_2$ (**I**). After coordination to the thiocarbamate (a), ortho C-H activation occurs to form rhodacyclic complex (**II**). Then the authors propose 2 pathways. By *pathway A* - desulfurization leading to intermediate (**III**) and insertion of the alkyne (**b**) form a seven-membered Rh intermediate (**V**). P*athway B* involves first alkyne insertion (**b**), which produces the eight-membered ring (**IV**) and then, desulfurization and formation of (**V**). Reductive elimination releases the iminium salt (**VI**) and $[Cp^*Rh^{I}]$ (**VII**). Nucleophilic attack of the acetate from the copper salt to the Iminium salt (**VII**)

[39] Rayabarapu, D. K.; Sambaiah, T.; Cheng, C.-H. *Angew. Chem. Int. Ed*. **2001**, 40 (7), 1286-1288
[40] Rayabarapu, D. K.; Shukla, P.; Cheng, C.-H. *Org. Lett.* **2003**, 5 (25), 4903-4906
[41] Reddy, M. S.; Thirupathi, N.; Haribabu, M. Beilstein J. *Org. Chem.* **2013**, 9, 180-184
[42] Yamamoto, Y.; Kirai, N. *Org. Lett.* **2008**, 10 (24), 5513-5516.
[43] Zhao, Y.; Han, F.; Yang, L.; Xia, C. *Org. Lett.* **2015**, 17 (6), 1477-1480

induces C-N bond cleavage, which results in coumarin (**c**) and dimethylacetamide. The catalytic cycle is then closed by oxidation of [Cp*Rh^{I}] (**VII**) by Cu^{II}/HOTf.

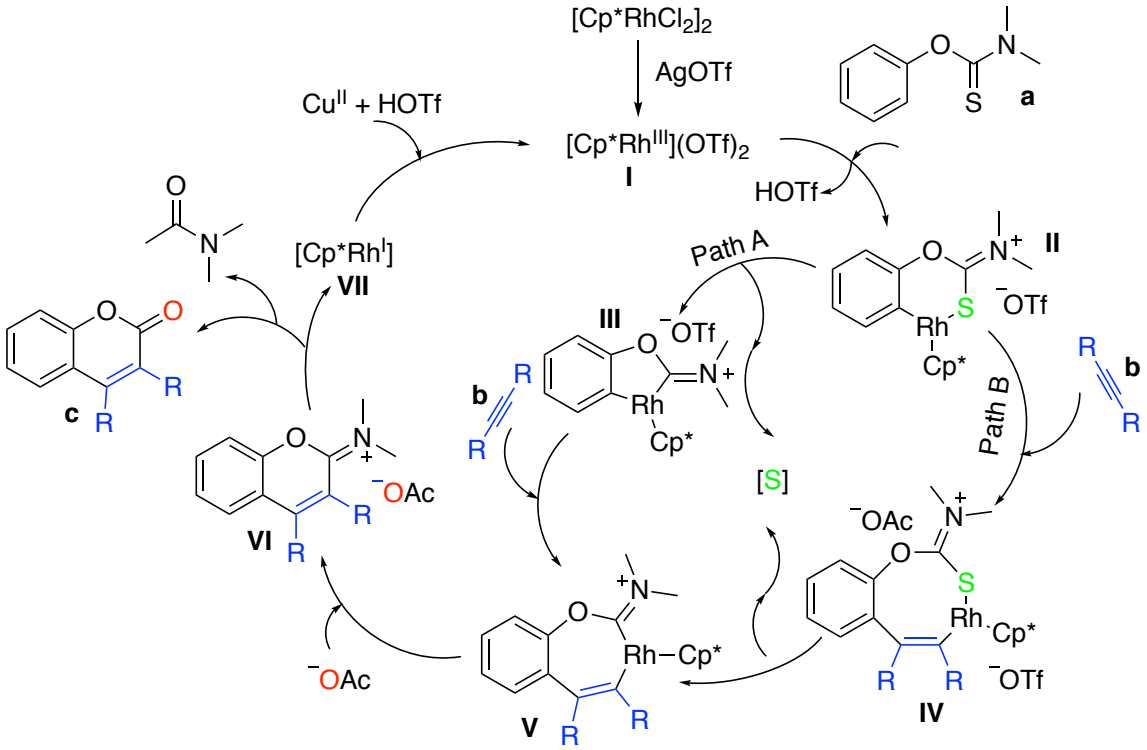

Scheme 9.

Rh is also able to promote cyclocarbonylation reactions of 2-vinylphenols producing coumarins (**Scheme 3, variant i**).[44] The catalytic system for this transformation is [Cp*RhCl$_2$]$_2$. A stoechiometric amount of Cu(OAc)$_2$·H$_2$O is also required. This method allows using readily available starting materials (2-vinylphenols and carbon monoxide) to assemble coumarins in a straightforward way with yields ranging from 69 to 85%.

Another variation in the use of a rhodium catalyst can be found in the synthesis of coumarins from phenolic acetates and acrylates by C−H bond activation (**Scheme 3, variant j**). In this case, the catalyst [Rh$_2$(OAc)$_4$] was activated by formic acid.[45] It is interesting to note that a wide range of substituted phenolic acetates was chosen as substrates, and in the case of a negative electronic effect on the phenolic ring, the yields of the final product did not fall below 64%

A very large number of works have been devoted to the use of palladium catalyst for the synthesis of coumarins. In my dissertation I present only a few of the most remarkable works.

Carbonylation is again one of the possibilities to obtain coumarin derivatives. Iodophenyl 3-butenoate reacts with carbon monoxide at atmospheric pressure In the presence of Pd(PPh$_3$)$_4$ and potassium butyrate (**Scheme 3, variant l**).[46] As a resultof this carbonylative coupling, 4-methylcoumarin were obtained with good yields. However, these reactions present some disadvantages: double-bond isomerization, formation of by-products (due to the use of anisole as a solvent), limited substrate scope.

Carbonylation of o-iodophenols with unsymmetrical alkynes could also be achieved, under the action of Pd (II) catalyst and CO in a mixture of base and DMF (**Scheme 3, variant k**).[47]

---

[44] Seoane, A.; Casanova, N.; Quinones, N.; Mascarenas, J. L.; Gulias, M. *J. Am. Chem. Soc.* **2014**, 136 (3), 834-837.
[45] Gadakh, S. K.; Dey, S.; Sudalai, A. *J. Org. Chem.* **2015**, 80 (22), 11544-11550
[46] Catellani, M.; Chiusoli, G. P.; Fagnola, M. C.; Solari, G. *Tetrahedron Lett.* **1994**, 35 (32), 5919-22
[47] a) Kadnikov, D. V.; Larock, R. C. *Org. Lett.* **2000**, 2 (23), 3643-3646. b) Kadnikov, D. V.; Larock, R. C. *J. Org. Chem.* **2003**, 68 (24), 9423-9432

However, this reaction led to the formation of a mixture of coumarin regioisomers. It has been observed that the size of the alkyne groups affects the regioselectivity. However, the total yield of coumarins ranges from low to medium high, probably because reactions took place at high temperatures and for a long time.

According to the authors, the mechanism of this reaction is as follows (**Scheme 10**). $Pd(OAc)_2$ is reduced to a Pd(0) complex due to the reducing effect of CO. The next step is the formation of the arylpalladium complex (**I**), due to the oxidative addition of 2-iodophenol to Pd(0). As a result of dissociation of one of the ligands of the complex, alkyne occupies the vacant position (**II**). As a result of internal rebuilding, the vinyl-palladium intermediate (**III**) is formed. Introduction of CO led to an acylpalladium complex (**IV**). As a result of the intramolecular attack of the phenolic oxygen to the carbonyl group, the final product is formed and the catalyst is released, ready for a new cycle.

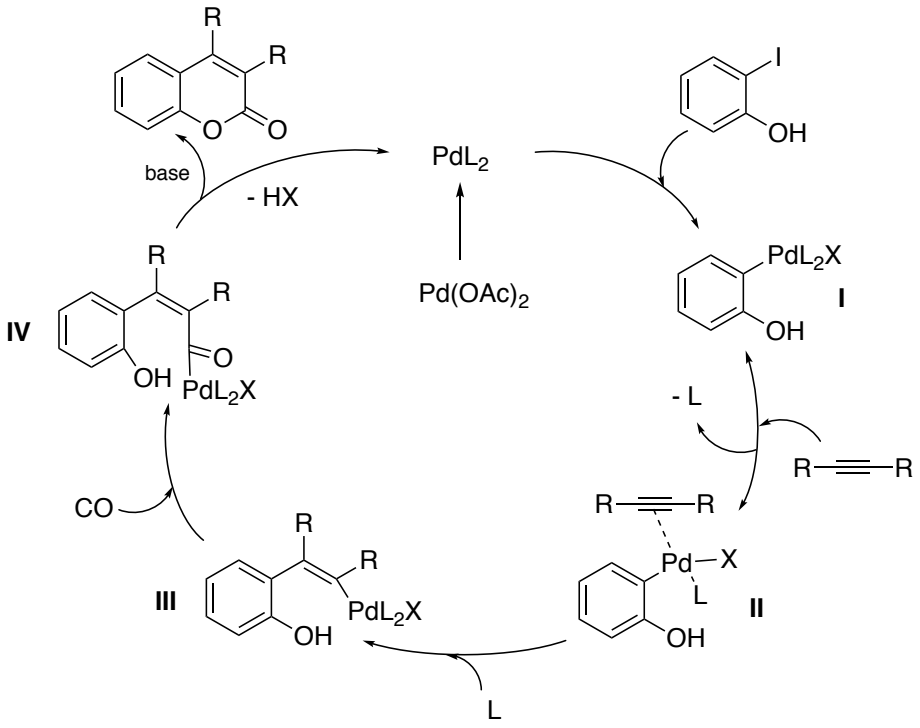

Scheme 10.

2.2. Intramolecular reactions under the action of Ru, Pd, Fe, Au, Pt complexes for the synthesis of coumarins

As seen above, various metal-catalyzed condensation-cyclization processes have been developed to produce coumarins. An interesting alternative is the direct cyclization of preformed compounds including an aryl moiety and at least one unsaturation. Two mains approaches have been developed: one based on ring-closing metathesis and the other based on the cyclization of *O*-aryl esters of propynoic acids. Both will be described here after.

The know classical ring-closing metathesis (RCM) catalyzed by ruthenium complexes have been applied to the synthesis of coumarin. The synthesis of coumarin from unsaturated aryl esters under the action of Ru complex was described by two independent groups in 2003 (**Scheme 11**). [48] [49] In both groups, unsubstituted coumarins were obtained successfully with high yields (70% or 89%). In the Grubbs group, 3,4-substituted coumarins were obtained in only 45% yield, but, in the case of coumarins substituted only at the 3 or 4 position, yields were high (74% or 80%, respectively. De Kimpe group worked with substituted aryl acrylates in the phenol ring. These experiments led to very good yields of the corresponding coumarins.

---

[48] Chatterjee, A. K.; Toste, F. D.; Goldberg, S. D.; Grubbs, R. H. *Pure Appl. Chem.* **2003**, 75 (4), 421-425.
[49] Nguyen, V. T.; Debenedetti, S.; De Kimpe, N. *Tetrahedron Lett.* **2003**, 44 (22), 4199-4201.

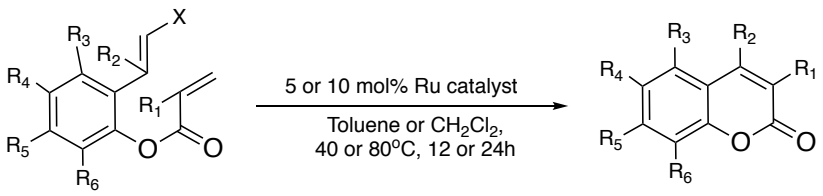

R_1 = H, Me; R_2 = H, Me; R_3 = H, OMe; R_4 = H, OMe;
R_5 = H; R_4+R_5 = O-CH_2-O; R_6 = H, OMe;
X = H or Me

Scheme 11.

The mechanism of this transformation is given below (**Scheme 12**). There are several important stages which should be noted: dissociation of a phosphine ligand (catalyst ligand replacement), formation of metalacyclobutane intermediate through [2+2] cycloaddition.

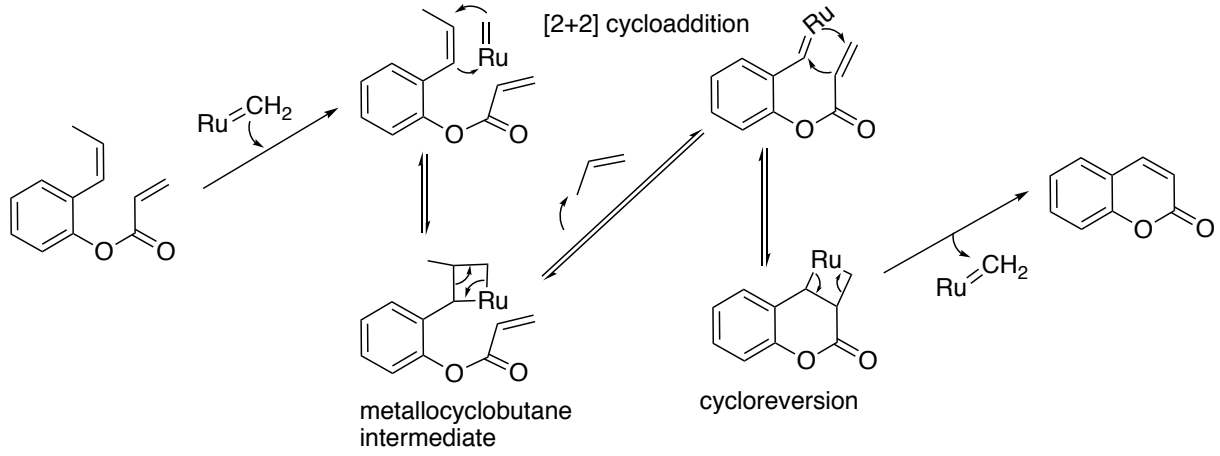

Scheme 12.

Alternatively, the intramolecular cyclization of *O*-aryl esters of propynoic acids into coumarins provides a very convenient way. Such reactions have been reported with various salts or metal complexes as catalyst.

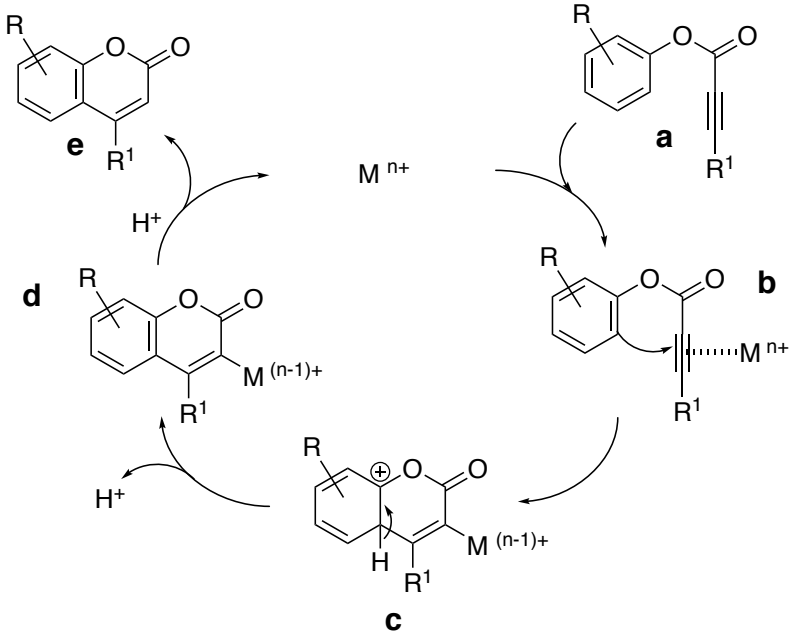

Scheme 13: Intramolecular hydroarylation of C≡C

In these reactions, the triple bond of O-aryl propynoate (**a**) is activated by an alkynophilic metal catalyst such as Pd, Au, Pt, and upon formation of intermediate (**b**), intramolecular cyclization occurs, leading to (**c**). Proton elimination then produces the rearomatized complex (**d**), which liberates the coumarin derivative (**e**) upon proto-demetallation and regenerates the catalyst (**Scheme 13**).

Ferric chloride (III) was chosen by Lu and his colleagues for addition reactions of arenes to aryl-substituted alkynes. [50] However, in the course of the work, the authors tested one variant of the propiolate cyclization. After 3 days at 80 °C in nitromethane, satisfactory yield of the corresponding coumarin was achieved. It is worth noting that reactions with iron in a catalytic amount are not popular and this work expands the range of economical catalysts for organic synthesis (**Scheme 14**).

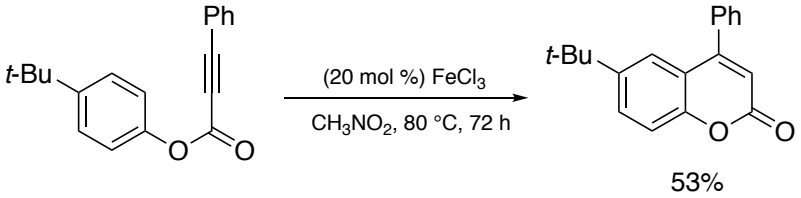

Scheme 14.

The group of scientists led by Fujiwara carried out the synthesis of coumarins from different aryl alkynoates using the intramolecular cyclization method. [51] This process was possible using 1 mol% of palladium acetate as catalyst and trifluoroacetic acid (**Scheme 15**). In this reaction, a high regioselectivity is observed. The most successful and fast reactions are those in which donor groups are present on the aryl moiety (R^1). The reaction mechanism was experimentally proved by NMR monitoring and deuteration experiments

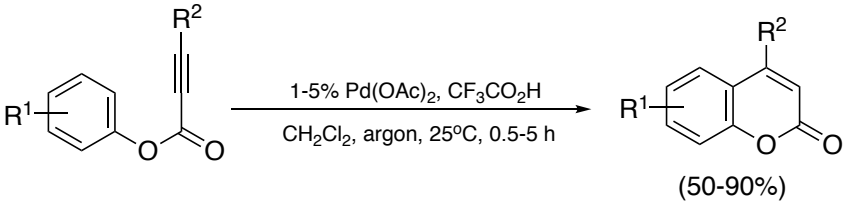

R^1= 2-Me, 3-Me, 4-Me, 4-t-Bu, 2-i-Pr-5-Me, 4-Br-3,4-Me_2, 2-CHO-5-MeO, 3,4,5-MeO_3, 3,4-benzo, 3,4-benzo, 3,4-[4,5-benzo] furano
R^2= H, Me, n-C_5H_{11}, Ph

Scheme 15.

Five years later, Tunge repeated this successful experience with brominated aryl propiolates as the starting material and, after formation of coumarin, reoriented the palladium catalyst from oxidation state +2 to 0 by changing the reaction conditions and implemented further Suzuki, Sonogashira, Heck, Hartwing-Buchwald couplings. [52]

Sames *et al.* tsted two variants of the Pt catalyst, $PtCl_2$ and $PtCl_4$ to obtain coumarin derivatives from the propiolate esters using the intramolecular cyclization method (**Scheme 16**).[53] [54] For alkyl substituted compound (a), the most successful result was achieved with $PtCl_4$ in DCE, which gave 73% yield after 36 h. After changing the solvent to dioxane, the yield dropped to 52%. $PtCl_2$ in toluene showed the lowest activity and even after 41 h, yield of coumarin was only 28%. Alkoxylated compound (b) was tested only with $PtCl_4$ in DCE and after 24h, the corresponding coumarin was obtained with 50% yield.

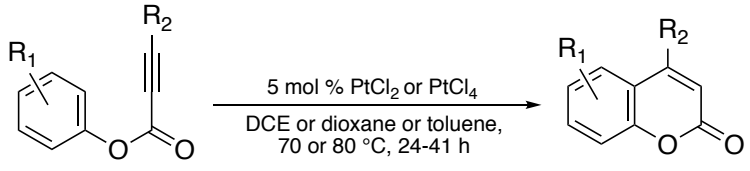

(a) R_1 = 3,5-Me_2, R_2 = Me
(b) R_1 = 3-OMe, R_2 = Ph

(a) 28 - 73%
(b) 50%

Scheme 16.

---

[50] Li, R.; Wang, S. R.; Lu, W. *Org. Lett.* **2007**, 9, 2219-2222
[51] Jia, C.; Piao, D.; Kitamura, T.; Fujiwara, Yu. *J. Org. Chem.* **2000**, 65, 7516-7522
[52] Li, K.; Zeng, Y.; Neuenswander, B.; Tunge, J. A. *J. Org. Chem.* **2005**, 70 (16), 6515-6518.
[53] Pastine, S. J.; Youn, S. W.; Sames, D. *Org. Lett.* **2003**, 5 (7), 1055-1058.
[54] Pastine, S. J.; Youn, S. W.; Sames, D. *Tetrahedron* **2003**, 59, 8859–8868

Another group, Kim *et al*, immersed us in the problem of the toxicity of gold (III) ions. They can cause damage to the liver, kidneys and peripheral nervous system. [55] To study these effects, the Kim group developed a coumarin as a probe to determine the amount of gold ions in the environment. The initial material 3-(diethylamino)phenyl 3-phenyl-propiolate exhibits a weak fluorescence, but under the action of gold ion, intramolecular hydroarylation turns this ester into the corresponding coumarin, which exhibits strong fluorescence (**Scheme 17**). Interestingly, ~~the~~ work in this direction was continued and after a while, an article about microfluidic "fireflies" for sensing applications was published. [56]

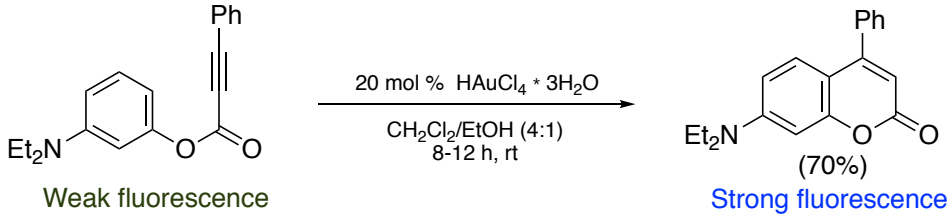

Scheme 17.

Similarly, Shi and He report on the possibility of intramolecular cyclization of aryl alkynoates using gold chloride (III) (**Scheme 18**). [57] However, the catalyst needs to be activated with AgOTf. All transformations were performed in very high yields, except for bromine-substituted aryl propiolates.

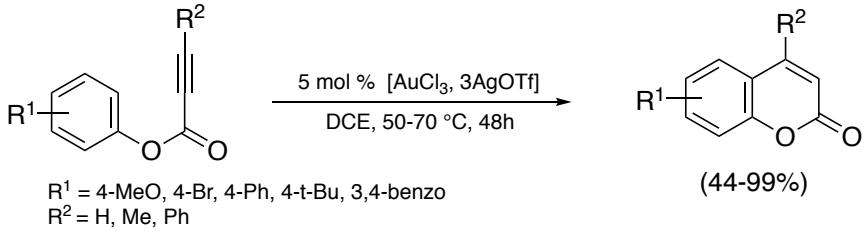

Scheme 18.

Other authors used a catalyst based on Au (I) for intramolecular hydroarylation of terminal alkynes (**Scheme 19**). [58] Among the reported products, two substituted coumarins were obtained. At room temperature in dichloromethane, methyl - substituted substrate reacted over two days, while methoxylated substrates only required two hours. This result is logically connected with the electron-donating ability of the substituents. This method of obtaining coumarins and other heterocyclic compounds does not require heat nor cocatalysts, and is thus very mild compared to others.

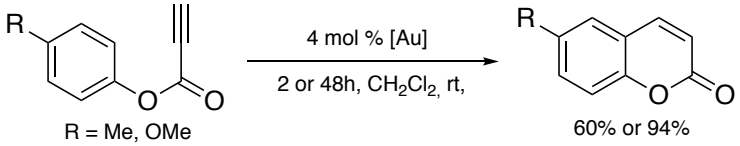

Scheme 19.

Aparece and Vadola tested the cyclization of aryl alkynoates under the action of gold catalyst $Au(PPh_3)Cl$ and activation agent AgOTf in the presence of water or in anhydrous conditions (**Scheme 20**). [59] They showed the selective formation of coumarin or of spirocyclic products depending on the presence or not of water. Having noticed by chance that a wet solvent was used, the scientists found that the reaction could proceed in two directions: effective *ortho*-cyclization under anhydrous conditions and *ipso*-cyclization in the presence of 1 equiv of water. High selectivity and high yields of spirocyclic products were obtained.

---

[55] Do, J. H.; Kim, H. N.; Yoon, J.; Kim, J. S.; Kim, H.-J. *Org. Lett.* **2010**, 12 (5), 932-934.
[56] Barikbin, Z.; Rahman, Md. T.; Khan, S. A. *Small* **2012**, 8 (14), 2152-2157
[57] Shi, Z.; He. C. *J. Org. Chem.* **2004**, 69 (11), 3669-3671
[58] Menon, R. J., Findlay, A. D., Bissember, A. C., Banwell, M. G. *J. Org. Chem.* **2009**, *74*, 8901–8903
[59] Aparece, M. D., Vadola, P. A. *Org. Lett.* **2014**, 16, 6008-6011

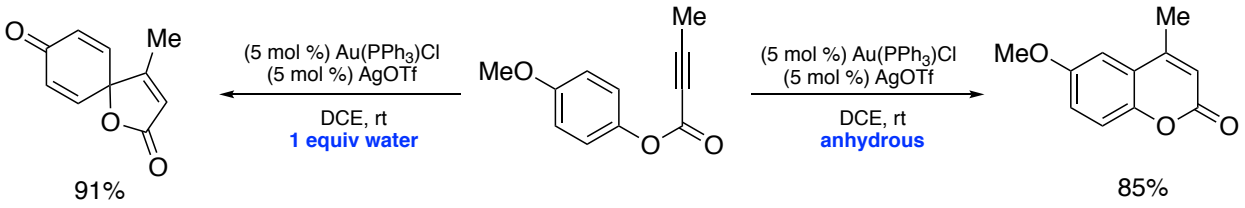

Scheme 20.

In a similar way Vadola and Sames worked on the creation of new aminocoumarins, which can be used in the study of brain activity (**Scheme 21**). [60] For cyclization reactions, they have chosen two catalytic systems: 5 mol% of $Au(PPh_3)Cl/AgSbF_6$ or 10 mol% of $PtCl_4$. In both cases, a mixture of 1,4-dioxane/DCE was used as solvents. The gold catalyst was effective at room temperature, while the platinum catalyst required heating at 80 °C.

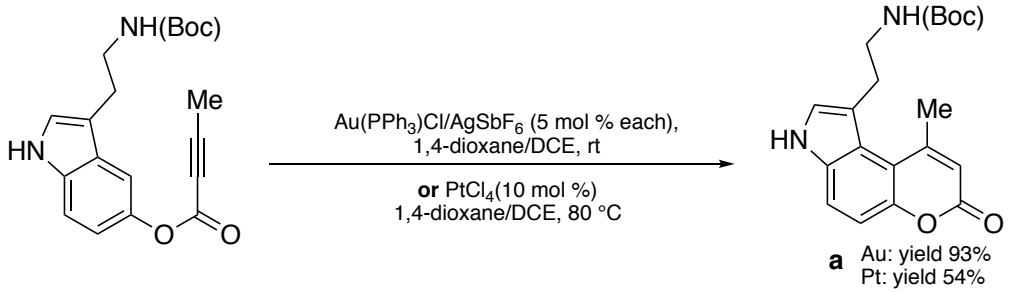

Scheme 21.

The authors investigated the influence of substituents on starting aryl alkynoate esters. In all reactions, gold showed good compatibility with amines and provides the best yields (components **a**, **b**, **d**), but platinum showed lower efficacy (see for example **Scheme 10** or **Table 1, entry 2, 3**) or unsuccessful cyclization due to coordination of the catalyst to the amine (for example **Table 1, entry 1**).

In the case of a highly reactive compound (**Table 1, entry 2**), the substance decomposed under the action of gold catalyst, despite very mild conditions. In contrast, the required aminocoumarin was formed after reaction with platinum chloride

Besides, both platinum and gold exhibit different regioselectivity. Gold catalyst does not provide great regioselectivity whereas the use of platinum becomes advantageous to ensure high regioselectivity (see **Table 1**, **entry 3**). For the Pt (IV) reaction, the yield was 69%, with a good d1:d2 selectivity of 5:1, while the selectivity was lower for the Au (I) reaction (d1:d2 = 1.7:1), despite higher yield (92%).

Entry	Starting material	Reaction product	
1	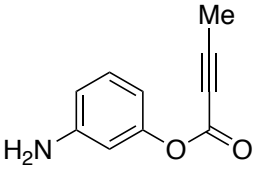	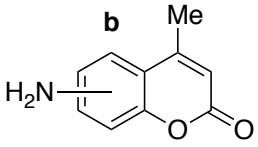	Au: yield 95% Pt: N.R. (not react)
2	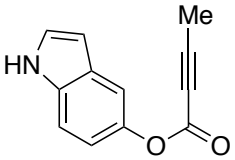	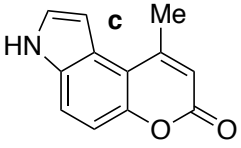	Au: decomposed Pt: yield 54%
3	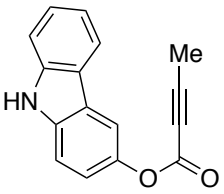	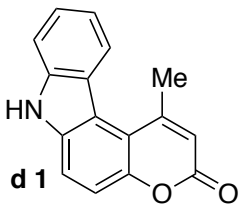 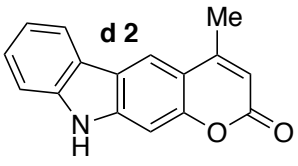	Au: yield 92%, 1:2 = 1.7:1 Pt: yield 69%, 1:2 = 5:1

Table 1.

[60] Vadola, P.A.; Sames, D. *J. Org. Chem.* **2012**, 77 (18), 7804-7814

Both catalysts effectively complement each other, although gold catalyst generally was very effective. Using it allowed to get the precursors of the substances FFN511 and PV139, which exhibit promising efficiency as fluorescent false neurotransmitters (FFNs) (**Fig. 7** and **8**).

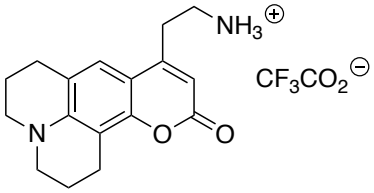

Figure 7, FFN511

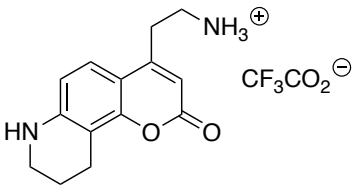

Figure 8, PV139

3. Platinum catalysts.

3.1 Platinum catalyst. History and properties.

Many sources claim, that platinum was found and studied a long time ago, but not used because of its high refractoriness.[62] [63] Nevertheless, for example, the Aztecs, many centuries before the development of metallurgy in Europe, made already in the 14th century "mirrors" of thin sheets. [64]

The active study of platinum began in the 17th and 18th centuries when this metal was brought from Peru by the Spanish colonizers. The explanation of the name is connected with the similarity of silver nuggets. Plata - silver; in Spanish, platino - small silver, poor silver. Often, this metal was found in places of gold mining and threw away as unsuitable heavy, bright nuggets. However, counterfeiters noticed that this metal mixes easily with gold, cooling its color quite a bit. This substance was described twice (1557 Scaliger, 1748 Antonio de Ulloa), but only in 1789 Lavoisier published his book, where in the "Tableau des substances simples" [65] he identified platinum as a simple, a new chemical element.

Figure 9.
Russian platinum coins [61]

Platinum gives the name to the whole group of metals, which includes Ru, Rh, Pd, Os, Ir, Pt. They were combined into one group for a combination of reasons: geolocation (this group of metals is found in the same places of mining); similarity in physical and chemical properties; configuration of external electron shells.

As a metal, it exhibits a face-centered cubic lattice, a very high melting point of 1769 °C and high refractoriness. In term of chemical properties, Pt is close to Pd, but is superior to this metal in chemical stability. For example, this metal can hardly be dissolved in hot sulfuric acid or aqua regia.

In the periodic system, platinum has an atomic number of 78, atomic mass of 195.09. The configuration of the outer electron shell of the atom is $5d^9\ 6s^1$. Therefore, the frequently encountered oxidation states are +2, +4. Various complex compounds are formed with Pt (II) and Pt (IV). Pt (II) is characterized by a square planar molecular geometry and Pt (IV) by an octahedral molecular geometry. Metal salts, such as chlorides, are often used for catalysis. As such, platinum offers several important industrial applications, such as exhaust afterburner catalyst, catalyst in petroleum refining and in organic synthesis.

---

[61] Decree of Nicholas I "Printing platinum coins in moderate amounts" **1828**, April 24
[62] Buslaeva T. M. *Soros Educational Journal*, **1999**, 11, 45–49.
[63] Kudryashov N. *Science and Life*, **2000**, 6, 46-52.
[64] Machines and technology of foundry production, A.N. Grablev, MGIU, 2010
[65] Lavoisier, A.-L. *Traité élémentaire de chimie. Paris: Cuchet,* **1789**, 192

We noticed, after studying the literature, that platinum catalysts are not very common, unlike gold or palladium. Nevertheless, Furstner and Davies described platinum in a review and pointed out that this metal is easy to work with, as there is no need for inert conditions, and also that this metal is practical, highly chemoselective towards alkenes, alkynes and carbophilic. [66]

3.2 Platinum catalyst. Activation of alkenes, alkynes.

Activation of alkenes by platinum can be traced back to the well-known Zeise salt, one of the first organometallic compounds, reported in 1831. Since, numerous applications have been developed, but we will only focus on those related to the present study.

Hydroarylation and hydroalkylation of alkenes. [67]

The research group of Widenhoefer developed several cyclization reactions mediated by platinum salts or complexes.

Alkenyl indoles can be transformed into tetrahydrocarbazoles under the influence of $PtCl_2$ and trace of HCl with high yields (**Scheme 22**). [68] The authors suggested that this cyclization occurs thanks to initial activation of an aryl C-H bond and olefin β-migratory insertion in later stages. This olefin hydroarylation allows to produce polycyclic indoles with wide biological activities, as for example, the capacity to imitate/mimic the chemical structure of peptides and possibility to reversibly create a link to proteins.

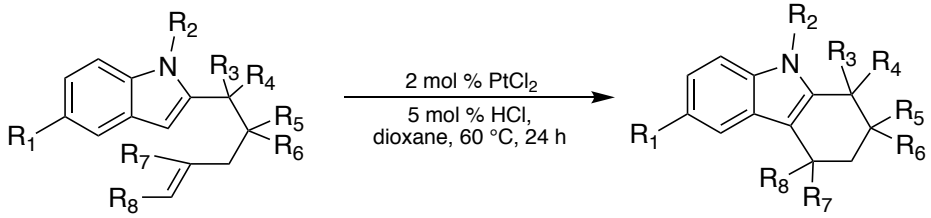

R_1 = H, OMe; R_2 = H, Me, Bn;
R_3 = H, Me; R_4 = H, Me
R_5 = H, CO_2Me; R_6 = H, CO_2Me;
R_7 = H, Me; R_8 = H, Et

74 - 98 %

Scheme 22:

This group also showed that the platinum-based compound $[PtCl_2(H_2C{=}CH_2)]_2$ can promote selective intermolecular olefin hydroalkylation (**Scheme 23**). Substituted diketones reacts with ethylene in the presence of this complex and a small amount of hydrochloric acid, that is used for the protonolysis of the Pt-C bond. High yields of α-ethyl β-diketones can thus be obtained. It is interesting to note that platinum (II) catalyst completely avoids β-hydride elimination contrary to palladium (II) used in the same reaction. [69]

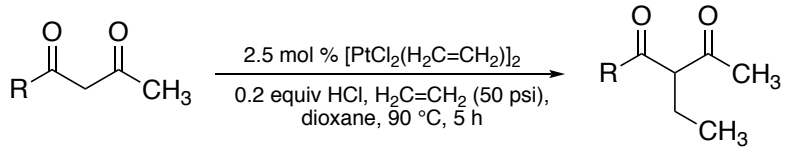

R = (a) *n*-C_5H_{11},
(b) Ph, (c) 2-furyl

(a, c) 68 %, (b) 72 %

Scheme 23:

Enynes

Besides effective transformation of alkenes, platinum-based catalysts proved able to promote skeletal reorganization of 1,n-enynes. For example, in 1996, $PtCl_2$ was tested as catalyst

---

[66] Furstner A.; Davies P. W. *Angew. Chem. Int. Ed. Engl*. **2007**, 46 (19), 3410-3449
[67] Chianese, A. R.; Lee, S. J.; Gagne, M. R. *Angew. Chem. Int. Ed.* **2007**, 46 (22), 4042-4059.
[68] Liu, X. Han, X. Wang, R. A. Widenhoefer, J. *Am. Chem. Soc*. **2004**, 126, 3700 – 3701.
[69] Wang, X.; Widenhoefer, R. A. *Chem. Commun.* **2004**, 6, 660-661.

for the cyclorearrangement of 1,6- and 1,7-ennynes into 1-vinylcycloalkenes (**Scheme 24**). [70] Organic chemists are interested in such reactions because they lead to cyclic derivatives with high structural complexity which can be used in further synthesis. [71]

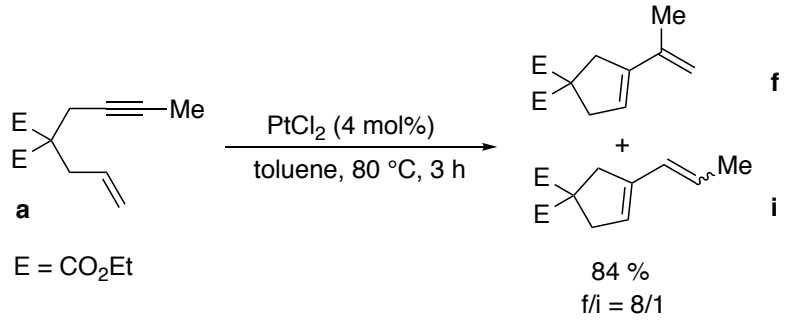

Scheme 24:

Later, Michelet, Toullec and Genet reviewed this chemistry and proposed a mechanism (**Scheme 25**).

At the first stage, coordination of the Pt^{II} - center occurs at the triple bond of the enynes (**a**) to form (**b**). The alkene group then insert in (**b**) to give (**c**) complex, which. Rearranges by a 1,2-alkyl shift to form (**d**). Subsequently, a possible fragmentation will lead to an intermediate alkene (**e**) and further elimination to give product (**f**). Alternatively, (**d**) could also isomerize through an additional 1,2-alkyl shift into the cyclopropyl intermediate (**j**). (**h**) is then formed by fragmentation and after 1,2-hybrid shift and elimination, the end product (**i**) is created.

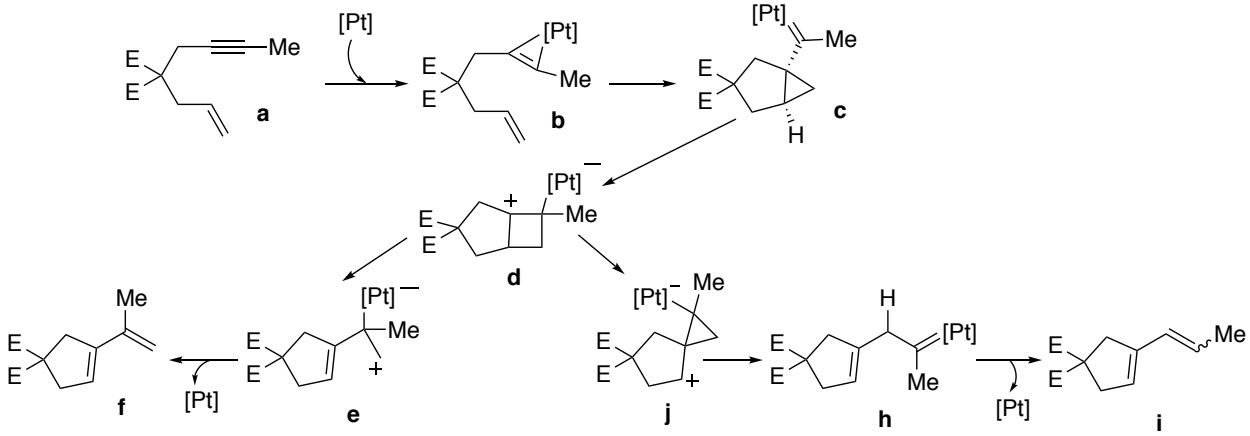

Scheme 25:

Similarly, allyl propargyl ethers undergo in the presence of a catalytic amount of $PtCl_4$ a cyclorearrangement, which produces cyclopropane-annulated dihydropyrans. [72] This work was published in 1995 by Blum *et al.* and scaled afterwards by Fürstner and Echavarren (**Scheme 26**).[73]

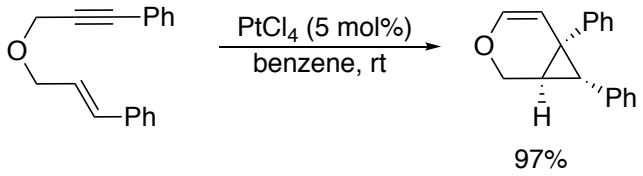

Scheme 26:

The mechanism of this transformation was clarified much later by Soriano (**Scheme 27**).[74] At the first stage, platinum ion is coordinated to the allyl propynyl ether (**a**) and form platinum-

---

[70] N. Chatani, T. Morimoto,T. Muto, S. Murai, *Organometallics,* **1996**, 15, 901.
[71] Michelet, V.; Toullec, P. Y.; Genet, J.-P. *Angew. Chem. Int. Ed.* **2008**, 47 (23), 4268-4315.
[72] Blum, J.; Beerkraft, H.; Badrieh, Y. *J. Org. Chem.* **1995**, 60, 5567.
[73] Michelet, V.; Toullec, P. Y.; Genet, J.-P. *Angew. Chem. Int. Ed.* **2008**, 47 (23), 4268-4315.
[74] Soriano, E., Ballesteros, P., Marco-Contelles J. *J. Org. Chem.* **2004**, 69, 8018.

cyclopropene (**I**). The following nucleophilic attack of the alkene group leads to the cyclopropylcarbene (**II**) through 6-endo cyclization. Next, 1,2-hydride shift occur leading to (**III**). The last stage is elimination as a result of which platinum and the final product (**b**) are released.

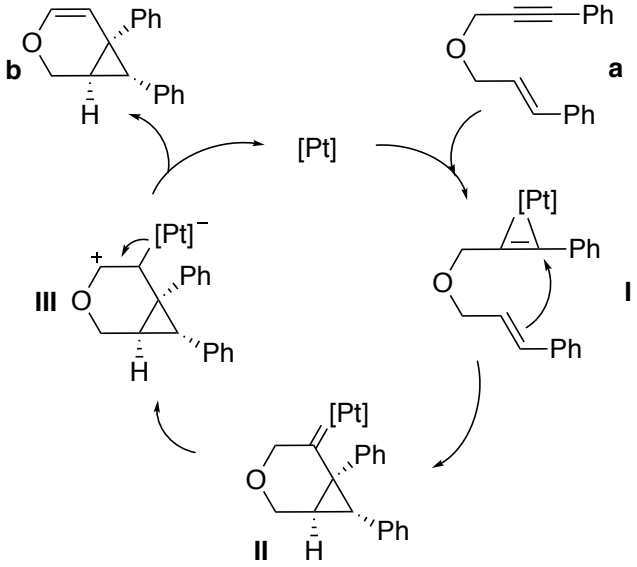

Scheme 27:

4. Conclusion.

In this chapter, we studied the variety of methods of coumarins synthesis. We started our journey in 1868 from the first synthesis of 2H-chromen-2-one by Perkin reaction. Then we mentioned the other popular named-reactions, such as Pechmann, Knoevenagel, Houben-Hoesch and Ponndorf. The most widespread reaction among them is Pechmann's one, amazingly, scientists have still been experimenting with catalytic systems or catalytic surfaces.

Later, chemistry of transition metal complexes appeared as a soft alternative to the traditional synthesis methods, requiring highly acidic or basic conditions. In this vein we divided our literature research into two subgroups: intermolecular and intramolecular reactions of transition metal complexes for the preparation of coumarins.

Intermolecular reactions concerning information about condensation-cyclization processes with metals such as Fe, Co, Ni, Cu, Zn, Ph, Pd, Pt.

On the other side, intramolecular reactions were presented in 2 approaches: one based on ring-closing metathesis, by Ru-catalysts and the other, based on the cyclization of *O*-aryl esters of propynoic acids by various salts or metal complexes as catalyst. Intramolecular reactions are interesting alternative to obtain coumarins. The main advantages of these methods include a simple, convergent and modular access to coumarin derivatives. We researched all the information and collected various examples of cyclization carried out with metals such as: Pd, Fe, Au, Pt.

We were surprised to find that $PtCl_4$ is one of the best catalysts for such a cyclization. $PtCl_2$ also been screened for this cyclization and mentioned in several publications, but usually showed a very low conversion. However, $PtCl_2$ usually exhibits similar and even better reactivity compared to $PtCl_4$, despite its lower electrophilicity; thus, it should correspond with Au (I) and Pt (IV) catalysts in the cyclization of aryl propynoates. Therefore, we have a look at the properties of platinum and found that with this metal is easy to work, also there is no need for inert conditions, and also that this metal is practical, highly chemoselective towards alkenes, alkynes.

CHAPTER II. Intramolecular cyclization of aryl 3-arylpropynoates into 4-arylcoumarins catalyzed by platinacycle complexes.

1. Introduction

In the literature background part (see Chapter 1), the main methods already developed for the synthesis of coumarins were surveyed. Among them, the intramolecular cyclization of aryl propynoates catalyzed by metals such as Pd (II), Au (I), Au (III), Fe (III), Pt (II) and Pt (IV) is probably the simplest and mildest method (**Scheme 28**). In the following table (**Table 2**) we tried to collect the most important informations, about these metal-catalyzed cyclizations of aryl propynoates.

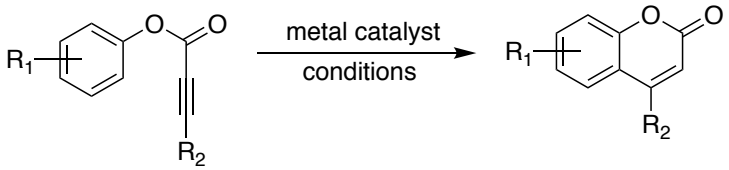

Scheme 28: Metal-catalyzed cyclizations of aryl propynoates

Entry	Catalyst	Reference	Catalyst	Conditions	Numb. of examples	Yields, %
1	Pd II	51	**Pd**$(OAc)_2$ (1-5 mol%)	TFA, CH_2Cl_2, rt, 0.5-5h	15	50-91
2	Au I	58	$BiPhtBu_2P$**Au**$(NCMe)^+$, SbF_6 (1-5 mol%)	CH_2Cl_2, rt, 1-48h	2	17-94
3		59, 60	PPh_3**Au**Cl (5 mol%) AgOTf or $AgSbF_6$ (5 mol%)	DCE or DCE/dioxane, rt, 10 min-6h	19	80-98
4	Au III	55	H**Au**Cl_4* $3H_2O$ (10 mol%)	CH_2Cl_2/EtOH, rt, 12h	1	70
5		57	**Au**Cl_3 (5 mol%) AgOTf (15 mol%)	DCE, 50-70 °C	9	44-99
6	Fe III	50	**Fe**Cl_3 (20 mol%)	CH_3NO_2, 80 °C, 72h	1	53
7	Pt II	53, 54	**Pt**Cl_2 (5 mol%)	Toluene, 80 °C, 41h	1	28
8	Pt IV	53, 54, 59	**Pt**Cl_4 (5-10 mol%)	DCE and/or dioxane rt to 80 °C, 8-24 h	14	34-92

Table 2. Known metal-catalyzed cyclizations of aryl propynoates

This table demonstrates that the simplest chloride salts of various metals were mainly used for this type of reaction (entries 3-8). In these cases, reactions can proceed with activating agents (AgOTf, $AgSbF_6$) or not. Complexes of Pd or Au (entry 1-3) were also used for these transformations. However, in almost all cases the effect of substituents often influenced the time and yield of the reaction.

The most active of the proposed catalyst is the cationic complex in situ produced from PPh_3**Au**Cl/$AgSbF_6$ (entry 3). It shows high activity at room temperature, usually requires short reaction times and its efficacy seems to be almost without negative influence of electron-withdrawing groups.

Platinum (IV) salt is also quite effective (entry 8). Although this catalyst allows to get medium to high yields of coumarins as for the Au catalyst mentioned above, it often requires heating.

Platinum (II) has not well been studied for this reaction (entry 7). Nevertheless, in the literature, there is evidence that this catalyst can be quite effective for other reaction [75]

[75] Cotton, A. F.; Wilkinson, G., *WILEY & SONS, New York,* **1999**, p 972

2. Platinum catalysts

Metal salts, such as chlorides, are often used for catalysis. However, it is known that the solubility of metals salts in organic solvents is often poor. For example, platinum chlorides are inorganic polymers, poorly soluble in most organic solvents. Coordinated organometallic complexes can be more soluble and effective for various catalytic reactions. For example, dichloro(cycloocta-1,5-diene)platinum or its diphosphine analog are fully soluble in organic solvent and often used in catalysis.

Cyclometalated platinum complexes offer several advantages compare to more classical complexes. The C-Pt bond demonstrates high stability, and therefore these complexes should be stable catalysts. The C-Pt bond also induces strong trans effect and strong back-bonding from platinum to other ligands, increasing the metal electrophilicity.

Interestingly for the case we are interested in, a strong electrophilic metal center is necessary for effective triple bond coordination, which then will ensure the successful cyclization.

Platinum Pt (IV) forms very thermally stable and kinetically inert complexes, unlike Pt (II). Therefore, platinum Pt (II) was selected as more promising. We thus look for complexes based on Pt (II) with high solubility and reactivity for intramolecular cyclization of aryl propynoates.

A range of catalysts based on Pt (II) was selected and synthesized (**Fig. 10 A-E**). We choose the complex *cis*-$PtCl_2(MeCN)_2$ **A**, because it proved to be quite effective as catalyst for the cyclization of furyl alkynes, [76] as well as for the cyclization of 1,6-enynes.[77] The preparation of this catalyst was carried out according to a reported method ref Its DMSO analog **B** was the most effective in obtaining a series of lactones [78] This catalyst was prepared by a known method. [79] The dimer **C** was also prepared according to a known method, [80] and also used as the starting component for obtaining **D** and **E**.

After synthesis, each complex was evaluated as catalysts for the intramolecular cyclization of aryl propynoates.

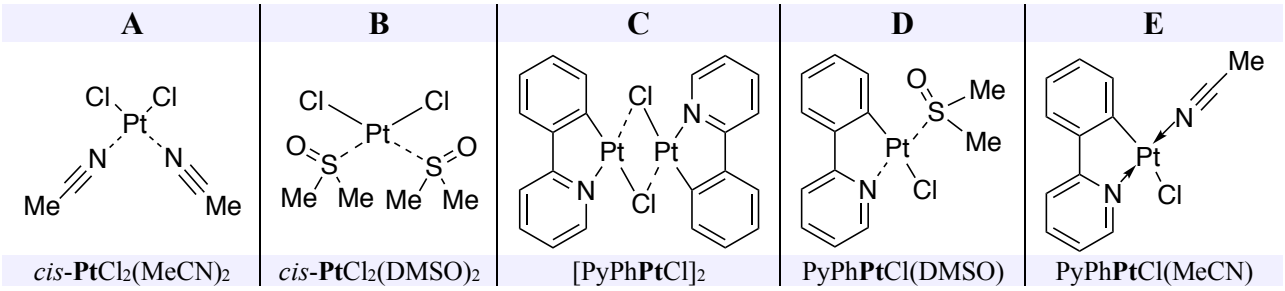

Fig 10: Cyclometalated complexes based on Pt (II)

[76] Martin-Matute, B.; Nevado, C.; Cardenas, D. J.; Echavarren, A. M. *J. Am. Chem. Soc.* **2003**, 125 (19), 5757-5766.
[77] Munoz, M. P.; Mendez, M.; Nevado, C.; Cardenas, D. J.; Echavarren, A. M. *Synthesis* **2003**, (18), 2898-2902.
[78] Aleman, J.; del Solar, V.; Martin-Santos, C.; Cubo, L.; Ranninger, C. N. *J. Org. Chem.* **2011**, 76 (17), 7287-7293.
[79] Han, X.; Wu, L.; Zhang, L.; Tung, C. *Sci. Bull.* **2006**, 51 (8), 1005-1009.
[80] Godbert, N.; Pugliese, T.; Aiello, I.; Bellusci, A.; Crispini, A.; Ghedini, M. *Eur. J. Inorg. Chem.* **2007**, 32, 5105-11.

3. Synthesis of *O*-aryl esters and *S*-aryl esters derived from 3-arylpropynoic acids

To explore the possibility of the cyclization reaction, we synthesized a series of *O*-and *S* esters of 3-arylpropynoic acids using the well-known reaction of acids with phenols or thiophenols under the action of DCC in CH_2Cl_2 (**Scheme 29**). Various propiolic acid derivatives, which carry a substituent at the acetylenic position were thus prepared

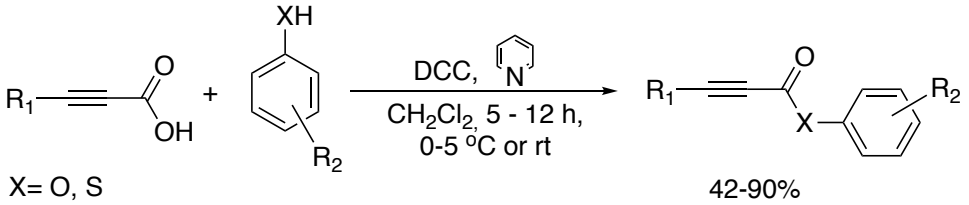

Scheme 29: Synthesis of the starting aryl propynoates and propynethioates.

The purification of the so-formed *O*-aryl esters and *S*-aryl esters was carried out classically by column chromatography on silica gel (eluent – pentane : diethyl ether (95:5)). The isolated yields of the esters were 40-90%. They were fully characterized by ^1H and ^{13}C NMR. All S-aryl esters were obtained for the first time.

4. Optimization of the catalyst and the reaction conditions.

Several experiments with phenyl 3-phenylpropynoate **2a** and various Pt-catalysts led to very low yields of 4-phenyl coumarin **3a**. It was decided to replace the starting material with **2b**, which contains two methyl groups (**Scheme 30**). With this more reactive substrate, a series of experiments was started to screen Pt catalysts (**Table 3**).

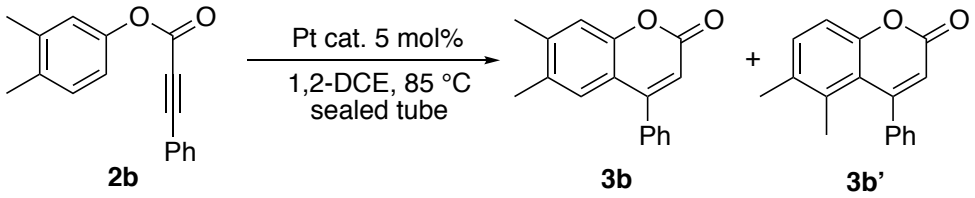

Scheme 30.

Entry	Catalyst*	Short name	Time	Yield[a] (%)	**3b** : **3b'**
1	none	-	24 h	0	-
2	$PtCl_2$	-	24 h	20	1 : 0.17
3	$PtCl_4$	-	24 h	14	1 : 0.18
4	*cis*- $PtCl_2(MeCN)_2$ **(A)**	**(A)**	76 h	20	1 : 0.15
5	*cis*- $PtCl_2(DMSO)_2$ **(B)**	**(B)**	76 h	19	1 : 0.2
6	PyPhPtCl(DMSO) **(D)**	**(D)**	192 h	37	1 : 0.2
7	$[PyPhPtCl]_2$ **(C)**	**(C)**	58 h	87	1 : 0.19
8	PyPhPtCl(MeCN) **(E)**	**(E)**	24 h	95	1 : 0.18

Table 3. Condition set up for the Pt-catalyzed cyclization of 3,4-dimethylphenyl phenyl propynoate **2b**.
*5 mol% loaded catalyst; [a] yields determined by ^1H NMR

First of all, a blank experiment without catalyst was carried out during 24h (Entry 1). As expected, no change was observed and the starting material was recovered. Next, commercially available platinum chlorides II and IV (Entry 2 and 3) were evaluated. After 1-day, low yields of 14% or 20% of cyclization products **3b** and **3b'** were achieved. Unfortunately, Pt II complexes **A** and **B** (Entry 4 and 5) did not show a better activity and the yield did not exceed 20%, even with reaction time increased up to 76 h. The platinacycle catalysts were then evaluated. They globally facilitated the reaction and improved yields, but with large variation. Complex **D** very slowly promotes the reaction and led to an increase in coumarin yield but after a very long time. Indeed,

it took more than 8 days to reach 37% yield (Entry 6). The dimeric complex **C** reacted with propynoate very effectively. Full conversion and 87% yield were achieved (Entry 7), but the reaction time was still long (2 days). Catalyst **E** turned out to be the most effective. With this catalyst, the yield of the corresponding coumarins were about 95 after 24 hours %.

Between the two monomeric complexes **D** and **E**, we can notice rather different cyclization abilities. This effect is associated with the more labile acetonitrile ligand, compare to DMSO. This lability provides a free coordination center on platinum, which facilitates the triple bond coordination and thus the formation of coumarin derivatives.

Interestingly, the different structural variations among the platinum (II) catalysts did not have an influence on the ratio between the two regio isomers **3b** and **3b'**, remaining approximately 1:0.2 whatever the catalyst.

After having determined the most effective catalyst, it was decided to test this catalyst on other substrates. Six aryl propynoates with methyl or methoxy substituents at position 2, 3 and 4 of the phenolic part were chosen (**Scheme 31** and **Table 4**). Only substrates with donor groups in position 3 were effectively cyclized (Entry 2 and 5). This result was quite expected since the electron density donation is favored in *ortho* and *para* position. In the other cases, the conversion was very low 2 - 9 % (Entry 1, 3, 4, 6).

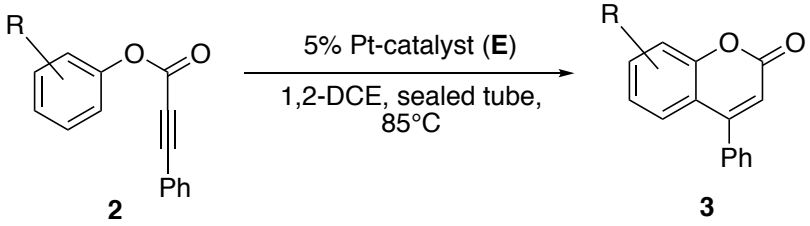

2 **3**

Scheme 31.

Entry	R	T, h	Conv. of **2** (%)
1	2-Me	24	8
2	3-Me	24	25
3	4-Me	24	9
4	2-OMe	24	2
5	3-OMe	5	100
6	4-OMe	24	7

Table 4: Catalyst tests on methyl or methoxy substituents of the phenolic part of aryl propynoates.

Based on the insufficient efficacy of the catalyst in the previous tests, it was decided to increase the electrophilicity of the platinum center. Silver salts have been chosen for this purpose. It is well known that silver salts are used as halide scavenger. Starting from complex **E**, silver ion will abstract the halide thus freeing one coordination center at the metal and rendering the resulting complex cationic. [81] All experiments from this series were performed on 2-methylphenyl 3-phenylpropynoate **2c** (**Scheme 32**), as a more challenging substrate and the results are presented in **Table 5**.

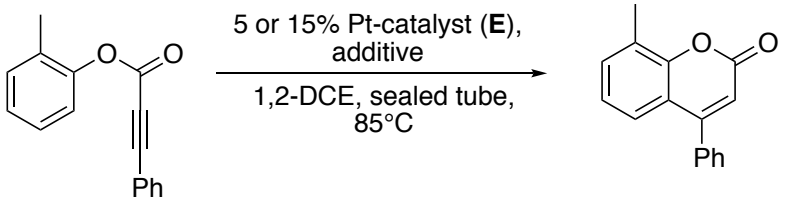

Scheme 32.

[81] Weibel, J.-M.; Blanc, A.; Pale, P. *Chem. Rev.* **2008**, 108 (8), 3149-3173.

Entry	Catalyst **E** (mol %)	Additive (mol %)	Conv. of **2c** (%)
1	5%	/	8
2	15%	/	11
3	5%	5% $AgBF_4$	4
4	5%	5% $AgSbF_6$	42
5	5%	10% $AgSbF_6$	91
6	5%	15% $AgSbF_6$	97
7	5%	20% $AgSbF_6$	100
8	/	20% $AgSbF_6$	11

Table 5: Optimization of the catalyst loading and additive for the cyclization of 2-methylphenyl phenylpropynoate **2c**.

As it can be seen from Table 5, the use of 5 mol% platinum catalyst **E** led only to 8% conversion of the starting material (Entry 1). By increasing 3 times the amount of catalyst (Entry 2), almost no improve in the conversion of **2c** propynoate could be observed. Two silver salts (silver tetrafluoroborate and silver hexafluoroantimonate) were used (Entry 3, 4). In the first case, the conversion remained low (Entry 3). However, $AgSbF_6$ increased 5 times the conversion of the starting material (entry 4 vs 1). Moreover, an additional increase in the silver catalyst amount from 5% to 20%, effectively raised the conversion from 42% to 100% (Entry 4-7). For comparison and to check the catalytic ability of silver salts alone in the cyclization, we have submitted **2c** to 20 mol% of $AgSbF_6$ and only a low conversion was observed (entry 8). Hence, effective and optimal proportions of the catalytic system were established as 5 mol% of Pt catalyst (**E**) and 15 mol% of silver activating agent $AgSbF_6$. This ratio will be further used for all transformations.

5. Intramolecular cyclization of *O*-aryl esters of 3-arylpropynoic acids into coumarins under the action of catalytic amounts of Pt (II) complexes

After the selection of the catalytic system (5 mol% PyPhPtCl(MeCN)/ 15 mol% $AgSbF_6$), the steric and electronic effects were studied with series of appropriately substituted aryl propynoates. The general scheme for all transformations is given below (**Scheme 33**). The experiments were carried out in a sealed tube, at a temperature of 85 °C, and using 1,2-dichloromethane (1,2-DCE) as the solvent and during a maximum reaction time of 24 h.

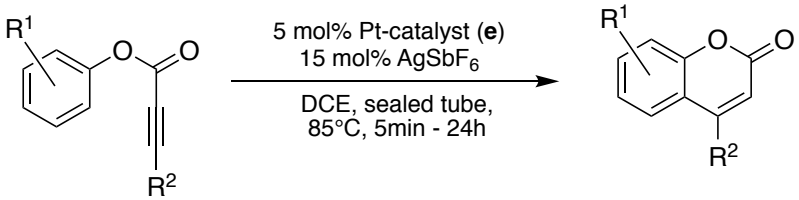

Scheme 33: General scheme for intramolecular cyclization of O-aryl esters of 3-arylpropynoic acids into coumarins under the action of PyPhPtCl(MeCN)/$AgSbF_6$ catalytic system

The strategy has been divided into three kind of transformations. In the first part, aryl propynoates were substituted at the ester moiety (**Table 6a** and **6b**); in the second part, the substitution occurred at the ynoate (**Table 6c**); in the third part, naphtyl esters were investigated (**Table 7**).

The simplest non-substituted phenyl 3-phenylpropynoate **2a**, was first re-investigated under the action of the updated catalyst system. After 24 h, this compound led to 54% yield of the expected coumarin **3a**. In the following experiments, (Entry 2-12), starting materials carrying electron-rich substituents at the ester moiety were submitted to the optimized conditions. They were converted to the corresponding coumarins with yields, from 77 to 94%. These fluctuations are related to the position of the substituent and its nature.

Methylated esters in the *ortho* **2c**, *meta* **2e** and *para* **2d** position gave the corresponding coumarins with significantly increased yields, compared to the reference ester **2a** (entries 2-4 vs

1). Interestingly, compound **2c**, with steric hindrance, gave a yield similar to compound **2d** (85 and 89%). The cyclization of substance **2e** was slightly faster (22h), but the yield of products **3e** and **3e'** were slightly lower than in the two previous cases (77%). The two dimethylated propynoate **2b** and **2f** react completely in a short time (2h or 4h) and the product yields were the same and achieved 88%. This relation could be due to the double effect of the methyl groups. We thus explored the behavior of substrates having stronger electro-donating substituents. Cyclohexylated **2g** esters were also very reactive substrates and after 5 h led to 72% yield of **3g**.

Entry	Propynoate		Coumarins		Time	Conv. (%)	Yield (%)[a] Ratio
1	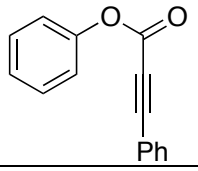	**2a**	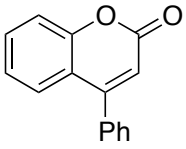	**3a**	24h	N.D.[b]	54
2	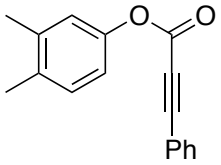	**2b**	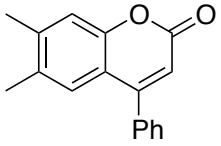 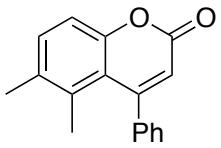	**3b** **3b'**	4h	100	88 5.5:1 1 : 0.18
3	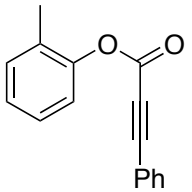	**2c**	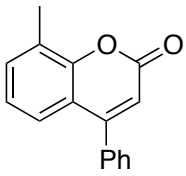	**3c**	24h	97	85
4	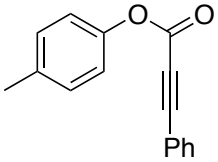	**2d**	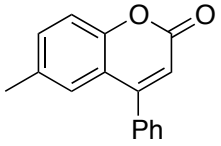	**3d**	24h	99	89
5	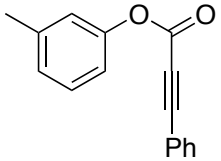	**2e**	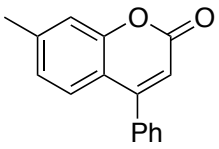 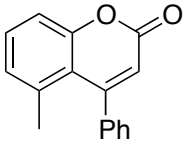	**3e** **3e'**	22h	100	77 4.3:1 1 : 0.23
6	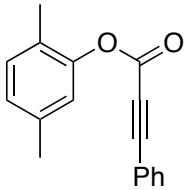	**2f**	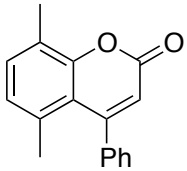	**3f**	2h	100	88
7	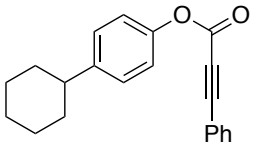	**2g**	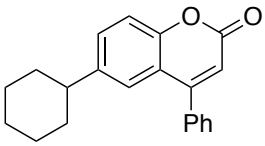	**3g**	5h	100	72

Table 6a: Pt(II)-catalyzed cyclization of aryl propynoates **2,** substituted at the ester moiety, to coumarins **3**.
[a] isolated yields; [b] N.D. : not determined

We then explored the behavior of substrates having stronger electro-donating substituents. As expected, the methoxylated esters **2h**, **2i**, **2j** led to very high product yields (84-86%). The *para*- and *ortho*- substituted starting materials **2h** and **2**i achieved complete conversion within 24 hours, while the *meta*-methoxylated **2j** fully reacted only after 1 h. Phenoxylated **2k** esters was very reactive substrates too. The time of its complete transformation was 2h and as a result, the corresponding coumarin was obtained with an excellent 82% yield. High reactivity of methoxylated **2j** or phenoxylated **2k** esters are again related to electron density donation in *ortho*- and *para*- position.

The opposite situation was observed with the electrodeficient bromo-substituted ester **2l**. After 24h, it was possible to only get 25% of **3l**. This yield is twice lower than that obtained for 4-phenyl coumarin **3a** (entry 12 vs 1).

As expected, the aryl esters of arylpropynoic acids containing donor groups as substituents gave higher conversions and yields of coumarins than those having electron-poor substituents.

Entry	Propynoate		Coumarins		Time	Conv. (%)	Yield (%)[a]
8	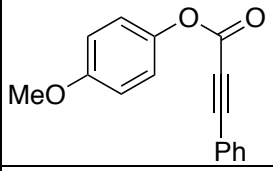	**2h**	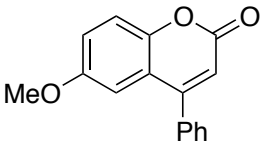	**3h**	24h	100	84
9	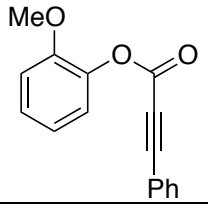	**2i**	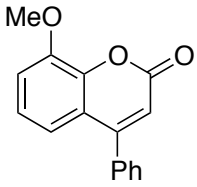	**3i**	24h	100	86
10	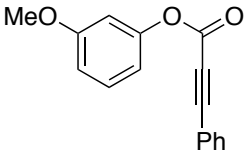	**2j**	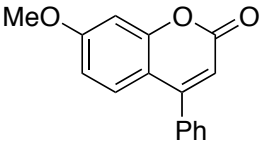 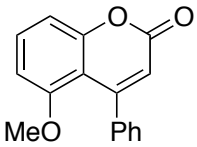	**3j** **3j'**	1h	100	94 3.2:1 1 : 0.31
11	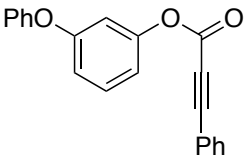	**2k**	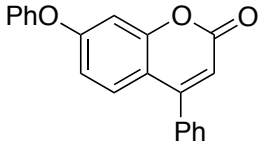 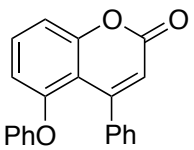	**3k** **3k'**	2h	100	82 4:1 1 : 0.25
12	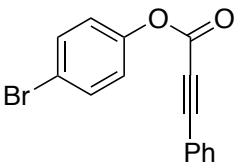	**2l**	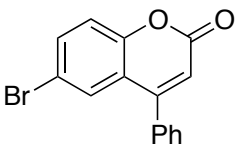	**3l**	24h	50	25

Table 6b: Pt(II)-catalyzed cyclization of aryl propynoates **2,** substituted at the ester moiety, to coumarins **3**.

After having checked electronic effects on the ester part, we also briefly accomplished several more experiments in which the electron density from the ynoate side was modulated by introducing various substituents (Entry 13-16). The fluoro-substituted derivative **2m** after 10 and

24 h led to the same yield 50-55% (entry 13). Unexpectedly, this yield was the same as in the unsubstituted compound **2a**. Reaction with the 4-methylated substrate **2n** increased yield only by a few percent and produced 59% of **3n** (entry 14). In compounds **2o** and **2n** substituted on both sides, we observed an obvious increase of conversion and yield by using donor substituents from the phenyl part (entries 15-16).

Entry	Propynoate		Coumarins		Time	Conv. (%)	Yield (%)[a]
13	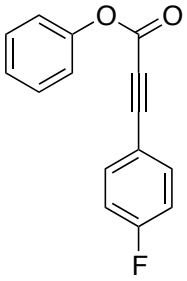	**2m**	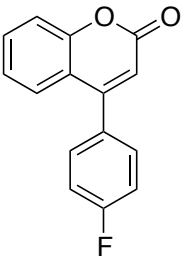	**3m**	10h 24h	N.D.	50-55
14	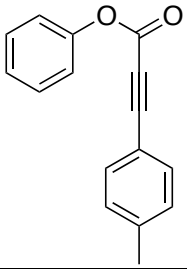	**2n**	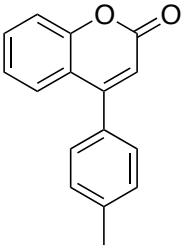	**3n**	24h	73	59
15	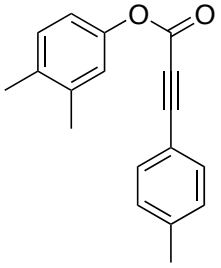	**2o**	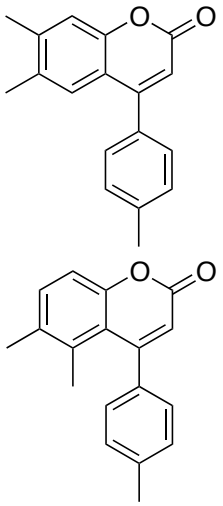	**3o** **3o'**	24h	80	60 3.8:1 1 : 0.26
16	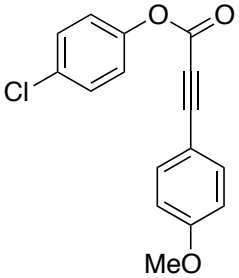	**2p**	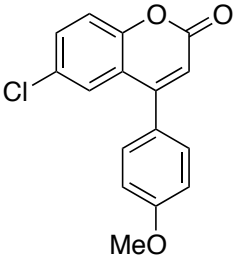	**3p**	24h	68	50

Table 6c. Pt(II)-catalyzed cyclization of aryl propynoates **2,** substituted at the ynoate moiety, to coumarins **3**

The benzocoumarins constitute a sub-class of the coumarin family. Due to the expanded nature of their π-electron system, they are highly efficient in photon-oriented applications. [82] They can act as a fluorescent probes and tags or photo-labile materials. [83] Based on the interest in this material, we thus prepared various naphthyl derivatives and submitted them to series of

[82] Tasior, M.; Kim, D.; Singha, S.; Krzeszewski, M.; Ahn, K. H.; Gryko, D. T. *J. Mater. Chem. C* **2015**, 3 (7), 1421-1446.

[83] Jung, Y.; Jung, J.; Huh, Y.; Kim, D. *J. Anal. Methods Chem.* **2018**, 5249765/1-5249765/11.

experiments. They turned out to be the more reactive of all the esters already studied. They indeed react very fast with a time of complete conversion ranging from 5 to 45 minutes. Various substituted benzocoumarins were obtained with very high yields (from 74 to 99%). We reasoned that the cyclization strategy we have developed could be easily extended to access to benzocoumarins, starting from naphthyl propynoate.

α-and β-Naphthyl esters **2q** and **2r** readily reacted within minutes in the presence of the Pt/Ag catalytic system and led to a quantitative yield of the expected benzocoumarins **3q** and **3r** products. Interestingly, the β substrate **2r** was completely converted to coumarin three times faster than its α-analog. This difference can be explained by the known higher nucleophilicity of the α-position in nathtyl system. The fluoro analog of β-naphthyl propynoate also reacted with the same uniquely fast reaction time and again quantitatively provided the fluoro benzocoumarin **3u**.

However, the methylated and methoxylated derivatives required longer reaction time (30–45 min). The methoxylated β-naphthyl ester **2t** was again quantitatively converted into the benzocoumarin **3t**. Surprisingly, the yield of the methylated **2s** derivative was the lowest in the series, but still good (74%).

Entry	Naphtyl propynoate		Benzocoumarin		Time	Conv (%)	Yield (%) [a]
1	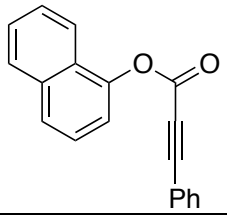	**2q**	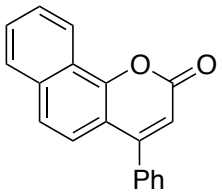	**3q**	15 min	100	99
2	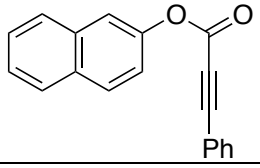	**2r**	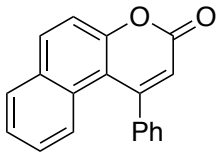	**3r**	5 min	100	99
3	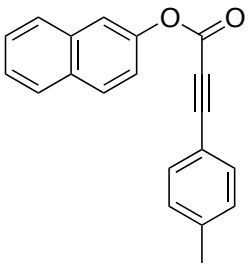	**2s**	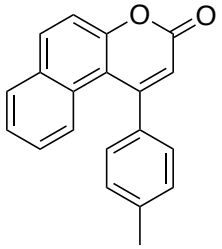	**3s**	30 min	100	74
4	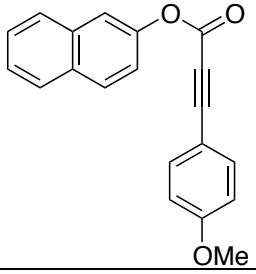	**2t**	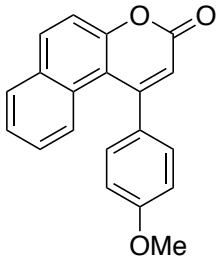	**3t**	45 min	100	99
5	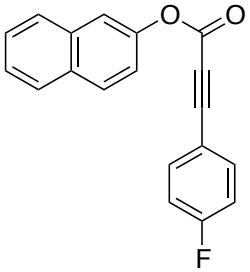	**2u**	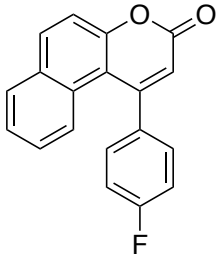	**3u**	5 min	100	99

Table 7: Pt(II)-catalyzed cyclization of naphtyl propynoates to benzocoumarins

It is worth noting that all the so-formed benzocoumarins almost did not require purification, as they crystallized. They can be recrystallized from a hot mixture of pentane with a few drops of diethyl ether. All the derivatives from this series were analyzed by XRD and excellent crystallographic data were obtained.

6. Conclusion

In chapter 2, we demonstrated an effective method of cyclization *O*-aryl esters of 3-arylpropynoic acids to coumarins and benzocoumarins by monomeric platinacycles. Among several dimeric or monomeric complexes based on platinum (II), the most effective was 2-(pyridin-2-yl) phenylPt(II)(acetonitrile) chloride complex. This complex was obtained in a very simple way by mixing 2-phenylpyridine with potassium tetrachloroplatinate in the appropriate solvents.

As a result of the optimization of the catalytic system and the choice of silver salt $AgSbF_6$ which abstract halide from metal halide complexes, thus liberating a coordination site on the metal, we managed to reduce the time and increase the reaction yield.

As a result of working with PyPhPtCl(MeCN) / $AgSbF_6$ we tested a wide range of substitutes with different functional groups. Regularities of the impact of electron-donor or electron-acceptor substituteы on both sides (ester or ynoate moiety) of aryl propynoates at the yield of the corresponding coumarin were fixed.

A very pleasant surprise was series of naphtyl esters experiments. They proved very reactive under the set-up conditions. In the light of their active study in in photon-oriented applications, benzocoumarins with a yield more 74% and did not exceed 45 min were obtained very timely.

SECOND PART. Zeolites

CHAPTER I. Literature background

1. Ζέωλίθος - the boiling stones.

1.1. Their story.

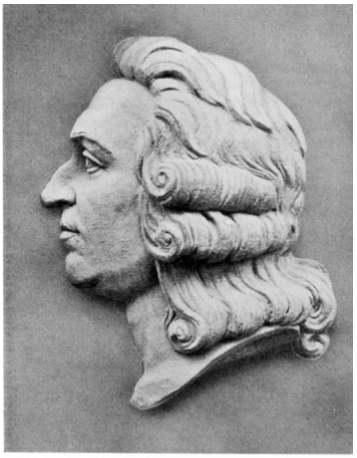

Figure 11. Sculpture of Baron Axel Fredrik Cronstedt who discovered zeolites.

In 1756, the mineralogist Baron Axel Fredrik Cronstedt (**Fig. 11**), from Sweden, first discovered a new mineral - zeolite. [84] He noticed, that during the heating of the stone, water began to rise from the stone, creating the appearance of boiling stone. Based on this property, by combining two greek words zέω - boil and λίθος - stone he defined the name of this new mineral, zeolite.

We'll skip the 140 years of inactive zeolite research and highlighted the next interesting stages:
- In 1896, Friedel published the idea of open spongy frames in zeolites. This discovery was based on the fact that some substances such as alcohol, benzene or chloroform remained inside calcined (dehydrated) zeolites
- Likewise, in 1909, Grandjean used anhydrous chabazite, as an adsorbent for new substances as ammonia, air, hydrogen
- Thereafter, in 1925 Weigel and Steinhoff first discovered a new property of zeolite - the ability to act as molecular sieve. Using again dehydrated chabazite, scientists noticed that water, methanol, formic acid could be easily and quickly adsorbed, whilst acetone or benzene did not.

In 1927, Leonard first applied X-ray diffraction to synthesized minerals.

In 1948, Richard M. Barrer succeeded to obtain the synthetic zeolite analogue of natural mordenite. [85] Barrer's group recreated the natural conditions for the synthesis of zeolites, namely, high temperature, high salt concentration, high autogeneous pressure. Hence, this discovery and the principles of synthesizing zeolites became the starting point for a number of new synthetic zeolites.

Between 1949 and 1955, Milton and Breck discovered type A, X, and Y zeolites.

Thanks to Union Carbide company, since 1954 the process of commercialization of synthetic zeolites has begun. They were mainly used for cleaning and separation of mixtures. However, in 1959, Union Carbide started producing and using Y-type zeolite as a catalyst for the isomerization of alkenes.

The first modification of zeolite occurred in 1969 from the Grace company. They created the first ultra-stable zeolite Y, obtained by steaming.

In 1974, Henkel proposed to replace phosphates in detergents by zeolite type LTA. A few years later in 1977, zeolites were introduced in ion exchange processes by Union Carbide.

So, we described the main historical moments from the discovery of zeolites as a new material to its synthesis in the laboratory, the choices of the properties of zeolites and to use at industrial scale. This historical information shows how the emerging interest in the properties of the mineral has grown into a huge scientific field, involving kaleidoscopic properties, the interest in which increases with time.

---

[84] Flanigen, Ed. M.; Broach, R. W.; Wilson, S. T. *Edited by Kulprathipanja, S. Zeolites in Industrial Separation and Catalysis,* **2010**, 1-26.
[85] Barrer, R. M. *J. Chem. Soc*. **1948**, 2158-2163

1.2. Natural zeolites.

Figure 12. Group of Faujasite crystals. Collection and photo Matteo Chinellato (1.83 mm)

The natural formation of zeolites, like many other minerals, occurred over thousands of years. It is impossible to recreate these natural processes occurring at geological time, but scientists think that the main component of zeolites — silica (SiO_2) — was released by hydrolysis from volcanic glass or chemogenic sediments followed by recrystallization under conditions of increased alkalinity. [86]

Natural zeolites (**Fig. 12**) are found either in cavities in basalt or volcanic rocks or in mineral deposits in sedimentary rocks. Usually, the natural zeolites found in these are chabazite, erionite, mordenite and clinoptilolite. Monomineral deposits are exploited for mining. They are used in construction, in pet litters, geological formations as adsorbents, fillers in paper, fertilizers.

Interestingly, semi-precious stones can form in the zeolite layer due to inclusions of metals in the structure of the zeolite. The stones are very beautiful and are thus collected in private collections and museums. [87] They can also be used in jewelry.

1.3. Synthetic zeolites

Natural zeolites are not homogeneous, they often contain impurities of other metals, other zeolite phases. Because of these nuances, their properties are not defined clearly enough for specific applications and are significantly inferior in the possible applications compared to well defined synthetic zeolites.

Figure 13. The main forms of synthetic zeolites (powder, ball, extenders)

At laboratory scale, it is possible to synthesize zeolites from aluminosilicate gels in an alkaline medium at high autogeneous pressure and temperature. By changing the parameters of the synthesis, one can vary the structure of the final zeolite product, [88] and obtain zeolites with well-defined properties. The application scope of those synthetic zeolites is much larger; they cover three main areas: catalysis, ion-exchange and sorption. Such synthesis can be scaled up to industrial level. Furthermore, the forms can also be adjusted depending on specific tasks (**Fig. 13**).

All currently known types of zeolites are systematized and classified. Structures, formations and properties are collected and most of them are stocked into an electronic database of the International Zeolite Association. IZA exists since 1977. Thanks to the activities of this organization, all confirmed topologies of zeolite frameworks are recorded, the data transferred to IUPAC and three-letter codes are assigned. At the moment, due to a constantly updated electronic resource, it is possible to get complete information on nearly 230 types of zeolites. These information reveal: material name, chemical formula, cell parameters, frame density, the number and type of building blocks, pore diameter, free volume, and also a moving 3D model.

---

[86] a) Hay, R. L. Geol. *Soc. Am., Spec. Papers* **1966**, 85, 1-130. b) Marantos I.; Christidis G. E.; Ulmanu M. *Natural Zeolites Handbook*, **2011**, 19-36

[87] http://www.minerant.org/home.html

[88] a) Anderson, M. W.; Agger, J. R.; Thornton, J. T.; Forsyth, N. *Angew. Chem. Int. Ed. Engl.* **1996**, 35 (11), 1210-1213. b) Mintova, S.; Olson, N. H.; Bein, T. *Angew. Chem. Int. Ed. Engl.* **1999**, 38 (21), 3201-3204.

2. Zeolites: what do we know about them?

2.1. Composition

Zeolites belong to the tectosilicate family of minerals. These materials are highly crystalline containing silicate (**Fig. 14**) and oxides of other metals. Their general formula for one-unit cell of aluminosilicates is given by:

$M_{x/n}(AlO_2)_x\ (SiO_2)_y \bullet {}_zH_2O$, where

M - is a cation, counterion, balancing the negative charge of the framework (Na, Ca, Mg)
x - is the amount of Al in one-unit cell
n - is the counterion charge
y - is the number of Si in one-unit cell
z - is the amount of water in the channel system

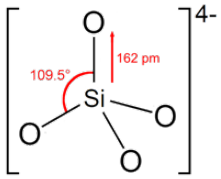

Figure 14. The primary unit of zeolite, SiO_4 tetrahedron

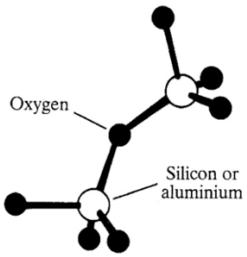

Figure 15. The basic constitution of aluminosilicates

In aluminosilicates, the framework consists of SiO_4 and AlO_4 tetrahedra linked by oxygen atoms. In **Fig. 15**, tetrahedra of silicate $[SiO_4]^{4-}$ and aluminate $[AlO_4]^{5-}$ are visualized. The SiO_4 tetrahedron is neutral because the Si atom formal charge (4^+) is balanced by the surrounding four oxygen atoms, each sharing a 2^- charge with the next tetrahedral atom. The Al atom with a formal charge of 3^+ is also associated with 4 oxygen atoms; this leave one unbalanced negative charge. [89] Therefore, the framework is negatively charged, and zeolite cavities or channels need to contain counterions to get neutrality of charge within the material.

Counterions in industrial or natural zeolites are usually alkali or alkaline earth metal cations, ammonium or simply protons. But today, using post-modification, counterions can be replaced with almost any metal cations or protons.

Due to this particular corner assembly, and the ability to change the angle between the tetrahedral element (called T-atom) and oxygen, multiple combinations of the tetrahedral framework and diverse structures arise. Channels of various sizes and shapes as well as pores can exist and generate a specific microporosity for each type of organization. Besides, the void volume of cavities and channels contains water molecules.

It is worthy to note, that a direct link between two AlO_4 units is impossible, since the negative charges on aluminates are unfavorable for building connections with each other a fact called the Löwenstein rule. [90] Even LTA zeolite which exhibits a high Al-content with a Si / Al = 1 possesses only alternating Si-O-Al-O-Si bonds.

Aluminosilicate zeolites are the most used in industry and the most well studied. But a variety of chemical compositions have been created for specific applications in which other metals act as the initial unit. About 20 other elements have been included in the tetrahedral positions in the framework. [91] These can be cations with a valency different from Si^{4+} (3+, 2+), that is allivalent, or with the same valence with Si^{4+}, that is isovalent. Cations of various sizes and valences from Li^+ to Ti^{3+} (as well as B^{3+}, Fe^{3+}, Ga^{3+}) range can be included in the tetrahedral framework. Although preserving the frame, these modifications retain the structural features and change the

[89] Cejka J., Corma A., Zones S., *Ed. WILEY-VCH Verlag GmbH & Co. KGaA, Weinheim,* **2010**, pp 173
[90] Loewenstein W, *Am. Mineral.* **1954**, 39, 92-96.
[91] http://europe.iza-structure.org/IZA-SC/ftc_table.php

chemical properties. [92] The present Thesis will not describe all the diversity of the zeolite world, but will focus on aluminosilicates.

By a proper understanding of the internal structure of a zeolite, we can "tune" properties: modify the chemical composition (for example, Si/Al ratio or counterions), change the 3D organization and thus the pore size.

2.2. Types and structures.

Tetrahedral TO_4 (T-being Si or Al) unit is the first and smallest building block, which is called the structural unit. They create what is called the secondary structural unit (SBU) with different arrangements when those tetrahedra are interconnect, in a special way relative unit.

Fig. 16 shows the three levels of self-organization of primary tetrahedra from simple to complex. For simplicity, only tetrahedra are indicated here with black dots and oxygens, balance ions, water are omitted. Rings with four to six tetrahedra are quite common (**Fig. 16 a**). They can self-organize into double 4 and 6-membered rings (D4R, D6R) (**Fig. 16 b**). More complex polyhedra can also be made: cancrinite cage, sodalite or β-cage and the α-cage (**Fig. 16 c**).

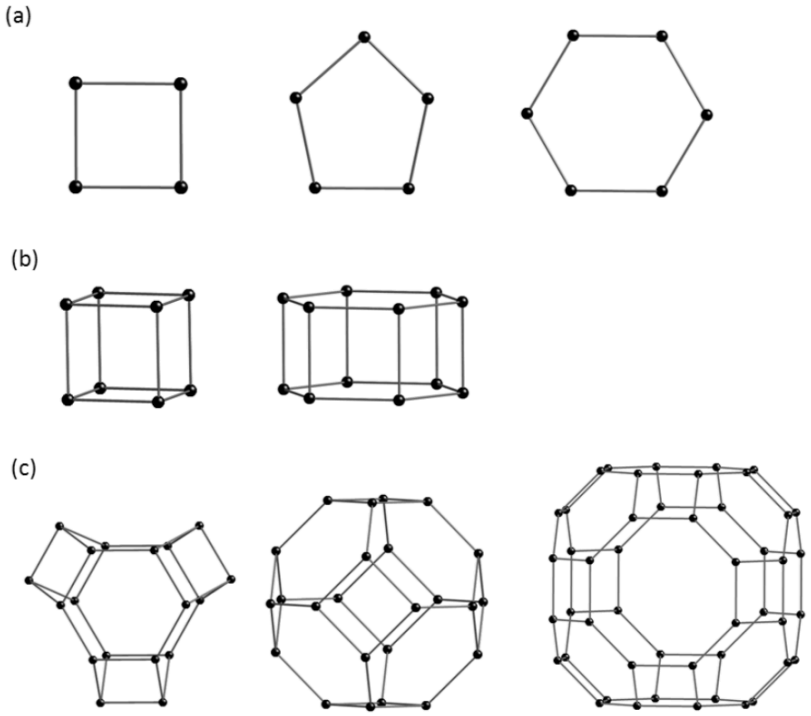

Figure 16. Some examples of SBU organization of primary tetrahedra from simple to complex: a) rings with different numbers of tetrahedral cations (4MR, 5MR, 6MR), b) D4R, D6R, c) cancrinite cage, β-cage and α-cage.

Cage can connect to itself in different ways, producing the framework of the most widely used zeolites in industry. Zeolites of the type: LTA (A), FAU (Y), MOR (Mordenite), MFI (ZSM-5), BEA (BETA), FER (ferrierite) are the most studied. Some of these structures are shown in the **Fig. 17-18**.

[92] Martínez C., Pérez-Pariente J. *Ed. Universitat Politècnica de València,* **2011**, pp 17-19

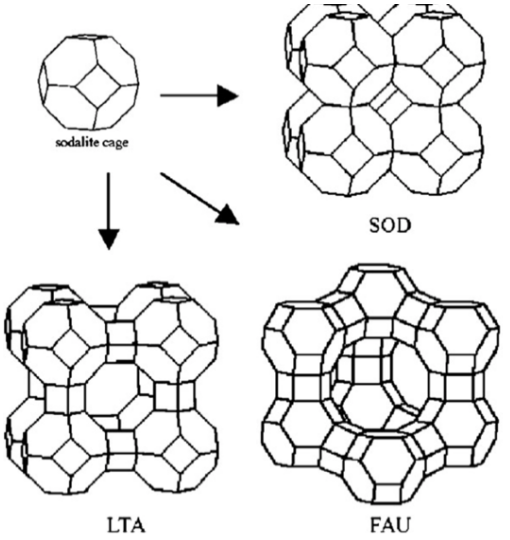

Figure 17. Three types of zeolite formed from β-cage: SOD, LTA, FAU [93]

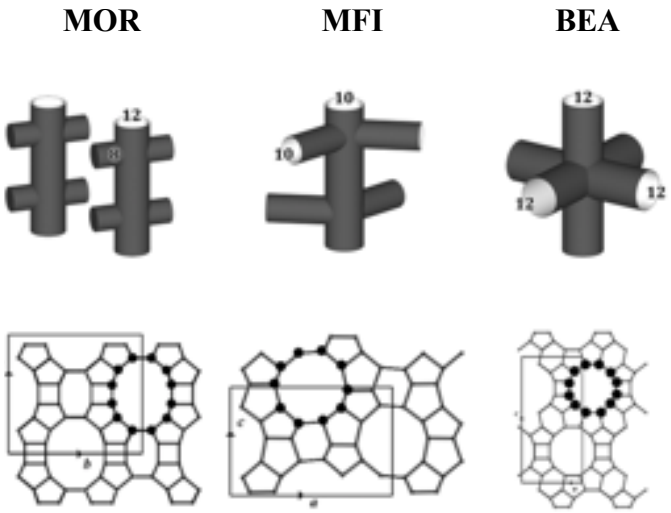

Figure 18. Schematic drawing of the channels structure for the zeolites MOR, MFI, BEA [94]

According to IZA, a large variety of different zeolite structures exists, each one being unique in terms of crystalline structure, chemical composition and physical properties.

The size of the corresponding channels and pores and their organization in space will drastically influence the crystal structures. Zeolite pore sizes roughly vary between 0.3 - 2 nm (**Fig. 19 a-d**). They can be divided into four subspecies:

a. 8-membered ring - small pore, 0.3 - 0.45 nm (LTA)
b. 10-membered ring - medium-pore, 0.45 - 0.6 nm (MFI)
c. 12-membered ring, large-pore, 0.6 - 0.8 nm (FAU)
d. 14 and more-membered ring, super large, 0.8 - 2nm (UTD)

For example, the channels inside the crystal can be one, two or three-dimensional. From the point of view of maximizing the molecular diffusion and adsorption-desorption properties, the last two are the most interesting.

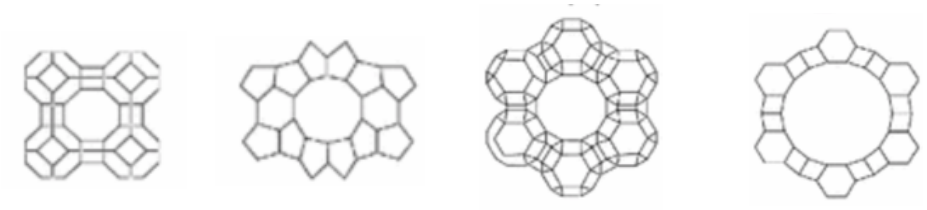

Figure 19: Schematic representation of pores such zeolites as LTA, MFI, FAU, UTD [95]

[93] Schwanke A. J.; Balzer R., Pergher S. *Eds Martínez & Kharissova & Kharisov Handbook of Ecomaterials* **2018**, 1-12
[94] Hartmann, M.; Machoke, A. G.; Schwieger, W. *Chem. Soc. Rev.* **2016**, 45 (12), 3313-3330.
[95] Xu, M.; Mukarakate, C.; Robichaud, D. J.; Nimlos, M. R.; Richards, R. M. *Top Catal,* **2016**, 59 (1), 73-85.

2.3. A typical case: FAU zeolites X and Y

Faujasite or FAU is one of the naturally occurring zeolites. [96] It is also one member from the "big five" zeolites used in industry. Synthetically, two subtypes X and Y can be obtained. Faujasite X is a zeolite with the highest Al content; usually, its Si / Al ratio is 1-1.5. [97] In turn, faujasite Y is enriched with silica, and its Si / Al ratio is above 2.

General formula for faujasite:
$(M)_{29}\ (H_2O)_{240}\ [Al_{58}Si_{134}\ O_{384}]$

The skeleton of zeolite Y is formed by sodalite cells that are articulated with hexagonal prisms (double six-membered rings, D6R). Such a connection of a sodalite cell and a hexagonal prism is called a “sodalite lantern”. This construction is repeated six times and forms a twelve-membered ring. This ring forms a large cavity, which is called a super cage. This cavity is accessible through a system of three-dimensional channels and cavities throughout the structure.

The total number of elements in the unit cell of faujasite is 8 sodalite cells, 16 double six-membered rings and 8 cavities (**Fig. 20**).

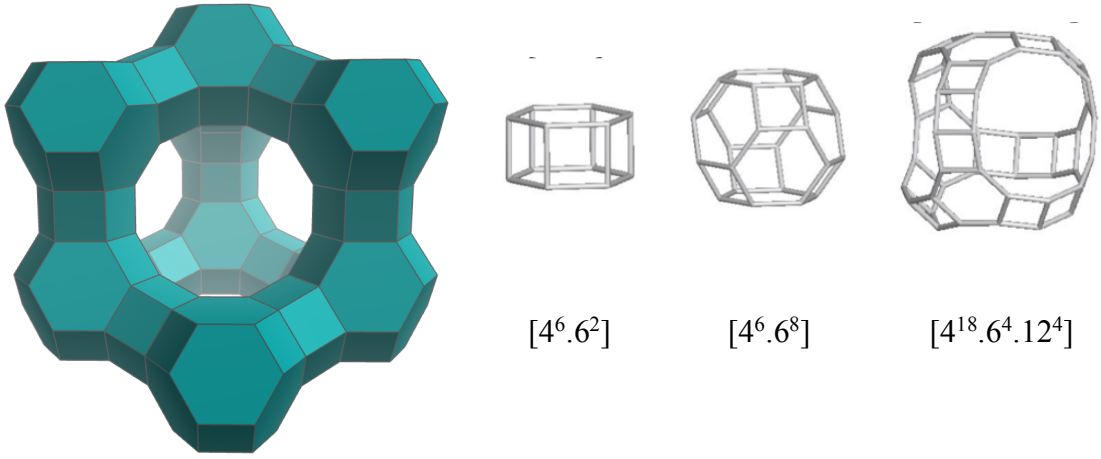

Figure 20. Construction of faujasite. [98] Unit cell size: a = 24.3 Å. The pore size of the supercell is 7.35 x 7.35 Å and in the sodalite cell 2.53 Å. Size (diameter) of the supercage 11.24 Å

The cations of balance (M) in faujasite can be: Ca^{2+}, Mg^{2+}, Na^{+}, and others. The places of their location are an important parameter that determines the catalytic properties and the possibility of adsorption. As we have already described in Chapter 2.1, negatively charged tetrahedra are balanced by metal cations, the cation location is thus mainly around aluminates, according to the following scheme (**Fig. 21**): (I) hexagonal prisms 1 and 1’, (II) sodalite cells 2 and 2’. These two locations are considered the most preferable, because they allow minimizing cation-cation repulsion together with interaction with negative tetrahedra sufficient. Position (III) in supercage can also, happens but rarely, after filling the first two positions.

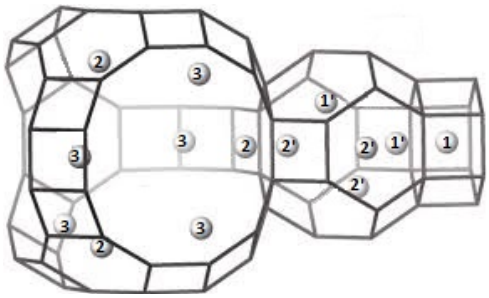

Figure 21. Localization of cations in the FAU cavities.

[96] Damour, M. *Annales des Mines*, **1842**, 4 (1), 395-399.
[97] Frising, T.; Leflaive, P. *Microporous Mesoporous Mater.* **2008**, 114 (1-3), 27-63.
[98] Available from: https://chemicalstructure.net/portfolio/faujasite/

2.4. Properties of zeolites

2. 4. 1. Acidity and basicity

What are the active sites?

While working with zeolites and choosing this material for catalytic or cation exchange purpose, we have to pay attention to the following points:
- the creation of active centers and their interplay (number, distribution, force)
- to distinguish what active sites are necessary for a reaction: Brønsted and/or Lewis
- to know about the accessibility to those active sites

Active sites are located in the framework of zeolite or within its channels / cavities. Thanks to the need to neutralize the negative charge surrounding the Al tetrahedron, positively charged (metal, complex) are needed and allow generating the main properties associated to zeolites: the ability to perform cationic exchange and catalysis.

Acidity

According to general rules, a Brønsted acid is a substance that is ready to lose a proton. The faster this acid gives away its proton, the stronger will be the acidity of this proton. [99] Alternatively, a Lewis acid is a substance possessing a free orbital, ready to accept a pair of electrons.

Acid sites in zeolites can be obtained through cationic exchange with ammonium salt and calcination according to the following equations:

$$NH_4^+ + Na^+Z^- \xrightarrow[-Na]{} NH_4^+Z^- \xrightarrow[-NH_3]{\approx 300 - 400\ ^\circ C} H^+Z^-$$

where Z - represents the negatively charged zeolite framework

There are three locations for **Brønsted** acid sites in zeolites:

- Hydrogen proton is associated with oxygen on the oxygen bridge Si-O(H)-Al (**Fig. 22 - a**), at the site of bonding of two tetrahedra of aluminate and silicate.
- The second location, related to weaker Brønsted acid site, is the hydroxyl group of SiOH (**Fig. 22 - b**), usually formed at places of structural defects or at the outer surface of the zeolite. Indeed, the continuity between the tetrahedra is interrupted at the surface. It can also occur upon partial destruction of the structure which may occur during any impact on the zeolite, such as high temperatures (calcination), alkali, acid or steaming treatment.
- A third type of hydroxyl groups may exist at aluminium nodes, that lead to the formation of AlOH (**Fig. 22 - c**). If the type of impact is strong enough, extra-framework aluminum species (EFAl) can be produced.

The Brønsted acid strength increases if the amount of aluminum in the framework decreases, as the average Sanderson electronegativity value increases. [100] It is logical to conclude from this that the zeolite with low aluminum content, that is to say when the Si / Al ratio is high, the strength of the acid is higher. For example, applying this concept to a FAU, a zeolite with Si/Al ~ 1 will exhibit lowest acid strength, despite the presence of numerous sites.

---

[99] Olah G. A.; Prakash G. K. S.; Molnar A.; Sommer J. *John Wiley & Sons, Inc.* **2009**, pp 39
[100] Cejka J., Corma A., Zones S., *WILEY-VCH Verlag GmbH & Co. KGaA, Weinheim*, **2010**, pp 495

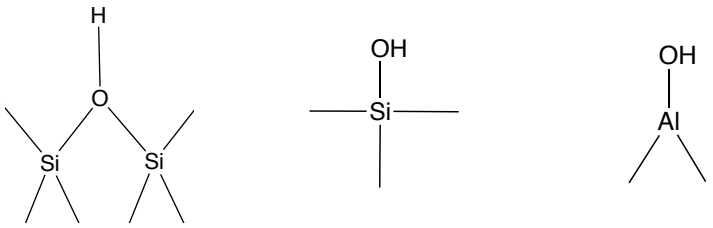

(a) (b) (c)

Figure 22. Schematic representation of the different types of hydroxyl groups in zeolites.

Usually, a homogeneous distribution and small amount of acidic sites are present in high silica zeolites. If the material has a high Al content, the number of acid sites increases. With a high concentration of acid sides, differences in acid strength can be expected. Highly acidic sites are those of aluminum tetrahedra.

Accordingly, the concentration of active sites depends on the primary units and their chemical composition. The amount of aluminum in the frame is directly related to the number of active centers, as well as to hydrophilicity / hydrophobicity (inverse relationship)

Basicity

Due to the inherently acidic nature of zeolites, their use as basic catalyst remains marginal. In order to give zeolite some basic character in catalysis, it is necessary to introduce free cation from the alkaline group, but with a large radius, for example, Cs. [101]

Thus, the best basic catalyst will be built from zeolites which have the highest possible Al content, with a Si / Al ratio close to 1.

In order to prevent a possible negative effect of zeolite acidic sites, ion exchange with alkaline cations is carried out. As a test of zeolite basic properties, Knoevenagel condensation can be performed. [102]

2. 4. 2 Shape selectivity

To improve catalyst efficiency, it is possible to vary not only the parameters of acidity, but also choose the shape of the zeolite, the type of pores and channels. Knowing the main factors, one can dig in depth to the possibility of using what is called the shape selectivity.

Weisz and Frilette proposed this term for the first time in 1960. [103] Shape selectivity occurs when the reactivity of a substance depends on its size and / or its spatial organization and when the selectivity of the reaction depends on the type of zeolite, its micropores and cavities.

There are three types of shape selectivity:

1. RSS (reactant shape selectivity). In this case, selectivity is obtained depending on the different sizes of reagents prior entering the zeolite. In other words, from a mixture of components, only the substances having a diameter inferior to the pores can diffuse within the pores. In contrast a larger molecule cannot diffuse inside and its transformation does not occur (**Fig. 23 - a**).
2. PSS (product shape selectivity). This type of selectivity is possible if the sizes of the reagents are very small, so they can freely and quickly penetrate inside, react at the active centers, but, only those reaction products, whose size is sufficiently small, quickly leave the channels (**Fig. 23 - b**).
3. TSS (transition shape selectivity). In this case, the reaction is governed by the possibility to form transition states with a suitable size (**Fig. 23 – c**).

---

[101] Barthomeuf, D. *Studies in Surface Science and Catalysis (Catal. Adsorpt. Zeolites)*. **1991**, 65, 157-169.
[102] Corma, A.; Fornes, V.; Martin-Aranda, R. M.; Garcia, H.; Primo, J. *Appl. Catal.* **1990**, 59 (2), 237-248.
[103] Weisz, P. B.; Frilette, V. J. *J. Phys. Chem.* **1960**, 64, 382.

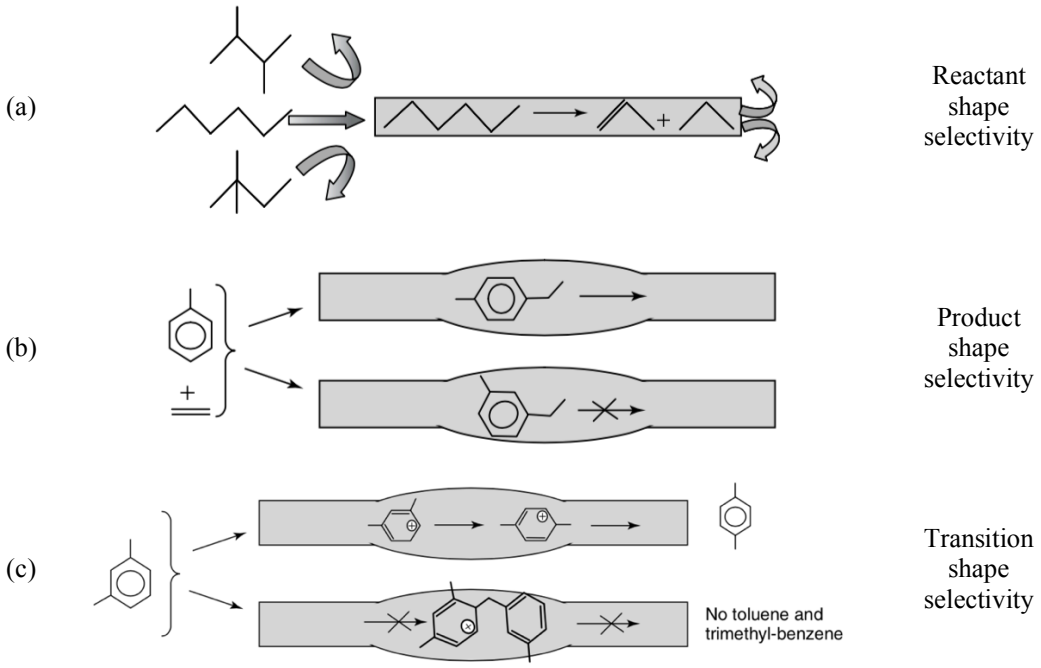

Figure 23. Schematic representation of the concept of shape selectivity.

Today, it is possible to calculate how the shape of a zeolite will affect the free energies of the formation of various components (this method is called "calculation of the free energy landscape of reacting systems" [104]). Such methods avoid practical errors and time loss.

2. 4. 3. Confinement effect

Two scientists have revealed and studied an unusual property of zeolites eventually called confinement effect.

- In 1979, Barthomeuf observed that a particular distribution of Al-sites and extra-framework cations creates an electric field gradient, which affects the reactivity of alkanes. She assumed that there was a weakening of some C-C bonds. [105]
- In 1986-88, Derouane first introduced the term "confinement" [106] describing some of the abilities of zeolites, although in his earlier works the concept of "nest effect" was used.

Generally, confinement effect combines two different forces: the Pauli repulsion acting at short range and Van der Waals interacting on a long range. This combination makes zeolite a unique material that exhibits enhanced diffusion (so-called molecule super mobility), shape selectivity and selective adsorption. The combination of these two forces is possible due to the angular assemblies of frame tetrahedra or the curvature of the framework. [107]

2. 4. 4. Zeolites - solid superacids

Due to the combination of three factors (acidic properties, shape selectivity, confinement effect), zeolites are sometimes called "solid superacids". [108] Usually, a Brønsted superacid [109] is defined as any acid system that is stronger than 100% sulfuric acid, and in the case of Lewis superacid system, it should be more electron deficient than aluminum trichloride.

---

[104] Smit, B.; Maesen, T. L. M. *Nature (London, United Kingdom)* **2008**, 451 (7179), 671-678.
[105] Barthomeuf, D. *J. Phys. Chem.* **1979**, 83, 249.
[106] Derouane E. G., Andre J. M.; Lucas, A. A. *J. Catal*. **1988**, 110 (1), 58-73
[107] Sastre, G.; Corma, A. *J. Mol. Catal. A: Chem.* **2009**, 305 (1-2), 3-7.
[108] Mirodatos, C.; Barthomeuf, D. *ChemComm,* **1981**, (2), 39-40.
[109] N. F. Hall and J. B. Conant, *J. Am. Chem. Soc.* **1927**, 49, 3047.

In addition to superacids such as the Lewis acid: SbF_5, BF_3 or the Brønsted acids: HSO_3F, CF_3SO_3H, binary (or ternary) systems are also known. They are produced by mixing strong Brønsted acids HF-HSO_3F or Brønsted – Lewis acids HSO_3F-SbF_5, HF-BF_3.

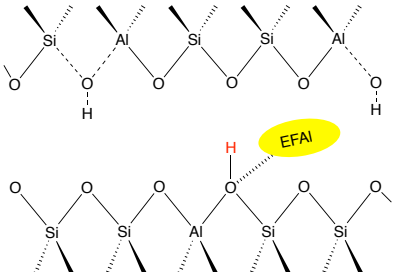

Figure 24. Schematic representation of the appearance of superacid sites in the zeolite structure

A similar behavior and rationale for superacidity in zeolites was given in 1981. It relies on the concept of partial transfer (or displacement) of electron density from OH to EFAl, which reduces the interaction strength between oxygen and hydrogen atoms and therefore leads to an increased proton mobility. As a result, it may create some "superacid" Si-O**H**$^+$-Al sites. (**Fig. 24**)

However, zeolite surfaces are not uniform, so it is difficult to measure their acidity. There are many methods (microcalorimetry of adsorbed probe molecules, amine thermal desorption, IR spectroscopy, MAS-NMR [110]), but so far checking the catalytic activity of zeolite on acid-catalyzed reactions remains the most effective.

3. Main applications of zeolites

Zeolites are materials whose possibility of application is so wide that it is only limited by human imagination. The history of these nanoreactors discovered more than two hundred and sixty years ago, seems just to begin.

From the world volume of zeolite consumption, it can be deduced that, natural zeolites are mostly used (60%) while synthetic zeolites account for the remaining 40%. Such large amount of natural zeolites use is due to their cheapness from 0.04 to 3.5 dollars per kg. Natural zeolites are mainly used in agriculture, animal food additives, hygiene, water purification and environmental protection and as construction material (cement additives). Synthetic zeolites are much more expensive, ranging from 2 to 20 dollars per kg. [111] Nevertheless, they exhibit a well-defined structure and properties, unlike natural zeolites, which often containing impurities of metals or mixture of zeolite phases.

Surprisingly, about 65% of all synthetic zeolites are employed as laundry detergents, as we highlighted in Chapter 1. In these detergents, poly phosphates are replaced by «green» zeolites.

According to 2018 data, about 18% are employed as catalysts and about 14% as adsorbers. However, there is a growing interest in the later area. The use of zeolites as drying agents or traps for impurity gases or for volatile organic compounds (VOCs) is correlated with a tendency to set cleaner processes.

3.1 Cationic exchange

As we have already mentioned (see **Chapter 2**), the smallest primary building in a zeolite is a T-atom surrounded by four oxygens. The presence of Al in the framework induces a negative charge, therefore cations are required to compensate this charge. Accordingly, the higher the aluminum content in the zeolite, the more the zeolite will contain counter-ions

As these cations are not incorporated into the framework, they can be displaced. This can be done by liquid-phase ion exchange or solid-state ion exchange. This process is commonly exploited for «water softening» during the washing process. In washing powders, multivalent ions from water, such as Mg^{2+}, Ca^{2+}, Fe^{3+}, are replaced with Na^+, K^+ from zeolite, usually using sodalite

[110] Derouane, E. G.; Vedrine, J. C.; Pinto, R. R.; Borges, P. M.; Costa, L.; Lemos, M. A. N. D. A.; Lemos, F.; Ribeiro, F. R. *Cat. Rev. - Sci. Eng.* **2013**, 55 (4), 454-515.
[111] IHS chemical. *Chemical economics handbook: IHS zeolite.* **2016**. Available from: www.ihs.com

or LTA zeolite type. As a result, to this ion-exchange process, surfactants freely migrate to the places of contamination and finally act as tensioactive agents.

This ion-exchange properties of zeolites as filters and barriers is also exploited to recover heavy metals and radionuclides present in ionic form, often released to the environment by technological processes or accidents. For example, zeolites have been used to trap radioactive Cs, released by the largest man-made accident, that caused the contamination of large areas after an explosion in April 1986 at the Chernobyl power plant in Ukraine.

Both natural and synthetic zeolites are used to purify water and soil from heavy metal cations, including radioactive Cs, Sr, Rb. The first is mainly clinoptilolite, and the second are zeolites A and X.

3.2 Adsorption

Adsorption is the concentration of a substance from a gas or liquid phase on the surface of a solid, as well as in its pores. The solid is called the adsorbent, and the adsorbed substance is the adsorbate.

For zeolites, their high surface curvature and, large internal volume allows a large capacity of adsorption.

The pores in the classical zeolites are not large, for example for FAU, MFI, LTA they are less than 7.5 Å. Accordingly, it is only possible to adsorb small molecules, such as water, carbon dioxide and sulfur or organic molecules of small-size. Therefore, zeolites can be used in separation or capture processes, such as the removal from gas mixtures purification of natural gas or the trapping of volatile organic compounds (VOCs). The last aspect is very interesting for us, because a large number of manufactories are involved in the processes of emissions like volatile organic compounds (VOCs). The negative effects of these organic compounds: photochemical smog, accelerated global warming and adverse effects on human health, in particular, eye irritation and breathing problems. The study of zeolites, as adsorbers, is increasing and we believe that in the future this trend will further gain popularity.

3.3 Catalytic properties

3. 3. 1. Cracking and hydrocracking

Zeolites are extensively used for petroleum refining. [112] Cracking and hydrocracking of oil are the most important processes in terms of tons of zeolites involved. [113]

Cracking is the largest chemical process using zeolites. After preliminary purification (dehydration, desalting, removal of impurities), crude oil is distilled at atmospheric pressure and at 350 °C, and then distilled under vacuum. Depending on the temperature, different products are recovered: gases (up to 30 °C), naphtha (up to 160 °C), kerosene (up to 230 °C), light and heavy gas oils (up to 340 °C and 430 °C respectively), fuel oil (up to 550 °C), tar (above 560 °C).

Hydrocarbon mixtures boiling at temperatures above 360 ^{o}C are then submitted to cracking catalyzed by zeolites. Several reactions occur during this cracking with saturated hydrocarbons: conversion of paraffins and naphthenes, isomerization, dealkylation, oligomerization and coke formation.

Which zeolite catalyst is used? For this process, three-layer spherical particles with a diameter around 60 μm are used. Their core is made of zeolite Y, more precisely USY in its acidic H form. The core matrix is surrounded by a layer made of amorphous aluminosilicate with a wide mesoporosity. This layer is used for heat removal from zeolite during regeneration processes. The particles are then covered by a shell for reduction of abrasion.

The main task of all the developments and research on zeolite catalysts for petrochemistry relies on maximizing the selectivity towards final products and minimizing the formation of coke.

---

[112] Rabo, J. A.; Schoonover, M. W. *Appl Catal A Gen.* **2001**, 222 (1-2), 261-275.
[113] Rigutto, M. Eds. Cejka, J.; Corma, A.; Zones, S. *Zeolites and Catalysis,* **2010**, 2, 547-584.

3. 3. 2. Organic synthesis

In addition to cracking and hydrocracking of petroleum, the unique properties of zeolites such as the presence of numerous acid sites (Lewis or Bronsted), shape selectivity and possible confinement effects zeolites have been used for applications in organic synthesis. With a large variety of zeolite types and possible post-modifications like cationic exchange, scientists have the opportunity to use zeolites as specific heterogeneous catalysts. Replacing the pristine zeolite cations with rare earth or transition metals ions, or with protons, unique solid catalysts can be produced to solve organic problems

In this work, we will only focus on organic reactions with acidic zeolites.

In the review written by S. Chassaing and co-workers, [114] two main applications of H-zeolites in organic synthesis are reported: **the functionalization of aromatic compounds** and **the chemistry of the carbonyl group.**

3. 3. 2. a) Functionalization of aromatic compounds:

- Halogenation of aromatic compounds. ***Chlorination of nitrobenzene***

Halogenation of aromatic compounds is mainly represented by chlorination reactions, in view of the industrial importance of chloroaromatics as bulk chemicals. Aromatics such as toluene, phenol or tert-butylbenzene can be chlorinated over H-zeolites (X, Y, ZSM-5). The main positive factor for using zeolites for this purpose is the absence of polyhalogenation and a clear tendency to mono-halogenated product selectivity. Furthermore, even electrodeficient aromatics can be chlorinated due to the superacid properties of zeolite.

As an example, the chlorination of the deactivated nitrobenzene has been carried out with a solid acid by our research group (**Scheme 34**). [115]

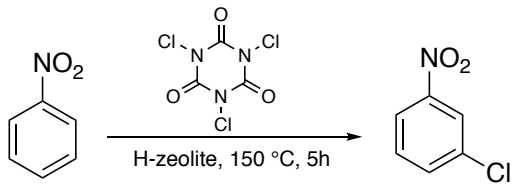

Scheme 34: The chlorination of nitrobenzene promoted by H-zeolite.

Trichloroisocyanuric acid (TCCA) is an inexpensive, available chemical reagent used as a disinfectant and bleaching agent for swimming pools. This substance can be used as a source of chlorine, the content of which is about 45% in weight. TCCA was used in the chlorination of nitrobenzene reaction promoted by various solid acids. The authors found that H-USY zeolite showed the best results. It showed the highest conversion (39%) and selectivity toward monochlorinated compound (99%). After removing all EFAl species by complexation with EDTA, it was possible to increase the conversion to 64% and keep the high selectivity (90–99%) towards the monochlorinated compound.

- Friedel-Crafts reactions

Friedel-Crafts reactions are widely used to produce aromatic ketones, which are further used in fine chemistry. In general, Friedel-Crafts reactions allow **alkylations** and **acylations** of aromatic compounds if acid catalysts are present in the reaction mixture. Usually, Lewis acids ($AlCl_3$, $FeCl_3$, $TiCl_4$) or Bronsted acids (HF and H_2SO_4) are used as acid promoters. Meanwhile, the presence of Lewis and Bronsted acids in zeolites and confinement effect renders possible

---

[114] Chassaing, S.; Beneteau, V.; Louis, B.; Pale, P. *Curr. Org. Chem.* **2017**, 21 (9), 779-793.
[115] Boltz, M.; de Mattos, M.C.S.; Esteves, P.M.; Pale, P.; Louis, B. *Appl. Catal. A*. **2012**, 449, 1-8

carrying out these reactions with zeolites. The mechanisms of these homogeneous and heterogeneous reactions are similar. [116]

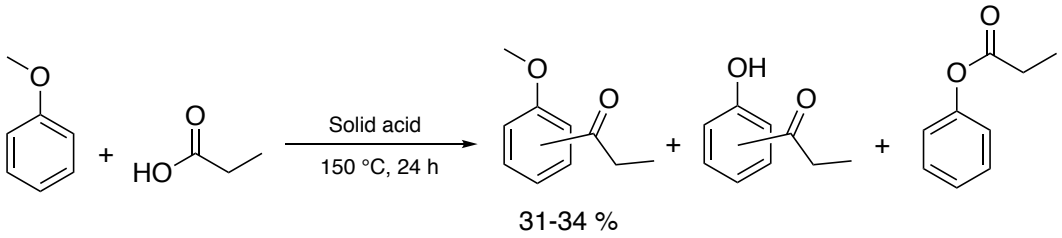

Scheme 35: Friedel-Crafts acylation of anisole with propanoic acid promoted by solid acid.

As an example, Friedel-Crafts acylation of anisole with propanoic acid has been reported (**Scheme 35)**. [117] The authors tested the catalytic activity of different H-zeolites structures (BEA, MFI) and of zeolites partially exchanged with metals (Ni, Ag, Fe). However, loaded metal cations impaired propanoic acid (PA) conversion. H-zeolites induced a better conversion, especially ZSM-5, with which PA conversion was about 75%. The yield of ortho and para-acylated products ranged from 31 to 34%. Among the proposed series, ZSM-5 led to the highest TOF value of 0.09 h^{-1}.

3. 3. 2. b) Chemistry of the carbonyl group

- Protection reactions

Another effective use of zeolite in organic synthesis is in protection reactions. These reactions are necessary for multistep synthesis, when it is necessary to temporarily deactivate a highly reactive group during the synthesis.

Some functional groups may be protected in the presence of H-zeolites: carbonyl group, diols on sugar derivatives. As an example, is presented below a method of preparation of fructone, [118] which is a flavoring agent (apple smell) (**Scheme 36)**.

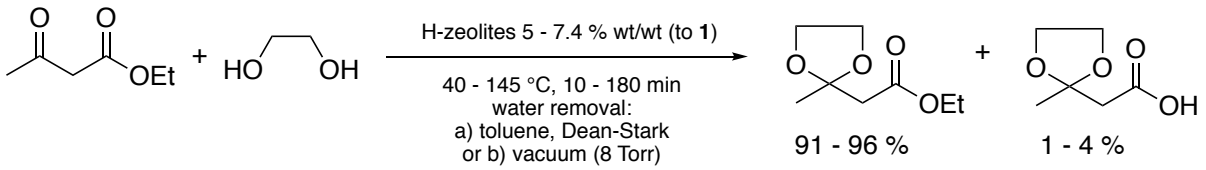

Scheme 36: Application of H-zeolite in protection reactions to produce fructone.

Usually, to produce ethyl 3,3-ethylenedioxybutyrate, strong acids (p-toluenesulfonic acid) are used, but this synthetic method leads to a by-product (3,3-ethylenedioxybutanoic acid), which can change organoleptic characteristics and reduces the overall yield of the desired ester. After testing several H-zeolites, two zeolites (Beta and USY) with high Si/Al (25-50 for Beta and 20 for USY) were selected. After optimization, fructone was obtained with high conversion and almost 100% selectivity.

- Additions on α, β-unsaturated carbonyl derivatives

Koltunov *et al.* [119] shed light on the fact that the cyclization of arylvinylketones to 1-indanones is possible not only in acidic or superacidic conditions, but also in H-USY zeolites.

---

[116] Sartori G.; Maggi R. *Chem. Rev.* **2006**, 106 (3), 1077-1104.
[117] Bernardon, C.; Ben Osman, M.; Laugel, G.; Louis, B.; Pale, P. *C. R. Chim.* **2017**, 20 (1), 20-29.
[118] Climent, M.J.; Corma, A.; Velty, A.; Susarte, M. *J. Catal.* **2000**, 196 (2), 345-351.
[119] a) Koltunov, K.Y.; Walspurger, S.; Sommer, *J. Tetrahedron Lett.*, **2005**, 46, 8391-8394; b) Sani Souna Sido, A.; Chassaing, S.; Kumarraja, M.; Pale, P.; Sommer, J. *Tetrahedron Lett.*, **2007**, 48 (33), 5911-5914.

Possible mechanisms for this reaction are considered through dicationic (or superelectrophilic) intermediates (**Scheme 37**).

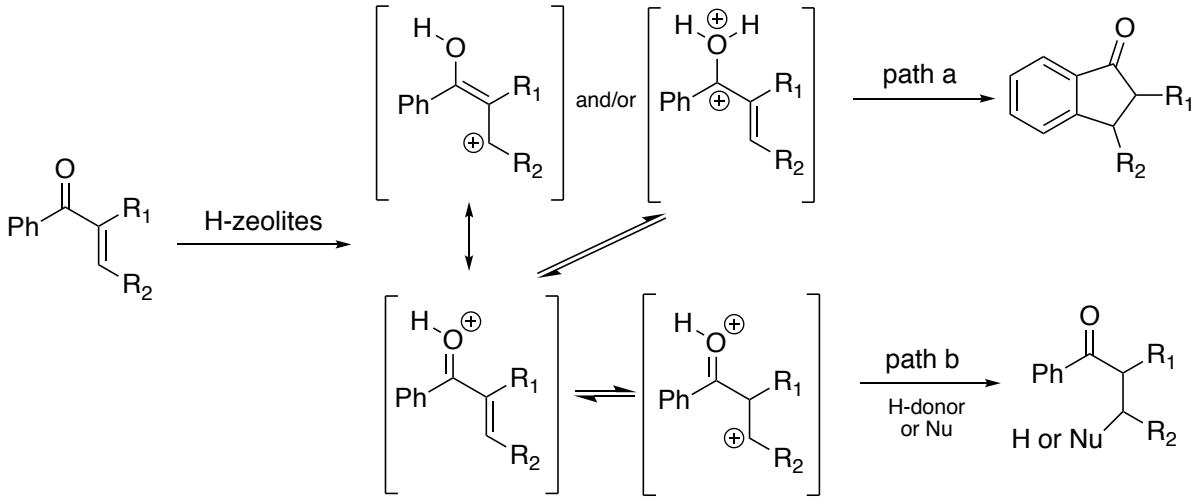

Scheme 37: Possible reaction mechanisms of arylvinylketones under the action of H-zeolites.

Arylvinylketones were tested for assessing the possible of mono- or/and di-protonations by zeolites. With this possibility, various intermediate products can be formed, which in turn can lead to different reaction products. Monoprotonation or/and diprotonation can take place, which may lead to either a Friedel-Crafts mechanism or Nazarov mechanism for the cyclization of the starting material (path a). The dication can be trapped by a nucleophile or an H-donor, the addition to which corresponds to a 1,4-reduction of enones (path b).

3. 3. 2. c) Intermolecular hydroarylation of carbon-carbon triple bond.

Under the action of an acidic H-USY zeolite, hydrophenylation of arylacetylenes were obtained. [120] It is nevertheless necessary that the starting arylacetylenes contained electron-withdrawing groups in their structure, such as SO_2Ph, $PO(OEt)_2$, COMe, CO_2Me (**Scheme 34)**. The reaction mechanism is not specified; however, the publication mentioned that it probably proceeds through electrophilic activation of alkynes with the formation of dications, as in the example above (see **Scheme 38)**.

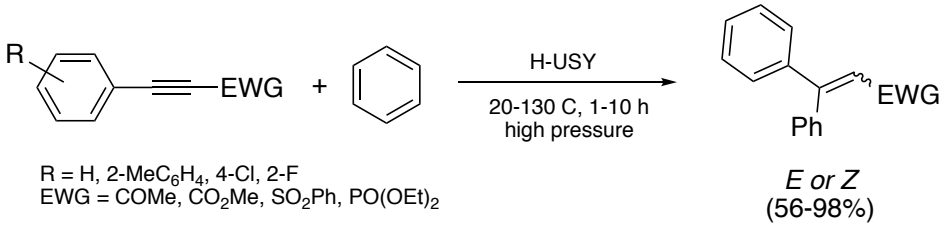

Scheme 38: Hydrophenylation of arylacetylenes promoted by H-USY zeolite.

In 2018, Vasilyev et *al.* performed the hydroarylation of triple bond of acetylenic tetrazoles, under the action of acidic zeolite H-USY (CBV-720). [121] These reactions formed arylated vinyl tetrazole derivatives (**Scheme 39)**. Reaction yields ranged from 52 to 81%. Here again, the formation of dicationc intermediates was postulated.

---

[120] Ryabukhin, D. S.; Vasilyev, A. V. *Mendeleev Commun.* **2016**, 26 (6), 500-501.
[121] Ryabukhin, D. S.; Lisakova, A. D.; Zalivatskaya, A. S.; Boyarskaya, I. A.; Starova, G. L.; Trifonov, R. E.; Ostrovskii, V. A.; Vasilyev, A. V. *Tetrahedron,* **2018**, 74 (15), 1838-1849

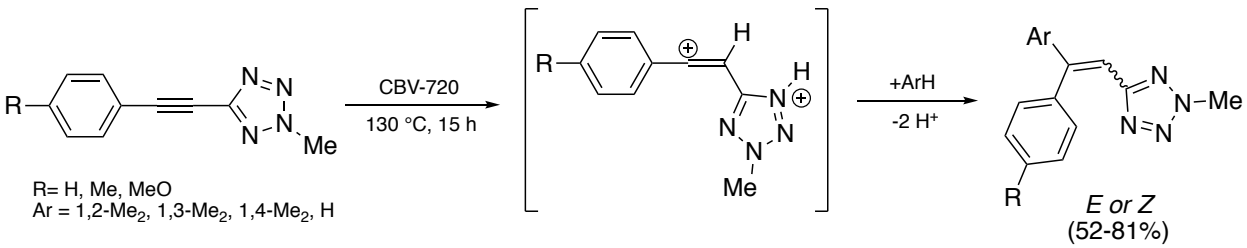

Scheme 39: Hydroarylation of acetylenic tetrazoles under the action of acidic zeolite

3. 3. 2. d) Intramolecular hydroarylation of carbon-carbon triple bond

For the first time, the intramolecular cyclization of *N*-aryl of 3-arylpropynamides under the action of acidic zeolite H-USY was tested by Koltunov *et al.* in 2004. [122] *N*-phenyl amide without substituent was used as the starting material in the presence of 10 equivalents of zeolite, in benzene at 130 °C under reflux. In 1 h, the reaction showed complete conversion and high yield (95%). This test reaction was very interesting and promising because of its high efficiency and the ability to use safe zeolites compared to strong Lewis or Brønsted acids (TfOH, FSO_3H, H_2SO_4, $AlCl_3$).[123]

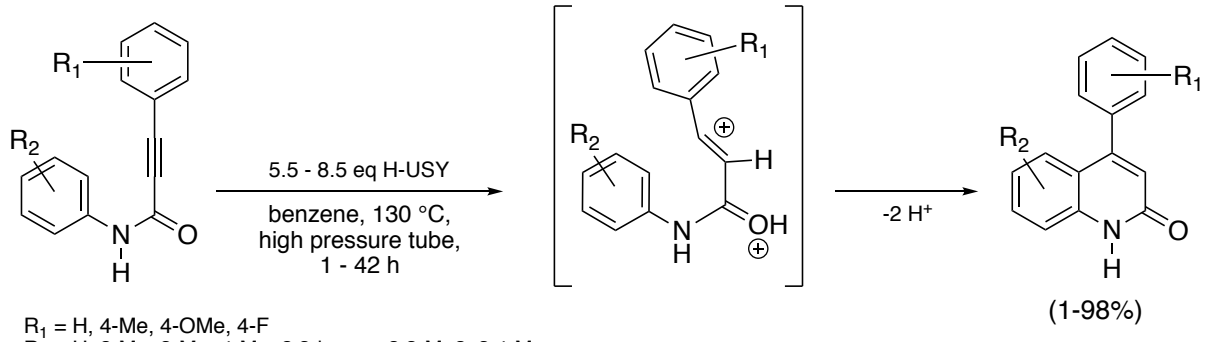

Scheme 40: The intramolecular cyclization of N-aryl of 3-arylpropynamides under the action of H-USY zeolite

In continuation of this work, a series of experiments was reported in a following article.[124] 4-aryl quinolin-2 (1H)-ones were obtained with 5.5 equivalents of USY zeolites (CBV-720), or 8.5 equivalents of USY zeolites (CBV 500), in benzene at 130 °C under reflux. Reaction times varied from 1 h to 42 h and yields from 1 to 97% (**Scheme 40**). It is worth noticing that, in order to extract all the components from the zeolite pores, the recovered zeolite was boiled in MeOH during 1 h.

3. 3. 2. e) Cycloaddition

A well-known example of cycloaddition remains the Diels-Alder reaction. Usually, this reaction is carried out under the action of Lewis acids. Several studies confirmed the possibility of using heterogeneous catalysts for such reactions.[125] For example, isoprene and methyl acrylate readily reacted in the presence of various zeolites (**Scheme 41**). ZSM-5 and Y were found as the most effective. Zeolite ZSM-5 was examined in more details and the following dependencies were established. It has been found that higher quality crystals contribute to higher productivity.[126] Notwithstanding the many transformations and optimizations made by the authors, yield of methyl 4-methylcyclohex-3-enecarboxylate remained low, due to high volatility of the product.

---

[122] Koltunov, K. Yu.; Walspurger, S.; Sommer, J. *Chem. Commun.* **2004**, (15), 1754-1755.
[123] Ryabukhin, D. S.; Gurskaya, L. Yu.; Fukin, G. K.; Vasilyev, A. V. *Tetrahedron* **2014**, 70 (37), 6428-6443.
[124] Ryabukhin, D. S.; Vasilyev, A. V. *Tetrahedron Lett.* **2015**, 56 (17), 2200-2202.
[125] Bernardon, C.; Louis, B.; Beneteau, V.; Pale, P. *ChemPlusChem*. **2013**, 78 (9), 1134-1141.
[126] Arichi, J.; Louis, B. *Cryst. Growth Des.* **2008**, 8 (11), 3999-4005.

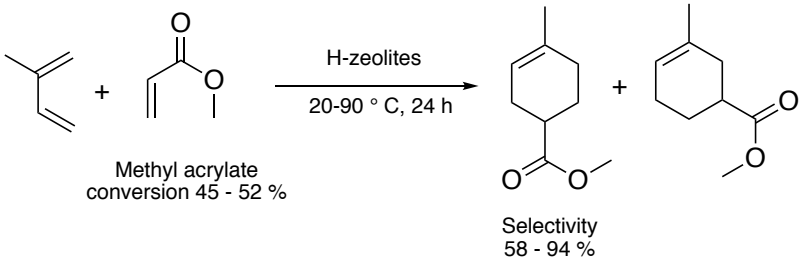

Scheme 41: The Diels-Alder cycloaddition reaction of isoprene and methyl acrylate in the presence of H-zeolites.

The Pechmann reaction appears popular for the synthesis of coumarins as we noted in Part I Chapter 1. Hegedues and Hell have proved that it is possible to use the clinoptilolite-type zeolite Ersorb-4 (E4a) (mineral belonging to group from row heulandite [127]) for the transformations of various phenols and β-ketoesters to 4-methylcoumarin derivatives (**Scheme 42**). [128] For the reaction, E4a with a pore size of 4 Å, was used in toluene as a solvent and at 110 °C during 3h. The yields of the reaction products were high. The effectiveness of the catalyst was almost unchanged after the third use of the catalyst.

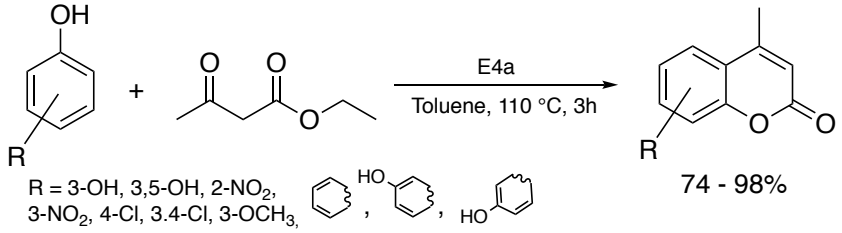

Scheme 42: The Pechmann reaction of various phenols and β-ketoesters under the action of acidic zeolite.

4. Mass transfer limitations and their solutions: generation of micro-mesoporous material

In all the applications mentioned above, molecules have to diffuse through and into zeolite particles. The resulting mass transfer is obviously dependent on zeolite structuration (crystal size and shape, pore size and shape).

Mass-transfer limitations are an important issue in heterogeneous-catalyzed reactions. The presence of only micropores in the zeolite structure leads to diffusion limitations. Creating a hierarchical porous structure in the catalyst increases the efficiency of diffusion and affects parameters such as activity, selectivity and catalyst lifetime.

4.1 Diffusion model: the Thiele-Weisz modulus and its consequences

Theories have been developed to better understand diffusion.

The Thiele-Weisz modulus (**Formula 1**) establishes the relationship between diffusion length in a particle (L), intrinsic rate coefficient (k_V) and effective diffusivity of an organic molecule (D_{eff}). [129]

$$\Phi = L \times \sqrt{\frac{k_V}{D_{eff}}} \qquad \textit{Form. 1}$$

When $\Phi \leq 0.1$, a full utilization of catalyst particles can be assumed and the experimental reaction rate equals the intrinsic rate of the chemical reaction, without any mass transfer limitation. [130] While increasing Thiele-Weisz modulus, only part of the catalyst particle is efficiently "used" and

---

[127] Ćwikła-Bundyra W. *Annales UMCS Sectio AA (Chemia).* **2011**, 66, 67-80.
[128] Hegedues, A.; Hell, Z. *Catalysis Letters.* **2006**, 112 (1-2), 105-108.
[129] Louis, B.; Ocampo, F.; Yun, H. S.; Tessonnier, J. P.; Pereira, M. M. *Chem. Eng. J.* **2010**, 161 (3), 397-402.
[130] Perez-Ramirez, J.; Christensen, C. H.; Egeblad, K.; Christensen, C. H.; Groen, J. C. *Chem. Soc. Rev.* **2008**, 37 (11), 2530-2542.

"seen" by the reagents. For example, in the case of Φ = 10, only 10% of the catalyst surface can be accessible, which is far from being efficient.

To keep the Thiele-Weisz module small, Perez-Ramirez offers 2 strategies: shorten the diffusion length (L) or increasing the effective diffusion capacity in the pores of the zeolite (D_{eff}) (if k_v constant). We are interested in the second strategy and will continue to study it.

As we mentioned in Chapter 2.2, a zeolite structure can have different structural geometries and the associated pore space. By manipulating various methods of synthesis, one can organize structures with small, medium and large pores. However, this is not the only one solution to solve the problem of diffusion and mass transfer. The secondary pore system or secondary mesoporosity increases the size and availability of a secondary network of pores, improves spatial diffusion. By changing the size of the micro-meso pores, you may be able to adjust selectivity, transition states, diffusion, and control the access to active sites. From the data existing in the literature, there are three main strategies to create efficient diffusion:

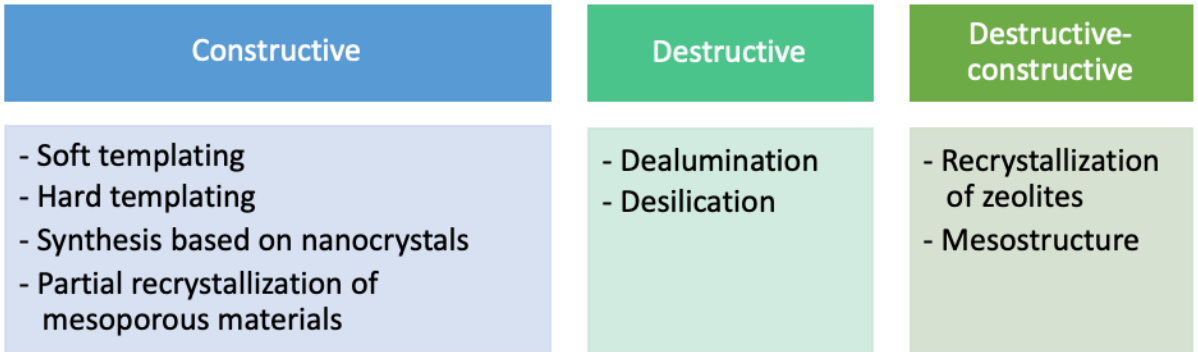

In order to understand which strategy is more suitable in our work, one may compile the data as done by Chal *et al*. They approached the creation of a new zeolite material in terms of economic costs, stability in hydrothermal conditions, field of application of the methods, possibility of using mesopores and their industrial introduction. [131] This can be compiled into graphs or tables (**Table 8**).

Synthetic method	Sub-method	Economic costs	Stability under hydrothermal conditions	Limits of sub-method application	The possibility of regulate mesopore	Flexibility in the Si/Al ratio	Industrial introduction
Constructive	Soft templating	Medium/ High	Medium/ High	Large	Yes/ sometimes	Yes	No
	Hard templating	High	High	Large	sometimes	Yes	No
Destructive	Dealumination	Low *	High	Medium	No	Medium	Yes
	Desilication	Low *	High	Low (Narrow, limits)	No	Low	No
Destructive-constructive	Recrystallization of zeolites	Medium	High	Large	Yes	Yes	No
	Mesostructure	Medium	High	Large	Yes	Yes	Yes

Table 8: Comparison of methods for creating synthetic zeolites in terms of economic costs, stability in hydrothermal conditions, field of application of the methods, possibility of using and their industrial introduction.
* If the zeolite was synthesized without a template

This table simply shows that the main weakness of the constructive method is its cost. Organic templates are expensive, compared to other methods, thus seriously hindering their implementation at an industrial scale. The undisputed advantage of this method is the possibility

[131] Chal, R.; Gerardin, C.; Bulut, M.; van Donk, S. *ChemCatChem.* **2011**, 3 (1), 67-81.

of designing materials with a tailored mesoporous structure and high stability under hydrothermal conditions.

Destructive methods are clearly distinguished by low costs and easy to use, due to long application time. But a major drawback is the inability to control the mesoporosity extent and size. In addition, it also depends on the Si/Al ratio of pristine zeolite.

Destructive-constructive method occupies an intermediate position in terms of economic costs, but it is very interesting because of the possible prospects: ability to vary the size of the mesopores, high thermal stability.

In order to make possible the synthesis of coumarins and thiocoumarins using zeolites, we consider herein both destructive and destructive-constructive methods.

4.2 Destructive methods.

4.2. a) Dealumination

Initially, dealumination was carried out to control the concentration and strength of the acid sites, increasing the Si / Al ratio of low-silica zeolites. However, it was shown, that the formation of mesopores also occurs during the dealumination of the zeolites. This process can be carried out in four different ways: calcination, steaming, acid leaching and combination of several methods.

Calcination. The calcination in air or inert atmosphere at high temperatures [132] (T > 600 ^{o}C) induces the mobility of aluminum atoms, escaping the zeolite framework to form extra-framework Al fragments (EFAl). The overall Si / Al ratio does not change, since aluminum remains in the zeolite pores, whereas the Si / Al ratio increases in the frame. The next step in this method is usually followed by an acid treatment under mild conditions that will remove the non-framed aluminum and form the final micro mesoporous material (MMM) without further extraction of aluminum from the zeolite lattice. But this method is considered obsolete and rarely used because of its small efficiency in the formation of the MMM. In addition, this treatment may also cause severe structural damages.

Steaming. This treatment can significantly increase the mobility of aluminum and silicon particles within large zeolite crystals. The temperature of the steam must be high enough to knock out Al- frame atoms. Indeed, during such heat treatment, part of the aluminum atoms leaves the zeolite framework as a result of the hydrolysis of the Si-O-Al bonds. An acidic extra treatment results in the removal of the EFAL frame particles and the formation of mesopores. [133]

Usually, in the course of hydrothermal dealumination, mesopores in the range of 5-20 nm size are formed. They are either cavities inside zeolite crystals, or cylindrical pores that connect the crystal outer surface to the inner one. The content of this kind of mesopores can be more than 70% of the total pore volume. [134] The effect of such treatment on the formation of mesopores has been studied for a large group of zeolites such as Y, ZSM-5, MOR. [135]

Acid Leaching. Acid treatment is generally used in the final step of modifying zeolites to remove amorphous fragments from zeolite pores. However, more concentrated aqueous solutions of an acid are also capable of effectively hydrolyze Si-O-Al bonds, extracting aluminum from the framework, thus forming mesopores in the zeolite structure. [136] This pattern is observed while using mineral acids (nitric, hydrochloric, sulfuric acids) and under the action of some organic acids (oxalic, acetic, tartaric acids). It is obvious that the main factor affecting the extent of the hydrolysis reaction is the nature /strength of the acid and the structure of the zeolite.

---

[132] Marques, J. P.; Gener, I.; Ayrault, P.; Lopes, J. M.; Ribeiro, F. R.; Guisnet, M. *Chem. Commun.***2004**, 20, 2290-91.
[133] Moreno, S.; Poncelet, G. *Microporous Mater.* **1997**, 12 (4-6), 197-222.
[134] Janssen, A. H.; Koster, A. J.; de Jong, K. P. *Angew. Chem. Int. Ed.* **2001**, 40 (6), 1102-1104.
[135] Janssen, A. H.; Koster, A. J.; de Jong, K. P. *J. Phys. Chem. B*. **2002**, 106 (46), 11905-11909.
[136] Silaghi, M.-C.; Chizallet, C.; Raybaud, P. *Microporous Mesoporous Mater.* **2014**, 191, 82-96.

Combination of several methods. The best effect is often achieved by combining several methods. For example: sequential steaming and acid treatment, steaming with calcination and after acid leaching. Usually, the stages are repeated one or two times.

4.2. b) Desilication

Another postsynthetic way of forming MMM is desilication. The essence of this method is the extraction of silicon atoms from the zeolite framework under alkaline treatment. This technique is well known as a method for obtaining zeolites with lower Si/Al ratio. [137] It was realized not a long time ago that such treatment leads to the formation of secondary mesoporosity. Extraction of silicon atoms leads to an increase in the proportion of mesopores. Places of mesopore formation are usually the outer boundaries of the crystal and defects in the structure of the zeolite. Datka et *al* showed that there is an optimal Si/Al ratio for desilication, which is in the range 20-40.[138]

Groen *et al.* proved that the charge due to framework aluminum prevents the extraction of an adjacent silicon atom from the zeolite framework. [139] Therefore, the presence of large concentrations of aluminum in the lattice of ZSM-5 zeolite prevents the extraction of silicon atoms. Indeed, with zeolites having a Si/Al ratio greater than 50, selective extraction was not observed, but amorphization (destruction) of the zeolite was observed.

Figure 25 schematically depicts the results of scanning electron microscopy (SEM) of ZSM-5 zeolite samples before and after desilication. It can be seen that the extraction of silicon-oxygen particles occurs predominantly in crystal regions that do not contain aluminum.

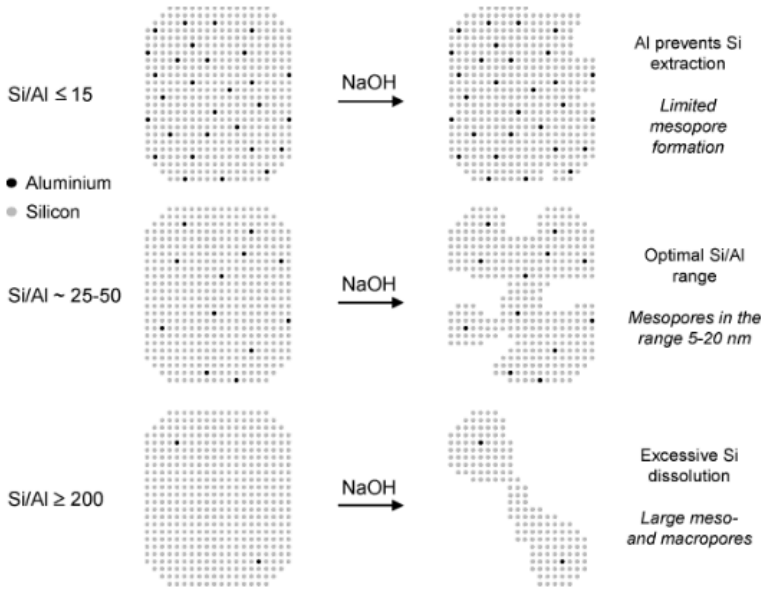

Figure 25: Schematic representation of the results of scanning electron microscopy of zeolite ZSM-5 samples before and after desilication.

Often, desilication is carried out with sodium hydroxide, which renders it possible to significantly increase the surface area and to create mesopores with a wide pore diameter distribution. The use of this technique for the preparation of mesopores has also been demonstrated for other zeolites such as mordenite, faujasite. Zeolite Y was synthesized with a combined micro and mesoporous structure in aqueous solutions of organic bases, such as tetrapropylammonium hydroxide (TPAOH) and tetrabutylammonium hydroxide (TBAOH).[140] It was shown that these bases are less reactive and less selective in the process of silicon dissolution than their inorganic analogues. Thus, treatment requires higher temperatures and / or longer reaction time.

---

[137] Ogura, M.; Shinomiya, S.-Ya; Tateno, J.; Nara, Y.; Kikuchi, E.; Matsukata, M. *Chem. Lett.* **2000**, 8, 882-883.
[138] Gackowski, M.; Kuterasinski, L.; Podobinski, J.; Sulikowski, B.; Datka, J. *Spectrochim. Acta A. Mol. Biomol. Spectrosc.* **2018**, 193, 440-446.
[139] Groen, J. C.; Moulijn, J. A.; Perez-Ramirez, J. *J. Mater. Chem.* **2006**, 16 (22), 2121-2131.
[140] Gackowski, M.; Tarach, K.; Kuterasinski, L.; Podobinski, J.; Jarczewski, S.; Kustrowski, P.; Datka, *J. Microporous Mesoporous Mater.* **2018**, 263, 282-288.

It is important to note that the use of organic hydroxides makes possible to obtain the proton form of MMM immediately after their calcination and does not require ion exchange.

4.3 Destructive-constructive methods

In the course of destructive-constructive methods, the destruction of the zeolite can take place in an alkaline medium. [141] [142] [143] This category of methods usually includes 2 stages: in the first stage, a partial destruction of the zeolite crystal occurs, and in the second one, the zeolitic fragments re-assemble into a micro-mesoporous material.

In the first step, it leads to partial or complete destruction of the zeolite structure as a result of the desilication process. In the second step, it leads to amorphization of the zeolite. The next step involves the assembly of the zeolite fragments, formed as a result of degradation into the mesoporous phase, which, depending on the degree of destruction of the zeolite, can form various mesoporous zeolitic materials. As structure-forming agent, the surfactant cetyltrimethylammonium bromide (CTAB) is often used, and the alkaline treatment is carried out with sodium hydroxide, ammonium or tetramethylammonium hydroxide. The literature also presents synthetic approaches in which cetyltrimethylammonium hydroxide (CTAOH) is used, combining the function of both bases and templates. [144]

4.3. a) Recrystallization of zeolites

Depending on the degree of destruction of the zeolite and the degree of growth of the mesoporous phase, it is possible to obtain 3 types of materials:

- mesostructured zeolites covered with a mesoporous phase;
- nanocomposites of zeolite-mesoporous phase;
- mesoporous materials with zeolite fragments in the walls.

These materials are schematically represented in **Fig. 26**

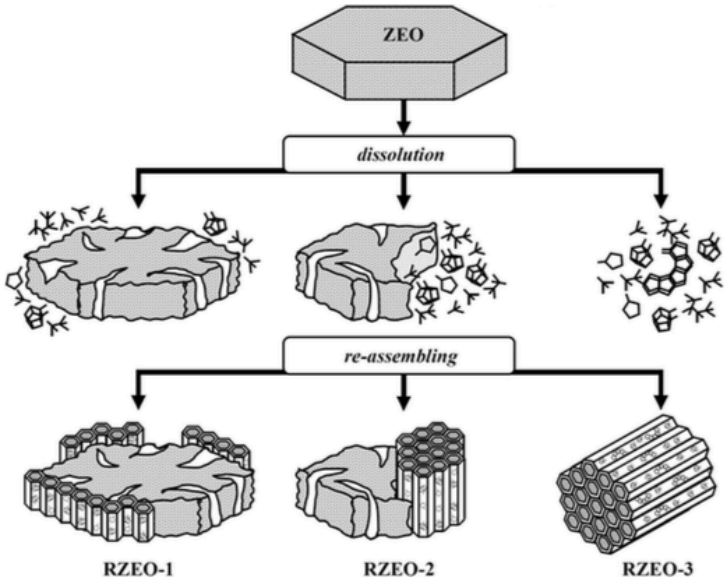

Figure 26: Schematic representation of recrystallization procedure leading to different types of materials. [145]

---

[141] Ivanova, I. I.; Kuznetsov, A. S.; Knyazeva, E. E.; Fajula, F.; Thibault-Starzyk, F.; Fernandez, C.; Gilson, J.-P. *Catal. Today.* **2011**, 168 (1), 133-139.
[142] Garcia-Martinez, J.; Johnson, M.; Valla, J.; Li, K.; Ying, J. Y. *Catal. Sci. Technol.* **2012**, 2 (5), 987-994.
[143] Garcia-Martinez, J.; Li, K.; Krishnaiah, G. *Chem. Commun.* **2012**, 48 (97), 11841-11843.
[144] Einicke, W.-D.; Uhlig, H.; Enke, D.; Glaeser, R.; Reichenbach, C.; Ebbinghaus, S. G. *Colloids Surf. A.* **2013**, 437, 108-112.
[145] Ivanova, I. I.; Knyazeva, E. E. *Chem. Soc. Rev.* **2013**, 42 (9), 3671-3688.

4. 3. b) Mesostructuring of zeolites

This approach is similar to the recrystallization step and was first described by García-Martínez, as the so-called Rive Technology.[146] The authors carried out the treatment of a zeolite with alkali simultaneously with the treatment of surfactants. They found out that in the alkaline medium, Si-O-Si bonds break, which brings some degree of freedom to the crystal structure to rearrange along the micelles of the organic template. As a result, zeolite crystals with homogeneous mesopores are formed (**Fig. 27**).

Unfortunately, scientists could not explain how the structural reorganization occurs at the molecular level. The authors called the obtained materials mesostructured. A detailed analysis of these materials shows that in their properties they are close to the recrystallized RZEO-1 materials (see **Fig. 26**).

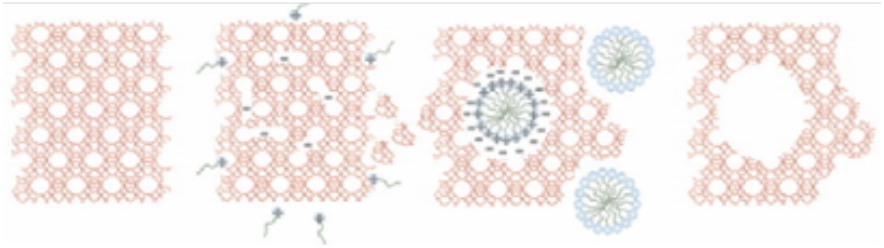

A B C D

Figure 27: Scheme of process of mesopore formation: A) initial zeolite; B) dissociation of Si-O-Si bonds under alkaline conditions C) reorganization of the structure for the inclusion of micelles; D) removal of the organic template.

5. Conclusion.

In this chapter, the main features of zeolites have been shown: their history, their origin their common structures and their properties have been highlighted. Their synthesis and mostly, the ways to create or induce mesoporosity in zeolites have been also briefly described.

Attention was paid to active sites, acidity, confinement effect and shape selectivity, because in organic synthesis and catalysis, each of these parameters affects the activity and selectivity of zeolites.

A wide range of applications of zeolites in adsorption, cation exchange processes, catalysis has been clearly mentioned, as well as their effectiveness.

---

[146] Garcia-Martinez, J.; Xiao, C.; Cychosz, K. A.; Li, K.; Wan, W.; Zou, X.; Thommes, M. *ChemCatChem*. **2014**, 6 (11), 3110-3115

CHAPTER II. Catalytic activity of different zeolites, Brønsted and Lewis acids in the synthesis of coumarins and thiocoumarins

As stated in the general introduction, coumarins are particularly interesting compounds, due to their numerous and wide application. As we have seen in Chapter 1-Part 1, the syntheses of coumarins, which do not involve metal catalysis, often require acidic conditions. Due to the similar behavior between strong acids and acidic zeolites, it seems worth to explore the use of zeolites in the synthesis of coumarins.

Furthermore, the group of Vasilyev showed the possible formation of superelectrophilic intermediates in hydroarylation of triple bond reactions occurring under the action of TfOH, FSO_3H, H_2SO_4 which are very strong Brønsted acids. Therefore, zeolites could replace these acids in hydroarylation reactions.

Applying this concept to the synthesis of coumarins led us to look for zeolites as catalyst/promoter in the intramolecular hydroarylation of aryl propynoates, according to the general **Scheme 35** below:

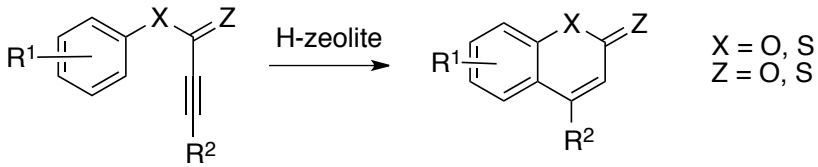

Scheme 43: General scheme for intramolecular hydroarylation of aryl propynoates

1. Liquid and solid acids.

In order to be able to compare reactions with zeolites, we also investigated the same reaction with representative strong Brønsted and Lewis acids.

Therefore, in a first series of experiments, the influence of the promoter nature was examined by submitting aryl propynoates to homogeneous Brønsted superacid triflic acid (TfOH) or strong Lewis acid such as $AlCl_3$ and BF_3 etherate complex (**Table 9**).

1. 1 Brønsted and Lewis (super) acids for the preparation of coumarins

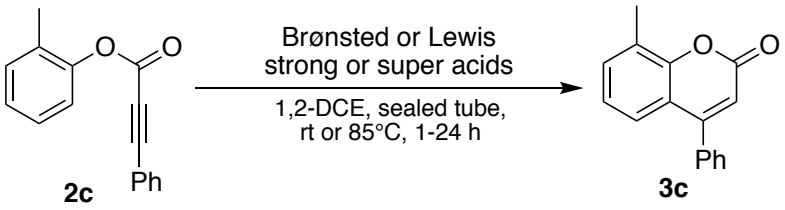

Scheme 44: Basic scheme of transformations for all test reactions.

It was decided to choose *O*-tolyl 3-phenylpropiolate (**2c**) as starting material, because this molecule presents in ^1H NMR a very easily visible singlet at 2.27 ppm, due to its methyl group. As the latter shifts to 2.52 ppm in the cyclization product **3c**, monitoring this shift significantly helps in screening various possible promoter for this cylization (**Scheme 44)**.

To start, catalyst-free test in 1,2-dichloroethane at 85 °C during 24h was performed with the ester **2c**. As expected, no reaction occurred and **2c** was recovered (Entry 1). Then two Lewis acids were tested at various loadings (1 or 5 eq), times (1 or 24h) and temperatures (rt or 85°C). These reactions led to the coumarin **3c**, but with different efficiencies (Entry 2-6). The maximum yield was achieved with 5 equivalents of promoter, within 1 h for both $AlCl_3$ and BF_3 (13% and 17%).

Then, we tested triflic acid, often mentioned as a liquid superacid (Entry 7-11). Within 1 hour, with 1eq of acid and at 85 °C, the conversion was complete, but high percentage of

degradation and addition products was found and we could only get 19% yield of the **3c** product. By lowering the temperature to rt, we were able to overcome this problem. 1-3 equivalents of TfSA did not significantly affect conversion and product yield, which ranged from 22 to 30%. The highest yield of **3c** was achieved with 5 equivalents (45%).

Promoter		Entry	Eq	T, ^{0}C	Time, h	Conv, %	Yield, %
No catalyst		1	-	85	24	0	0
Lewis acid	$AlCl_3$	2	1eq	85	1	2	0
		3	1eq	85	24	10	5
		4	5eq	85	1	30	13
	BF_3 * Et_2O	5	5 eq	85	1	30	17
		6	5 eq	rt	1	7	4
Brønsted superacids	TfSA	7	1 eq	85	1	100	19
		8	1 eq	rt	1	30	23
		9	2 eq	rt	1	28	22
		10	3 eq	rt	1	41	30
		11	5 eq	rt	1	60	45

Table 9: Cyclization of *O*-aryl ester of propynoic acid **2c** to coumarin **3c** in the presence of Brønsted and Lewis (super) acids

1. 2 Zeolites as heterogeneous catalysts for the preparation of coumarins

The starting material (**2**), due to its structure, has two centers of high electron density (**Scheme 45**). The first is a —C≡C— triple bond, the second is the carbonyl group. As a result of exposure to Brønsted acids sites, a dication might be formed, [147] which is highly electrophilic, even considered as super-electrophilic. Such dication might induce an intramolecular cyclization (**4**), which should produce coumarin (**3**).

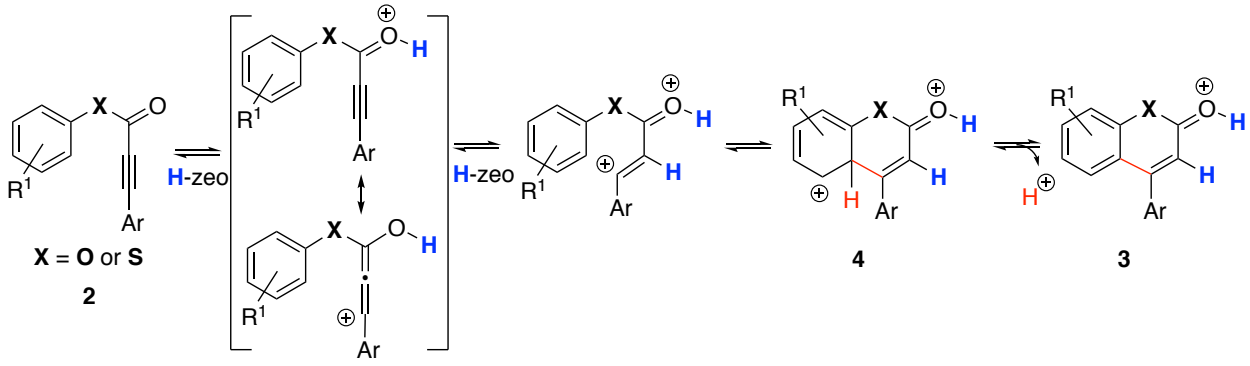

Scheme 45: Possible reaction mechanism

As already postulated for related cyclization reactions, [148] acidic zeolites might induce the formation of such dicationic intermediate. Zeolites were thus evaluated as heterogeneous solid acids in order to replace strong and toxic acids.

Mainly used zeolites containing both Lewis and Brønsted acids (MFI, BEA, MOR and FAU, **Table 10**) have been screened with the one of the simplest 2-methylphenyl 3-phenylpropynoate **2c**.

---

[147] a) Walspurger, S.; Vasilyev, A. V.; Sommer, J.; Pale, P. *Tetrahedron,* **2005**, 61 (14), 3559-3564; b) Ryabukhin, D. S.; Vasilyev, A. V. *Russ. J. Org. Chem.* **2008**, 44 (12), 1849-1851; c) Ryabukhin, D. S.; Vasilyev, A. V.; Vyazmin, S. Yu. *Russ. Chem. Bull.* **2012**, 61 (4), 843-846.

[148] Sani-Souna-Sido, A., Chassaing, S., Pale, P., Sommer, *J. Appl. Cat. A* **2008**, 336, 101-108.

Zeolite type	Channel and cavities size, Å	Si/Al	Acidity *	Conv, %	Yield, %	Structures
MFI	5.6	25	0.86	3	1	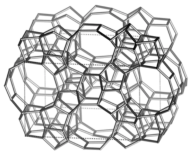
BEA	6.7	14	1.07	9	5	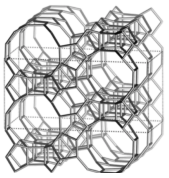
MOR	7	10	1.9	16	10	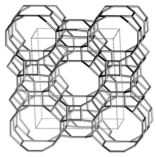
FAU	7.4 11.24	37	0.71	30	18	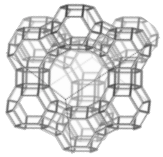

Table 10: Cyclization of *O*-tolyl 3-phenylpropiolate **2c**. Conditions: 1 eq H^+ zeolites, 1h, 85 °C. Conversion and yield (%) data were obtained by NMR standard method. *Acidity (mmol H^+/g) data was obtained by H/D method

MFI zeolite, which has the smallest sizes of micropores (5.6 Å) only gave trace amount of the expected coumarin **3c**. In contrast, FAU zeolite with the largest micropores (7.4 Å and 11.24 Å for supercage) gave the highest conversion and yield. However, the acidity (mmol H^+/g) is about the same in both zeolites (0.86 for MFI and 0.71 for FAU). It is thus obvious that acidity is not the main parameter, but that the pore size favors the reaction.

The pore sizes of BEA and MOR zeolites do not seem large enough for an effective conversion of molecule **2c**. Nevertheless, the MOR zeolite has a higher acidity than BEA (1.9/1.07 mmol H^+/g respectively) in the proposed set, and this acidity provides some advantage to MOR over BEA.

Hence, it can be concluded that the pore size has a key effect on the conversion and yield of *O*-aryl ether **2c**. If the pore size is an important parameter, we can repeat the same reaction with mesoporous materials and micro-mesoporous materials with larger pores, up to 6.4 nm.

For comparison purposes, mesoporous materials with Si/Al 10 and 25 (MS 1 and MS 2) have been used. These materials were prepared by Qian JIANG, as part of her Thesis at ICPEE. Amorphous morphology with the presence of unordered worm-like mesopores has been proved.[149]

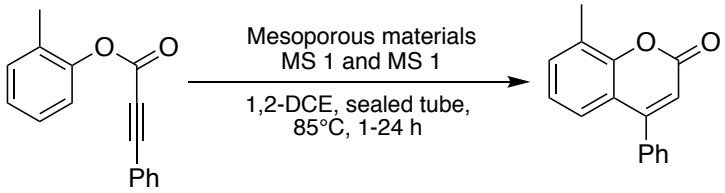

Scheme 46: Cyclization of *O*-aryl ester of propynoic acid **2c** to coumarin **3c** in the presence of amorphous mesoporous materials

[149] Thesis JIANG Q. *"Synthèse directe de diméthyl éther àpartir de CO_2/H_2" Université de Strasbourg*, **2017**. Mesoporous material with Si/Al 10 and 25 corresponds to the code Al-TUD-1

Characteristic	Si/Al	Acidity, mmol H^+/g (H/D method)	Type of material	Conv, %	Yield, %	Pore Diameter (nm)
MS 1	10	3	Mesoporous	1	0	0-5
MS 2	25	1.4	material	3	0	0-6.4

Table 11: Cyclization of *O*-tolyl 3-phenylpropiolate (**2c**). Conditions: 1 eq H^+ zeolites, 1h, 85 °C. Conversion and yield (%) data were obtained by NMR standard method.

In MS 1 and MS 2 series of experiments, no cyclization occurred (**Table 11**, **Scheme 46**). Therefore, high acidity (3 and 1.4 mmol H^+/g) and large pore sizes (MS1 - 5 nm, MS2 - 6.4), are not enough to promote cyclization. It is thus clear that a crystalline structure is required for cyclization.

Having determined the main parameters for the reaction: pore size, presence of a crystalline structure, we can proceed to further experiments with the H-USY group of zeolites (**Table 12, Scheme 47**). We screened a series of commercial crystalline, micro-mesoporous zeolites H-USY, which were obtained from FAU zeolite by the methods of steaming and acid washing.

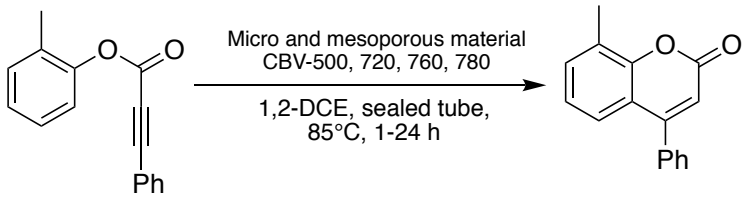

Scheme 47: Cyclization of *O*-aryl ester of propynoic acid **2c** to coumarin **3c** in the presence of micro-mesoporous materials

Entry	Characteristic	Si/Al	Acidity mmol H^+/g	Type of material	Conv, %	Yield, %	Yield of by-product, %
1	H-USY, CBV-500	3.4	3.9	Micro and mesoporous material	37	15[a]	0
2	H-USY, CBV-720	21	2.4		55	40[b]	3
3	H-USY, CBV-760	41	2.2		50	40[b]	7
4	H-USY, CBV-780	57	2		39	30[b]	1

Table 12: Cyclization of *O*-tolyl 3-phenylpropiolate (**2c**). Conditions: 1 eq H^+ zeolites, 1h, 85 °C. [a] NMR standard method, [b] isolated yield

Low yields of coumarin **3c** were obtained over the zeolite CBV-500, even lower than the pristine FAU. In order to understand this part, we need to look at the mesopore volume column (**Table 13**), where it can be seen that this feature for CBV-500 practically does not differ from the FAU (0.05 cm^3/g for FAU and 0.07 cm^3/g for CBV-500). Therefore, it is clear that this version of a commercial zeolite does not solve yield problems. Nevertheless, higher acidity in CBV-500 (3.9 mmol H^+/g) slightly increases conversion (up to 7%) compared to FAU.

CBV-720, CBV-760, CBV-780 zeolites gave approximately the same yield of coumarin **3c**, from 30 to 40%. However, conversion decreases with decreasing acidity. The smallest acidity (2 mmol H^+/g) and conversion (39%) are observed for CBV-780. The corresponding values gained with CBV-720 and 760 zeolites are very close (entry 2, 3), but the amount of by-products ($\mathbf{3c_{b\text{-}p}}$) in the CBV-760 is the largest (7%). The result similarity for these three zeolites can be also considered BET analyses.

Entry	Name	Surface Area, m^2/g	t-Plot Micropore Area, m^2/g	Pore Volume, cm^3/g			Pore Diameter (nm)
				Pore volume	Micropore volume	Mesopore volume	
1	FAU	653 ± 15	541	0.31	0.26	0.05	1.2
2	CBV-500	535 ± 12	452	0.29	0.22	0.07	13
3	CBV-720	535 ± 12	452	0.43	0.25	0.18	13
4	CBV-760	777 ± 15	491	0.41	0.24	0.17	13
5	CBV-780	680± 13	463	0.39	0.22	0.17	13

Table 13: BET surface areas, pore volume and pore diameter (max) for microporous and micro-mesoporous zeolites of Y series. The experimentally established pore size and volume correlates with literature data, for example in [150]

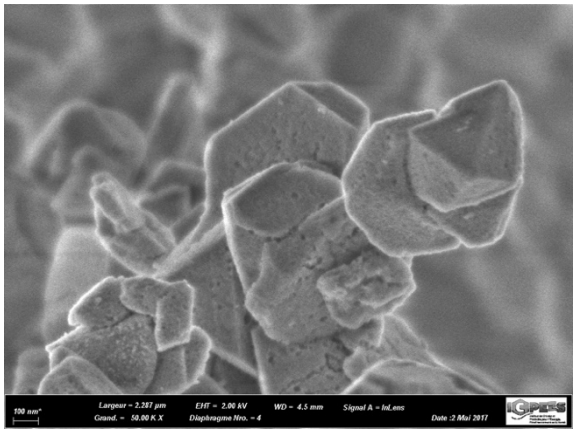

Figure SEM 1: Commercial USY zeolite **CBV 720**.

Thanks to the SEM CBV 720 (**Fig. SEM 1**) and pore distribution data (N_2 adsorption / desorption method), the average mesopore size for USY zeolites (CBV 720, 760, 780) was set approximately at 13 nm. We observe differences in surface area volume range from 535 to 777 m^2/g, as well as micropore volume from 0.22 to 0.25 cm^3/g and mesopore volume from 0.17 to 0.18 cm^3/g.

2. Post-modification of commercial microporous FAU zeolite.

The fact that good conversion and yield for the studied cyclization could only be achieved with micro-mesoporous zeolites with a certain acidity suggest to improve the mesoporous system. As seen above, this can be achieved by various post-modification treatments.

2. 1 Dealumination. Steaming and acid leaching

2.1.a) Steaming. The commercial zeolite Y (Zeochem 200, Si/Al = 37) 1 g was placed in the reactor. The test sample was subjected to steaming in the oven at the 550 °C, under N_2 flow (45 ml/min), while water was heated until 95 °C. The dealumination process lasted for 24 h, the samples received codes S1. After, the zeolite was filtered and calcined (550°C, 15 h).

2.1.b) Acid leaching. Zeolite S1 with long steam exposure time was further treated with EDTA (ethylenediaminetetraacetic acid). Test sample 0.5 g was stirred at 60 °C, during 5h in 30 ml EDTA-solution with a selected concentration (0.25M). After, the zeolite was filtered and calcined (550°C, 15 h). Test samples are named S1Ac0.25.

S1 and S1Ac0.25 two experiments have been selected and their BET and SEM results are presented in **Table 14** and **Fig. SEM 2 and 3**.

---

[150] Salzinger, M.; Fichtl, M. B.; Lercher, J. A. *Appl. Catal. A-Gen.* **2011**, 393 (1-2), 189-194.

Name	Surface Area, m²/g	Micropore Area, m²/g	Pore Volume, cm³/g			Pore diameter (nm)
			Pore volume	Microp. volume	Mesop. volume	
S1	872 ± 21	726	0.44	0.35	0.09	11
S1Ac0.25	667 ± 15	528	0.31	0.25	0.06	11

Table 14: BET surface areas, pore volume and pore diameter (max) for micro-mesoporous zeolites.

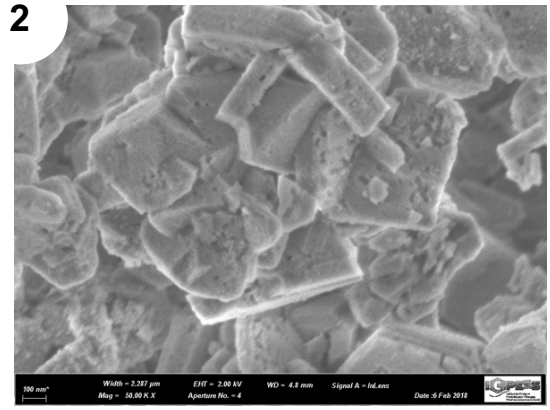

Figure SEM 2: Steamed Y-zeolite **S1**

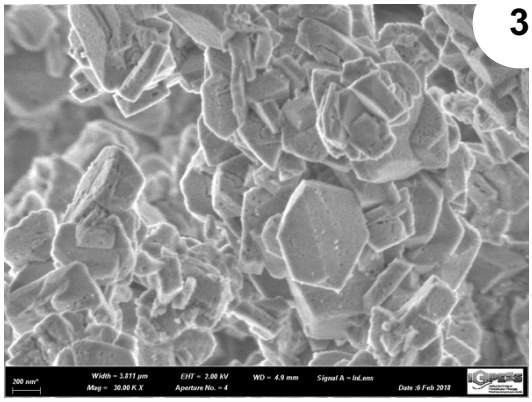

Figure SEM 3: Steamed and acid leached Y-zeolite **S1Ac0.25**

S1 has a very large area and micropore area due to many fragments, that have broken away as a result of water exposure during dealumination step. This picture is very visible on SEM image 3. The volume of mesopores in S1 and S1Ac0.25 is 0.09 and 0.06 cm³/g, respectively. The pore diameter does not exceed 11 nm in both samples.

2. 2. Desilication

2.2.a) Desilication with NaOH.

The commercial Y zeolite (Zeochem 200, Si / Al = 37, Na^+ form) was treated with NaOH. In this case, three aqueous solutions with different concentrations of sodium hydroxide were tested: 0.5M, 0.15M, 0.1M, and the reaction was carried out at different reaction times, from 1 h to 10 min. Test samples were named from D1- to D9. 0.5 g of zeolite was stirred at room temperature for the required time in a 20 ml alkaline solution with a selected concentration. After this, solid precipitate was filtered and calcined (550°C, 15 h). **Table 15** presents all the experiments in details.

#	Conc. of NaOH	Reaction time
D1	0.5 M	1 h
D2	0.5 M	30 min
D3	0.5 M	10 min
D7	0.1 M	1 h
D8	0.1 M	30 min
D9	0.1 M	10 min

Table 15. Summary reaction conditions of desilication with NaOH

In D1-D9, experiments only amorphous materials could be found. It was a surprise for us that even the smallest impact in the D9 experiment (0.1M of NaOH) for 10 min destroyed the entire crystalline structure.

2.2.b) Desilication with NH_4OH.

Another common method of zeolite desilication, was chosen: desilication with NH_4OH.[151] The parent zeolite 0.5g was dispersed in the aqueous solution of 20 ml ammonium hydroxide at

[151] Gackowski, M.; Kuterasinski, L.; Podobinski, J.; Sulikowski, B.; Datka, J. *Spectrochim Acta A Mol Biomol Spectrosc.* **2018**, 193, 440-446

different concentrations and stirred at room temperature for different durations (**Table 16**). This zeolite was then filtered and calcined (550°C, 15 h). Depending on the concentration and reaction time, samples received code numbers D10-D13.

#	Conc. of NH_4OH	Reaction time
D10	0.25	10h
D11	0.15	
D12	1	1h
D13	0.5	

Table 16. Summary reaction conditions of desilication with NH4OH

As a result of experiments from series D10-D14, the crystal structure was preserved only in two samples D11 and D13. The N_2 adsorption/desorption results of these samples are presented below (**Table 17**).

Name	Surface Area, m^2/g	Micropore Area, m^2/g	Pore Volume, cm^3/g			Pore diameter (nm)
			Pore volume	Microp. volume	Mesop. volume	
D11	943 ± 16	534	0.52	0.26	0.28	7
D13	1013 ± 17	566	0.62	0.27	0.35	14

Table 17: BET surface areas, pore volume and pore diameter (max) for micro-mesoporous zeolites.

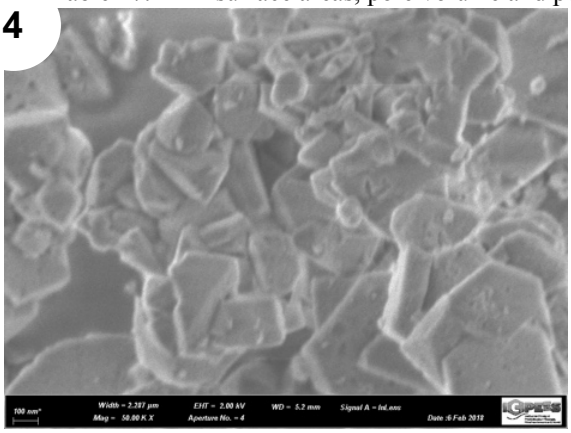

Figure SEM 4: Desilicated by NH_4OH Y-zeolite **D11**

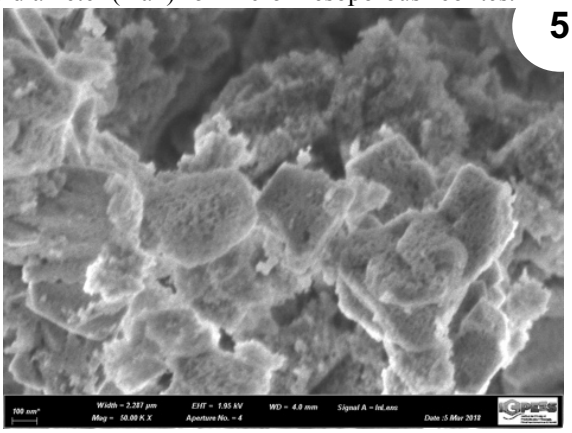

Figure SEM 5: Desilicated by NH_4OH Y-zeolite **D13**

Simple and cheap agent NH_4OH was very effective to create secondary mesoporosity. According to the results of the SEM (**Fig. SEM 4 and 5**) the structure of D11 looks robust with a bit of melted edges - an obvious result of dissolution.

However, D13 exhibits visible areas of amorphization and very large mesopores, due to the effect of a more concentrated alkali solution, although in a shorter time. This zeolite is thus not suitable for further experiments.

Regarding the N_2 adsorption/desorption results, both samples show a large surface area (943/1013 m^2/g for D11 / D13) and mesopore volume (0.28 / 0.35 cm^3/g for D11 / D13). Pore diameter is not uniform, with a maximum value of 14 nm (according to SEM and N_2 adsorption/desorption method)

2.2.c) Desilication with TBAOH or TPAOH or TEAOH.

Next, the less common but interesting method of desilication with TBAOH, TPAOH, TEAOH was chosen.[152] In such organic base treatments were performed in an aqueous solution with 20 ml of the appropriate base, while the base concentration varied from 0.25 to 1M (**Table**

[152] Verboekend, D.; Vile, G.; Perez-Ramirez, J. *Adv. Funct. Mater.* **2012**, 22 (5), 916-928.

18), added 0.5g to parent zeolite. The mixture was stirred at rt for 10 h. The zeolite was then filtered and calcined (550°C, 15 h) to remove organic residues.

#	Conc. of organic base	Reaction time
DTE-1M	1	
DTB-0.5M	0.5	10 h
DTP-0.25M	0.25	

Table 18. Summary reaction conditions of desilication with TBAOH or TPrAOH or TEtAOH

In each of the presented experiments, the crystal structure was retained. The N_2 adsorption/desorption results of these samples are presented below (**Table 19**).

Name	Surface Area, m^2/g	Micropore Area, m^2/g	Pore Volume, cm^3/g			Pore diameter (nm)
			Total pore volume	Microp. volume	Mesop. volume	
DTE-1M	654 ± 15	536	0.43	0.26	0.06	9
DTB-0.5M	657 ± 15	540	0.43	0.26	0.05	8
DTP-0.25M	662 ± 12	397	0.33	0.20	0.12	7

Table 19: BET surface areas, pore volume and pore diameter (max) for micro-mesoporous zeolites.

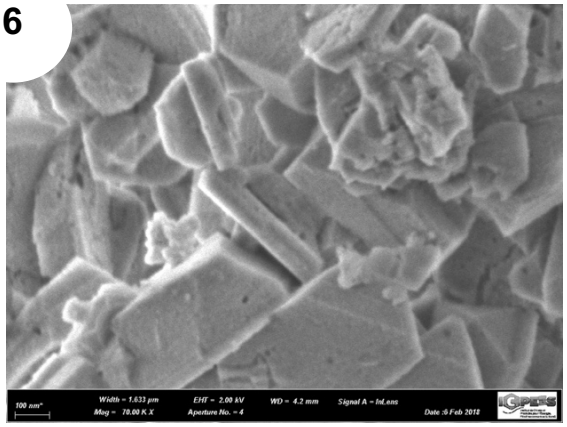

Figure SEM 6: Desilicated by TBAOH Y-zeolite **DTB-0.5M**

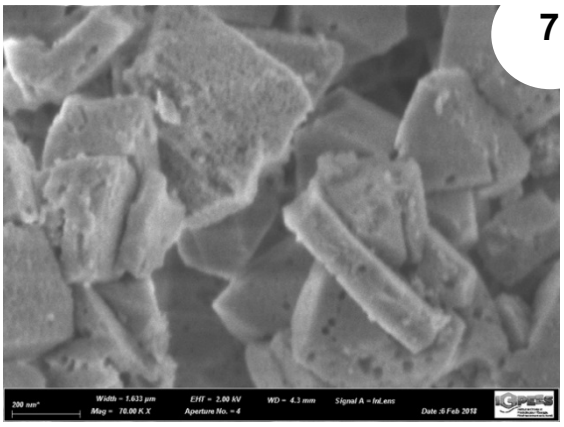

Figure SEM 7: Desilicated by TPAOH Y-zeolite **DTP-0.25M**

In all zeolites, it was possible to create secondary mesoporosity. This is proved by the results of BET (pore diameter from 9 to 7 nm) and SEM images (**Fig. SEM 6 and 7**)

The largest mesoporosity was present in DTP-0.25M, in a weakly alkaline solution. Its pore diameter turned out to be the smallest (up to 7 nm), but pores are more common than in DTE-1M and DTB-0.5M. This conclusion is based on mesopore volume for DTP-0.25M, being 0.12 cm^3/g, while for DTB-0.5M and DTE-1M samples, it ranges between 0.05 and 0.06 cm^3/g.

2.2.d) Desilication with TBAOH or TPAOH or TEAOH and NaOH.

This method was found in the literature and tested over the parent zeolite. [153] Preparing a solution consisting of 0.2M NaOH and an organic base (it was or TBAOH or TPAOH or TEAOH), also 0.2M. The total volume of the solution used for 0.5 g of zeolite was 20 ml. Stirring at room temperature lasted 30 min for all experiments. After, the zeolite was filtered and calcined (550°C, 15 h). The samples were named D14-D16 (**Table 20**).

[153] Gackowski, M.; Tarach, K.; Kuterasinski, L.; Podobinski, J.; Jarczewski, S.; Kustrowski, P.; Datka, J. *Microporous and Mesoporous Mat.* **2018**, 263, 282-288.

#	Conc. of bases	Reaction time
D14	0.2M NaOH + 0.2M TBAOH	
D15	0.2M NaOH + 0.2M TPAOH	30 min
D16	0.2M NaOH + 0.2M TEAOH	

Table 20. Summary reaction conditions of desilication with NaOH and TBAOH or TPrAOH or TEtAOH

Treatment with 0.1M NaOH in our case led to amorphization of the crystalline structure, but in the mixture of NaOH and organic base, all the experiments withstand the effects of a concentration of 0.2M NaOH and 0.2M TBAOH (or TPAOH, TEAOH). The BET results of these samples are presented below (**Table 21**).

Name	Surface Area, m²/g	Micropore Area, m²/g	Pore Volume, cm³/g			Pore diameter (nm)
			Pore Volum	Microp. volume	Mesop. volume	
D14	861 ± 19	677	0.44	0.33	0.11	10
D15	574 ± 12	439	0.3	0.21	0.09	9
D16	603 ± 13	471	0.3	0.23	0.07	9

Table 21: BET surface areas, pore volume and pore diameter (max) for micro-mesoporous zeolites.

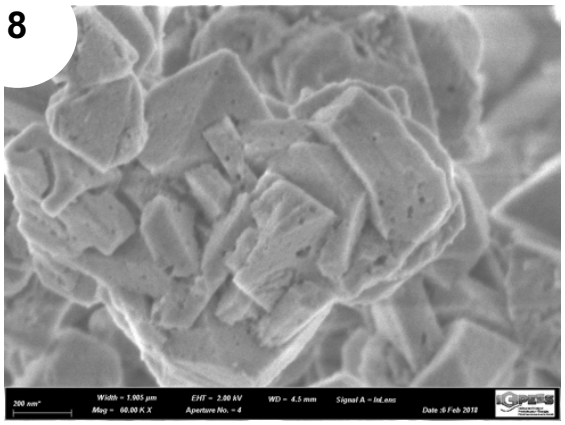

Figure SEM 8: Desilicated by with TBAOH and NaOH Y-zeolite **D14**

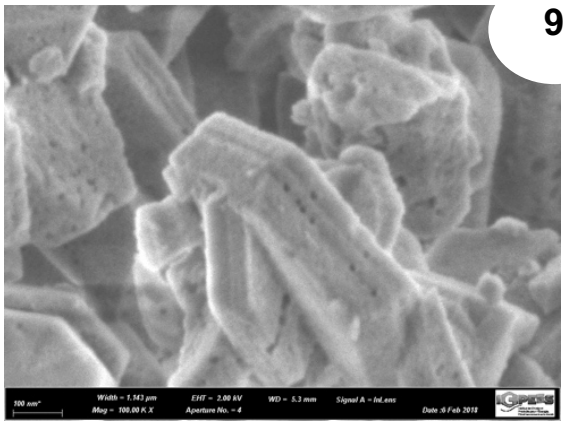

Figure SEM 9: Desilicated by with TPAOH and NaOH Y-zeolite **D15**

This impact has approximately the same effect with all the three organic bases. So, D14 (0.2M NaOH + 0.2M TBAOH) presents pores up to 10 nm and mesopore volume is 0.11 cm³/g. In the two other experiments D15-D16, all the parameters are nearly identical (mesopore volume from 0.07 to 0.09 cm³/g, micropore volume from 0.21-0.23 cm³/g, pore diameter with a maximum of 10 nm). These data were confirmed by SEM analyses (**Fig. SEM 8 and 9**)

2.3 Destructive-constructive synthesis strategy. Mesostructuring of zeolites

The general method for all **A1-A25** experiments is the following: parent zeolite (Zeochem company, H-Y form, Si/Al mole ratio: 37) was mixed with solution of TEtAOH or TPrAOH (5 min - 96h), then hydrolysed lignin(L) or oxidized lignin (LO) was added and mixed (for 5-15 min). The whole mixture was quantitatively transferred to an autoclave. After that, it was heated in the oven during 10-25h at 150 °C. When the recrystallization time was over, the autoclave was cooled down to room temperature, filtered and placed ~~it~~ in muffle oven (550°C, 15 h). All information and details are presented in **Table 22**.

	#	Conditions			% of lost weight of zeo
-	**A0**	0.1 M TEtAOH	10 min mix	0	12%
-	**A1**	1 M TEtAOH		0.1g LO	100%
-	**A2**	0.5 M TEtAOH	5-10 min	0.1g LO	100%
+	**A3**	0.2 M TEtAOH	mix	0.1g LO	96%
+	**A4**	0.1 M TEtAOH		0.1g LO	59%
-	**A5**	0.05 M TEtAOH		0.1g LO	13%
-	**A6**	0.2 M TEtAOH	5-10 min	0.1g L	
-	**A7**	0.1 M TEtAOH	mix	0.1g L	44%
-	**A8**	0.05 M TEtAOH		0.1g L	17%
-	**A9**	0.1 M TEtAOH	5-10 min mix	0.05g LO	63%
-	**A10**	0.1 M TEtAOH		0.15g LO	64%
-	**A11**	0.1 M TEtAOH		0.2g LO	32%
+	**A12**	0.1 M TEtAOH	1h mix	0.1g LO	54%
+	**A13**	0.1 M TEtAOH	96h mix	0.1g LO	57%
-	**A14**	0.1 M TEtAOH, 15h in autoclave	5-10 min mix	0.1g LO	78%
-	**A15**	0.1 M TEtAOH, 25h in autoclave		0.1g LO	72%
+	**A16**	0.1 M TPrAOH		0.1g L	46%
-	**A17**	0.15 M TPrAOH	5-10 min	0.1g L	32%
-	**A18**	0.2 M TPrAOH	mix	0.1g L	86%
-	**A19**	0.25 M TPrAOH		0.1g L	79%
+	**A20**	0.1 M TPrAOH	5-10 min	0.1g LO	51%
-	**A21**	0.25 M TPrAOH	mix	0.1g LO	78%
+	**A22**	0.1 M TPrAOH	5-10 min mix	0.05g L	50%
+	**A23**	0.1 M TPrAOH		0.15g L	52%
-	**A24**	0.1 M TPrAOH		0.2g L	43%

Table 22. Mesostructuring of zeolites with biomass; summary reaction conditions

Blank experiment without the addition of any biomass was carried out under the number A0. Experiments A1-A5 were carried out to study the effect of TEtAOH concentration, for experiments with constant amount of LO. Experiments A6-A8 were done to determine the best concentration of the same organic base, but for L. A9-A11 experiments were necessary to check the optimal amount of organic template. The following two experiments, A12-A13 investigated the effect of the mixing time of the zeolite with a solution of weak base and the subsequent effect of mesostructuring process. Attention was paid to the duration of the mixing process with the zeolite, lignin and organic base were in the autoclave. In experiments A14 and A15, the time was varied from 15 to 25 h. In the A15 experiment, we ended up working with the TEtAOH and switched to TPrAOH. Working concentrations were checked in A16-A19, for experiments with lignin and A20-A21 for oxidized hydrolysis lignin. Finally, the last three experiments A22-A24 were done to determine the best amount of lignin to produce micro-mesoporous material.

Among post-modifications, the last method allowed the mesostructuring of zeolites using an organic base (TEAOH or TPAOH) in the presence of organic templates, such as hydrolysed lignin (L) or oxidized hydrolysed lignin (LO).

The test experiment A0, without organic template, was amorphous. This result proves that under high temperature and pressure, an organic template is necessary to preserve the zeolite structure, while introducing mesoporosity.

In the series A1 - A5, the required concentration of TEAOH as a solvent was tested (from 1M to 0.05M), with the same LO (0.1 g) organic template, only two samples A3 and A4 (0.2M and 0.1M TEAOH, respectively) retained the crystal structure. However, the mass loss (by

dissolution) in sample A4 was 96%. Only A4 from this series is selected for further work (BET data are in **Table 23**).

In the series A6-A8, we tried to used lignin (L) at different concentrations of TEAOH, however TEAOH did not work with this organic template, all the material was amorphous.

In the series A9-A11, we added different mass of LO (0.05g, 0.15g, 0.2g) at the same concentration TEAOH (0.1 M). All solids in this series were amorphous.

When we examined the effect of mixing all the components (before transferring to autoclave), the experiments of the A12-A13 series, with a mixing time from 1h to 96 h, preserved the crystal structure. However, A12 will not be considered further due to its high similarity to A4. Only A13 was selected for further experiments (BET data are listed in **Table 23**).

Change in the autoclaving time in experiments A14 and A15 (15h and 25h, respectively) led to negative results. The obtained material was also amorphous.

The second variant of the solvent (TPAOH) unexpectedly started working with L. A series of experiments A16-A19, clearly proves the possibility of creating mesoporosity in A16 with TPAOH with the concentration of 0.1M (BET data are listed in **Table 23**), but the remaining concentrations in experiments A17, A18, A19 (0.15M, 0.2M, 0.25M, respectively), give damaged material.

At the same time, the TPAOH solvent in experiment A20 can work with LO (0.1 g) (BET data are listed in **Table 23**), but in A21 with the concentration of 0.25 is not effective.

When checking the optimal amount of L in experiments A21-A24, it turned out that experiments A22 and A23 (0.05g and 0.15g, respectively) were positive. The structure in them is saved. However, in A24 (0.2 g), the zeolite is amorphous. (BET data are listed in **Table 23**).

From these results, A3, A4, A12, A13, A16, A20, A22, A23 have retained the FAU crystalline fine structure.

The TEtAOH works effectively only at a concentration of 0.1 M and only with LO, when its amount is equal to 0.1g. However, the mixing time of the components (before transfer to the autoclave) can be from 10 min to 96 h.

The TPrAOH showed more opportunities. It saves crystalline structure at concentration of 0.1M with L, in an amount of 0.1g, 0.5g, 0.15g. And also, at a concentration of 0.1M with 0.1g OL. Successful in experiments, where the structure of zeolite was preserved, were analyzed using BET (**Table 23**) and SEM (**Fig. SEM 10-17**)

Name	Surface Area, m^2/g	Micropore Area, m^2/g	Pore Volume, cm^3/g			Pore diameter (nm)
			Pore Volum	Microp. volume	Mesop. volume	
A4	402 ± 5	146	0.31	0.07	0.24	15
A13	463± 6	198	0.46	0.1	0.36	22
A16	429 ± 10	318	0.27	0.15	0.12	21
A20	474 ± 9	298	0.24	0.14	0.1	17
A22	432 ± 8	247	0.21	0.12	0.09	17
A23	468 ± 9	292	0.26	0.14	0.12	19

Table 23: BET surface areas, pore volume and pore diameter (max) for micro-mesoporous mesostructured zeolites

Samples A4 and A13 formed the largest mesoporosity. Their mesopore volume was 0.24 and 0.36 cm^3 / g, respectively. The microporous volume was reduced from parent zeolite to 0.07 and 0.1 cm^3 / g. The pore diameter was up to 15 and up to 22 nm.

The remaining experiments A16, A20, A22, A23 showed approximately the same microporous volume from 0.12 to 0.15 cm^3 / g, their mesopore volume ranged from 0.09 to 0.12 cm^3 / g, and pore diameter from 17 to 21 nm.

This series of experiments is unique. We managed to create a family of micro- mesoporous materials with a high degree of mesoporosity, while preserving the zeolite crystal structure (data confirmed by XRD, SEM results).

The SEM images show that each of the samples described resembles a “sponge” or “Emmental cheese” (**Fig. SEM 10-17**)

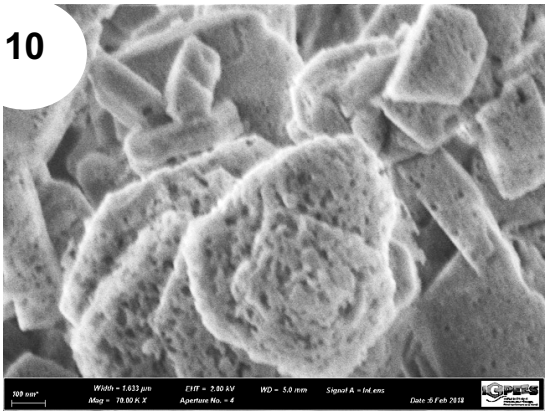

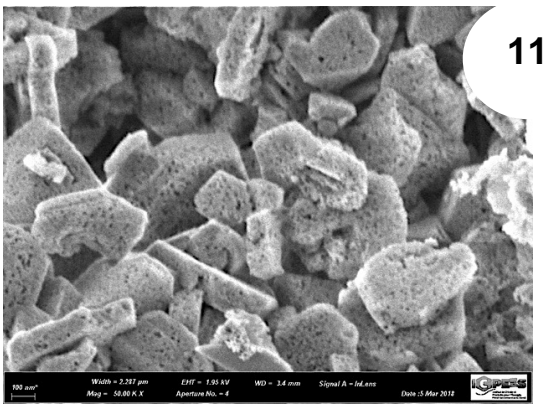

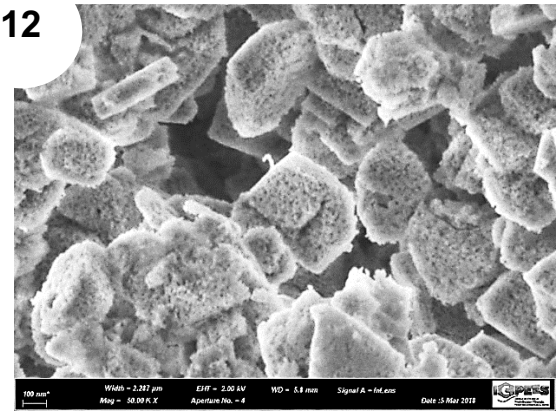

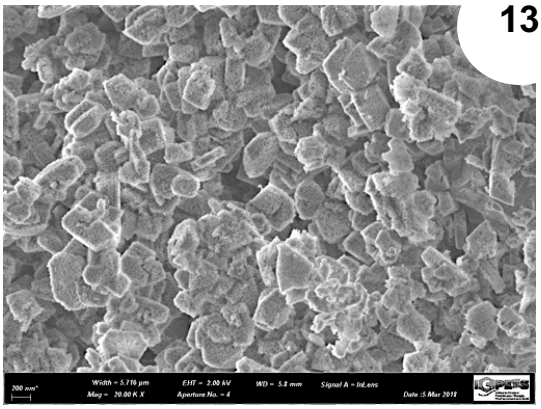

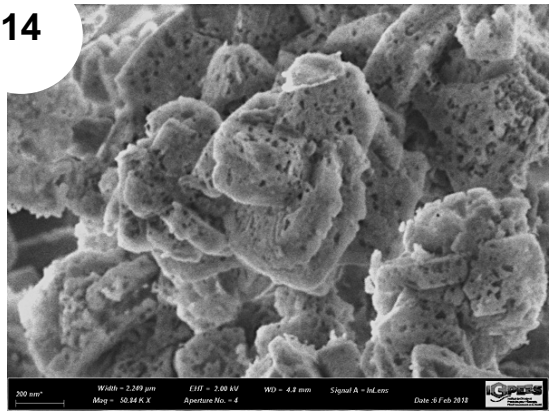

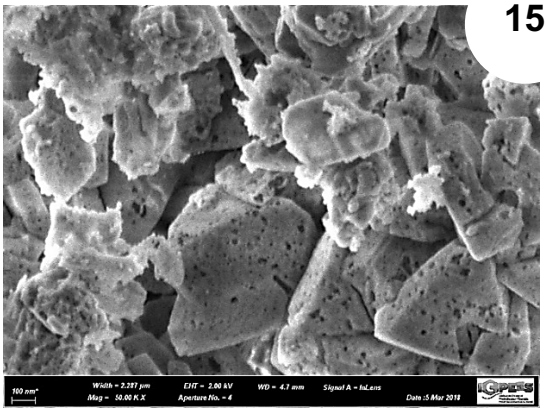

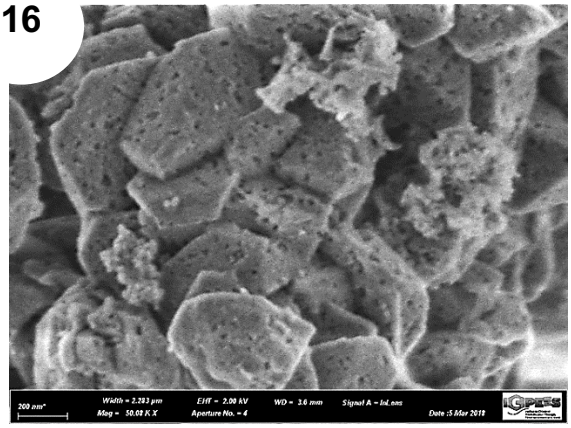

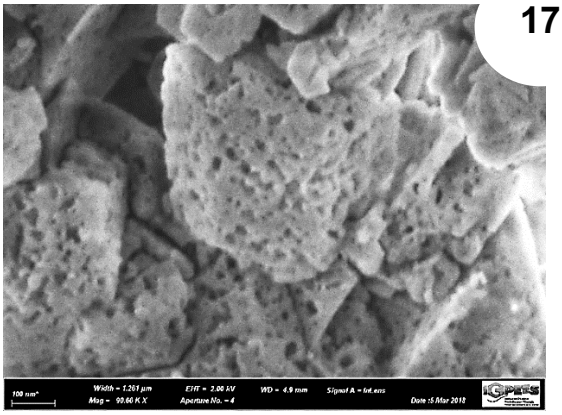

Figure SEM 10-16: Mesostructured Y-zeolites
10 — **A4**; 11 — **A4**; 12 — **A13**; 13 — **A13**; 14 — **A16**; 15 — **A20**; 16 — **A22**; 17 — **A23**

The TEM results (**Fig. TEM I - VI**) confirmed the crystal structure by the presence of linear bands (or zone) corresponding to the microporous crystalline organization of the zeolite. With zoom at 20 nm, visible areas with the defect of linearity, which corresponds to the mesopores formed due to the effect of meso-structuring agents. The largest number or breaches in the structure are noticeable in sample A13, which is completely correlated with SEM and BET analyzes

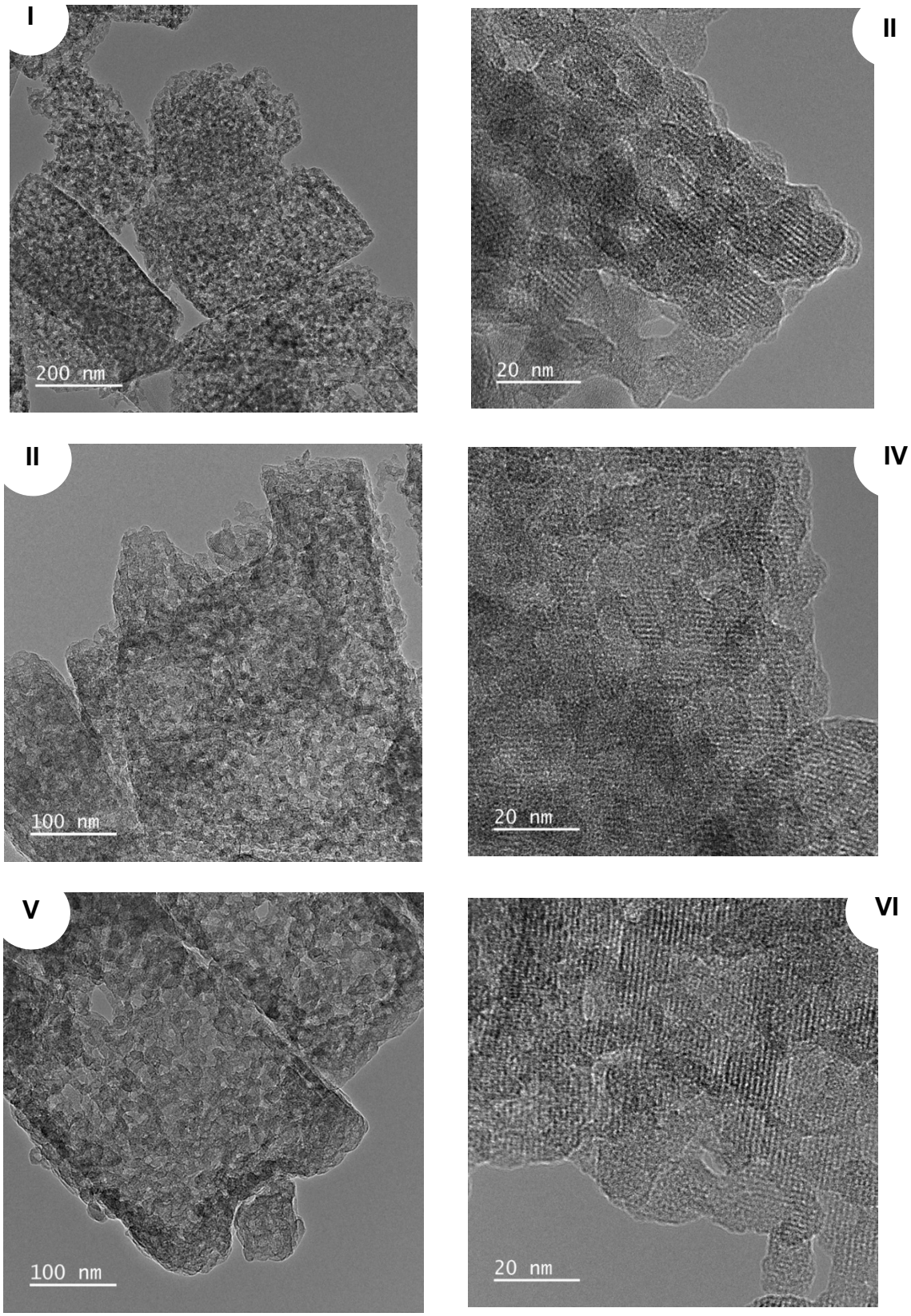

Figure **TEM I - VI**: Mesostructured Y-zeolites
I — **A4**; II — **A4**; III — **A13**; IV — **A13**; V — **A16**; VI — **A16**

3. Checking the effectiveness of catalysts, prepared by different treatments, on the intramolecular cyclization reaction of 2-methylphenyl-3-phenylpropiolate.

The best potential catalysts, according to post-modifications were evaluated in the intramolecular cyclization 2-methylphenyl 3-phenylpropiolate **(Scheme 48)**. Data on conversion and yield are listed in **Table 24** and a graph expressing the dependence between the pore volume and the yield of coumarin is plotted (**Fig. 28**)

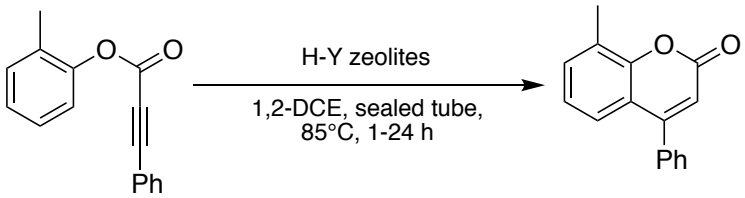

Scheme 48: Cyclization of *O*-aryl ester of propynoic acid **2c** to coumarin **3c** in the presence of post-modificated Y-zeolites

Zeolites	Conv, %	Yield, %	Mesopore volume, cm³/g	Si/Al
FAU	30	18	0.05	37
CBV-720	55	40	0.18	21
S1	14	5	0.09	36
S1Ac0.25	30	14	0.06	57
D11	22	10	0.28	30
DTP-0.25M	40	27	0.12	30
D14	47	20	0.11	40
A4	56	29	0.24	18
A13	18	7	0.36	15

Table 24: Conversion, yield, mesopore volume and Si/Al ratio of post-modificated Y-zeolites

All experiments were performed by using the same mass of starting material and catalyst, corresponding to 1 eq of CBV 720 (26.5 mg). The highest yield of coumarin was achieved with the commercial zeolite CBV 720. However, DTP-0.25M, A4, D14 (yield 27%, 29% and 20%) improved the yield of the parent FAU zeolite (18%).

The remaining samples of zeolites worsened the values obtained with parent zeolite. S1, S1Ac0.25, D11, A13 (5%, 14%, 10%, 7%).

The graph below **Fig. 28** shows the dependence between the mesoporous volume to the yield of coumarin. An “effective and optimal mesopore range” can be observed from 0.11 to 0.24 cm³/g with a peak at 0.18 cm³/g, which allowed producing 8-methyl-4-phenyl coumarin.

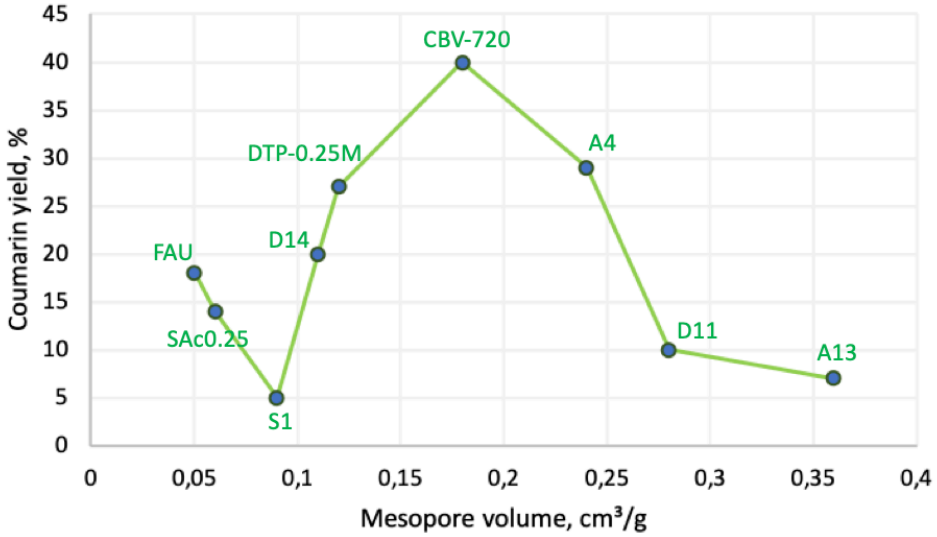

Figure 28. «Effective and optimal mesopore range »

Summing up those tests, we can conclude that our transformations of the FAU zeolite did not have a positive effect on cyclization. However, we established «effective mesopore range» and chose a catalyst for further scope.

4. Towards optimised conditions.

Having chosen the best catalyst, we needed to set optimized conditions. We chose several different starting materials : phenyl 3-phenylpropiolate **2a**, 2-methylphenyl 3-phenylpropiolate **2c**, 4-methylphenyl 3-phenylpropiolate **2d**. Under the action of different amounts of CBV 720 (1-5 equivalents mmol H^+), these compounds gave the corresponding coumarins **3a**, **3c** and **3d**. The results are graphically presented in **Fig. 29.**

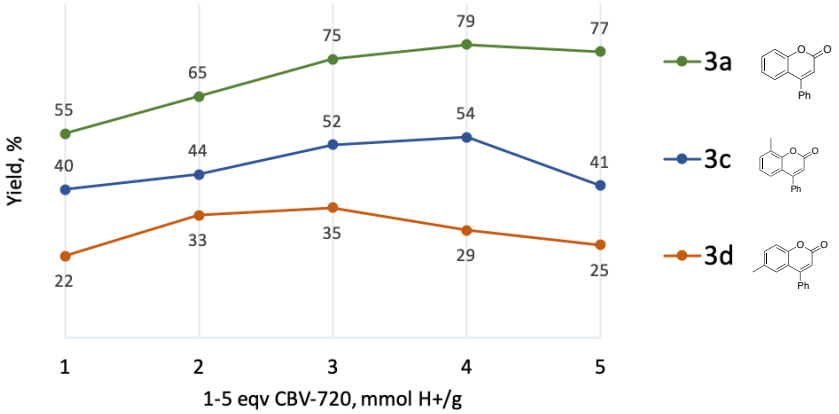

Figure 29. Dependence graph of yields (%) of 3a, 3c and 3d from number of equivalents CBV-720 (mmol H^+)

For substrates **3a** and **3c**, the use of 4 eq CBV 720 turned out to be the most effective. Indeed, 100 % conversion was reached within 1 hour, and good to high yields were obtained: 77% for **3a**, 54% for **3c**. However, the use of 5 eq induced a decrease in ~~the~~ yield; this was probably due to the blocking of organic material in an excessive amount of zeolite. Such difficulty to extract the product from the pores was also observed with the next example **3d**; the overall yield remains modest and its yield began to decrease already at 4 eq (29%). The peak efficiency to be around 3eq, with a yield of 35%.

Having determined that for **3a** and **3c**, the use of 4 eq does not significantly increase yields compared to 3 eq (4% and 2%), and the decrease for the **3d** is 6%, we decided to choose 3 eq for further experiments. With 3 equivalents, the conversion was 100% for **2a**, the other two starting material, the conversion was 85-95%.

Using 3 eq, we increased the reaction time to 2 h (**Fig. 30**), in order to reach full conversion for all components. The yields towards all coumarins increased by 5-9%. By complementing a MeOH washing of the filtrate solid after reaction, we increased the yields by another 2-5%.

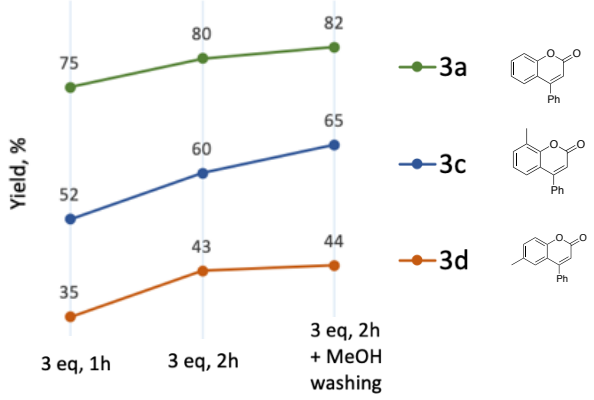

Figure 30. Dependence graph of yields (%) of 3a, 3c and 3d depending from reaction conditions.

After having tested several series of conditions, we were able to select the best catalyst and get optimized conditions. We then attempted to developed a general method for the intramolecular cyclization of aryl propynoates to coumarins with zeolites.

5. Intramolecular cyclization of *O*-(*S*-)aryl esters of 3-arylpropynoic acids into coumarins and thiocoumarins under the action of CBV-720

After having selected the optimal reaction conditions, we started a series of experiments to broaden the scope with various organic substrates to identify trends and effectiveness (**Schemes 49 - 50**, **Tables 25 - 26**).

First, we investigated aryl propynoates which contained various electro-donating or withdrawing groups at either the phenolic or the 2-propynoic acid sites. This was done to evaluate the possible electronic effect on cyclization (**Table 25**).

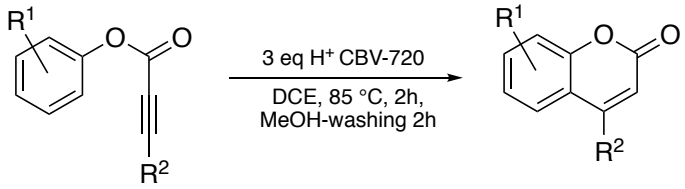

Scheme 49: Zeolite-promoted cyclization of aryl propynoates to coumarins

Entry	Propynoate		Products		Conv (%)	Yield [a] (%)
1	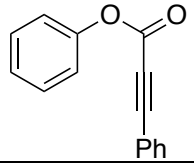	**2a**	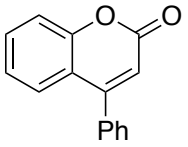	**3a**	100	82
2	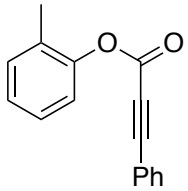	**2c**	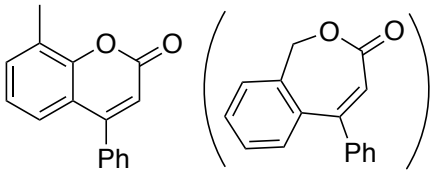	**3c** **3c$_{b-p}$**	100	65 (14)
3	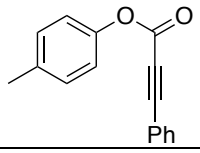	**2d**	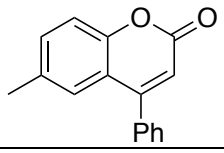	**3d**	100	44[b]
4	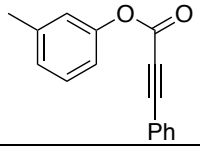	**2e**	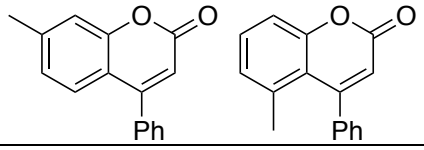	**3e** **3e'**	100 (1/0.4)	80
5	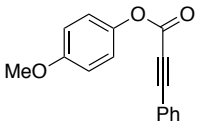	**2h**	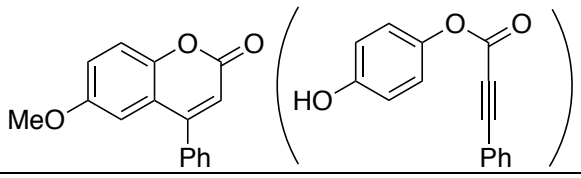	**3h** **3h$_{b-p}$**	100	60 (20)
6	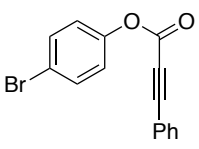	**2l**	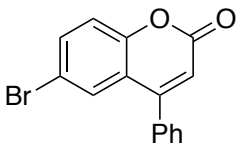	**3l**	100	84

7	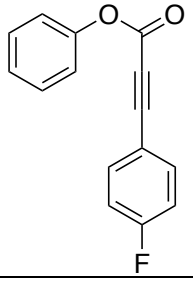	**2m**	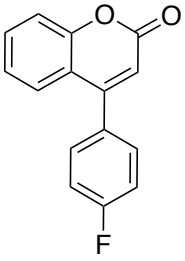	**3m**	87	73
8	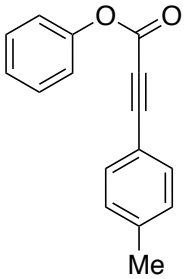	**2n**	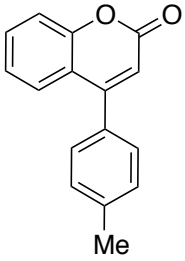	**3n**	100	80
9	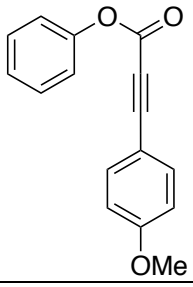	**2v**	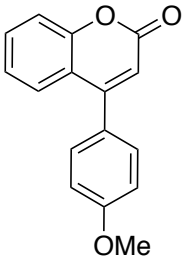	**3v**	100	88
10	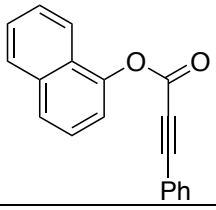	**2q**	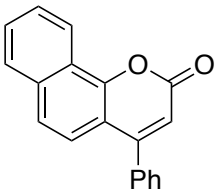	**3q**	100	28 [b, c]
11	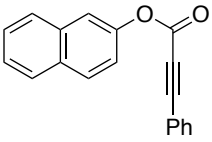	**2r**	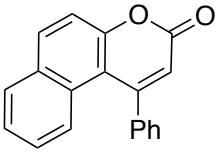	**3r**	100	65

Table 25. Zeolite-promoted cyclization of aryl propynoates to coumarins. (a) isolated; (b) not all the organic matter could be extracted from the solid catalyst; (c) formation of unidentified side-products

As can be seen from **Table 25**, zeolite CBV-720 are effective for the cyclization of most substrates into coumarins (entries 1-11). This heterogeneous catalyst generally provides complete conversion and high yields (65-88%), with two exceptions **3d**, **3q**.

Compound **3d** was formed in moderate yield (44%), possibly due to extraction problems. We assume that organic matter is blocked in the pores. During testing this material three times, we did not detect any by-product in the combined organic mixture after filtration. In contrast, compound **2p**, due to its high reactivity, formed many by-products that could not be isolated nor determined.

As seen from the results, electronic effects do not seem to have a significant influence when substituents are placed on the ester moiety. Electrodonating and electrowithdrawing substituents gave similar conversion and yields (entries 4,5 vs 6). When placed on the arylpropiolate moiety, such substituents induced small variations in yields in line with their electronic effects (entry 7 vs 8 vs 9).

These results seems consistent with the proposed mechanism: the more electron-rich the arylpropiolate moiety, the more facile would be the formation of a dicationic intermediate. Once

formed, such very reactive (superelectrophilic) intermediate would induce cyclization, whatever the electronic modification at the aryl moiety.

While studying the intramolecular cyclization of *O*-esters, we noticed the formation of several by-products **3c$_{b-p}$**, **3h$_{b-p}$**. The formation of **3c$_{b-p}$** could not be explained by comparison to the literature, but the second (**3h$_{b-p}$**) was formed as a result of the demethoxylation during the synthesis.

In the following series of experiments, we used *S*-aryl esters of 3-phenylpropynoic acids (**4a-h**). The conditions were the same as for the *O*-esters mentioned above (**Schemes 50**).

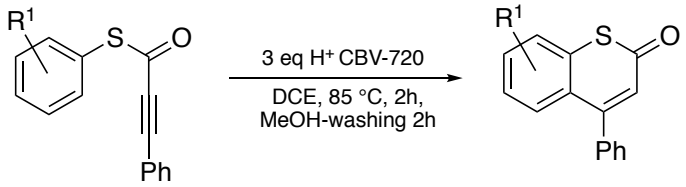

Scheme 50: Zeolite-promoted cyclization of aryl propynethioates to thiocoumarins

Entry	Propynoate		Thiocoumarins		Conv (%)	Yield[a] (%)
1	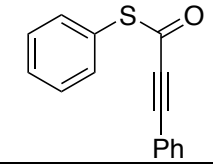	**4a**	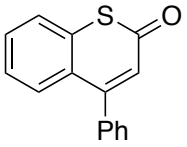	**5a**	100	84
2	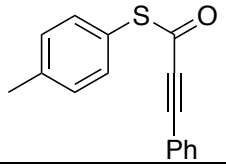	**4b**	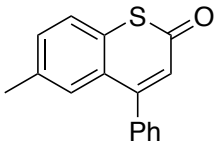	**5b**	100	99
3	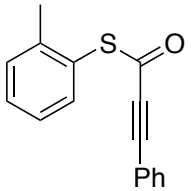	**4c**	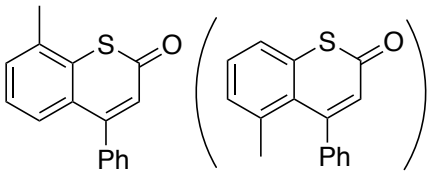	**5c** **5c$_{b-p}$**	95-100	0 (40) [b]
4	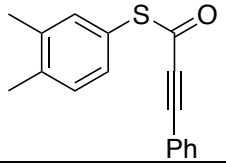	**4d**	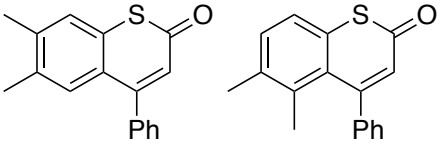	**5d** **5d'**	100 1:0.45	99
5	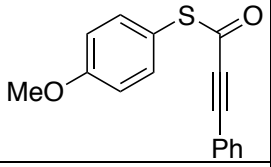	**4e**	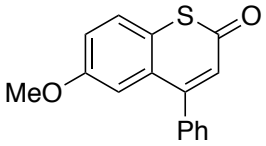	**5e**	95-100	90
6	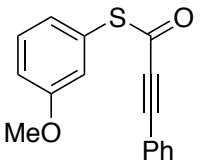	**4f**	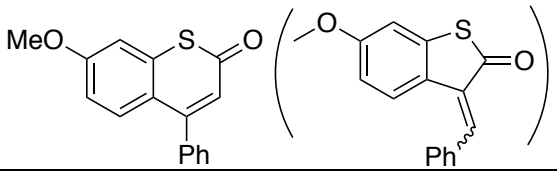	**5f** **5f$_{b-p}$**	70	24 [b, c] (8)
7	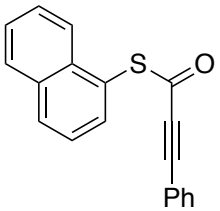	**4g**	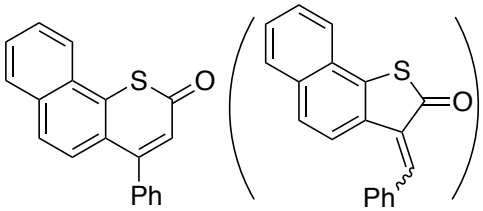	**5g** **5g$_{b-p}$**	95-100	33 [b, c] (5)

8	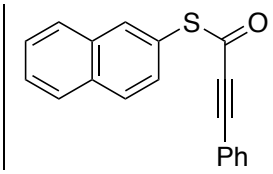	**4h**	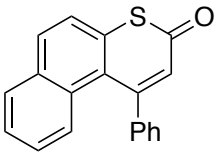	**5h**	100	95

Table 26. Zeolite-promoted cyclization of aryl propynethioates to thiocoumarins. (a) isolated; (b) not all the organic matter could be extracted from the solid catalyst; (c) formation of unidentified side-products

Under the action of acidic zeolites, thioesters **4** provided the expected thiocoumarins **5**. In most cases, conversions were complete and yields usually very high, almost quantitative (84-99%). In a few examples, low yields were obtained and side products were produced (entries 6-7).

Unsubstituted thioester **4a**, *para*-methyl thioester **4b**, 3,4-dimethyl thioester **4d** as well as *para*-methoxy thioester **4e**, gave very efficiently the corresponding thiocoumarins **5a**, **5b**, **5d**, **5e** (entries 1, 2, 4, 5, 8)

As in the ester series, extraction problems also occurred with thiocoumarins, but the substances were different from coumarins. If for the *O*-tolyl ester, that was the *para*-methyl isomer, it was *ortho*-methyl for the *S*-aryl ester. Interestingly, these two reactions showed a very similar yield (40-44%)

As a result of the study of this intramolecular cyclization of *S*-esters, we noticed the formation of new heterocycles **4f'** and **4g'**. The latter clearly result from an exo-cyclization process, in sharp contrast to all the other examples, which only gave endo-cyclization products

6. Conclusion

In Chapter 2 was tested catalytic activity of different zeolites, Brønsted and Lewis acids in the synthesis of coumarins and thiocoumarins.

We began our experiments with comparing several Lewis and Brønsted (super) acids and several heterogeneous materials for the cyclization of aryl propiolates. During these experiments, zeolites were effective as an alternative to acidic or superacid media.

Further, we found that among several types of zeolites (MFI, MOR, BEA, FAU) FAU-type exhibits prevailing values in conversion and yield of desired organic material. Having continued experiments in this vein, several commercial ultrastable Y zeolites (USY) showed even better results.

We have noticed that the presence of micro-meso porous in the structure affects the yield of coumarins. We have created a post-modification of commercial microporous zeolite FAU to influence pore size by dealumination and desilication methods. All of these zeolites were tested for cyclization to coumarins. As a result of this series of experiments, we managed to create an "effective and optimal mesopore range", by which it became apparent that the commercial USY was the most effective.

Having defined the zeolite promoter and reaction conditions, we activated a series of experiments with *O*- or *S*-aryl esters of 3-arylpropynoic acids. We obtained coumarins and thiocoumarins in high yields, with a few exceptions.

Quick and easy way to get coumarins and especially thiocoumarins through the use of zeolites as a promoter was found. Work in this direction will allow the use of more green methods of synthesis in organic chemistry.

CHAPTER III. FAU zeolites and toluene adsorption

While working with zeolites, we created series of micro-mesoporous materials, with different mesoporosity. We increased the mesopore volume of commercial microporous FAU from 0.05 to 0.24 cm^3/g.

In Chapter 1, Subsection 3.2, we have seen that zeolites can potentially be effective in adsorption processes, such as VOCs adsorption, because of their structure, curvature, different pore diameter and large internal volume. In this chapter, we want to study the adsorption properties of zeolites within Y group with different mesoporosity. For this study we selected microporous and micro-mesoporous materials obtained by three different ways: desilication with alkaline solvents, dealumination and mesostructurization by using organic templates. Those experiments were performed at the Beijing Forest University.

1. Introduction

VOCs (volatile organic components) are a common problem in industrial plants. The most common examples are ethyl acetate, acetone, benzene, tetrachloroethylene, toluene, xylene and 1,3-butadiene. These VOC are mainly released in companies producing paints, printed materials, plastics, resins, household chemicals.

It is difficult to fully study the effect of these substances on the human body. However, workers who are constantly in contact with these substances have deteriorated health, increased allergic reactions, breath problems, draining mucous membranes and burning feeling in eyes. [154] At the same time, there are evidences in the literature that VOCs contribute to the formation of tropospheric ozone [155] and smog. [156]

The adsorption method is recognized as an efficient way to reduce VOCs. [157] The main issues in favor of this method are: low operating cost; no chemical degradation and as a result, the possibility of reusing trapped components.

Zeolites have a high adsorption capacity and can be used to capture VOCs. Research in this direction is growing in popularity. The undoubted positive aspects are the possibility to reuse zeolites, the wide variation of zeolite types, high thermal stability, tailorable hydrophilicity.

Among the volatile organic compounds toluene is a common and toxic agent. Toluene is an organic solvent mainly extracted from oil, coke gas, or as a by-product in certain organic reactions (for example, in the manufacture of styrene).

The domain of application is broad. It is used as a solvent for the production of varnishes and paints, in printing houses (for example, gravure printing). To maintain a high rate of printing the paint contains toluene, as a rapidly evaporating solvent. A significant consumption of this product is also noted in the leather industry (at the stages of dyeing and washing)

According to the literature (for example Takeuchi & Hidaka [158]) we know that zeolite Y exhibits good toluene adsorption abilities. The diameter of a 12-membered ring is 0.74 nm and the diameter of the super-cage in Y zeolites surrounded by 10 sodalite cages is 1,2 nm, while the diameter of toluene molecule is 0.65/0.89 nm. The authors consider that the similarity in size enhances the dispersion interaction.

Thus, we can conclude that the adsorption of released toluene is an interesting and very important aspect to preserve the environment and help companies meeting high environmental standards.

---

[154] Disease Control and Prevention (CDC) Organization https://www.cdc.gov/nceh/clusters/fallon/glossary-voc.pdf
[155] Lillo-Rodenas, M. A.; Cazorla-Amoros, D.; Linares-Solano, A. *Carbon,* **2005**, 43 (8), 1758-1767.
[156] Qin, Y.; Wang, Y.; Wang, H.; Gao, J.; Qu, Z. *Procedia Environ. Sci.* **2013**, 18, 366-371.
[157] Zhang, W.; Qu, Z.; Li, X.; Wang, Y.; Ma, D.; Wu, J. *J. Environ. Sci. (China),* **2012**, 24 (3), 520-528
[158] Takeuchi, M.; Hidaka, M.; Anpo, *M. Res. Chem. Intermed.* **2014**, 40 (6), 2315-2325.

2. Material selection. Physical characteristics of selected materials

The following zeolites FAU, DTP-0.25M, CBV-720, A4 were selected for testing adsorption capacity of toluene. All zeolite samples belong to class Y and were prepared by post-modification such as: desilication, dealumination and mesostructurization. They retain their crystal structure and have different quantities of mesopores and correspondingly degradation (XRD results). For comparison the results are duplicated in this section in **Fig. 31**.

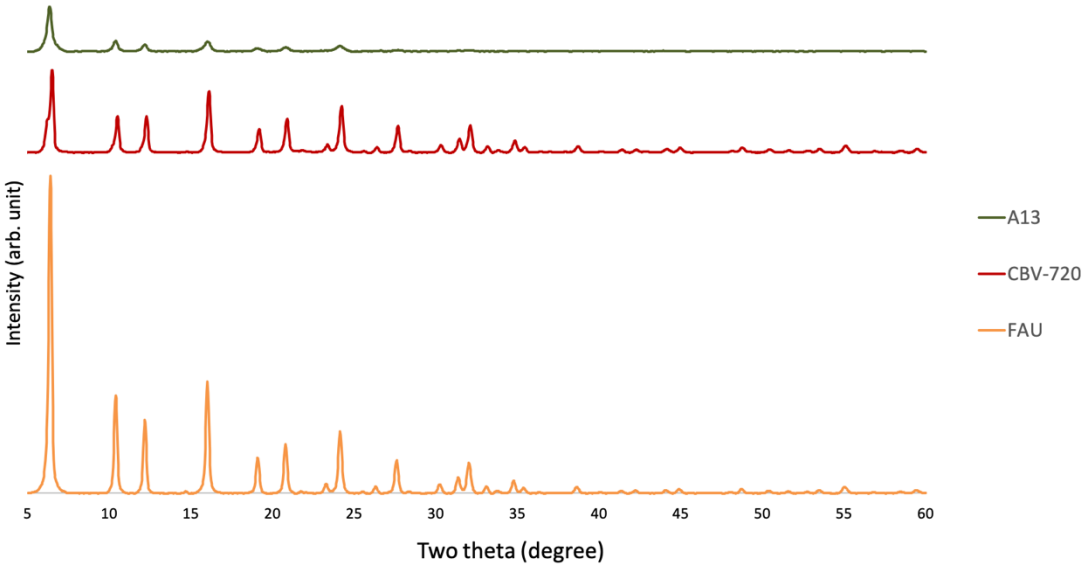

Figure 31. X-ray diffraction patterns of five Y-zeolites

For such comparison, the FAU parent zeolite is the standard. This zeolite exhibits main diffraction peaks at 6.3°, 10.4°, 12.2°, 16°, 19°, 20.7°, 24°, 27.5°, 32°, with intensity at 64300, 19400, 15000, 20500, 6400, 8500, 10700, 6200, 6200 respectively.

The intensity of the signals decreases (after steaming and acid leaching for CBV-720 or mesostructured for A13) while exposure intensity increases. If we use the ratio: parent zeolite/modified * 100, according to the first, most powerful and characteristic peak, then the percentage of crystallinity retention becomes clear. If for FAU, crystallinity is obviously 100%, crystallinity dropped to 14% for CBV, and to 4% for A4.

These data are correlated with the BET results in all cases. From FAU to A4 a gradual decrease in micropore area and an increase in mesopore volumes (**Table 27**) can be observed.

Name	Surface Area, m^2/g	Micropore Area, m^2/g	Pore Volume, cm^3/g			Pore diameter, max (nm)
			Total pore volume	Microp. volume	Mesop. volume	
HY	653 ± 15	541	0.31	0.26	0.05	1.2
CBV720	535 ± 12	452	0.43	0.25	0.18	13
A4	402 ± 5	146	0.31	0.07	0.24	15

Table 27. BET surface areas, pore volume and pore diameter (max) for microporous and micro-mesoporous zeolites of Y series.

Thus, we have zeolites of the same type, but modified in various ways with their own unique textural properties. They were then investigated for toluene adsorption.

3. Adsorption dynamics

This work was done at the Beijing Forestry University, in the laboratory EFN led by Professor Qiang Wang. Testing the adsorption capacity of zeolites was performed in two ways. At first, all samples were tested regarding their total adsorption capacity in anhydrous conditions. After selection of the best samples, additional tests of toluene adsorption capacity under wet conditions were carried out. Thus, hydrophilic abilities were checked or in other words, the ability to continue to capture toluene despite the presence of water vapor. This kind of testing conditions brings the laboratory approach closer to real situation in a factory, where obviously there are no ideal conditions (dry mixture of VOCs gases).

The basic formula for calculating the absorption capacity of toluene is given by [159]:

$$q = \frac{F * C_o * 10^{-6}}{W} * \left[t_s - \int_0^{t_s} \frac{C_t}{C_0} * d_t\right], \text{ where}$$

q (mg/g) - absorption capacity of toluene
F (ml/min) - gas flow velocity
C_t (mg/m^3) – the concentration of gas at t minutes C_t/ C_0
C_0 (mg/m^3) – initial concentration of the intake
W (g) – the amount of zeo
t (min) – the absorption time
t_s (min) – the time of absorption saturation

All adsorption diagrams can be divided into three segments: a) breakthrough time (btt) that corresponds to the time of complete adsorption of toluene in zeolite; b) stage during which pores of the zeolite can no longer hold all toluene flow and the concentration of the output toluene begins to sharply increase over time (usually, giving a S-shaped curve); c) zeolite channels are filled, the curve of unhurried achievement of the initial concentration ($C/C_0 = 1$) and the end of the activity of the catalyst.

3.1 Comparison of the adsorption diagrams FAU (Na/H)

First, the acidic FAU zeolite (FAU-H) and its parent sodium zeolite FAU (FAU-Na) were selected as typical microporous material. The results of toluene adsorption are shown in **Fig. 32** and **Fig. 33**.

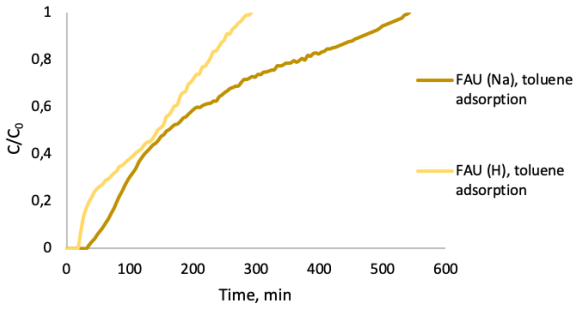

Figure 32: Toluene adsorption diagrams of FAU (Na/H)

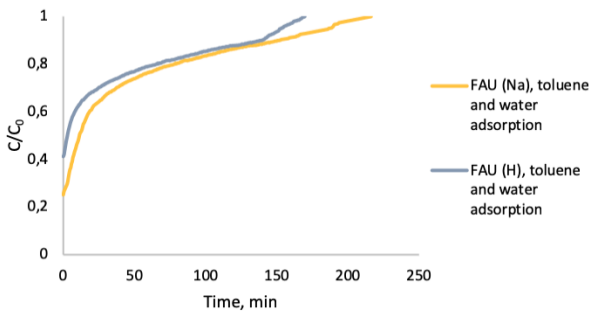

Figure 33: Toluene adsorption diagrams of FAU (Na/H) in the presence of water

The parent microporous zeolite FAU-Na without any changes exhibits a breakthrough time (btt) value of 43.8 min and absorption capacity of toluene (q) 87.4 mg/g. The same experiment with the acidic version FAU-H, provided very different values: btt 17.5 min and capacity 55.6 mg/g (**Table 28**).

---

[159] Li, R.; Xue, T.; Bingre, R.; Gao, Y.; Louis, B.; Wang, Q. *ACS Appl. Mater. Interfaces.* **2018**, 10 (41), 34834-34839.

Name	Toluene		Toluene + H_2O	
	Breakthrough time (btt), min	Adsorption capacity of toluene (q), mg/g	Breakthrough time, min	Adsorption capacity of toluene (q_{H2O}) mg/g
FAU-Na	43,8	87,4	0	16,63
FAU-H	17,5	55,6	0	12,9

Table 28: Toluene adsorption of FAU (Na/H) in the presence of water or without.

The large differences between breakthrough time and capacity in these experiments can be explained by a stronger chemical interaction between toluene and Na^+ than between toluene and H^+. We made this conclusion on the basis of results published in 2014 by the group of Anpo. [160] They studied the ability of Na-Y, H-Y and H-USY zeolites to adsorb benzene. Using FT-IR and UV methods, they proved that there is an interaction between benzene and hydroxyl group, H^+ and Na^+ ions. Moreover, the authors of this work found the strongest interaction between Na^+ and benzene, since these organic molecules were barely removed during the desorption process.

The high adsorption capacity of FAU-Na zeolite is explained in terms of ordering in the structure, ideal size of the micropores for adsorption of toluene.[161] The sodium ions act as a Lewis acid and provide a strong interaction between the organic molecule and the zeolite framework.

Experiments in the presence of water, H- and Na-FAU materials provided very different results (**Fig. 33**). Btt in both cases, decreased to zero (no adsorption), q for FAU (Na) decreased from 87,4 to 16,63, and for FAU (H), from 55,6 to 12,9. These results confirmed the information taken from the literature [162] on the high hydrophilicity of microporous zeolites. Microporous Na-Y, H-Y zeolites are hydrophilic because these zeolites are capable of adsorbing polar water molecules by coordination and interaction between zeolites and water.

3.2 Comparison of adsorption diagrams with zeolite A-13 (Na/H)

The following tests were performed with zeolite A-13 containing either sodium or proton ions. Zeolites from the whole series «A» were obtained by mesostructured method in the presence of organic templates. The results of toluene adsorption were surprising (**Fig. 34**).

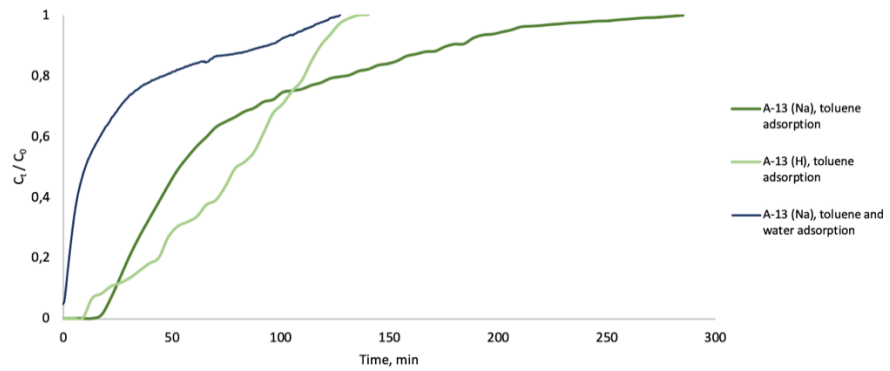

Figure 34: Toluene adsorption diagrams of A-13 (Na/H) without or in the presence of water

The bbt values are 8.7 for A-13 (H) and 17.5 for A-13 (Na), while the capacities are 30.35 for A-13 (H) and 33.08 for A-13 (Na) (**Table 29**). Although the ratio between the H and Na form remains the same, the adsorption capacity of this zeolite diminished compared to the parent

[160] Takeuchi, M.; Hidaka, M.; Anpo, M. *Res. Chem. Intermed.* **2014**, 40 (6), 2315-2325.
[161] Zhang W.; Qu Z.; Li X.; Wang Y.; Ma D.; Wu J. *J. Environ. Sci. (Beijing, China)* **2012**, 24 (3), 520-528.
[162] Sung, C.-Y.; Al Hashimi, S.; McCormick, A.; Cococcioni, M.; Tsapatsis, M. *Microporous and Mesoporous Mater.* **2013**, 172, 7-12.

microporous zeolite. This decrease could be due to the fact that the dimensions of the mesopores are large and toluene is simply washed out with the flow of other gases, not having time to adsorb to the surface.

Name	Toluene		Toluene + H_2O	
	Breakthrough time (btt), min	Adsorption capacity of toluene (q), mg/g	Breakthrough time, min	Adsorption capacity of toluene (q_{H2O}) mg/g
A-13 (Na)	17,5	33,08	0,52	10,94
A-13 (H)	8,7	30,35	-	-

Table 29: Toluene adsorption of A-13 (Na/H) in the presence of water or without.

A-13 (Na), which showed higher adsorption capacity than the H-form, was also tested in the presence of water. Under such conditions, the bbt value dropped to 0,52 and q = 10,94. These results are also lower than in FAU-Na. But, in percentage, falling adsorption capacity in the experiment for micro-mesoporous zeolite A-13 (Na) was not as low as in the experiment for the microporous zeolite FAU-Na. In sample A-13 (Na) it was 67%, and in FAU-Na it was 81%.

3.3 Comparison of adsorption diagrams CBV-720 (H)

The zeolite, which proved to be the best catalyst for organic reactions, was also evaluated regarding adsorption of toluene and hydrophilicity/hydrophobicity. We used only the proton form of CBV-720. The results are presented in **Fig. 35**

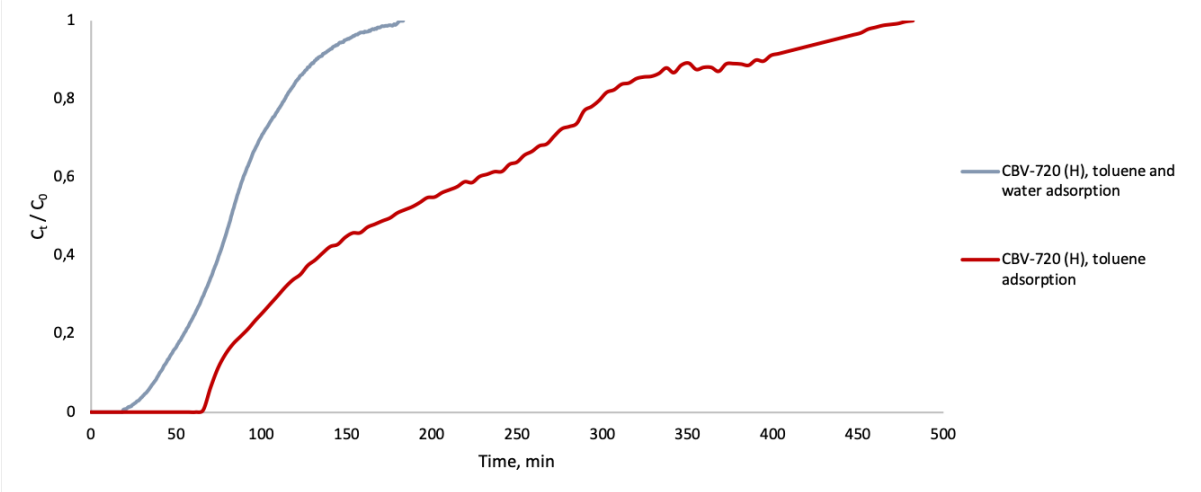

Figure 35: Toluene adsorption of CBV-720 (H) in the presence of water or without.

As can be seen on the adsorption diagram (**Fig. 35, red curve**), the curve (CBV-720 (H), toluene adsorption) has two hills. The first is observed after of 120–200 minutes, the second between 290–370 minutes. It seems logical to assume that these data are correlated to pore size distributions of BET-analysis (**Fig. 36**). The CBV zeolite exhibit clearly two major pore size one well defined from 3 to 6 nm and another set less defined from 7 to 13 nm. Apparently, large volumes of gases penetrate through large mesopores, and then diffused into micropores. In a second stage, the penetration of gases through smaller pores from 3 to 6 nm, sequentially forming the first and second areas on the toluene adsorption diagram.

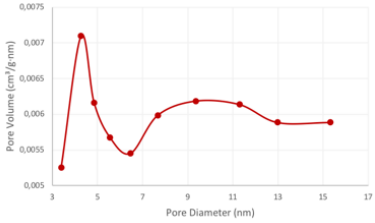

Figure 36. Pore size distributions of the sample CBV-720.

This zeolite exhibits the following values: btt of 65.7 and q = 82.54 (**Table 30**). Its total adsorption is almost the same as the commercial microporous zeolite FAU-Na, that showed the best toluene adsorption. This is possible due to the connections between mesopores and micropores.

Name	Toluene		Toluene + H_2O	
	Breakthrough time (btt), min	Adsorption capacity of toluene (q), mg/g	Breakthrough time, min	Adsorption capacity of toluene (q_{H2O}) mg/g
CBV-720 (H)	65,7	82,54	31,9	34,89

Table 30: Toluene adsorption of CBV-720 (H) in the presence of water or without.

For this zeolite, water effect on the ability of toluene adsorption was significant. Indeed, btt value fell to 31.9, and the adsorption capacity fell to 34.89 (**Table 32 and Fig. 35,** blue curve). These results are the best results from the presented series.

The literature presents some data on the hydrophobicity of dealuminated zeolites.[163] Hydrophobic zeolites are those that are dealuminated and have a minimal amount of hydroxy groups. He tested the CBV-901 CBV-780 CBV-100, in which Si / Al is 41.5, 40, 1.3. According to the results of experiments, CBV-901 was hydrophobic, CBV-780 partially, and CBV-100 hydrophilic. Our study on zeolite CBV-720 (Si / Al = 21), show partial hydrophobicity in agreement with the publication of the Marcus group.

4. Conclusion

As a result of our work, it was confirmed that the substitution of protons for sodium ions in a microporous zeolite significantly affects toluene adsorption. These results correlated with literature data. Hydrophilicity in micro-mesoporous zeolites increases with decreasing Si/Al ratio.

From all the experiments, we can conclude what, large mesopores are not effective for the adsorption of toluene.

[163] Halasz I.; Kim S.; Marcus B. *Mol. Phys.* **2002**, 100 (19), 3123-3132.

GENERAL CONCLUSIONS

The results of the work «Development of new synthetic tools for the preparation of coumarins and thiocoumarins» carried out in the context of this thesis, is divided into the development of two strategies to reach this goal, homogeneous catalysis with a platinum complex and parallel to heterogeneous catalysis with acidic zeolites.

According to the results it was possible to reveal the conditions for the cyclization of O- and S- arylpropynoates to coumarins and thiocoumarins. Although it was shown that the Pt (II) complex (PyPhPtCl(MeCN)) acts to cyclize O-arylpropynoates into coumarins, zeolites (H-Y, H-USY) are effective acid catalysts for access not only to coumarins, but also to very poorly described in literature thiocoumarins

All these results are the subject of two publications, which will be submitted very soon. One of them is «Zeolite-promoted synthesis of coumarins and thiocoumarins», the other is «Intramolecular cyclization of aryl 3-arylpropynoates into 4-arylcoumarins catalyzed by platinacycle complexes».

COMMUNICATIONS

Oral presentation:

1) Zaitceva O., Louis B., Vasilyev A., Pale P.
Development of new synthetic tools for the preparation of coumarins and thiocoumarins.
Journée des Doctorant en Chimie 2017 (JDC 2017), 10 November 2017, Strasbourg, France.

Posters:

1) Zaitceva O., Bénéteau V., Louis B., Vasilyev A., Pale P.
New methods for the synthesis of coumarin and thiocoumarin from acetylene compounds catalyzed by platinum or H-zeolite catalysts.
GECat-2017, 29 Mai - 1er Juin, L'île d'Oléron, France.

2) Zaitceva O., Bénéteau V., Louis B., Vasilyev A., Pale P.
Comparison of strong Brønsted and Lewis acids with H-zeolites through the cyclization reaction of O-aryl ester of propynoic acid in to coumarin derivative.
GECat-2018, 22-25 Mai, Bretagne, a coté de Quimper (Finistère), Azureva de Trégunc, France.

EXPERIMENTAL SECTION
ZEOLITE PART

1. Experimental set-up

1. 1 Toluene adsorption

Principle of operation: Adsorption of toluene (gas) through Y-zeolite. Registration intensity of toluene signals by GC, breakthrough time of each of the studied catalysts, the total adsorption capacity of toluene and influence of water for toluene adsorption

Experimental equipment:

The prepared sample (drying at 120 °C overnight) 0.1 g was placed inside a fixed-bed reactor, which is a stainless-steel tube with diameter outside 20 mm, diameter inside 10 mm, 40 cm long. The reactor temperature throughout the experiment was constant and equal 40 ° C.

The total gas flow is 100 ml/min, containing a mixture of three gases: toluene (400 ppm), O_2 (15%) and Ar, where this gas filled the rest percentage to a constant flow. It was controlled by mass flow controllers. For the series of experiments called «toluene adsorption capacity under wet conditions» the relative humidity was controlled to be 50%. After stabilization, gas flow directed into the reactor (on the reactor way).

To analyze the effluents of the adsorbate, we used a gas chromatograph (GC) Agilent Technologies 7890A with a flame ion detector (FID) and thermal conductivity detector (TCD) (**Figure 37**).

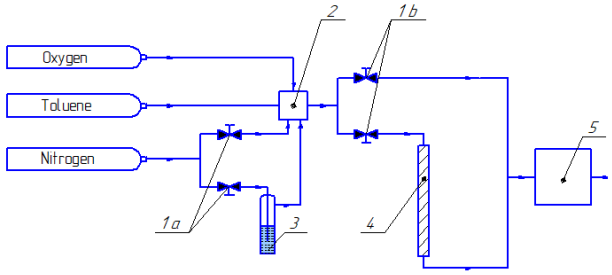

Figure 37. Schematic image of the setup for the toluene adsorption. (1 a, b) stop valve, (2) mass flow controller, (3) water saturator (4) reactor, (5) gas chromatograph with a flame ion detector (FID) and thermal conductivity detector (TCD).

1.2 Ion exchange process

All samples were used in their H^+ form, after being ion-exchanged. For this purpose, zeolite 0.2 g was added in 30 ml of 1M NH_4NO_3 aqueous solution, heated at 80 °C and stirred for 1 h. After that, it was filtered through nylon membrane (0.2 μm) and dried for 1 h in an oven at 110 °C. To replace all the Na^+ ions from the channel space with NH_4^+, this stage of ion exchange was repeated three times. At the end of this process, NH_4^+-zeolite was calcined in an atmosphere of air at 550 °C for 15 h. As a result of thermal exposure, NH_3 was released, leaving H^+-zeolite (as shown in **Fig. 38**)

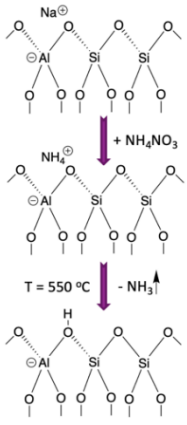

Fig. 38. Schematic representation of the ion exchange process

2. Characterization of zeolites

2. 1 X-ray fluorescence (XRF)

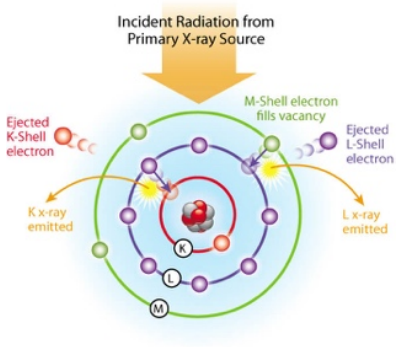

Figure 39. Schematic representation of the effect of X-rays on the electrons of the test substance using XRF

Principle of operation: X-ray excitation of the sample, knocking out electrons from the orbitals, collecting and analyzing the unique wavelength and energy emitted by electrons coming from the upper orbitals to vacant sites (**Fig. 39**). The emission of X-ray photons is characteristic from each element that generates them. The more intense the emission of a certain wavelength, the higher the concentration of chemical element. Thus, using this device, it is possible to register which elements are included in the composition of the test substance and the percentages of each element.

To measure elemental analysis in our work, we used the device SPECTRO XEPOS. In this equipment, the X-ray source is a 50-watt X-ray tube. Due to the selection of the optimal excitation conditions and also to the detection system which is represented by semiconductor Si-Drift Detector (SDD - 10 mm2) with Peltier cooling element, this spectrometer can analyze all substances from Na to U. The resolution of this spectrometer is less than 155 eV at Mn Kα. To avoid influence of light elements from the air, the experiment was conducted in helium atmosphere.

2. 2 X-ray diffraction (XRD)

Principle of operation: When X-rays interact on crystals, the primary beam (rays coming out of the device) is scattered into a large number of deflected rays. This occurs due to the interaction of the primary beam on the electrons of the substance, the wavelength (however) does not change. The intensity of the secondary rays and the direction depend on the structure of the studied substance (scattering object) **Fig. 40**.

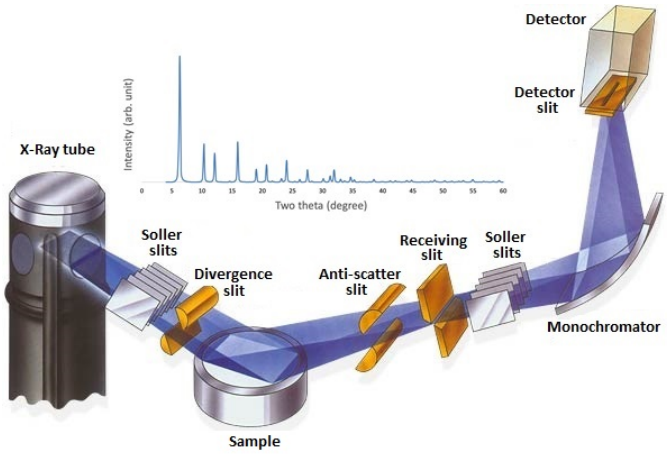

Figure 40. Schematic representation of the X-ray diffraction method

Our scientific team has the ability to use an automated Bruker D8 Advance diffractometer. X-ray tube with a copper anode λ Cu Kα = 1.5418. The detector is made of nickel. The angle interval was 2θ 4–60 with a step size of 0.02° and a step time of 2 s. After there was data processing in programs EVA and Excel.

2. 3 Specific surface area and porosimetry measurements (BET)

Brunauer Emmett Teller method. The calculation allows to mathematically describe the physical adsorption. These calculations are based on the theory of monolayer adsorption.

Principle of operation: physical adsorption-desorption of nitrogen on the surface of the material. Using this method and analyzing the data we can answer questions about specific surface area, specific pore volume, pore size and their distribution.

Our zeolites were tested on ASAP2020M equipment (Micromeritics). A prerequisite before the start of the adsorption-desorption nitrogen process was the degassing of the sample at temperature T= 250°C.

Physical adsorption was carried out at -196,15°C with gas pressure that was gradually increased from 0.1 to 1 p/p_o. First of all, gas fills a monolayer on the surface. With increasing pressure and gas in the system, several layers are collected on the surface. While increasing the pressure, capillary condensation appears in the mesopores **(Fig. 41)**.

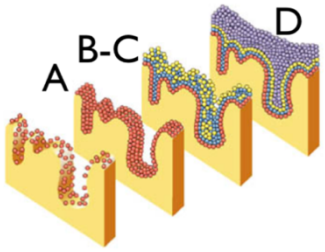

Figure 41. Stages of filling micro-meso pore with nitrogen. A-monolayer formation, B-C-capillary condensation, D-saturation

Measuring the amount of gas used during pore saturation determines the total pore volume. The desorption process goes the opposite way. The gas is removed with decreasing pressure.
Thus, by recording data and using special software, it becomes possible to build an adsorption isotherm (constant temperature, measures the amount of gas that is adsorbed on the surface at a large range of relative pressures) and desorption isotherm (the pressure decreases and the removed gas is measured)

Construction of the pore distribution diagram in zeolite (micro-meso-macro) is based on Barrett-Joyner-Halenda (BJH) method. To create this desorption isotherm is pressure range of p/p_0 = 0.4 - 0.967 was used. This method is limited for material with macropores below 60 nm.

2. 4 Scanning electron microscopy (SEM)

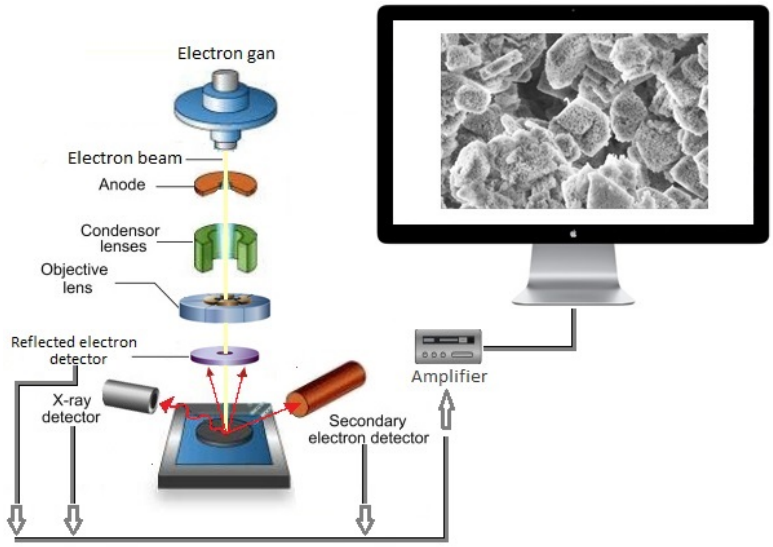

Figure 42. Schematic representation of the scanning electron microscopy method

The use of a directional electron beam to scan a test surface, with subsequent data analysis of electron scattering and absorption data. Then the data is converted into images. The following parameters can be determined by this method: phase aggregation (amorphous, crystallinity), shape and size of the crystals, morphology (surface modification) **Fig. 42**

The microscope was a JEOL FEG 6700F. An electron beam fed from an electron gun is accelerated at a voltage of 9 kV. The intense beam enters the system of guiding lenses, focused on the selected area of the material and the electron beam penetrates into the matter.
This microscope detects 3 main signals: (i)reflected electrons - electrons of the beam, which flew back due to collisions with atoms or electrons of a tested substance; (ii) secondary electrons - electrons from the material, which were knocked out by the accelerated electrons of the beam; (iii) X-rays (2 types): a) bremsstrahlung - radiation emitted as a result of electron deceleration from an accelerated electron beam; b) characteristic - this radiation is unique to the atoms of each chemical element (resulting from the excitation of the atoms of the substance under study by the accelerated electrons of the beam).

Each signal is then recorded with its own detector, and after the collection and processing are completed, the data is displayed on the screen as an image.

2. 5 Transmission electron microscopy (TEM)

In this method, as in SEM, electron beams are used. But instead of studying the interaction of an electron beam - test material (and subsequent analysis of reflected electrons, secondary electrons and X-rays), we pass the electron beam through test material and register the interacting electron beam (passed through the substance).

This kind of research was conducted for us by colleagues from South Korea on the device Hitachi HF-3300kV. the samples were dispersed in $CHCl_3$, sonicated for few seconds and drop-deposited on a copper TEM grid with a holey carbon film. The electron beam on this equipment came out of an electron gun, using a condenser lens, focuses the sample on a spot with a diameter of 2-3 μm and passes the substance through. With the passage of the sample through, the electron beam loses its intensity, scattering, being absorbed or reflected from the crystal. Not scattered electrons enter the diaphragm, and then into the projection lens. This lens transfers the image to a fluorescent screen (glowing under the influence of electrons).
In our case, we used bright field TEM and HAADF (high-angle annular dark-field).

2. 6 H/D isotope exchange method

Principle of operation:

This method allows to titrate all acid centers of Brønsted in zeolite and it is based on the exchange of hydrogen protons for deuterium of any type of solid acids with H_2O/D_2O [164]

This is a homemade installation. The average experiment time is 6 h. The general scheme is presented in **Fig. 43**. Zeolite 0.2 g, pre-dried overnight in the oven at 110 °C, placed in reactor 1. Activation of zeolites (removing excess water) is carried out at 400 °C during 1 h at a constant nitrogen flow 40 ml/min. To remove possible impurities from the N_2 flow, all the feed gas is first passed through a U-shaped tube, 3, which was cooled (with liquid nitrogen) to -173 °C. After 1 h from the start of activation, the temperature in the reactor is cooled to 200°C and will remain unchanged until the end of the experiment. After the temperature is stabilized, we bubbled N_2 flow through a U-shaped tube 4 (the temperature of this tube is rt) containing D_2O, for 1 h. At this stage, all protons in zeolite are replaced by deuterium atoms (formula X). After this time, only dry N_2 gas was passed through the sample in order to be sure that all the D_2O residues went to zeolite. The time of this step is also 1 h. Then, N_2 was bubbled through the current U-shaped tube 5 (rt) which contains H_2O. At this stage, sections of zeolite O–D are titrated with distilled water (**Formula X**). This stage is accompanied by trapping in a cold U-shaped-trap-tube (we dry overnight, we establish the exact mass) at t = 156°K. H_xOD_y - water, which is a mixture of H_2O, D_2O and HDO. At the end of an hour, the bubbling of the water stops and for 30 min - 1 h the excess of H_xOD_y was removed from all elements of the equipment in order to be sure that all the material was caught in the U-shaped trap. When the U-shaped trap tube (6) is heated to room temperature, it is weighed.

$$\text{Zeol-OH} \xrightarrow[\text{excess}]{D_2O} \text{Zeol-OD} + H_2O + \text{HDO} + D_2O$$

$$\text{Zeol-OD} \xrightarrow[\text{excess}]{H_2O} \text{Zeol-OH} + H_2O + \text{HDO} + D_2O$$

The next step is preparation of the NMR tube.
For this, trifluoroacetic anhydride 0.6 ml, was added directly in the U-shaped tube with mix of different water and it was shaken up. This mixture was transferred to NMR tubes in an amount of 0.4 ml. A mixture of $CDCl_3$ / $CHCl_3$ in the ratio 10/90 was used as a standard.

$$H_xOD_y \xrightarrow[\text{excess}]{(CF_3CO)_2O} \mathbf{x}\ CF_3COOH + \mathbf{y}\ CF_3COOD$$

---

[164] Louis, B.; Vicente, A.; Fernandez, C.; Valtchev, V. *J. Phys. Chem. C.* **2011**, 115 (38), 18603-18610.

Finally, the spectra was calculated on a Bruker AM600, by integrating the peaks ^{1}H and ^{2}H in $CF_3COOH(D)$ and $CH(D)Cl_3$, and then calculated the exact amount of Brønsted acidic centers according to the formula proposed in the literature [4].

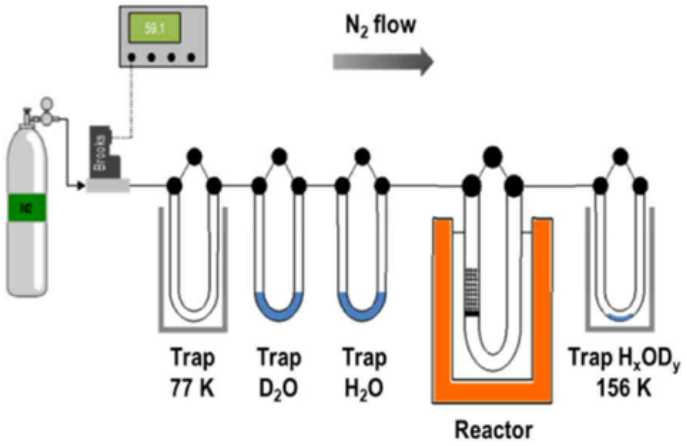

Figure 43. Schematic representation of the experimental equipment for H/D isotope exchange method.

ORGANIC PART

1. Synthesis of aryl esters of 3-arylpropynoic acid

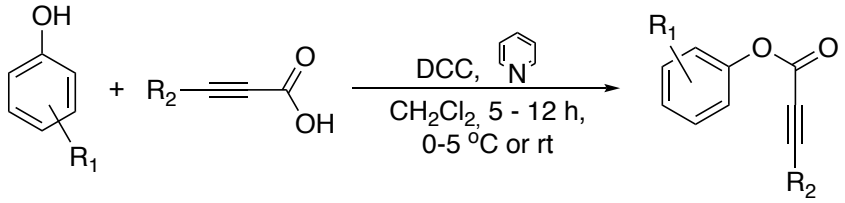

General procedure:

To a solution of propiolic acid derivative (6.8 mmol, 1eq) and phenol derivative (6.8 mmol, 1eq) in 10 mL of CH_2Cl_2 was added DCC (7.53 mmol, 1.1eq) and 10 drops of pyridine. The reaction mixture was stirred for 5-12 hours at 0 ^{0}C or rt. This mixture was treated with water (50 ml), extracted with chloroform (3 × 50 ml). The combined organic phases were washed with 0.2 N NaOH (2 × 50 ml), water (2 × 50 ml) and dried over Na_2SO_4. After filtration the solvent was removed under reduced pressure. The crude product purified by column chromatography on silica gel, eluent – pentane : diethyl ether (95:5).

2. Synthesis of coumarins and thiocoumarins

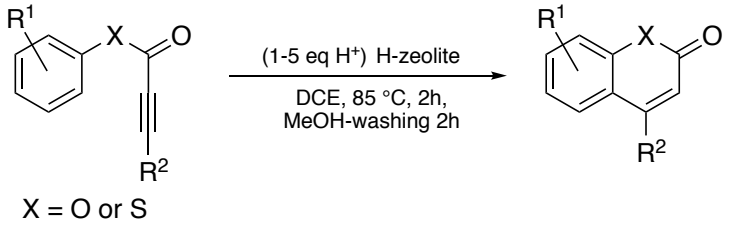

General procedure:

In a sealed tube (with a screw cap) O-aryl or S- aryl esters of 3-arylpropynoic acid (45 mg, 1eq) was added, along with H-zeolite (1-5 eq mmol H^+/g) and 2ml of 1,2-DCE. The reaction was performed at 85°C with stirring, during 2 h. At the end of the reaction, the mixture was filtered through nylon membrane (0.2 μm) and washed with 2-5 ml DCE. The zeolite (from the filter) was collected in a 50 ml round bottom flask and stirred with 20 mL of methanol at room temperature for 2 h. After filtration, the two filtrates were combined and the solvents were removed under reduced pressure. The resulting reaction product was purified by column chromatography on silica gel, eluents - cyclohexane : ethyl acetate (90:10)

3. Synthesis of Pt(II) complexes, $[Pt(PPy)(\mu\text{-}Cl)]_2$ and PyPhPtCl(MeCN)

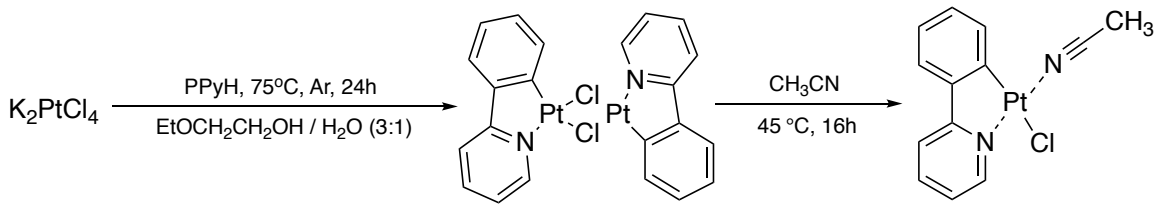

General procedure for (**C**)[165]

To a degassed water-ethoxyethanol (1:3) solution was added 0.58 g (3.7 mmol) of 2-

[165] Jain, V. K.; Jain, L. *Coord. Chem. Rev.* **2005**, 249 (24), 3075-3197.

phenylpyridine and 1.55 g (3.7 mmol) of potassium tetrachloroplatinate(II). The reaction mixture was heated at 75 °C for 24h. After cooling to room temperature, the reaction mixture was poured into 40 ml of distilled water. The precipitate was filtered, washed with 10 ml of water and 5 ml of acetone, twice with 5 ml of dichloromethane and dried in air at room temperature. As a result obtained pale-yellow powder $[Pt(PPy)(\mu\text{-}Cl)]_2$ with 44% yield.

General procedure for (**E**)[166]

A mix of the dimeric complex $[Pt(PPy)(\mu\text{-}Cl)]_2$ 60 mg (0.078 mmol) in 0.5 ml of acetonitrile was stirred at 45 °C for 16h. The precipitate was filtered, washed with diethyl ether and dried in air at room temperature. As a result obtained yellow powder of 2-(pyridin-2-yl)phenyl Pt(II) or PyPhPtCl(MeCN) with 91% yield.

4. Characterization of organic materials

Proton (^{1}H NMR) and Carbon (^{13}C NMR) nuclear magnetic resonance spectra were recorded on 300, 400 or 500 MHz instruments. The chemical shifts are given in part per million (ppm) on the delta scale. The solvent peak was used as reference values. For ^{1}H NMR: $CDCl_3$ = 7.26 ppm. For ^{13}C NMR: $CDCl_3$= 77.16 ppm. Data are presented as followed; chemical shift, multiplicity (s = singlet, d = doublet, t = triplet, q = quartet, quint = quintet, m = multiplet, b = broad), coupling constants (*J* in Hz) and integration and carbons with the same chemical shift as follows: chemical shift (x carbons).

Infrared spectra were recorded neat. Wavelengths of maximum absorbance (ν_{max}) are quoted in wave numbers (cm^{-1}).

High resolution mass spectra (HRMS) data were recorded on a microTOF spectrometer equipped with an orthogonal electrospray interface (ESI). The parent ions $[M]^+$, $[M+H]^+$, $[M+K]^+$ $[M+Li]^+$ or $[M+Na]^+$ are quoted.

Analytical thin layer chromatography (TLC) was carried out on silica gel 60 F_{254} plates with visualization by ultraviolet light.

Flash column chromatography was carried out using SiO_2 60 (40−63 μm) and the procedures included the subsequent evaporation of solvents in vacuo.

1,2-Dichloroethane (DCE) was distilled from CaH_2. All other commercially available reagents were used as received, all extractive procedures were performed using technical grade solvents, and all aqueous solutions were saturated unless details are given. All air- and moisture-sensitive reactions were carried out in flame-dried glassware under an argon atmosphere. AgSbF6 (98%), AgBF4 (99%), were purchased from STREM Chemicals.

5. Spectra description.

Structural formula	Description
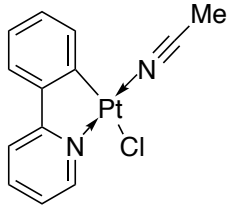	2-(pyridin-2-yl)phenyl Pt(II) (**E**). Yield: 91%. **^{1}H NMR** (300 MHz, $CDCl_3$): δ= 2.57 (s, 3H, CH_3), 7.09-7.17 (m, 1H, $H_{arom.}$), 7.29-7.32 (m, 1H, $H_{arom.}$), 7.43-7.46 (m, 1H, $H_{arom.}$), 7.59-7.66 (m, 1H, $H_{arom.}$), 7.82 (td, 1$H_{arom.}$, *J* = 8.0, 1.5 Hz, $H_{arom.}$), 9.55-9.72 (m, 1H, $H_{arom.}$). **^{13}C NMR** (125MHz, CD_3CN): δ = 4.6, 116.5, 118.4, 122.0, 123.8, 124.3, 130.5, 132.0, 139.5, 139.6, 144.0, 151.0, 167.8. **IR (neat)**: 413, 480, 556, 628, 725, 743, 857, 1030, 1068, 1124, 1158, 1237, 1276, 1318, 1425, 1440, 1485, 1584, 1609, 2090, 3045 cm^{-1}. **HRMS** (ESI-μTOF): *m/z* $[M+H]^+$ calcd for $C_{15}H_{14}N_3Pt$: 431.0831; found: 431.0841

[166] Ha, K., Kristallogr. *New Cryst. Struct.* **2014**, 229 (2), 151-152.

Structural formula	Description
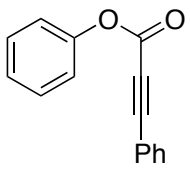	Phenyl 3-phenylpropynoate (**2a**). Yield: 90% ^{1}H NMR (500 MHz, $CDCl_3$): δ= 7.20 (d, 2H, *J* =7.7 Hz, $H_{arom.}$), 7.29 (t, 1H, *J* =7.5 Hz, $H_{arom.}$), 7.40-7.44 (m, 4H, $H_{arom.}$), 7.49 (t, 1H, *J* =7.5 Hz, $H_{arom.}$), 7.63 (d, 2H, *J* =7.1 Hz, $H_{arom.}$)
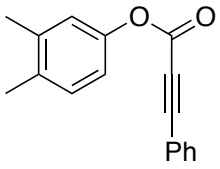	3,4-dimethylphenyl 3-phenylpropynoate (**2b**). Yield: 70% ^{1}H NMR (300 MHz, $CDCl_3$): δ= 2.26 (s, 3H, CH_3), 2.28 (s, 3H, CH_3), 6.90-6.97 (m, 2H, $H_{arom.}$), 7.16 (d, 1H, *J* =8.1 Hz, $H_{arom.}$), 7.40 (t, 2H, *J* = 7.2 Hz, $H_{arom.}$), 7.49 (t, 1H, *J* =7.4 Hz, $H_{arom.}$), 7.63 (d, 2H, *J* =6.8 Hz, $H_{arom.}$)
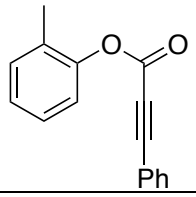	2-Methylphenyl 3-phenylpropynoate (**2c**). Yield: 85% ^{1}H NMR (300 MHz, $CDCl_3$): δ= 2.27 (s, 3H, CH_3), 7.11 (d, 1H, *J* =5.9 Hz, $H_{arom.}$), 7.17-7.29 (m, 3H, $H_{arom.}$), 7.38-7.44 (m, 2H, $H_{arom.}$), 7.47-7.52 (m, 1H, $H_{arom.}$), 7.63 (d, 2H, *J* =6.9 Hz, $H_{arom.}$)
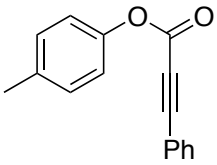	4-Methylphenyl 3-phenylpropynoate (**2d**). Yield: 43% ^{1}H NMR (300 MHz, $CDCl_3$): δ= 2.37 (s, 3H, CH_3), 7.07 (d, 2H, *J* =8.5 Hz, $H_{arom.}$), 7.21 (d, 2H, *J* =8.1 Hz, $H_{arom.}$), 7.40 (t, 2H, *J* =7.2 Hz, $H_{arom.}$), 7.49 (t, 1H, *J* =7.4 Hz, $H_{arom.}$), 7.63 (d, 2H, *J* =6.8 Hz, $H_{arom.}$)
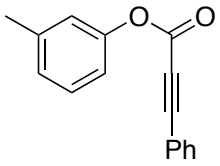	3-Methylphenyl 3-phenylpropynoate (**2e**). Yield: 79% ^{1}H NMR (400 MHz, $CDCl_3$): δ= 2.39 (s, 3H, CH_3), 6.98-7.01 (m, 2H, $H_{arom.}$), 7.08 (d, 1H, *J* =7.6 Hz, $H_{arom.}$), 7.30 (t, 1H, *J* =7.7 Hz, $H_{arom.}$), 7.41 (t, 2H, *J* =7.5 Hz, $H_{arom.}$), 7.49 (t, 1H, *J* =7.5 Hz, $H_{arom.}$), 7.63 (d, 2H, *J* =7.0 Hz, $H_{arom.}$)
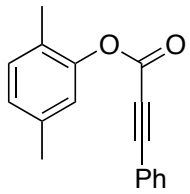	2,5-dimethylphenyl 3-phenylpropynoate (**2f**). Yield: 74%. White solid; m.p =74.5–76 °C; R_f = 0.57 (10% diethyl ether/pentane). **^{1}H NMR** (300 MHz, $CDCl_3$): δ= 2.21 (s, 3H, CH_3), 2.34 (s, 3H, CH_3), 6.92 (s, 1H, $H_{arom.}$), 6.99 (d, 1H, *J* = 7.7 Hz, $H_{arom.}$), 7.14 (d, 1H, *J* = 7.7 Hz, $H_{arom.}$), 7.41 (t, 2H, *J* = 7.2 Hz, $H_{arom.}$), 7.49 (t, 1H, *J* = 7.4 Hz, $H_{arom.}$), 7.63 (d, 2H, *J* = 6.8 Hz, $H_{arom.}$). **^{13}C NMR** (125MHz, $CDCl_3$): δ = 15.9, 21.0, 80.3, 88.5, 119.4, 122.3, 127.0, 127.5, 128.8, 131.1, 133.3, 137.2, 148.6, 152.4. **IR (neat):** 451, 534, 557, 602, 689, 737, 758, 816, 904, 998, 1149, 1182, 1238, 1280, 1440, 1487, 1572, 1623, 1718, 2215, 2920 cm^{-1}. **HRMS (ESI)**: *m/z* $[M+H]^+$ calcd for $C_{17}H_{15}O_2$: 251.1067; found: 251.1068
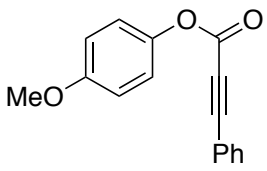	4-methoxyphenyl 3-phenylpropynoate (**2h**). Yield: 86% ^{1}H NMR (300 MHz, $CDCl_3$): δ= 3.81 (s, 3H, OCH_3), 6.92 (d, 2H, *J* =9.2 Hz, $H_{arom.}$), 7.11 (d, 2H, *J* =9.2 Hz, $H_{arom.}$), 7.40 (t, 2H, *J* =7.2 Hz, $H_{arom.}$), 7.49 (t, 1H, *J* =7.4 Hz, $H_{arom.}$), 7.63 (d, 2H, *J* =6.9 Hz, $H_{arom.}$)

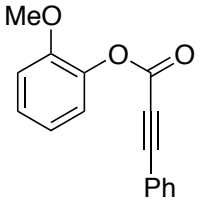	2-methoxyphenyl 3-phenylpropynoate (**2i**). Yield: 58% ^{1}H NMR (500 MHz, $CDCl_3$): δ= 3.87 (s, 3H, OCH_3), 6.97-7.02 (m, 2H, $H_{arom.}$), 7.14 (dd, 1$H_{arom.}$, *J* = 8.9, 2.4 Hz, $H_{arom.}$), 7.25 (dt, 1$H_{arom.}$, *J* = 7.9, 1.6 Hz, $H_{arom.}$), 7.40 (t, 2H, *J* =7.5 Hz, $H_{arom.}$), 7.48 (t, 1H, *J* =7.5 Hz, $H_{arom.}$), 7.63 (d, 2H, *J* =7.1 Hz, $H_{arom.}$)
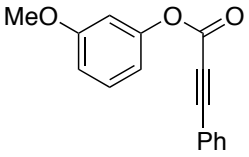	3-methoxyphenyl 3-phenylpropynoate (**2j**). Yield: 71% ^{1}H NMR (300 MHz, $CDCl_3$): δ= 3.82 (s, 3H, OCH_3), 6.75 (t, 1H, *J* =2.3 Hz, $H_{arom.}$), 6.78-6.85 (m, 2H, $H_{arom.}$), 7.31 (t, 1H, *J* =8.28 Hz, $H_{arom.}$), 7.38-7.44 (m, 2H, $H_{arom.}$), 7.47-7.52 (m, 1H, $H_{arom.}$), 7.61-7.65 (m, 2H, $H_{arom.}$)
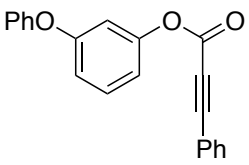	3-phenoxyphenyl 3-phenylpropynoate (**2k**). Yield: 50% ^{1}H NMR (300 MHz, $CDCl_3$): δ= 6.84 (t, 1H, *J* =2.2 Hz, $H_{arom.}$), 6.91-6.96 (m, 2H, $H_{arom.}$), 7.06 (d, 2H, *J* =7.6 Hz, $H_{arom.}$), 7.15 (t, 1H, *J* =7.4 Hz, $H_{arom.}$), 7.33-7.43 (m, 5H, $H_{arom.}$), 7.49 (t, 1H, *J* =7.4 Hz, $H_{arom.}$), 7.62 (d, 2H, *J* =6.9 Hz, $H_{arom.}$)
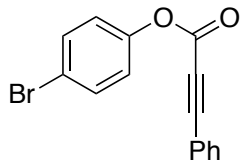	4-bromophenyl 3-phenylpropynoate (**2l**). Yield: 62% ^{1}H NMR (400 MHz, $CDCl_3$): δ= 7.09 (d, 2H, *J* =8.9 Hz, $H_{arom.}$), 7.42 (t, 2H, *J* = 7.4 Hz, $H_{arom.}$), 7.50 (t, 1H, *J* =7.4 Hz, $H_{arom.}$), 7.53 (d, 2H, *J* = 8.9 Hz, $H_{arom.}$), 7.64 (d, 2H, *J* =7 Hz, $H_{arom.}$)
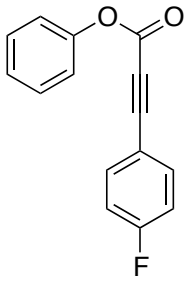	Phenyl 3-(4- fluorophenyl)propynoate (**2m**). Yield: 67% ^{1}H NMR (300 MHz, $CDCl_3$): δ= 7.07-7.14 (m, 2H, $H_{arom.}$), 7.17-7.21 (m, 2H, $H_{arom.}$), 7.27-7.31 (m, 1H, $H_{arom.}$), 7.39-7.45 (m, 2H, $H_{arom.}$), 7.60-7.66 (m, 2H, $H_{arom.}$)
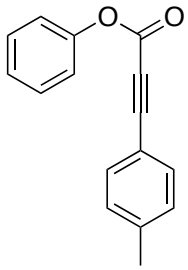	Phenyl 3-(4-methylphenyl)propynoate (**2n**). Yield: 28% ^{1}H NMR (300 MHz, $CDCl_3$): δ= 2.40 (s, 3H, CH_3), 7.18-7.23 (m, 4H, $H_{arom.}$), 7.27-7.30 (m, 1H, $H_{arom.}$), 7.39-7.45 (m, 2H, $H_{arom.}$), 7.51-7.54 (m, 2H, $H_{arom.}$)
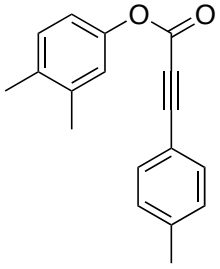	3,4-dimethylphenyl 3-(4-methylphenyl)propynoate (**2o**). Yield: 53% White solid; m.p =100.3–101.8°C; R_f = 0.6 (10% diethyl ether/pentane). **^{1}H NMR** (500 MHz, $CDCl_3$): δ = 2.25 (s, 3H, CH_3), 2.27 (s, 3H, CH_3), 2.40 (s, 3H, CH_3), 6.91 (dd, 1H, *J* = 8.2, 2.5 Hz, $H_{arom.}$), 6.96 (d, 1H, *J* = 2.3 Hz, $H_{arom.}$), 7.15 (d, 1H, *J* = 8.2 Hz, $H_{arom.}$), 7.21 (d, 2H, *J* = 8.0 Hz, $H_{arom.}$), 7.52 (d, 2H, *J* = 8.1 Hz, $H_{arom.}$). **^{13}C NMR** (125MHz, $CDCl_3$): δ = 19.3, 20.0, 21.8, 80.2, 89.1, 116.3, 118.6, 122.4, 129.5, 130.5, 133.3, 134.8, 138.2, 141.8, 148.1, 152.9. **IR (neat):** 428, 536, 578, 710, 734, 819, 916, 1155, 1185, 1236, 1288, 1495, 1717, 2220, 2915 cm^{-1}. **HRMS (ESI)**: *m/z* $[M+K]^+$ calcd for $C_{18}H_{16}KO_2$: 303.0782; found: 303.0789

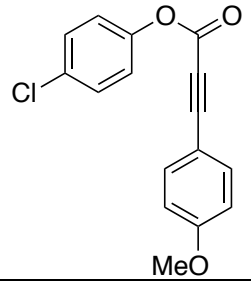

4-chlorophenyl 3-(4-methoxyphenyl)propynoate (**2p**). Yield: 51%

^{1}H NMR (300 MHz, $CDCl_3$): δ= 3.85 (s, 3H, OCH_3), 6.91 (d, 2H, *J* =8.9 Hz, $H_{arom.}$), 7.13 (d, 2H, *J* =8.9 Hz, $H_{arom.}$), 7.37 (d, 2H, *J* =8.9 Hz, $H_{arom.}$), 7.58 (d, 2H, *J* =8.9 Hz, $H_{arom.}$)

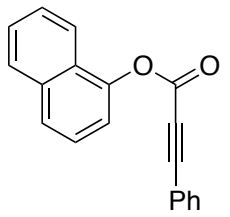

naphthalen-1-yl 3-phenylpropynoate (**2q**). Yield: 79%

^{1}H NMR (500 MHz, $CDCl_3$): δ = 7.42 (t, 2H, *J* =7.4 Hz, $H_{arom.}$), 7.48-7.51 (m, 2H, $H_{arom.}$), 7.56 (t, 1H, *J* =7.8 Hz, $H_{arom.}$), 7.59-7.62 (m, 1H, $H_{arom.}$), 7.63-7.66 (m, 1H, $H_{arom.}$), 7.70-7.71 (m, 2H, $H_{arom.}$), 7.85 (d, 1H, *J* =8.2 Hz, $H_{arom.}$), 7.96 (d, 1H, *J* =7.7 Hz, $H_{arom.}$), 8.18 (d, 1H, *J* =8.4 Hz, $H_{arom.}$)

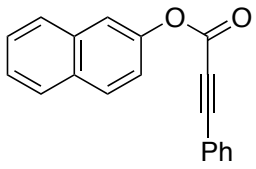

naphthalen-2-yl 3-phenylpropynoate (**2r**). Yield: 60%

^{1}H NMR (300 MHz, $CDCl_3$): δ= 7.33 (dd, 1H, *J* = 8.9, 2.4 Hz, $H_{arom.}$), 7.39-7.45 (m, 2H, $H_{arom.}$), 7.47-7.55 (m, 3H, $H_{arom.}$), 7.64-7.68 (m, 3H, $H_{arom.}$), 7.82-7.91 (m, 3H, $H_{arom.}$)

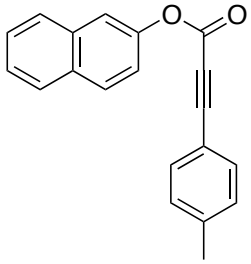

naphthalen-2-yl 3-(4-methylphenyl)propynoate (**2s**). Yield: 53%.Pale yellow solid; m.p = 104.5–106.9 °C; R_f = 0.5 (10% diethyl ether/pentane).

^{1}H NMR (300 MHz, $CDCl_3$): δ= 2.40 (s, 3H, CH_3), 7.21 (d, 2H, *J* =7.9 Hz, $H_{arom.}$), 7.32 (dd, 1$H_{arom.}$, *J* = 8.9, 2.4 Hz, $H_{arom.}$), 7.48-7.55 (m, 4H, $H_{arom.}$), 7.66 (d, 1H, *J* =2.5 Hz, $H_{arom.}$), 7.82-7.90 (m, 3H, $H_{arom.}$). **^{13}C NMR** (125MHz, $CDCl_3$): δ = 21.9, 80.1, 89.6, 116.2, 118.7, 120.9, 126.1, 126.8, 127.9, 129.6, 129.7, 131.8, 133.3, 133.8, 142.0, 147.9, 152.7. **IR (neat)**: 404, 481, 533, 570, 733, 761, 814, 896, 960, 1141, 1184, 1206, 1238, 1288, 1355, 1506, 1600, 1715, 2209, 2913 cm^{-1}. **HRMS (ESI)**: *m/z* $[M+H]^+$ calcd for $C_{20}H_{15}O_2$: 287.1067; found: 287.1074

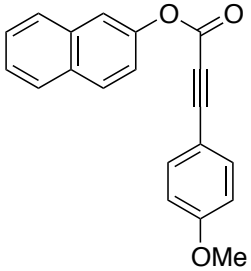

naphthalen-2-yl 3-(4-methoxyphenyl)propynoate (**2t**). Yield: 48%
Pale beige solid; m.p=91–93°C; R_f = 0.2 (10% diethyl ether/pentane).

^{1}H NMR (300 MHz, $CDCl_3$): δ= 3.85 (s, 3H, CH_3), 6.91 (d, 2H, *J* =6.8 Hz, $H_{arom.}$), 7.32 (dd, 1H, *J* = 8.8, 2.3 Hz, $H_{arom.}$), 7.45-7.54 (m, 2H, $H_{arom.}$), 7.59 (d, 2H, *J* =8.9 Hz, $H_{arom.}$), 7.66 (d, 1H, *J* =2.3 Hz, $H_{arom.}$), 7.81-7.90 (m, 3H, $H_{arom.}$). **^{13}C NMR** (125MHz, $CDCl_3$): δ = 55.6, 80.0, 90.0, 111.1, 114.5, 118.8, 120.9, 126.1, 126.8, 127.91, 127.94, 129.7, 131.7, 133.8, 135.4, 147.9, 152.8, 162.0. **IR (neat)**: 468, 536, 577, 729, 759, 800, 827, 853, 889, 965, 1024, 1138, 1185, 1211, 1257, 1289, 1509, 1603, 1710, 2204, 2847, 2928, 3008, 3063, 3283 cm^{-1}. **HRMS (ESI)**: *m/z* $[M+H]^+$ calcd for $C_{20}H_{15}O_3$: 303.1016; found: 303.0995

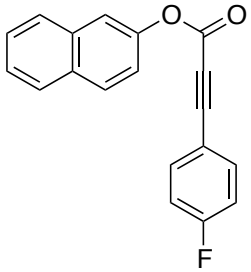	naphthalen-2-yl 3-(4-fluorophenyl)propynoate (**2u**). Yield: 59%. Pale yellow solid; m.p =103–105.9 °C; R_f = 0.5 (10% diethyl ether/pentane). **^{1}H NMR** (500 MHz, $CDCl_3$): δ= 7.09 - 7.14 (m, 2H, $H_{arom.}$), 7.32 (dd, 1H, *J* = 8.8, 2.3 Hz, $H_{arom.}$), 7.48 - 7.53 (m, 2H, $H_{arom.}$), 7.63 - 7.67 (m, 3H, $H_{arom.}$), 7.82 - 7.90 (m, 3H, $H_{arom.}$). **^{13}C NMR** (125MHz, $CDCl_3$): δ = 80.3, 87.9, 115.50, 115.53, 116.3, 116.5, 118.7, 120.8, 126.2, 126.9, 127.92, 127.96, 129.8, 131.8, 133.7, 135.6, 135.7, 147.8, 152.5, 163.3, 165.3 **IR (neat)**: 470, 536, 573, 731, 762, 776, 821, 839, 865, 896, 938, 962, 1153, 1174, 1204, 1227, 1291, 1502, 1597, 1708, 2215, 3066, 3408 cm^{-1}. **HRMS (ESI)**: *m/z* $[M+H]^+$ calcd for $C_{19}H_{12}FO_2$: 291.0816; found: 291.0810

Structural formula	Description
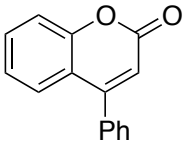	4-phenyl-2H-chromen-2-one (**3a**). Yield: 54% ^{1}H NMR (300 MHz, $CDCl_3$): δ= 6.39 (s, 1H, =CH-), 7.21-7.24 (m, 1H, $H_{arom.}$), 7.42 (dd, 1H, *J* = 8.3, 0.9 Hz, $H_{arom.}$), 7.44-7.59 (m, 7H, $H_{arom.}$)
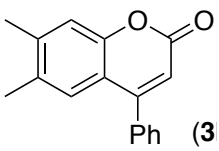 (**3** 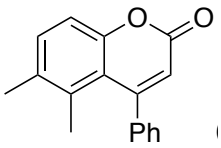	6,7-dimethyl-4-phenyl-2*H*-chromen-2-one/5,6-dimethyl-4- phenyl-2*H*-chromen-2-one (**3a**). Yield: 88%. (**3b**) / (**3b′**) : 1 / 0.2 3b : ^{1}H NMR (300 MHz, $CDCl_3$): δ = 2.23 (s, 3H, CH_3), 2.36 (s, 3H, CH_3), 6.29 (s, 1H, =CH-), 7.20 (s, 2H, $H_{arom.}$), 7.43-7.47 (m, 2H, $H_{arom.}$), 7.51-7.55 (m, 3H, $H_{arom.}$)
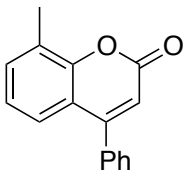	8-methyl-4-phenyl-2H-chromen-2-one (**3c**). Yield: 85% ^{1}H NMR (300 MHz, $CDCl_3$): δ = 2.52 (s, 3H, CH_3), 6.37 (s, 1H, =CH-), 7.13 (t, 1H, *J* = 7.7 Hz, $H_{arom.}$), 7.32 (dd, 1$H_{arom.}$, *J* = 8.0, 1.1 Hz, $H_{arom.}$), 7.40-7.47 (m, 3H, $H_{arom.}$), 7.50-7.54 (m, 3H, $H_{arom.}$)
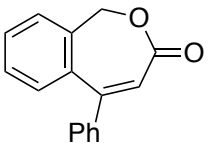	5-phenylbenzo[c]oxepin-3(1H)-one (**3c$_{b-p}$**). Yield: 14%; colorless solid; m.p = 110 °C; R_f = 0.31 (20% EtOAc/cyclohexane). **^{1}H NMR** (500 MHz, $CDCl_3$): δ = 5.07 (large s, 1H, -CH_2-), 5.30 (large s, 1H, -CH_2-), 6.54 (s, 1H, CH_3), 7.13 (d, 1H, *J* = 7.7 Hz, $H_{arom.}$), 7.36-7.52 (m, 8H, $H_{arom.}$). **^{13}C NMR** (125MHz, $CDCl_3$): δ = 68.9, 120.5, 128.7, 129.0, 129.3, 129.5, 129.6, 130.1, 130.9, 136.1, 137.6, 140.5, 151.6, 168.7. **IR (neat)**: 442, 504, 623, 650, 671, 698, 775, 875, 1038, 1208, 1267, 1377, 1488, 1702, 2952, 2992, 3057, 3391 cm^{-1}. **HRMS** (ESI-µTOF): *m/z* $[M+H]^+$ calcd for $C_{16}H_{13}O_2$: 237.0910; found: 237.0911
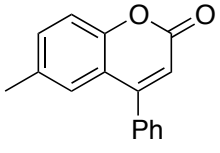	6-methyl-4-phenyl-2*H*-chromen-2-one (**3d**). Yield: 89% ^{1}H NMR (300 MHz, $CDCl_3$): δ= 2.34 (s, 3H, CH_3), 6.35 (s, 1H, =CH-), 7.25 (s, 1H, H_{arom}), 7.03 (d, 1H, *J* = 8.4 Hz, $H_{arom.}$), 7.36 (dd, 1$H_{arom.}$, *J* = 8.5, 1.9 Hz, $H_{arom.}$), 7.43-7.48 (m, 2H, $H_{arom.}$), 7.51-7.56 (m, 3H, $H_{arom.}$)

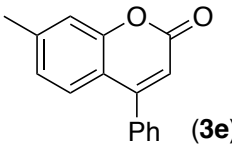
(**3e**)

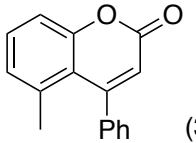
(**3e'**)

7-methyl-4-phenyl-2H-chromen-2-one / 5-methyl-4-phenyl-2H-chromen-2-one
Yield: 77%. (**3e**) / (**3e′**) : 1 / 0.23.
3e ^{1}H NMR (300 MHz, $CDCl_3$): δ = 2.46 (s, 3H, CH_3), 6.32 (s, 1H, =CH-), 7.04 (ddd, 1H, *J* = 8.2, 1.6, 0.6 Hz), 7.22 (s, 1H, H_{arom}), 7.03 (d, 1H, *J* = 8.1 Hz, $H_{arom.}$), 7.43-7.48 (m, 2H, $H_{arom.}$), 7.50-7.54 (m, 3H, $H_{arom.}$)

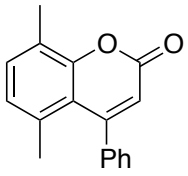

5,8-dimethyl-4-phenyl-2*H*-chromen-2-one (**3f**). Yield: 88%. White solid; m.p =97.4–99.4 °C; R_f = 0.25 (20% diethyl ether /pentane).

^{1}H NMR (300 MHz, $CDCl_3$): δ = 2.39 (s, 3H, CH_3), 2.42 (s, 3H, CH_3), 6.30 (s, 1H, =CH-), 7.03 (d, 1H, *J* = 8.2 Hz, $H_{arom.}$), 7.20 (d, 1H, *J* = 8.2 Hz, $H_{arom.}$), 7.41 – 7.45 (m, 2H, $H_{arom.}$), 7.48 – 7.52 (m, 3H, $H_{arom.}$). **^{13}C NMR** (125MHz, $CDCl_3$): δ = 11.8, 20.6, 113.8, 116.9, 124.0, 125.1, 125.7, 128.6, 128.9, 129.6, 135.9, 141.8, 152.5, 156.3, 161.4. **IR (neat)**: 424, 497, 570, 619, 638, 699, 712, 757, 778, 817, 890, 953, 1090, 1176, 1258, 1370, 1448, 1597, 1707, 2853, 2921, 2973, 3059 cm^{-1}. **HRMS** (ESI- µTOF): *m/z* $[M+K]^+$ calcd for $C_{17}H_{14}KO_2$: 289.0625; found: 289.0588

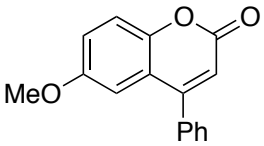

6-methoxy-4-phenyl-2*H*-chromen-2-one (**3h**). Yield: 84%

^{1}H NMR (300 MHz, $CDCl_3$): δ = 3.74 (s, 3H, OCH_3), 6.38 (s, 1H, =CH-), 6.93 (d, 1H, *J* = 2.9 Hz, $H_{arom.}$), 7.13 (dd, 1H, *J* = 9.0, 2.9 Hz $H_{arom.}$), 7.35 (d, 1H, *J* = 9.0 Hz, $H_{arom.}$), 7.43 – 7.48 (m, 2H, $H_{arom.}$), 7.51 – 7.55 (m, 3H, $H_{arom.}$)

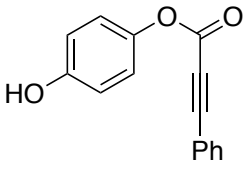

4-hydroxyphenyl 3-phenylpropynoate (**3h$_{b-p}$**). Yield: 20%; white solid; m.p = 102 °C; R_f = 0.33 (20% EtOAc/cyclohexane).

^{1}H NMR (400 MHz, $CDCl_3$): δ = 6.50 (d, 2H, *J* = 10.1 Hz, $H_{arom.}$), 6.56 (s, 1H, -OH), 6.71 (d, 2H, *J* = 10.1 Hz, $H_{arom.}$), 7.37 – 7.41 (m, 2H, $H_{arom.}$), 7.46 – 7.50 (m, 3H, $H_{arom.}$). **^{13}C NMR** (125MHz, $CDCl_3$): δ = 81.4, 116.9, 127.3, 128.9, 129.4, 131.9, 132.2, 143.5, 165.4, 170.7, 184.2. **IR (neat)**: 425, 561, 687, 775, 875, 938, 1014, 1067, 1169, 1195, 1277, 1387, 1610, 1667, 1790, 2923, 3089 cm^{-1}. **HRMS** (ESI-µTOF): *m/z* $[M+H]^+$ calcd for $C_{15}H_{11}O_3$: 239.0703; found: 239.0705

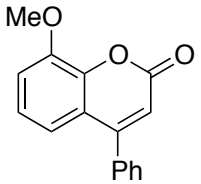

8-methoxy-4-phenyl-2H-chromen-2-one (**3i**). Yield: 86%

^{1}H NMR (300 MHz, $CDCl_3$): δ= 3.99 (s, 3H, OCH_3), 6.39 (s, 1H, =CH-), 7.05 (dd, 1H, *J* = 7.5, 2.0 Hz, $H_{arom.}$), 7.10 (dd, 1H, *J* = 8.1, 2.0 Hz, $H_{arom.}$), 7.16 (t, 1H, *J* = 8.1 Hz, $H_{arom.}$), 7.43-7.48 (m, 2H, $H_{arom.}$), 7.50-7.54 (m, 3H, $H_{arom.}$)

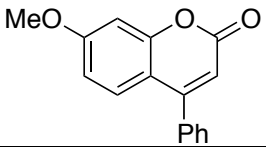

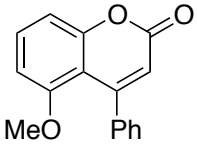

7-methoxy-4-phenyl-2*H*-chromen-2-one / 5-methoxy-4-phenyl-2*H*-chromen-2-one.
Yield: 94%. (**3j**) / (**3j′**) = 1 / 0.31

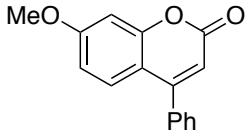

(**3j**) **^{1}H NMR** (300 MHz, $CDCl_3$): δ = 3.89 (s, 3H, OCH_3), 6.22 (s, 1H, =CH-), 6.80 (dd, 1H, *J* = 8.9, 2.6 Hz, $H_{arom.}$), 6.90 (d, 1H, *J* = 2.5 Hz, $H_{arom.}$), 7.39 (d, 1H, *J* = 8.9 Hz, $H_{arom.}$), 7.42 – 7.47 (m, 2H, $H_{arom.}$), 7.49 – 7.54 (m, 3H, $H_{arom.}$)

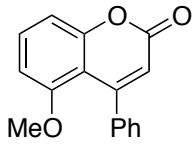

(**3j'**) **^{1}H NMR** (300 MHz, $CDCl_3$): δ = 3.46 (s, 3H, OCH_3), 6.18 (s, 1H, =CH-), 6.67 (dd, 1H, *J* = 8.3, 0.8 Hz $H_{arom.}$), 7.03 (dd, 1H, *J* = 8.4, 1.0 Hz $H_{arom.}$), 7.27 – 7.31 (m, 2H, $H_{arom.}$), 7.37 – 7.41 (m, 3H, $H_{arom.}$), 7.47 (t, 1H, *J* = 8.3 Hz, $H_{arom.}$)

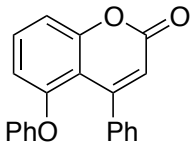

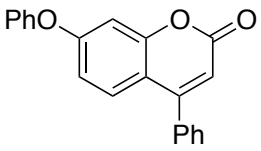

7-phenoxy-4-phenyl-2H-chromen-2-one / 5-phenoxy-4-phenyl-2*H*-chromen-2-one. Yield: 82%. (**3k**) / (**3k′**) = 1 / 0.25. White solid; R_f = 0.3 (20% diethyl ether / cyclohexane)

IR (neat): 404, 429, 466, 496, 570, 614, 644, 689, 731, 771, 797, 818, 836, 850, 868, 936, 999, 1049, 1072, 1113, 1147, 1182, 1241, 1271, 1339, 1374, 1449, 1484, 1550, 1586, 1712, 2853, 2923, 3051, 3088 cm^{-1}. **3j and 3j′** : **^{1}H NMR** (300 MHz, $CDCl_3$): δ = 6.23 (s, 0.25H, =CH-), 6.26 (s, 1H, =CH-), 6.42 – 6.45 (m, 0.5H, $H_{arom.}$), 6.77 (dd, 0.26H, *J* = 8.2, 1.1 Hz $H_{arom.}$), 6.87 (dd, 1H, *J* = 8.8, 2.5 Hz, $H_{arom.}$), 6.92 (d, 1H, *J* = 2.4 Hz, $H_{arom.}$), 6.96 – 6.99 (m, 0.26H, $H_{arom.}$), 7.07 – 7.15 (m, 2.54H, $H_{arom.}$), 7.20 – 7.25 (m, 2.26H, $H_{arom.}$), 7.38 – 7.48 m (5.22H, $H_{arom.}$), 7.50 – 7.54 (m, 3H, $H_{arom.}$). **HRMS** (ESI-μTOF): *m/z* $[M+H]^+$ calcd for $C_{21}H_{15}O_3$: 315.1016; found: 315.1001

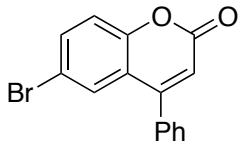

6-bromo-4-phenyl-2*H*-chromen-2-one (**3l**). Yield: 25%

^{1}H NMR (400 MHz, $CDCl_3$): δ = 6.40 (s, 1H, =CH-), 7.30 (d, 1H, *J* = 8.8 Hz, $H_{arom.}$), 7.42 – 7.45 (m, 2H, $H_{arom.}$), 7.55 – 7.57 (m, 3H, $H_{arom.}$), 7.59 (d, 1H, *J* = 2.3 Hz, $H_{arom.}$), 7.64 (dd, 1H, *J* = 8.7, 2.3 Hz $H_{arom.}$)

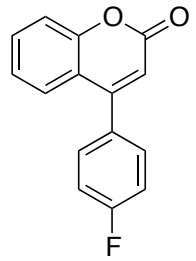

4-(4-fluorophenyl)-2*H*-chromen-2-one (**3m**). Yield: 50%

^{1}H NMR (500 MHz, $CDCl_3$): δ = 6.37 (s, 1H, =CH-), 7.21-7.27 (m, 3H, $H_{arom.}$), 7.41-7.47 (m, 4H, $H_{arom.}$), 7.55 – 7.59 (m, 1H, $H_{arom.}$)

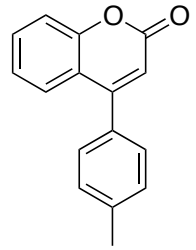

4-(*p*-tolyl)-2*H*-chromen-2-one (**3n**). Yield: 59%

^{1}H NMR (300 MHz, $CDCl_3$): δ = 2.46 (s, 3H, CH_3), 6.37 (s, 1H, =CH-), 7.20-7.25 (m, 1H, $H_{arom.}$), 7.31-7.42 (m, 5H, $H_{arom.}$), 7.52-7.57 (m, 2H, $H_{arom.}$)

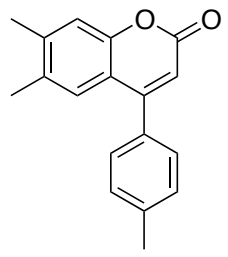

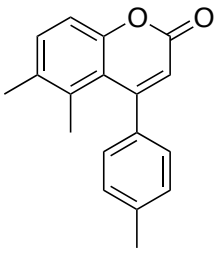

6,7-dimethyl-4-(*p*-tolyl)-2*H*-chromen-2-one /5,6-dimethyl-4-(*p*-tolyl)-2*H*-chromen-2-one. Yield: 60%; (**3o**) / (**3o′**) = 1 / 0.26. White solid; R_f = 0.2(20% diethyl ether /pentane).

(**3a**): **^{1}H NMR** (400 MHz, $CDCl_3$): δ = 2.23 (s, 3H, CH_3), 2.35 (s, 3H, CH_3), 2.46 (s, 3H, CH_3), 6.27 (s, 1H, =CH-), 7.19 (s, 1H, $H_{arom.}$), 7.23 (s, 1H, $H_{arom.}$), 7.31-7.37 (m, 4H, $H_{arom.}$). **3n** : **^{13}C NMR** (125MHz, $CDCl_3$): δ = 19.5, 20.3, 21.5, 114.0, 116.8, 118.0, 127.1, 128.5, 129.6, 132.8, 133.0, 139.8, 142.1, 152.7, 155.9, 161.6 **HRMS** (ESI-μTOF): *m/z* $[M+H]^+$ calcd for $C_{18}H_{17}O_2$: 265.1223; found: 265.1219

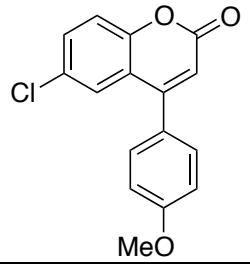	6-chloro-4-(4-methoxyphenyl)-2*H*-chromen-2-one (**3p**). Yield: 50% ^{1}H NMR (300 MHz, $CDCl_3$): δ= 3.90 (s, 3H, OCH_3), 6.38 (s, 1H, =CH-), 7.07 (d, 2H, *J* = 8.8 Hz, $H_{arom.}$), 7.35 (dd, 1$H_{arom.}$, *J* = 8.5, 0.6 Hz, $H_{arom.}$), 7.37 (d, 2H, *J* = 8.8 Hz, $H_{arom.}$), 7.31-7.42 (m, 2H, $H_{arom.}$)
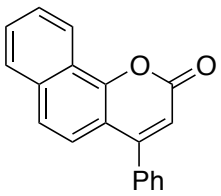	4-phenyl-2*H*-benzo[*h*]chromen-2-one (**3q**). Yield: 99% ^{1}H NMR (500 MHz, $CDCl_3$): δ = 6.48 (s, 1H, =CH-), 7.45 – 7.53 (m, 3H, $H_{arom.}$), 7.54 – 7.59 (m, 3H, $H_{arom.}$), 7.63 (d, 1H, *J* = 8.8 Hz, $H_{arom.}$), 7.65 – 7.69 (m, 2H, $H_{arom.}$), 7.86 – 7.88 (m, 1H, $H_{arom.}$), 7.63 – 7.65 (m, 1H, $H_{arom.}$)
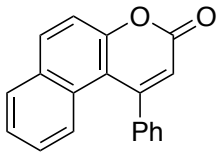	1-phenyl-3*H*-benzo[*f*]chromen-3-one (**3r**). Yield: 99% ^{1}H NMR (300 MHz, $CDCl_3$): δ = 6.39 (s, 1H, =CH-), 7.13 – 7.18 (m, 1H, $H_{arom.}$), 7.25 (d, 1H, *J* = 8.3 Hz, $H_{arom.}$), 7.35 – 7.39 (m, 2H, $H_{arom.}$), 7.41 – 7.44 (m, 1H, $H_{arom.}$), 7.48 – 7.55 (m, 4H, $H_{arom.}$), 7.85 (d, 1H, *J* = 8.5 Hz, $H_{arom.}$), 8.02 (d, 1H, *J* = 9.0 Hz, $H_{arom.}$)
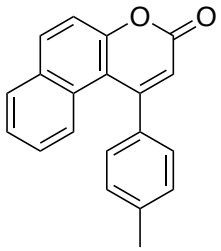	1-(*p*-tolyl)-3*H*-benzo[*f*]chromen-3-one (**3s**). Yield: 74%; White solid; m.p=124.8–126.6°C;R_f= 0.19(20% diethyl ether /pentane). **^{1}H NMR** (300 MHz, $CDCl_3$): δ = 2.50 (s, 3H, CH_3), 6.37 (s, 3H, =CH-), 7.17 – 7.22 (m, 1H, $H_{arom.}$), 7.25 (d, 2H, *J* = 8.2 Hz, $H_{arom.}$), 7.31 – 7.37 (m, 3H, $H_{arom.}$), 7.40 – 7.45 (m, 1H, $H_{arom.}$), 7.51 (d, 1H, *J* = 8.9 Hz, $H_{arom.}$), 7.85 (dd, 1H, *J* = 8.1, 1.3 Hz $H_{arom.}$), 7.99 (d, 1H, *J* = 8.9 Hz, $H_{arom.}$). **^{13}C NMR** (125MHz, $CDCl_3$): δ = 21.6, 113.3, 116.8, 117.6, 125.4, 126.2, 126.8, 127.5, 129.1, 129.6, 129.9, 131.4, 134.0, 136.8, 139.4, 154.9, 156.8, 160.6. **IR (neat)**: 408, 459, 566, 603, 747, 811, 933, 996, 1055, 1454, 1509, 1546, 1622, 1721, 2852, 2921 cm^{-1}. **HRMS** (ESI-µTOF): *m/z* $[M+H]^+$ calcd for $C_{20}H_{15}O_2$: 287.1067; found: 287.1093
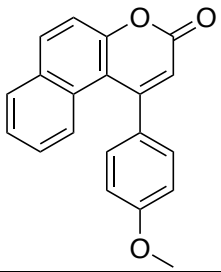	1-(4-methoxyphenyl)-3*H*-benzo[*f*]chromen-3-one (**3t**). Yield: 99% ^{1}H NMR (500 MHz, $CDCl_3$): δ = 3.92 (s, 3H, OCH_3), 6.37 (s, 1$H_{arom.}$, =CH-), 7.02 (d, 2H, *J* = 8.7 Hz, $H_{arom.}$), 7.18 – 7.22 (m, 1H, $H_{arom.}$), 7.29 (d, 2H, *J* = 8.8 Hz, $H_{arom.}$), 7.38 – 7.43 (m, 2H, $H_{arom.}$), 7.52 (d, 1H, *J* = 9.0 Hz, $H_{arom.}$), 7.85 (d, 1H, *J* = 8.0 Hz, $H_{arom.}$), 8.00 (d, 1H, *J* = 9.0 Hz, $H_{arom.}$)
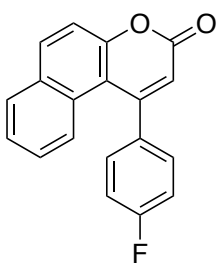	1-(4-fluorophenyl)-3*H*-benzo[*f*]chromen-3-one (**3u**). Yield: 99%; White solid; m.p = 116.5–121.4°C; R_f=0.15(20% diethyl ether /pentane). **^{1}H NMR** (300 MHz, $CDCl_3$): δ = 6.37 (s, 1H, =CH-), 7.17 – 7.28 (m, 4H, $H_{arom.}$), 7.33 – 7.39 (m, 2H, $H_{arom.}$), 7.40 – 7.46 (m, 1H, $H_{arom.}$), 7.54 (d, 1H, *J* = 9.0 Hz, $H_{arom.}$), 7.87 (dd, 1H, *J* = 8.1, 1.2 Hz $H_{arom.}$), 8.02 (d, 1H, *J* = 8.9 Hz, $H_{arom.}$). **^{13}C NMR** (125MHz, $CDCl_3$): δ = 113.0, 116.4, 116.6, 117.2, 117.7, 125.6, 125.9, 127.0, 129.3, 129.4, 129.5, 129.6, 131.5, 134.3, 135.6, 135.7, 155.0, 155.6, 160.4, 162.4,

	164.4. **IR (neat)**: 402, 503, 532, 565, 600, 685, 698, 723, 750, 817, 848, 893, 933, 996, 1074, 1092, 1154, 1182, 1214, 1267, 1319, 1394, 1430, 1454, 1503, 1546, 1599, 1622, 1717, 2849, 2920, 3069 cm^{-1}. **HRMS** (ESI-µTOF): *m/z* $[M+H]^+$ calcd for $C_{19}H_{12}FO_2$: 291.0816; found: 291.0817

Structural formula	Description
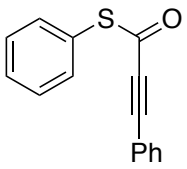	*S*-phenyl 3-phenylprop-2-ynethioate (**4a**). Yield: 50%; brown oil **^{1}H NMR** (300 MHz, $CDCl_3$): δ = 7.34 - 7.40 (m, 2H, $H_{arom.}$), 7.41 - 7.51 (m, 6H, $H_{arom.}$), 7.51 - 7.58 (m, 2H, $H_{arom.}$). **IR (neat)**: 453, 533, 636, 685, 744, 785, 919, 990, 1012, 1257, 1440, 1477, 1488, 1645, 2193, 3058 cm^{-1}. **HRMS** (ESI-µTOF): *m/z* $[M+H]^+$ calcd for $C_{15}H_{11}OS$: 239.0525; found: 239.0514.
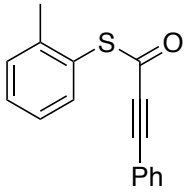	*S*-(*o*-tolyl) 3-phenylprop-2-ynethioate (**4c**). Yield: 60%; yellow solid; **^{1}H NMR** (300 MHz, $CDCl_3$): δ = 2.45 (s, 3H, CH_3), 7.27 - 7.31 (m, 1H, $H_{arom.}$) or 7.29 (dd, 1H, *J* = 7.5, 2.3 Hz, $H_{arom.}$), 7.33 - 7.41 (m, 4H, $H_{arom.}$), 7.43 - 7.49 (m, 3H, $H_{arom.}$), 7.50 - 7.53 (m, 1H, $H_{arom.}$) or 7.29 (dd, 1H, *J* = 7.7, 1.2 Hz, $H_{arom.}$). **^{13}C NMR** (125MHz, $CDCl_3$): δ = 21.1, 85.2, 93.8, 119.5, 126.9, 127.0, 128.8, 130.9, 131.1, 131.2, 133.2, 136.5, 142.7, 176.1. **IR (neat)**: 425, 480, 530, 645, 686, 750, 790, 915, 991, 1017, 1205, 1282, 1376, 1487, 1643, 2200, 2850, 2918, 3057, 3270 cm^{-1}. **HRMS** (ESI-µTOF): *m/z* $[M+H]^+$ calcd for $C_{16}H_{12}OS$: 253.0682; found: 253.0676.
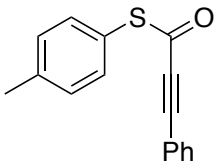	*S*-(*p*-tolyl) 3-phenylprop-2-ynethioate (**4b**). Yield: 65%; yellow solid; m.p = 71 °C; R_f = 0.5 (10% ethyl acetate /cyclohexane). **^{1}H NMR** (300 MHz, $CDCl_3$): δ= 2.41 (s, 3H, CH_3), 7.27 - 7.30 (m, 2H, $H_{arom.}$), 7.34 - 7.41 (m, 3H, $H_{arom.}$), 7.42 - 7.49 (m, 4H, $H_{arom.}$). **^{13}C NMR** (125MHz, $CDCl_3$): δ = 21.5, 85.3, 94.2, 119.6, 123.8, 128.7, 130.4, 131.1, 133.2, 135.0, 140.7, 176.8. **IR (neat)**: 474, 533, 636, 687, 759, 786, 805, 988, 1006, 1255, 1398, 1441, 1486, 1572, 1592, 1652, 2186, 2850, 2918 cm^{-1}. **HRMS** (ESI-µTOF): *m/z* $[M+H]^+$ calcd for $C_{16}H_{13}OS$: 253.0682; found: 253.0667.
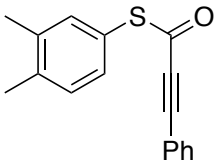	*S*-(3,4-dimethylphenyl) 3-phenylprop-2-ynethioate (**4d**). Yield: 65%; yellow solid; m.p = 68 °C; R_f = 0.45 (10% ethyl acetate /cyclohexane). **^{1}H NMR** (300 MHz, $CDCl_3$): δ = 2.29 (s, 3H, CH_3), 2.31 (s, 3H, CH_3), 7.21 - 7.29 (m, 3H, $H_{arom.}$), 7.34 - 7.40 (m, 2H, $H_{arom.}$), 7.43 - 7.48 (m, 3H, $H_{arom.}$). **^{13}C NMR** (125MHz, $CDCl_3$): δ = 19.9, 19.9, 85.4, 94.0, 119.6, 123.8, 128.7, 130.9, 131.1, 132.5, 133.1, 136.0, 138.2, 139.4, 176.9. **IR (neat)**: 432, 534, 567, 638, 688, 761, 786, 818, 988, 1010, 1027, 1256, 1383, 1442, 1485, 1654, 2190, 2852, 2922, 3021, 3060, 3289 cm^{-1}. **HRMS** (ESI-µTOF): *m/z* $[M+H]^+$ calcd for $C_{17}H_{15}OS$: 267.0838; found: 267.0838.

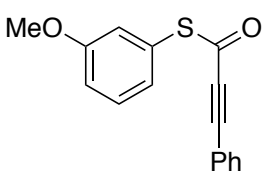

S-(3-methoxyphenyl) 3-phenylprop-2-ynethioate (**4f**). Yield: 78%; yellow oil; R_f = 0.39 (10% ethyl acetate /cyclohexane).

^{1}H NMR (300 MHz, $CDCl_3$): δ = 3.83 (s, 3H, OCH_3), 7.02 (dd, 1H, *J* = 8.3, 0.9 Hz, $H_{arom.}$), 7.08 (t, 1H, *J* = 2 Hz, $H_{arom.}$), 7.13 (dt, 1H, *J* = 7.7, 1.2 Hz, $H_{arom.}$), 7.35 - 7.40 (m, 3H, $H_{arom.}$), 7.44 - 7.50 (m, 3H, $H_{arom.}$). **^{13}C NMR** (125MHz, $CDCl_3$): δ = 55.6, 85.2, 94.2, 116.5, 119.5, 119.9, 127.2, 128.2, 128.8, 130.3, 131.2, 133.2, 160.1, 176.2. **IR (neat)**: 440, 532, 636, 684, 755, 784, 847, 989, 1012, 1232, 1247, 1283, 1425, 1442, 1479, 1589, 1649, 2193, 2836, 2906, 2936, 2959, 3003, 3063 cm^{-1}. **HRMS** (ESI-μTOF): *m/z* $[M+H]^+$ calcd for $C_{16}H_{12}NaO_2S$: 291.0450; found: 291.0444.

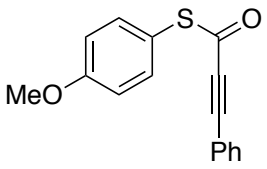

S-(4-methoxyphenyl) 3-phenylprop-2-ynethioate (**4e**). Yield: 69%; yellow solid; m,p = 84 °C; R_f = 0.33 (10% ethyl acetate /cyclohexane).

^{1}H NMR (500 MHz, $CDCl_3$): δ = 3.85 (s, 3H, OCH_3), 6.99 (d, 2H, *J* = 8.9 Hz, $H_{arom.}$), 7.37 (t, 2H, *J* = 7.6 Hz, $H_{arom.}$), 7.44 (d, 2H, *J* = 8.9 Hz, $H_{arom.}$), 7.46 - 7.48 (m, 3H, $H_{arom.}$). **^{13}C NMR** (125MHz, $CDCl_3$): δ = 55.6, 85.3, 94.3, 115.2, 118.0, 119.6, 128.8, 131.1, 133.2, 136.7, 161.3, 177.5. **IR (neat)**: 500, 533, 632, 690, 754, 791, 822, 992, 1012, 1176, 1249, 1288, 1444, 1494, 1572, 1591, 1650, 2195, 2839, 2928 cm^{-1}. **HRMS** (ESI-μTOF): *m/z* $[M+H]^+$ calcd for $C_{16}H_{13}O_2S$: 269.0631; found: 269.0631.

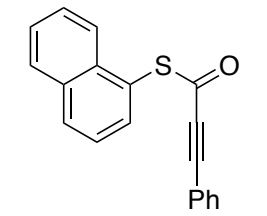

S-(naphthalen-1-yl) 3-phenylprop-2-ynethioate (**4g**). Yield: 70%; yellow solid; m.p = 82 °C; R_f = 0.44 (10% ethyl acetate /cyclohexane).

^{1}H NMR (300 MHz, $CDCl_3$): δ = 7.28 - 7.36 (m, 4H, $H_{arom.}$), 7.39 - 7.46 (m, 1H, $H_{arom.}$),
7.53 - 7.64 (m, 3H, $H_{arom.}$), 7.84 (dd, 1H, *J* = 7.2, 1.2 Hz, $H_{arom.}$), 7.93 (d, 1H, *J* = 7.4 Hz, $H_{arom.}$), 8.02 (d, 1H, *J* = 8.3 Hz, $H_{arom.}$), 8.32 (d, 1H, *J* = 8.2 Hz, $H_{arom.}$). **^{13}C NMR** (125MHz, $CDCl_3$): δ = 85.2, 94.4, 119.4, 124.8, 125.6, 125.8, 126.8, 127.7, 128.7, 128.8, 131.1, 131.7, 133.1, 134.4, 134.4, 135.7, 176.5. **IR (neat)**: 405, 492, 534, 638, 688, 760, 790, 968, 993, 1015, 1261, 1442, 1486, 1502, 1592, 1643, 2196, 3035, 3056, 3267 cm^{-1}. **HRMS** (ESI-μTOF): *m/z* $[M+H]^+$ calcd for $C_{19}H_{13}OS$: 289.0682; found: 289.0682.

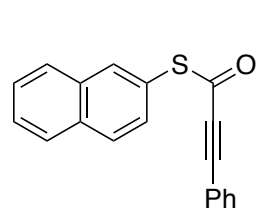

S-(naphthalen-2-yl) 3-phenylprop-2-ynethioate (**4h**). Yield: 65%; yellow solid; m.p = 106 °C; R_f = 0.47 (10% ethyl acetate /cyclohexane).

^{1}H NMR (300 MHz, $CDCl_3$): δ = 7.29 - 7.47 (m, 5H, $H_{arom.}$), 7.52 - 7.61 (m, 3H, $H_{arom.}$), 7.86 - 7.94 (m, 3H, $H_{arom.}$), 8.32 (d, 1H, *J* = 1.2 Hz, $H_{arom.}$). **^{13}C NMR** (125MHz, $CDCl_3$): δ = 31.1, 85.3, 94.5, 119.4, 124.6, 126.9, 127.7, 128.0, 128.3, 128.7, 129.2, 131.2, 133.2, 133.7, 133.8, 135.2, 176.5. **IR (neat)**: 474, 530, 628, 685, 751, 788, 819, 867, 990, 1014, 1194, 1256, 1442, 1487, 1650, 2193, 3055, 3283 cm^{-1}. **HRMS** (ESI-μTOF): *m/z* $[M+H]^+$ calcd for $C_{19}H_{13}OS$: 289.0682; found: 289.0682.

Structural formula	Description
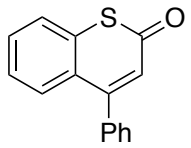	4-phenyl-2*H*-thiochromen-2-one (**5a**). Yield: 84%; **^{1}H NMR** (300 MHz, $CDCl_3$): δ = 6.54 (s, 1H, =CH-), 7.27 - 7.32 (m, 1H, $H_{arom.}$), 7.38 - 7.43 (m, 2H, $H_{arom.}$), 7.45 - 7.52 (m, 4H, $H_{arom.}$), 7.52 - 7.56 (m, 2H, $H_{arom.}$). **^{13}C NMR** (125MHz, $CDCl_3$): δ = 124.9, 126.4, 126.4, 126.9, 128.8, 128.8, 129.1, 129.9, 130.7, 138.0, 138.4, 155.6, 184.8. **IR (neat)**: 413, 427, 559, 651, 670, 696, 734, 758, 773, 789, 867, 1183, 1245, 1265, 1360, 1428, 1539, 1583, 1626, 3028, 3054 cm^{-1}. **HRMS** (ESI-µTOF): *m/z* $[M+H]^+$ calcd for $C_{15}H_{11}OS$: 239.0525; found: 239.0513.
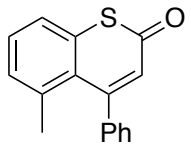	8-methyl-4-phenyl-2*H*-thiochromen-2-one (**5c$_{b\text{-}pr}$**). Yield: 40%; yellow solid; m.p = 68 °C; R_f = 0.54 (20% EtOAc/cyclohexane). **^{1}H NMR** (400 MHz, $CDCl_3$): δ = 1.81 (s, 3H, CH_3), 6.53 (s, 1H, =CH-), 7.12 (d, 1H, *J* = 7.2 Hz, $H_{arom.}$), 7.29 - 7.30 (m, 2H, $H_{arom.}$), 7.34 - 7.40 (m, 2H, $H_{arom.}$), 7.42 - 7.44 (m, 3H, $H_{arom.}$). **^{13}C NMR** (125MHz, $CDCl_3$): δ = 25.2, 124.5, 126.3, 127.7, 128.6, 128.8, 128.8, 129.3, 131.3, 139.0, 140.2, 142.6, 155.6, 184.7. **IR (neat)**: 442, 540, 598, 695, 769, 852, 1029, 1076, 1138, 1191, 1250, 1345, 1414, 1441, 1488, 1576, 1644, 1695, 2197, 2852, 2923, 3055 cm^{-1}. **HRMS** (ESI-µTOF): *m/z* $[M+H]^+$ calcd for $C_{16}H_{13}OS$: 253.0682; found: 253.0699.
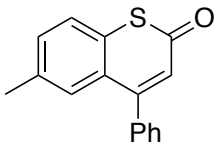	6-methyl-4-phenyl-2*H*-thiochromen-2-one (**5b**). Yield: 99%; yellow solid; m.p = 115 °C;R_f=0.54(20% EtOAc/cyclohexane) **^{1}H NMR** (500 MHz, $CDCl_3$): δ = 2.43 (s, 3H, CH_3), 6.48 (s, 1H, =CH-), 7.54 (dd, 1H, *J* = 8.3, 1 Hz, $H_{arom.}$), 7.35 - 7.39 (m, 3H, $H_{arom.}$), 7.42 (d, 1H, *J* = 8.3 Hz, $H_{arom.}$), 7.48 - 7.52 (m, 3H, $H_{arom.}$). **^{13}C NMR** (125MHz, $CDCl_3$): δ = 21.5, 124.0, 124.6, 126.5, 127.7, 128.7, 128.8, 129.0, 130.6, 138.1, 138.7, 140.8, 155.7, 185.0. **IR (neat)**: 437, 544, 633, 666, 698, 725, 780, 821, 862, 913, 1158, 1183, 1219, 1245, 1269, 1357, 1381, 1440, 1483, 1531, 1597, 1629, 1725, 2852, 2918, 3027, 3052cm^{-1}. **HRMS** (ESI-µTOF): *m/z* $[M+H]^+$ calcd for $C_{16}H_{13}OS$: 253.0682; found: 253.0670.
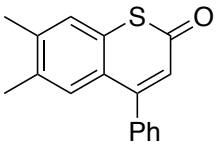 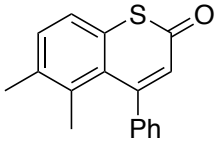	6,7-dimethyl-4-phenyl-2*H*-thiochromen-2-one /5,6-dimethyl-4-phenyl-2*H*-thiochromen-2-one (**5d**) / (**5d**). Yield: 99%; yellow solid; R_f= 0.54 (20% EtOAc/cyclohexane) **^{1}H NMR** (500 MHz, $CDCl_3$): δ = 2.21 (s, 3H, CH_3), 2.34 (s, 3H, CH_3), 2.41 (d, 2.6 H, *J* = 4.3 Hz, $H_{arom.}$), 6.46 (s, 1H, =CH-), 6.49 (s, 0.45H, =CH-), 7.10 (d, 0.45H, *J* = 8.3 Hz, $H_{arom.}$), 7.27 (s, 1H, $H_{arom.}$), 7.29 (d, 0.57H, *J* = 8.6 Hz, $H_{arom.}$), 7.31 (s, 1H, $H_{arom.}$), 7.36 - 7.39 (m, 3H, $H_{arom.}$), 7.46 - 7.53 (m, 4.6H, $H_{arom.}$). **IR (neat)**: 439, 493, 544, 605, 649, 697, 763, 782, 859, 1020, 1182, 1339, 1383, 1440, 1602, 1629, 1724, 2862, 2915, 2934, 2967, 3048 cm^{-1}. **HRMS** (ESI-µTOF): *m/z* $[M+H]^+$ calcd for $C_{17}H_{15}OS$: 267.0838; found: 267.0842.
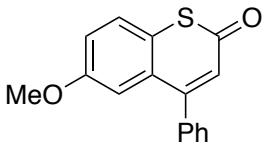	6-methoxy-4-phenyl-2*H*-thiochromen-2-one (**5e**). Yield: 90%; yellow oil; R_f = 0.41 (20% EtOAc/cyclohexane) **^{1}H NMR** (400 MHz, $CDCl_3$): δ = 3.88 (s, 3H, OCH_3), 6.40 (s, 1H, =CH-), 6.84 (d, 1H, *J* = 9 Hz, $H_{arom.}$), 7.01 (s, 1H, $H_{arom.}$), 7.37 - 7.39

	(m, 2H, $H_{arom.}$), 7.44 (d, 1H, *J* = 9 Hz, $H_{arom.}$), 7.48 - 7.49 (m, 3H, $H_{arom.}$). **^{13}C NMR** (125MHz, $CDCl_3$): δ = 55.9, 109.5, 114.6, 120.4, 122.3, 128.7, 128.7, 129.0, 132.2, 138.9, 140.6, 155.9, 160.7, 184.7. **IR (neat)**: 416, 442, 543, 564, 699, 780, 837, 1027, 1060, 1181, 1235, 1282, 1361, 1441, 1529, 1587, 1631, 1733, 2838, 2905, 2936, 2964, 3056 cm^{-1}. **HRMS** (ESI-μTOF): *m/z* $[M+H]^+$ calcd for $C_{16}H_{13}O_2S$: 269.0631; found: 269.0622.
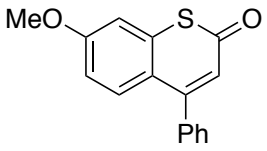	7-methoxy-4-phenyl-2*H*-thiochromen-2-one (**5f**). Yield: 24%. R_f = 0.40 (20% EtOAc/cyclohexane) **^{1}H NMR** (300 MHz, $CDCl_3$): δ = 3.70 (s, 3H, OCH_3), 6.55 (s, 1H, =CH-), 7.03 (d, 1H, *J* = 2.7 Hz, $H_{arom.}$), 7.12 (dd, 1H, *J* = 8.8, 2.7 Hz, $H_{arom.}$), 7.35 - 7.42 (m, 2H, $H_{arom.}$), 7.44 (d, 1H, *J* = 8.8 Hz, $H_{arom.}$), 7.48 - 7.53 (m, 3H, $H_{arom.}$).
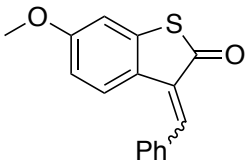	3-benzylidene-6-methoxybenzo[*b*]thiophen-2(3*H*)-one (**5f$_{b-p}$**). Yield: 8%; yellow solid 120 °C; R_f = 0.21 (20% EtOAc/cyclohexane) **^{1}H NMR** (300 MHz, $CDCl_3$): δ = 3.93 (s, 3H, OCH_3), 7.06 (d, 1H, *J* = 2.2 Hz, $H_{arom.}$), 7.11 (dd, 1H, *J* = 8.9, 2.5 Hz, $H_{arom.}$), 7.18 (s, 1H, $H_{arom.}$), 7.47 - 7.54 (m, 3H, $H_{arom.}$), 7.65 - 7.71 (m, 2H, $H_{arom.}$), 8.48 (d, 1H, *J* = 8.9 Hz, $H_{arom.}$). **^{13}C NMR** (125MHz, $CDCl_3$): δ = 55.9, 108.7, 116.7, 123.6, 124.9, 127.1, 129.4, 130.7, 130.8, 136.7, 140.1, 152.2, 162.1, 180.5. **IR (neat)**: 442, 477, 576, 591, 617, 660, 691, 738, 755, 779, 832, 1010, 1051, 1078, 1105, 1124, 1222, 1259, 1321, 1399, 1447, 1487, 1580, 1595, 1618, 1730, 2852, 2922, 3022, 3059 cm^{-1}. **HRMS** (ESI-μTOF): *m/z* $[M+H]^+$ calcd for $C_{16}H_{13}O_2S$: 269.0631; found: 269.0640.
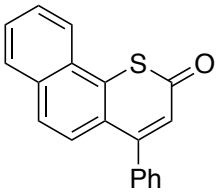	4-phenyl-2*H*-benzo[*h*]thiochromen-2-one (**5g**). Yield: 33%; yellow solid;m.p = 140 °C;R_f = 0.49 (20% EtOAc/cyclohexane) **^{1}H NMR** (400 MHz, $CDCl_3$): δ = 6.71 (s, 1H, =CH-), 7.07 (t, 1H, *J* = 8.1 Hz, $H_{arom.}$), 7.28 - 7.31 (m, 2H, $H_{arom.}$), 7.37 - 7.46 (m, 4H, $H_{arom.}$), 7.53 (d, 1H, *J* = 8.8 Hz, $H_{arom.}$), 7.83 (d, 1H, *J* = 7.9 Hz, $H_{arom.}$), 7.92 (d, 1H, *J* = 8.7 Hz, $H_{arom.}$). **^{13}C NMR** (125MHz, $CDCl_3$): δ = 123.3, 123.8, 126.0, 126.1, 127.4, 127.6, 128.0, 128.8, 128.9, 129.3, 131.4, 131.7, 133.2, 139.9, 143.0, 155.2, 183.9. **IR (neat)**: 496, 539, 556, 620, 694, 740, 773, 813, 896, 961, 1029, 1109, 1158, 1186, 1250, 1301, 1389, 1445, 1501, 1623, 3024, 3051 cm^{-1}. **HRMS** (ESI-μTOF): *m/z* $[M+H]^+$ calcd for $C_{19}H_{13}OS$: 289.0682; found: 289.0695.
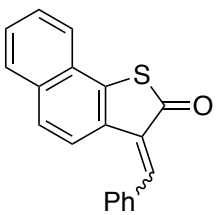	3-benzylidenenaphtho[1,2-*b*]thiophen-2(3*H*)-one (**5g$_{b-p}$**). Yield: 5%; yellow solid; m.p = 150 °C; R_f = 0.32 (20% EtOAc/cyclohexane) **^{1}H NMR** (300 MHz, $CDCl_3$): δ = 7.38 (s, 1H, =CH-), 7.53 - 7.59 (m, 3H, $H_{arom.}$), 7.66 - 7.75 (m, 2H, $H_{arom.}$), 7.76 - 7.82 (m, 2H, $H_{arom.}$), 7.92 - 8.02 (m, 2H, $H_{arom.}$), 8.43 - 7.49 (m, 1H, $H_{arom.}$), 8.56 (d, 1H, *J* = 8.8 Hz, $H_{arom.}$). **^{13}C NMR** (125MHz, $CDCl_3$): δ = 123.8, 124.0, 124.3, 127.3, 127.5, 128.2, 129.1, 129.2, 129.5, 129.7, 129.8, 131.0, 134.2, 136.9, 137.5, 151.4, 181.3. **IR (neat)**: 407, 450, 471, 580, 699, 771, 782, 824, 861, 1029, 1077, 1116, 1260, 1350, 1445, 1488, 1596, 1731, 2851, 2921, 3052 cm^{-1}. **HRMS** (ESI-μTOF): *m/z* $[M+H]^+$ calcd for $C_{19}H_{13}OS$: 289.0682; found: 289.0690.

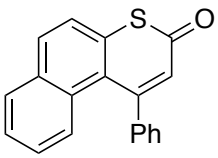

1-phenyl-3*H*-benzo[*f*]thiochromen-3-one (**5h**). Yield: 95%; green solid; m.p = 120 °C; R_f = 0.51 (20% EtOAc/cyclohexane)

^{1}H NMR (500 MHz, $CDCl_3$): δ = 6.65 (s, 1H, =CH-), 7.42 - 7.44 (m, 2H, $H_{arom.}$), 7.51 - 7.56 (m, 4H, $H_{arom.}$), 7.64 - 7.68 (m, 3H, $H_{arom.}$), 7.86 - 7.91 (m, 1H, $H_{arom.}$), 8.29 - 8.32 (m, 1H, $H_{arom.}$). **^{13}C NMR** (125MHz, $CDCl_3$): δ = 123.8, 124.6, 124.8, 126.3, 126.4, 127.6, 128.7, 128.8, 128.8, 129.0, 129.3, 133.0, 137.7, 139.1, 156.9, 183.7. **IR (neat)**: 412, 455, 537, 660, 698, 724, 751, 773, 813, 857, 955, 1028, 1073, 1124, 1159, 1260, 1305, 1390, 1442, 1500, 1537, 1631, 3021, 3053 cm^{-1}. **HRMS** (ESI-μTOF): *m/z* $[M+H]^+$ calcd for $C_{19}H_{13}OS$: 289.0682; found: 289.0686.

6. XRD data description.

Figure S1. Image of XRD packing for (E)

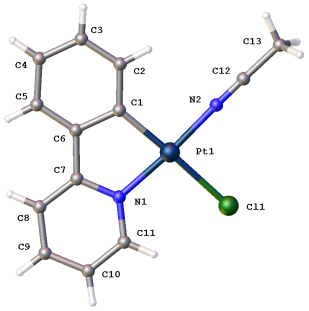

Table S1. Crystal data and refinement details for (E)

Identification Code	Compound (**E**)
Formula	$C_{13}H_{11}ClN_2Pt$
Formula weight	425.78
Crystal system	monoclinic
Space group	$P2_1/n$
a (Å)	11.3968(3)
b (Å)	5.44964(13)
c (Å)	20.0079(5)
α (°)	90
β (°)	105.150(3)
γ (°)	90
V ($Å^3$)	1199.48(5)
Z	4
Density (g cm^{-3})	2.358
Mu (MoKα) (mm^{-1})	11.896
F(000)	792.0
Data collection	
Temperature (K)	100.01(11)
Radiation (Å)	MoKα (λ = 0.71073)
Theta min - max	6.444 to 54.976
Dataset [h, k, l]	$-14 \le h \le 12$, $-7 \le k \le 4$, $-11 \le l \le 25$
Tot., Uniq. Data, R(int)	5078, 2740, 0.0244
Refinement	
Nreflections, Nparameters, Nrestrains	2740, 155, 0
R2, R1, wR2, wR1,	R_1 = 0.0256, wR_2 = 0.0484
	R_1 = 0.0308, wR_2 = 0.0505
Goof	1.050
Max. and Av. Shift/Error	0.001, 0.000
Min, Max. Resd Dens. (e-/$Å^3$)	1.399/-1.496

Figure S2. Image of XRD packing for (3g)

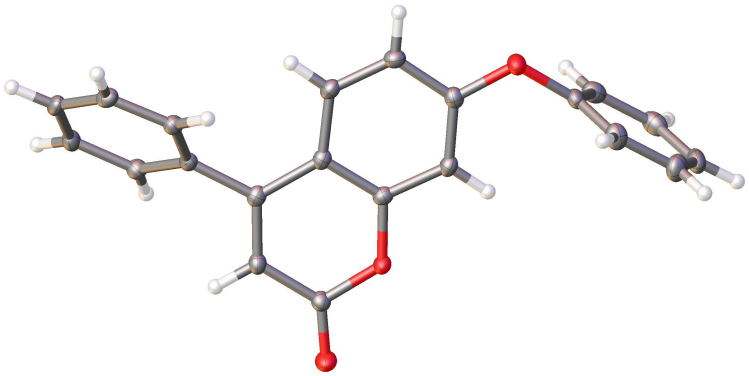

Table S2. Crystal data and refinement details for (3g)

Identification Code	Compound (3g)
Formula	$C_{21}H_{14}O_3$
Formula weight	314.32
Crystal system	monoclinic
Space group	$P2_1/c$
a (Å)	8.8762(3)
b (Å)	9.53546(17)
c (Å)	20.4998(6)
α (°)	90
β (°)	120.523(4)
γ (°)	90
V (Å^3)	1494.64(9)
Z	4
Density (g cm^{-3})	1.397
mu (MoKα) (mm^{-1})	0.752
F(000)	656.0
Data collection	
Temperature (K)	100.01(10)
Radiation (Å)	CuKα (λ = 1.54184)
Theta min - max	4.9870 to 75.9130
Dataset [h, k, l]	-10 ≤h≤ 10, -11≤k≤11, -24 ≤l≤ 24
Tot., Uniq. Data, R(int)	18401, 2831, 0.0276
Refinement	
Nreflections, Nparameters, Nrestrains	2831, 217, 0
R2, R1, wR2, wR1,	R_1 = 0.0325, wR_2 = 0.0833 R_1 = 0.0362, wR_2 = 0.0868
Goof	1.038
Max. and Av. Shift/Error	0.003, 0.000
Min, Max. Resd Dens. (e-/Å^3)	0.221/-0.198

Figure S3. Image of XRD packing for (3n)

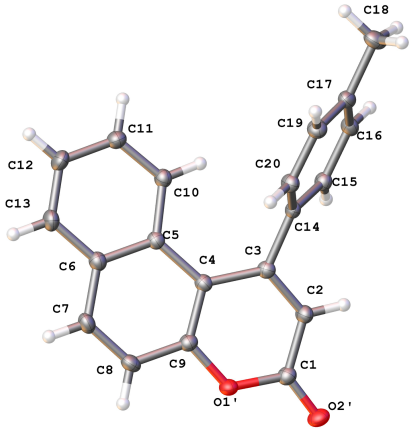

Table S3. Crystal data and refinement details for (3n)

Identification Code	Compound (3n)
Formula	$C_{20}H_{14}O_2$
Formula weight	286.31
Crystal system	monoclinic
Space group	$P2_1/c$
a (Å)	16.7399(2)
b (Å)	6.42919(8)
c (Å)	13.27782(18)
α (°)	90.00
β (°)	95.9314(12)
γ (°)	90.00
V (Å^3)	1421.36(3)
Z	4
Density (g cm^{-3})	1.338
mu (MoKα) (mm^{-1})	0.680
F(000)	600
Data collection	
Temperature (K)	100.01(10)
Radiation (Å)	CuKα (λ = 1.5418)
Theta min - max	5.3020 – 75.8750
Dataset [h, k, l]	-21/21, -8/8, -16/16
Tot., Uniq. Data, R(int)	34278, 2979, 0.0457
Refinement	
Nreflections, Nparameters, Nrestrains	2979, 200, 0
R2, R1, wR2, wR1, Goof	0.0398, 0.0382, 0.1173, 0.1151, 1.075
Max. and Av. Shift/Error	0.001, 0.000
Min, Max. Resd Dens. (e-/Å^3)	-0.264, 0.255

Figure S4. Image of XRD packing for (3m)

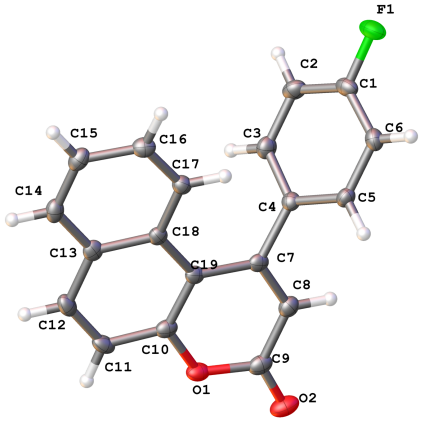

Table S4. Crystal data and refinement details for (3m)

Identification Code	Compound (**3m**)
Formula	$C_{19}H_{11}F_1$
Formula weight	373.01
Crystal system	monoclinic
Space group	$P2_1/c$
a (Å)	7.6932(5)
b (Å)	6.0149(4)
c (Å)	14.4236(9)
α (°)	90.00
β (°)	91.028(6)
γ (°)	90.00
V (Å^3)	667.33(7)
Z	2
Density (g cm^{-3})	1.856
mu (MoKα) (mm^{-1})	0.235
F(000)	370
Data collection	
Temperature (K)	100.01(10)
Radiation (Å)	MoKα – 0.7107
Theta min - max	2.82– 27.50
Dataset[h, k, l]	-23/25, -25/25, -25/25
Tot., Uniq. Data, R(int)	5534, 2656, 0.0182
Refinement	
Nreflections, Nparameters, Nrestrains	2656, 199, 2
R2, R1, wR2, wR1, Goof	0.0341, 0.0315, 0.0734, 0.0715, 1.022
Max. and Av. Shift/Error	0.000, 0.000
Min, Max. Resd Dens. (e-/Å^3)	-0.162, 0.218

Figure S5. Image of XRD packing for ($3c_{b-p}$)

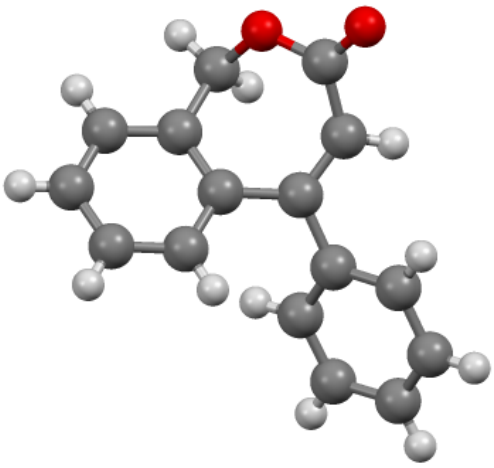

Table S5. Crystal data and refinement details for ($3c_{b-p}$)

Identification Code	Compound **($3c_{b-p}$)**
Formula	$C_{16}H_{12}O_2$
Formula weight	236.26
Crystal system	orthorhombic
Space group	$P2_1/c$
a (Å)	5.27450(10)
b (Å)	8.6629(2)
c (Å)	26.3674(5)
α (°)	90.00
β (°)	90.00
γ (°)	90.00
V (Å^3)	1204.79(4)
Z	4
Density (g cm^{-3})	1.303
mu (MoKα) (mm^{-1})	0.682
F(000)	496
Data collection	
Temperature (K)	173(2)
Radiation (Å)	MoKα – 1.54178
Theta min - max	3.352 – 66.641
Dataset [h, k, l]	-6/6, -10/10, -31/31
Tot., Uniq. Data, R(int)	11604, 2130, 0.0395
Refinement	
Nreflections, Nparameters, Nrestrains	2130, 164, 0
R2, R1, wR2, wR1, Goof	0.0430, 0.0389, 0.0981, 0.0956, 1.060
Max. and Av. Shift/Error	0.000, 0.000
Min, Max. Resd Dens. (e-/Å^3)	-0.204, 0.142

Figure S6. Image of XRD packing for ($5c_{b-p}$)

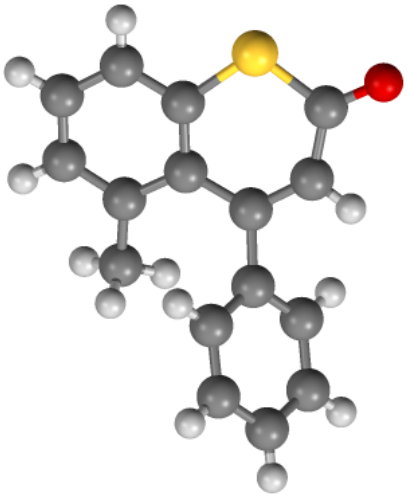

Table S6. Crystal data and refinement details for ($5c_{b-p}$)

Identification Code	Compound (**$5c_{b-p}$**)
Formula	$C_{16}H_{12}OS$
Formula weight	252.32
Crystal system	orthorhombic
a (Å)	14.4980(10)
b (Å)	9.0605(7)
c (Å)	18.9450(17)
α (°)	90.00
β (°)	90.00
γ (°)	90.00
V ($Å^3$)	2488.6(3)
Z	8
Density (g cm^{-3})	1.347
mu (MoKα) (mm^{-1})	0.243
F(000)	1056
Data collection	
Temperature (K)	173(2)
Radiation (Å)	MoKα – 0.71073
Theta min - max	2.150– 28.094
Dataset [h, k, l]	-19/17, -11/11, -25/25
Tot., Uniq. Data, R(int)	32938, 3024, 0.0688
Refinement	
Nreflections, Nparameters, Nrestrains	3024, 164, 0
R2, R1, wR2, wR1, Goof	0.0743, 0.0469, 0.1096, 0.0996, 1.047
Max. and Av. Shift/Error	0.001, 0.000
Min, Max. Resd Dens. (e-/$Å^3$)	-0.223, 0.311

Figure S7. Image of XRD packing for (5h)

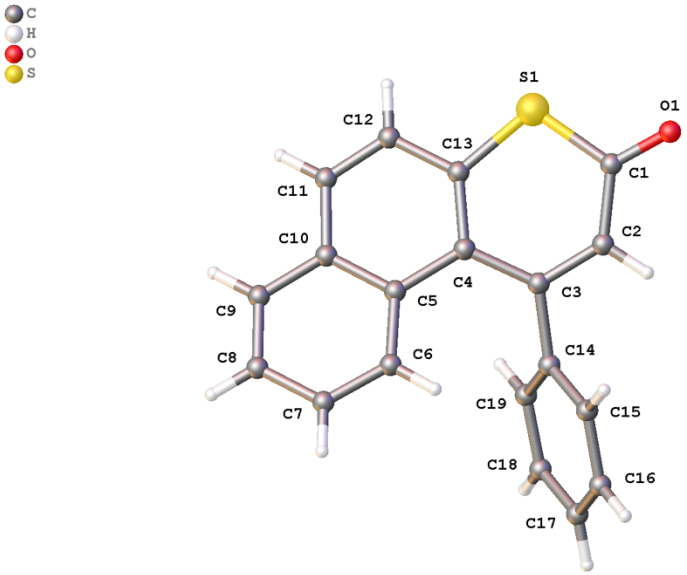

Table S7. Crystal data and refinement details for (5h)

Identification Code	Compound (5**h**)
Formula	$C_{19}H_{12}OS$
Formula weight	288.35
Crystal system	monoclinic
Space group	$P2_1/c$
a (Å)	14.7930(4)
b (Å)	5.99640(10)
c (Å)	20.2355(5)
α (°)	90.00
β (°)	128.973(2)
γ (°)	90.00
V (Å^3)	1395.5
Z	4
Density (g cm^{-3})	1.372
mu (MoKα) (mm^{-1})	0.227
F(000)	600
Data collection	
Temperature (K)	173 (2)
Radiation (Å)	MoKα – 0.71073
Theta min - max	1.771– 28.035
Dataset [h, k, l]	-19/19, -7/7, -26/26
Tot., Uniq. Data, R(int)	35542, 3350, 0.0776
Refinement	
Nreflections, Nparameters, Nrestrains	3350, 190, 0
R2, R1, wR2, wR1, Goof	0.0641, 0.0397, 0.0970, 0.0870, 1.009
Max. and Av. Shift/Error	0.001, 0.000
Min, Max. Resd Dens. (e-/Å^3)	-0.406, 0.346